Wave Splitting in Direct and Inverse Scattering Problems

Gustafsson, Mats

2000

Wave Splitting in Direct and Inverse Scattering Problems

by

Mats Gustafsson

Department of Applied Electronics
Electromagnetic Theory
Lund University
P.O. Box 118, S-221 00 Lund
Sweden

No. 16
ISSN 1402-8662
ISBN 91-7874-068-1

Printed in Sweden
KFS AB
Lund, May 2000

Abstract

The focus of this thesis is on the use of wave splitting in electromagnetic direct and inverse scattering problems. Wave splitting offers a decomposition of wave fields into appropriate input and output wave constituents. Several different wave splittings are studied including one-dimensional, multi-dimensional energy-flux, and multi-dimensional locally exact wave splittings.

The Bremmer series is naturally connected to wave splitting as a method to decompose a complex scattering problem into a sequence of single scattering problems. The one-dimensional Bremmer series is reviewed and time-domain convergence is shown for the acoustic locally exact wave splitting.

The emphasis of the inverse scattering problems is on the identification of the spatial structure of complex medium models in multi-dimensions from time-domain data. The parameter identification is determined in an iterative fashion with a conjugate-gradient algorithm where the least-squares error of the output field is minimized. The gradient is determined from the solution of an additional adjoint problem. The energy-flux split fields are shown to give a good representation of the boundary fields in the inverse scattering problem. Several multi-parameter identifications are performed in two spatial dimensions.

A detailed analysis is included about electromagnetic modeling. The non-uniqueness of the instantaneous response and the long-time behavior is specially emphasized.

Finally, time-reversal mirrors and time-reversal cavities are discussed.

Contents

Acknowledgments

This thesis is the result of my research during the past five years. It would not have been possible without a lot of assistance, encouragement, and support.

First, I would like to express my deep gratitude to my supervisor Prof. Gerhard Kristensson for his guidance as well as valuable discussions concerning the preparation of this thesis. I also appreciate that he has encouraged me to visit several universities abroad and his assistance in finding support for these visits.

I am grateful to Doc. Sailing He, Dept. of Electromagnetic theory, Royal Institute of Technology, Sweden, for initiating the least-squares time-domain inverse scattering project and the many stimulating discussions during the project.

Prof. Yahya Rahmat-Samii and the graduate students at the Antenna Lab, University of California Los Angeles (UCLA), USA, are gratefully acknowledged for giving me an invaluable year as a graduate student at the UCLA 1995-96. 'Gemzéus stipendiefond, Gålöstiftelsen' is also acknowledged for its support during this year.

The work on Bremmer series and time-reversal mirrors was initiated during a visit to the Center of Wave Phenomena (CWP), Colorado School of Mines, USA, spring and summer 1998. I thank Prof. Maarten V. de Hoop at the CWP for inviting me to CWP and introducing me to Bremmer series, time-reversal mirrors, and geophysics in general. The CWP is also acknowledged for its hospitality and support during the visit.

Prof. David Wall and the department of mathematics and statistics, Canterbury University, Christchurch, New Zealand, are gratefully acknowledged for their hospitality during a very stimulating visit in fall 1998.

I thank all former and present colleagues at the department for creating a stimulating scientific atmosphere. In particular I wish to thank Bengt Stjernberg and Erik Jonsson for general computer assistance, Elsbieta Szybicka for solving practical problems, Richard Lundin for his encouragement and support in my work as teaching assistant and lecturer, Anders Karlsson for reading and criticizing various manuscripts, Margaret Cheney for discussions on the English language, and Daniel Sjöberg for sharing his knowledge of LaTeX.

I thank MSc. Lars Jonsson at the Dept. of Electromagnetic theory, Royal Institute of Technology, Sweden, Prof. Anders Melin at the Center for Mathematical Sciences, Lund University, Sweden, and Prof. Ari Laptev at the Dept. of Mathematics, Royal Institute of Technology, Sweden, for fruitful discussions about wave splitting and Bremmer series.

My brother Lars Gustafsson is acknowledged for invaluable C-program consultations.

Finally, I would like to thank family and friends for distracting me from doing too much research and making these years to a truly good time.

This work is partially funded by a grant from the Swedish Research Council for Engineering Sciences and their support is gratefully acknowledged. Several travel grants from the Crafoord foundation, Ernhold Lundström foundation, the Royal Swedish Academy of Sciences, the Royal Physiographic Society in Lund, and the L M Ericsson foundation are gratefully acknowledged.

Chapter 1

Introduction

This introductory chapter starts with a brief introduction to electromagnetics in Section 1.1. It continues with a discussion about direct and inverse scattering problems in Section 1.2 and an outline of the thesis in Section 1.3.

1.1 Electromagnetics

Electromagnetics offers a description of many phenomena that affect our everyday life. Among many products, *e.g.*, the power lines that supply our society with electrical energy, motors and generators that transform electrical energy to mechanical force and vice versa, wired and wireless communication such as telephone, optical fibers and cellular phones, radio, and television. Microwaves are used in microwave ovens to heat food as well as in radar applications such as traffic control and weather forecasting. Visual light is obviously essential for our vision and X-rays are used in tomography to image the interior of our body. These apparently very different products illustrate the variety of electromagnetics. The frequency span of the electromagnetic field offers an understanding of the different electromagnetic phenomena. The frequencies of the above products range from the powerlines at approximately 50 Hz, *i.e.*, 50 oscillations per second, up to X-rays at about 10^{17} Hz. The difference is maybe more clearly illustrated by the equivalent free-space wavelengths that range from 10^{7} m down to 10^{-9} m in powerlines and X-rays, respectively. The electromagnetic applications together with their frequencies and equivalent free-space wavelengths are depicted in Figure 1.1.

Electric, magnetic, and optical theories have been studied by several famous scientists such as Cavendish, Coulomb, Ampère, Faraday, and Gauss. In 1864, J.C. Maxwell unified the electric, magnetic, and optical theories to an electromagnetic theory [181, 182]. His famous equations constitute the basic model for all macroscopic electromagnetic phenomena. This macroscopic electromagnetic theory is accurate up to frequencies somewhere between visual light and X-rays. At higher frequencies it is necessary to include microscopic effects [128, 73].

The rapid development of electromagnetic theory and electrical equipments at the end of the 19th century led to the development of radio by Marconi, Tesla, *et al.,* [31, 9]. The use of wireless communication have exploded during the 20th century

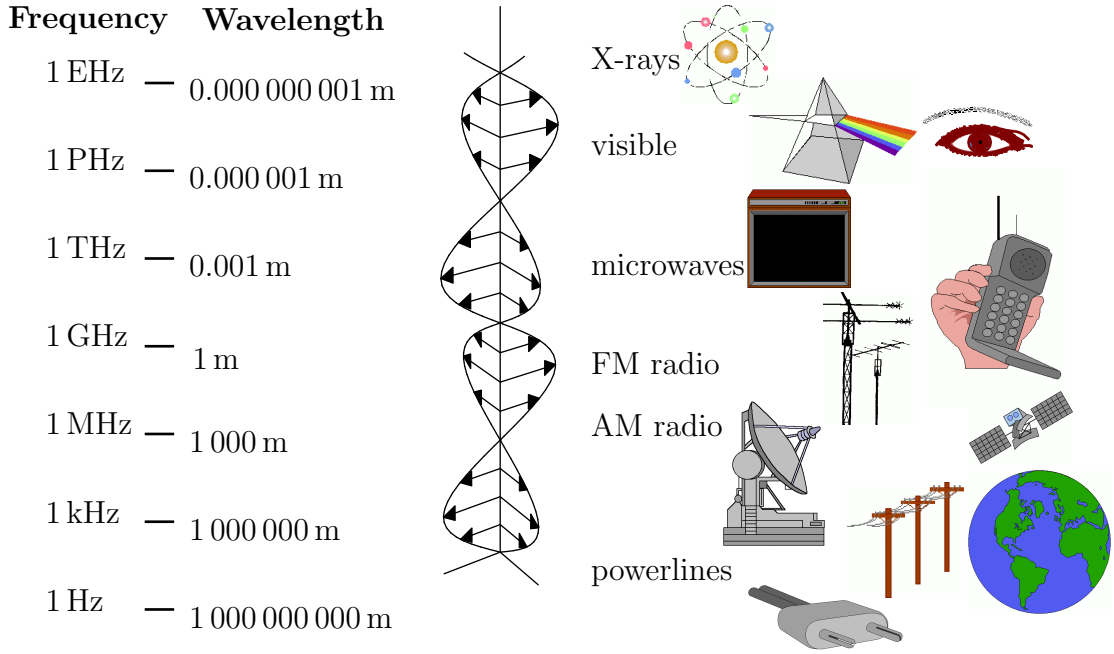

Figure 1.1: Electromagnetic theory is used to describe a variety of phenomena ranging from the low frequency power lines up to X-ray radiation. Each frequency is related to its free-space wavelength.

and today it is a natural part of our society. A basic application of electromagnetic theory in wireless communication is to determine the signal strength, *i.e.*, the amplitude of the electromagnetic field, far away from a transmitting antenna. The wireless communication problem is illustrated in Figure 1.2.

With due respect to the modern information society and its use of electromagnetic fields, the profound application of electromagnetic fields is to investigate our world. For example, our eyes observes an object by the light that is scattered from the object. A technical application based on similar principles is found in medical imaging where electromagnetic fields are induced in a body and the scattered electromagnetic field is measured. Knowledge about the incident field and the scattered field together with a model of electromagnetic wave propagation can be used to determine an image of the internal structure of the body. The X-ray computer tomography is probably the most well-known imaging system. It uses X-rays to obtain an image of the body [123]. Magnetic resonance imaging (MRI) is another well-known imaging system [7]. In Figure 1.3a part of the impedance imaging system at Rensselaer Polytechnic Institute, Troy, NY is shown [32]. In impedance imaging a low frequency current is induced at one spot of the body and the voltage is measured around the body. The internal structure of the identified body is shown in Figure 1.3b. Similar techniques are used in areas such as mineral prospecting and non-destructive testing.

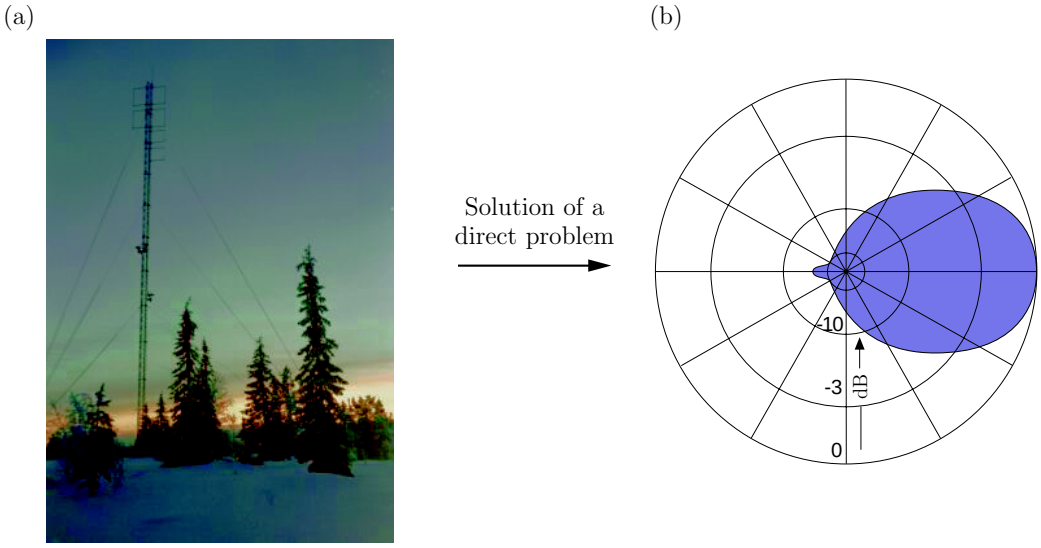

Figure 1.2: Example of the use of electromagnetic waves to transmit information. (a) The mobile communication base station antenna in Nattavaaraby, Sweden, at noon Christmas eve 1999. (b) An antenna pattern that represents the signal strength far away from the antenna. The antenna pattern is determined from the solution of an electromagnetic problem where the excitation of the antenna and the material parameters are known and the electromagnetic fields are sought.

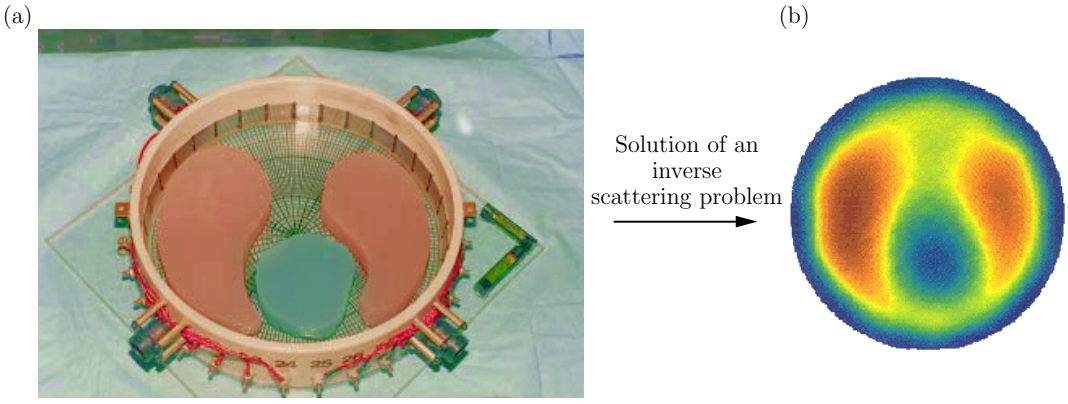

Figure 1.3: Example of the use of electromagnetic waves to infer information about the internal structure of an object. (a) Experimental setup of impedance tomography at Rensselaer Polytechnic Institute, Troy, NY. (b) The identified internal structure of the object. (Courtesy of the impedance tomography group at Rensselaer Polytechnic Institute, Troy, NY.).

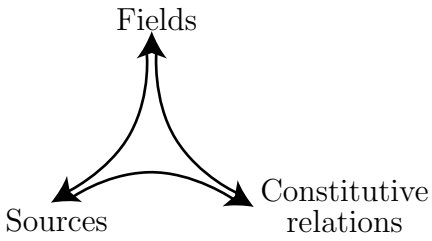

Figure 1.4: In electromagnetics there are three different quantities involved, *i.e.*, the electromagnetic fields, the sources, and the constitutive relations. The sources are the origin of the electromagnetic fields and the constitutive relations model the interaction between the electromagnetic fields and material. In the direct problem, the field are determined from knowledge about the source and the constitutive relations. In inverse scattering problems the constitutive relations are determined.

1.2 Direct and inverse problems

In electromagnetics, there are three equally important parts: the electromagnetic fields, the sources, and the constitutive relations, see Figure 1.4. The electromagnetic fields originate from the sources and the constitutive relations model the interaction between electromagnetic fields and material.

The antenna example in Figure 1.2 and the tomography example in Figure 1.3 are fundamentally different with respect to given and requested data. In the antenna example, the sources and a model of the surrounding region are given and the electromagnetic fields are sought. Electromagnetic theory is used to determine the electromagnetic field that originates from the sources and that is scattered by the surrounding medium. It is natural to interpret the fields as an effect caused by the currents and material. The antenna example is a typical direct problem, *i.e.*, a direct problem is to determine the effects from given causes.

The tomography example is an example of the opposite type of procedure, *i.e.*, an inverse problem. In an inverse problem the effects are given and a possible cause is sought.

The classification of electromagnetic problems as either direct problems or inverse problems gives a good characterization of the fundamental problems in electromagnetic theory. However, the majority of engineering applications of electromagnetics involves the design of a product. These types of electromagnetic problems are neither direct nor inverse problems although their solution typically involves the solution of basic direct and/or inverse problems. Another fundamental problem in electromagnetics is to determine effective models of the interaction between electromagnetic fields and material.

1.3 Outline of the thesis

One of the most interesting application of electromagnetics is the use of electromagnetic fields to infer information about the internal structure of an object from

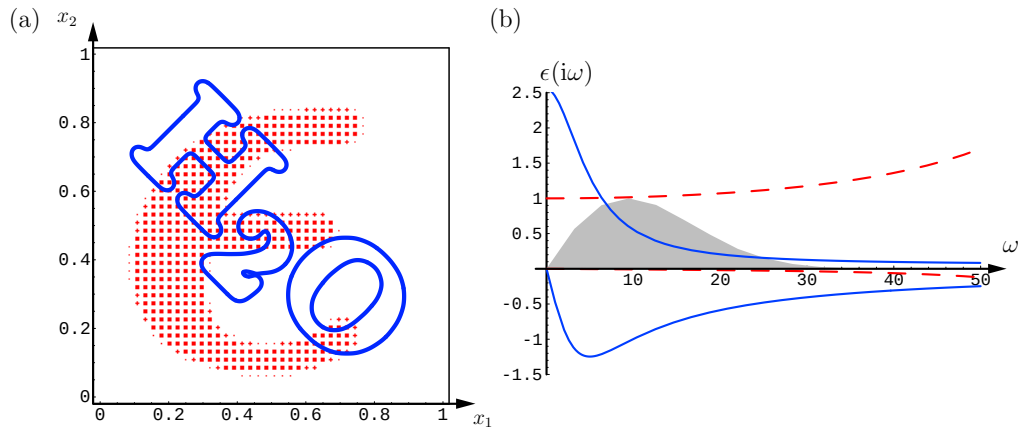

Figure 1.5: An object partly filled with crystal and water. (a) The crystal portion is illustrated by the (red) dotted ϵ-shaped part and the water is contained in the (blue) H_2O-shaped region. (b) The interaction between electromagnetic fields and the medium is modeled by a frequency dependent permittivity. The (red) dashed and (blue) solid graphs correspond to the frequency dependence of the crystal and water, respectively.

measurements of the electromagnetic fields at the surface of the object. Impedance tomography, X-ray tomography, and magnetic resonance imaging are typical medical applications where electromagnetic fields are used to create an image of a body. Other applications include non-destructive testing, mine detection, and mineral prospecting.

In this thesis, we focus on the case where it is possible to measure the fields at a surface surrounding the object. As an example consider the two-dimensional object depicted in Figure 1.5a. This object consists of a mixture of crystal and water. The crystal is the dotted (red) ϵ-shaped portion and the water is contained in the (blue) H_2O-shaped portion. We try to infer information about the object from a set of measurements at the surface of the object.

To be able to identify a material with electromagnetic fields it is essential to know how electromagnetic fields interact with the material. In general, the interaction differs with the frequency of the electromagnetic field, the amplitude of the field, and with the direction (polarization) of the field. Our vision is sensitive to frequency dependent and directional dependent materials. The color of an object can be explained by the fact that the object scatters some frequencies (colors) and absorbs other frequencies. In a similar context, we are also familiar with directional dependence from polarized sun glasses. In microwave applications, many materials display a directional dependence due to a small scale directionality of the material, such as the fiber structure of muscle tissues. The material depicted in Figure 1.5a is dispersive but not directional dependent. The frequency dependence is modeled by a frequency dependent permittivity, see Figure 1.5b. The amplitude dependence can often be ignored if the amplitude of the electromagnetic field is sufficiently small. Modeling of the interaction between electromagnetic fields and material is discussed

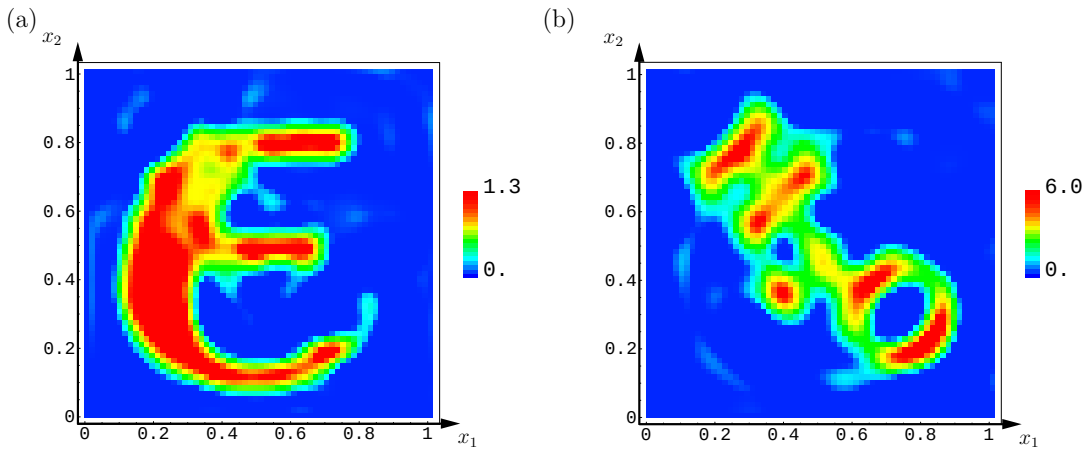

Figure 1.6: The identified distribution of the water and crystal medium. (a) The crystal portion is identified as a smooth ϵ-shaped region. The amplitude corresponds to an effective medium representation of the originally dotted crystal medium. (b) The identified amount of water resembles the original distribution of water.

in Chapter 2.

The object is identified from information about how it interacts with electromagnetic fields. It is natural to interpret the interaction as the relation between incident and scattered wave fields. The wave splitting concept generalizes this decomposition of a wave field into a decomposition in input and output fields. The wave splitting is studied in Chapter 4.

The output fields of a given object and prescribed input fields are determined as solutions of the Maxwell equations together with the constitutive relations. Here the equations are solved with a finite-difference time-domain (FDTD) scheme. This direct problem is studied in Chapter 5.

At this stage, we are ready to infer some information about the object depicted in Figure 1.5a. The solution is defined as the object that minimizes the difference between the given output fields and a set of calculated output fields. The identification process starts with an initial guess of the spatial distribution of the object. This guess is improved with a gradient based optimization algorithm, *i.e.*, the identified parameters are updated such that the output fields resemble the given output fields even better. In the crystal and water example, an initial guess of zero crystal and zero water is used. The algorithm tries to find the distribution of water and crystal that gives the same output fields as the original crystal and water configurations. The identified crystal and water profiles are depicted in Figure 1.6. The identification algorithm as well as the crystal and water example are discussed in more detail in Chapter 8. The identified material parameters resembles the original parameters. However, it is only the coarse structure of the crystal that is retrieved. We also note a slight deficiency in the water identification, *i.e.*, the identification deteriorates in regions that contain both crystal and water.

Moreover, we include a brief discussion of the acoustic wave equation in Chapter 3. In Chapter 6, a direct solution strategy of half-space problems is discussed. A

general description of inverse problems is given in Chapter 7. Time-reversal mirrors and time-reversal cavities are considered in Chapter 9. Finally, the used notation is outlined in Appendix A.

Chapter 2

Electromagnetic modeling

The evolution of electromagnetic fields is governed by the Maxwell equations and a set of constitutive relations. The constitutive relations model the interaction between electromagnetic fields and the material.

In Sections 2.1 and 2.2, we discuss the Maxwell equations and the constitutive relations, respectively. Characterization of passive medium models is considered in Section 2.3. The instantaneous, the long-time limits, and the static limit are analyzed in Sections 2.4, 2.5, and 2.6, respectively. Section 2.7 treats a state-variable representation of the constitutive relations. An alternative form of the constitutive relations is discussed in Section 2.8 and a few inequalities are outlined in Section 2.9.

2.1 Maxwell equations

The electromagnetic phenomena are described by the electric and magnetic fields, *i.e.*, the electric field intensity $\boldsymbol{E}$, the magnetic field intensity $\boldsymbol{H}$, the electric flux density $\boldsymbol{D}$, and the magnetic flux density $\boldsymbol{B}$, see Table 2.1. The electromagnetic fields originate from the (electric) current density $\boldsymbol{J}$ and the charge density ϱ. In many problems it is convenient to include a magnetic current [12]. The electromagnetic fields are related through the Maxwell equations. The Maxwell equations consist of the Ampere's law and the Faraday's law

$$\begin{cases} \partial_t \boldsymbol{D} - \nabla \times \boldsymbol{H} = -\boldsymbol{J}, \\ \partial_t \boldsymbol{B} + \nabla \times \boldsymbol{E} = \boldsymbol{0} \end{cases} \tag{2.1}$$

together with the divergence equations

$$\begin{cases} \nabla \cdot \boldsymbol{D} = \varrho, \\ \nabla \cdot \boldsymbol{B} = 0. \end{cases} \tag{2.2}$$

The divergence equations express the relation between the flux densities and the charge densities. Observe that the continuity equation for the current and charge density

$$\partial_t \varrho + \nabla \cdot \boldsymbol{J} = 0 \tag{2.3}$$

Description	Symbol	SI unit	Scaled unit
Electric fields intensity	$\boldsymbol{E}$	V/m	$(\mathrm{Ws/m^3})^{1/2}$
Magnetic fields intensity	$\boldsymbol{H}$	A/m	$(\mathrm{Ws/m^3})^{1/2}$
Electric flux density	$\boldsymbol{D}$	$\mathrm{As/m^2}$	$(\mathrm{Ws/m^3})^{1/2}$
Magnetic flux density	$\boldsymbol{B}$	$\mathrm{Vs/m^2}$	$(\mathrm{Ws/m^3})^{1/2}$
(Electric) Current (density)	$\boldsymbol{J}$	$\mathrm{A/m^2}$	$(\mathrm{Ws/m^5})^{1/2}$
(Electric) Charge (density)	ϱ	$\mathrm{As/m^3}$	$(\mathrm{Ws/m^5})^{1/2}$

Table 2.1: The electromagnetic fields and sources.

follows from the Maxwell equations.

We model the interaction on a macroscopic level with a set of constitutive relations. The field intensities are treated as fundamental quantities and the corresponding flux densities as derived quantities. The constitutive relations are given by a map from the field intensities to the flux densities

$$\begin{pmatrix} \boldsymbol{E} \\ \boldsymbol{H} \end{pmatrix} \xrightarrow{\boldsymbol{\varepsilon}} \begin{pmatrix} \boldsymbol{D} \\ \boldsymbol{B} \end{pmatrix}. \tag{2.4}$$

Under very general constitutive relations, the Maxwell equations (2.1) uniquely define the electromagnetic fields for all times $t > 0$ from knowledge of the electromagnetic fields up to a time $t = 0$ together with knowledge about the current $\boldsymbol{J}$ for times $t > 0$. These fields also satisfy the divergence equation (2.2) if these equations are satisfied at time $t = 0$. This implies that the Ampere's law and the Faraday's law are the fundamental ones as long as the initial conditions are consistent with the divergence equations (2.2).

However, in a typical problem it is not possible to have a priori information about the field values for all previous times in all of space. We consider a general problem where the current $\boldsymbol{J}(\boldsymbol{x}, t)$ and the charge density $\varrho(\boldsymbol{x}, t)$ are given for $\boldsymbol{x} \in \mathbb{R}^3$ and $t > 0$ and we want to determine the electromagnetic fields in a region $\Omega \subset \mathbb{R}^3$ for times $t > 0$.

The electromagnetic fields are not given for $t \leq 0$, *i.e.*, neither the initial values of the equations (2.1) nor the history of the fields for (2.4) are prescribed. To be able to predict the fields in the region Ω, it is necessary that the response of the fields at $t = 0$ as well as the effect of the prehistory $t < 0$ decay as time evolves. In Sections 2.5, 2.6, and 5.4, we study this decay and its restrictions on the constitutive relations (2.4).

In numerical implementations as well as in theoretical discussions it is convenient to scale the electromagnetic field quantities. The scaling is similar to the rationalized Gaussian units and all the fields are measured in an energy unit, *i.e.*, $\boldsymbol{E}, \boldsymbol{H}, \boldsymbol{D}$ and $\boldsymbol{B}$ have the unit $(\text{Energy/Volume})^{1/2}$. The transformation to SI units is made by the substitution

$$\begin{aligned} \boldsymbol{E} &\mapsto \sqrt{\epsilon_0}\boldsymbol{E}_{\mathrm{SI}}, \;\; \boldsymbol{D} \mapsto \epsilon_0^{-1/2}\boldsymbol{D}_{\mathrm{SI}}, \;\; \boldsymbol{J} \mapsto \sqrt{\mu_0}\boldsymbol{J}_{\mathrm{SI}}, \\ \boldsymbol{H} &\mapsto \sqrt{\mu_0}\boldsymbol{H}_{\mathrm{SI}}, \;\; \boldsymbol{B} \mapsto \mu_0^{-1/2}\boldsymbol{B}_{\mathrm{SI}}, \;\; t \mapsto c_0 t_{\mathrm{SI}} = (\epsilon_0\mu_0)^{-1/2} t_{\mathrm{SI}}. \end{aligned} \tag{2.5}$$

In the analysis, we use the shorthand notation in the scaled fields

$$\boldsymbol{e} = \begin{pmatrix} \boldsymbol{E} \\ \boldsymbol{H} \end{pmatrix}, \quad \boldsymbol{d} = \begin{pmatrix} \boldsymbol{D} \\ \boldsymbol{B} \end{pmatrix} \quad \text{and} \quad \boldsymbol{j} = \begin{pmatrix} \boldsymbol{J} \\ \boldsymbol{0} \end{pmatrix} \tag{2.6}$$

for the field intensities, flux densities and current densities, respectively. With this notation, the constitutive relations (2.4) are written

$$\boldsymbol{d} = \boldsymbol{\varepsilon}[\boldsymbol{e}] \tag{2.7}$$

and the Maxwell equations (2.1) are

$$\partial_t \boldsymbol{d} - \nabla \times \mathrm{J}\boldsymbol{e} = -\boldsymbol{j},$$

see Appendix A.2 on page 149 for details about this notation.

2.2 The constitutive relations

Electromagnetic interaction with material is diverse. It ranges from the simplest case of diluted gases to the complex structure of iron (highly nonlinear effects, such as hysteresis). The material interacts with the electromagnetic field through the dynamics of the microscopic charges of the material, *i.e.*, the charges of the atoms and the molecules. This implies phenomena such as direction dependence and memory effects. The mathematical models of the interaction, *i.e.*, the constitutive relations, have been thoroughly investigated, see *e.g.*, Refs [55, 74, 128, 26, 199, 139, 64, 65, 167, 177] for a general discussion about electromagnetic modeling.

The electromagnetic interaction with material is modeled by the constitutive relations (2.4). The constitutive relations of a material are determined either from direct measurements or from a priori knowledge of the microscopic structure of the material. In general, this offers an accurate description of the material interaction with the electromagnetic field in a specific frequency and amplitude range. The set of constitutive relations can be used in an electromagnetic application as long as the fields of the application are restricted to the same frequency and amplitude range. In time-domain applications it is necessary to extend the constitutive relations to all frequencies. The constitutive relations can be extended outside the range of validity as long as their values do not affect the solubility of the Maxwell equations.

We start with a few assumptions that offer a good representation of the constitutive map. The assumptions for a linear dispersion law are

Causal: Effects follow causes

$$\boldsymbol{e}(\boldsymbol{x}, t) = 0 \quad \text{for} \quad t \leq T \quad \text{implies} \quad \boldsymbol{\varepsilon}[\boldsymbol{e}(\boldsymbol{x}, \cdot)](t) = 0 \quad \text{for} \quad t \leq T.$$

Spatially pointwise: Information is only allowed to propagate in space through the Maxwell equations (2.1).

$$\boldsymbol{d}(\boldsymbol{x}, t) = \boldsymbol{\varepsilon}[\boldsymbol{x}, \boldsymbol{e}(\boldsymbol{x}, \cdot)](t).$$

We restrict the discussion to a treatment of temporally dispersive media, *i.e.*, we do not include the interesting modeling of phenomena associated with spatially dispersive media [167].

Continuous: Small causes give small effects, *i.e.*, we assume that the map $\boldsymbol{e} \to \boldsymbol{d}$ is bounded. This statement is specified below.

Linear: The constitutive relations (2.4) are linear, *i.e.*,

$$\boldsymbol{\varepsilon}[\boldsymbol{x}, \alpha_1 \boldsymbol{e}_1(\boldsymbol{x}, \cdot) + \alpha_2 \boldsymbol{e}_2(\boldsymbol{x}, \cdot)](t) = \alpha_1 \boldsymbol{\varepsilon}[\boldsymbol{x}, \boldsymbol{e}_1(\boldsymbol{x}, \cdot)](t) + \alpha_2 \boldsymbol{\varepsilon}[\boldsymbol{x}, \boldsymbol{e}_2(x, \cdot)](t)$$

for all $\alpha_1, \alpha_2 \in \mathbb{R}$ and all fields $\boldsymbol{e}_1, \boldsymbol{e}_2$. The majority of materials behaves linearly for small amplitudes of the field intensities (or equivalent small energies).

Time-invariant: The medium does not age

$$\boldsymbol{d}(\boldsymbol{x}, t + \tau) = \boldsymbol{\varepsilon}[\boldsymbol{x}, \boldsymbol{e}(\boldsymbol{x}, \cdot + \tau)](t).$$

This assumption is convenient for the Laplace-domain analysis.

A map $\boldsymbol{e} \to \boldsymbol{d}$ satisfying the requirements above has a representation in the form of a temporal convolution [139]

$$\boldsymbol{d}(\boldsymbol{x}, t) = \int_{-\infty}^{t} \left(\boldsymbol{\varepsilon}_\infty(\boldsymbol{x})\delta(t - \tau) + \boldsymbol{\chi}(\boldsymbol{x}, t - \tau)\right) \boldsymbol{e}(\boldsymbol{x}, \tau)\, \mathrm{d}\tau, \tag{2.8}$$

where a Dirac delta function is included for future convenience. Time invariance gives the convolution structure. Causality implies that time t enters as the upper limit of integration, or, equivalently, the requirement $\boldsymbol{\chi}(\boldsymbol{x}, t) = \boldsymbol{0}$ for $t < 0$. In the convolution representation (2.8), we clearly observe the memory interpretation of the interaction, *i.e.*, all previous field values affect the present field value [139].

The Laplace domain is frequently used in the analysis. The Laplace transformed wave-field quantities are denoted with a hat, *i.e.*,

$$\hat{\boldsymbol{e}}(\boldsymbol{x}, s) = \int_{0-}^{\infty} \mathrm{e}^{-st} \boldsymbol{e}(\boldsymbol{x}, t)\, \mathrm{d}t, \tag{2.9}$$

where the Laplace transform parameter s is restricted to a right half plane $s = \eta + \mathrm{i}\omega$, with $\eta \geq 0$. The time-domain wave-field quantities are recovered by the inverse Laplace transform

$$\boldsymbol{e}(\boldsymbol{x}, t) = \frac{1}{2\pi} \int_{-\infty}^{\infty} \mathrm{e}^{(\eta + \mathrm{i}\omega)t} \hat{\boldsymbol{e}}(\boldsymbol{x}, \eta + \mathrm{i}\omega)\, \mathrm{d}\omega. \tag{2.10}$$

Before we can transform the Maxwell equations to the Laplace domain, the history ($\boldsymbol{e}(\boldsymbol{x}, t)$ for $t < 0$) of the field has to be removed. Decompose the temporal convolution (2.8) into two parts, *i.e.*, for $t \geq 0$ the flux density is

$$\boldsymbol{d}(\boldsymbol{x}, t) = \int_{0-}^{t} \left(\boldsymbol{\varepsilon}_\infty(\boldsymbol{x})\delta(t - t') + \boldsymbol{\chi}(\boldsymbol{x}, t - t')\right) \boldsymbol{e}(\boldsymbol{x}, t')\, \mathrm{d}t' + \int_{-\infty}^{0-} \boldsymbol{\chi}(\boldsymbol{x}, t - t') \boldsymbol{e}(\boldsymbol{x}, t')\, \mathrm{d}t'.$$

The first part depends only on the present ($t \geq 0$) values of the field and the second part depends only on the past ($t < 0$) field values. In the Laplace domain, the first part has the well-known matrix relation

$$\hat{\boldsymbol{d}}(\boldsymbol{x}, s) = \boldsymbol{\varepsilon}(\boldsymbol{x}, s)\hat{\boldsymbol{e}}(\boldsymbol{x}, s), \tag{2.11}$$

where $\boldsymbol{\varepsilon}$ can be identified with a complex-valued 6×6 matrix, see (2.17) and Appendix A.2 on page 151. Causality is guaranteed by the requirement that the elements of $\boldsymbol{\varepsilon}(\boldsymbol{x}, s)$ are analytic functions of s for $\operatorname{Re} s > \eta_0$ for some $\eta_0 > -\infty$. Furthermore, the matrix elements are real-valued if the Laplace parameter is real-valued.

The second part is reinterpreted and included as a current term, *i.e.*, the Laplace domain current is defined as

$$\hat{\boldsymbol{\jmath}}(\boldsymbol{x}, s) = \int_0^\infty \mathrm{e}^{-st} \left(\boldsymbol{\jmath}(\boldsymbol{x}, t) + \partial_t \int_{-\infty}^{0-} \boldsymbol{\chi}(\boldsymbol{x}, t - t')\boldsymbol{e}(\boldsymbol{x}, t') \, \mathrm{d}t' \right) \mathrm{d}t - \boldsymbol{\varepsilon}_\infty(\boldsymbol{x})\boldsymbol{e}(\boldsymbol{x}, 0).$$

The Maxwell equations are written

$$s\boldsymbol{\varepsilon}(\boldsymbol{x}, s)\hat{\boldsymbol{e}} - \nabla \times \mathrm{J}\hat{\boldsymbol{e}} = -\hat{\boldsymbol{\jmath}}(\boldsymbol{x}, s)$$

in the Laplace domain.

The basic assumptions above are not sufficient to give a well-posed form of the Maxwell equations and to satisfy the energy-decay property. Here, we add a set of assumptions to obtain a well-defined form of the Maxwell equations. These additional assumptions are:

Passive: The constitutive relations (2.4) are (pointwise) passive, *i.e.*, the material does not produce energy. The time-domain characterization of passive constitutive relations is [139]

$$\int_0^T \boldsymbol{e}(\boldsymbol{x}, t)^{\mathrm{T}} \cdot \partial_t[\boldsymbol{\varepsilon}\boldsymbol{e}](\boldsymbol{x}, t) \, \mathrm{d}t \geq 0 \quad \text{for all } T \geq 0 \tag{2.12}$$

and all fields $\boldsymbol{e}$. The Laplace-domain characterization is

$$\operatorname{Re} s\boldsymbol{\varepsilon}(\boldsymbol{x}, s) \geq 0 \quad \text{for} \quad s \in \mathbb{C}_+ = \{s = \eta + \mathrm{i}\omega : \eta > 0, \omega \in \mathbb{R}\},$$

see Section 2.3. This inequality is a shorthand notation for a non-negative definite symmetric part of the constitutive map, *i.e.*,

$$\boldsymbol{u}^{\mathrm{H}} \frac{s\boldsymbol{\varepsilon}(\boldsymbol{x}, s) + (s\boldsymbol{\varepsilon}(\boldsymbol{x}, s))^{\mathrm{H}}}{2} \boldsymbol{u} \geq 0 \quad \text{for all } \boldsymbol{u} \in \mathbb{C}^6 \text{ and } s \in \mathbb{C}_+.$$

Instantaneous response: The constitutive relations are decomposed into an instantaneously reacting part and non-instantaneous part. The instantaneous (or optical, or high frequency) response is modeled by a symmetric positive

definite 6×6 matrix and the non-instantaneous (or dispersive) part is modeled by a 6×6 integral operator, *i.e.*,

$$\boldsymbol{d}(\boldsymbol{x},t) = \boldsymbol{\varepsilon}_\infty(\boldsymbol{x})\boldsymbol{e}(\boldsymbol{x},t) + \int_{-\infty}^{t} \boldsymbol{\chi}(\boldsymbol{x},t-\tau)\boldsymbol{e}(\boldsymbol{x},\tau)\,\mathrm{d}\tau = \boldsymbol{\varepsilon}_\infty\boldsymbol{e} + \boldsymbol{\chi} * \boldsymbol{e}. \quad (2.13)$$

In the Laplace-domain, the instantaneous response corresponds to the high frequency behavior, *i.e.*,

$$\boldsymbol{\varepsilon}(\boldsymbol{x},s) = \boldsymbol{\varepsilon}_\infty(\boldsymbol{x}) + \mathrm{o}(1) \quad \text{as} \quad \mathbb{C}_+ \ni s \to \infty. \quad (2.14)$$

The instantaneous response is discussed in Section 2.4.

Long-time response: The long-time behavior of $\boldsymbol{\varepsilon}$ defines the conductivity, *i.e.*,

$$\boldsymbol{\chi}(\boldsymbol{x},t) \to \boldsymbol{\varsigma}(\boldsymbol{x}) \quad \text{as} \quad t \to \infty$$

where the conductivity is positive semi-definite, *i.e.*, $\boldsymbol{e}^{\mathrm{T}} \cdot \boldsymbol{\varsigma}(\boldsymbol{x})\boldsymbol{e} \geq 0$ for all fields $\boldsymbol{e}$ and points $\boldsymbol{x}$. Moreover, the temporal differential of the susceptibility kernel decays sufficiently fast for large times, *i.e.*,

$$\int_{0+}^{\infty} |\partial_t \boldsymbol{\chi}(\boldsymbol{x},t)|\,\mathrm{d}t < \infty. \quad (2.15)$$

The long-time behavior corresponds to the behavior of the Laplace-domain constitutive map at the imaginary axis. The conductivity translates to a simple pole at $s = 0$ and the absolute integrability of the susceptibility kernel translates to continuity of $\boldsymbol{\varepsilon}(\boldsymbol{x},s)$ at the imaginary axis, *i.e.*,

$$\boldsymbol{\varepsilon}(\boldsymbol{x},s) = \frac{\boldsymbol{\varsigma}(\boldsymbol{x})}{s} + \mathrm{O}(1) \quad \text{as} \quad s \to 0$$

and

$$\mathrm{i}\omega\boldsymbol{\varepsilon}(\boldsymbol{x},\mathrm{i}\omega) \quad \text{depends continuously on} \quad \omega.$$

The long-time response is discussed in Section 2.5.

Statics: To get a well-behaved static limit, the susceptibility kernel is restricted such that

$$\int_{0}^{\infty} |\boldsymbol{\chi}(\boldsymbol{x},t) - \boldsymbol{\varsigma}(\boldsymbol{x})|\,\mathrm{d}t < \infty. \quad (2.16)$$

This restriction is more accessible in the Laplace domain, where it corresponds to the asymptotic behavior

$$\boldsymbol{\varepsilon}(\boldsymbol{x},s) = \frac{\boldsymbol{\varsigma}(\boldsymbol{x})}{s} + \boldsymbol{\varepsilon}_{\mathrm{s}}(\boldsymbol{x}) + \mathrm{o}(1) \quad \text{as} \quad s \to 0.$$

The conductivity $\boldsymbol{\varsigma}(\boldsymbol{x})$ and the static limit $\boldsymbol{\varepsilon}_{\mathrm{s}}(\boldsymbol{x})$ are symmetric positive semidefinite, see Section 2.6.

The constitutive relations are characterized by the constitutive map. The model is non-dispersive if the constitutive map $\boldsymbol{\varepsilon}$ is independent of the Laplace parameter. The constitutive relations are further characterized by the symmetries of $\boldsymbol{\varepsilon}$. In the Laplace domain the constitutive map has the representation

$$\boldsymbol{\varepsilon} = \begin{pmatrix} \boldsymbol{\epsilon} & \boldsymbol{\xi} \\ \boldsymbol{\zeta} & \boldsymbol{\mu} \end{pmatrix} = \begin{pmatrix} \epsilon_{1,1} & \epsilon_{1,2} & \epsilon_{1,3} & \xi_{1,1} & \xi_{1,2} & \xi_{1,3} \\ \epsilon_{2,1} & \epsilon_{2,2} & \epsilon_{2,3} & \xi_{2,1} & \xi_{2,2} & \xi_{2,3} \\ \epsilon_{3,1} & \epsilon_{3,2} & \epsilon_{3,3} & \xi_{3,1} & \xi_{3,2} & \xi_{3,3} \\ \zeta_{1,1} & \zeta_{1,2} & \zeta_{1,3} & \mu_{1,1} & \mu_{1,2} & \mu_{1,3} \\ \zeta_{2,1} & \zeta_{2,2} & \zeta_{2,3} & \mu_{2,1} & \mu_{2,2} & \mu_{2,3} \\ \zeta_{3,1} & \zeta_{3,2} & \zeta_{3,3} & \mu_{3,1} & \mu_{3,2} & \mu_{3,3} \end{pmatrix}, \tag{2.17}$$

see Appendix A.2 on page 151. The general model (2.17) models a bi-anisotropic material. If the map is invariant under rotations of the coordinate system (has the same representation in all rotated coordinate systems), *i.e.*, $\boldsymbol{\epsilon} = \epsilon\mathbf{I}$, $\boldsymbol{\mu} = \mu\mathbf{I}$, $\boldsymbol{\xi} = \xi\mathbf{I}$, and $\boldsymbol{\zeta} = \zeta\mathbf{I}$ the model is bi-isotropic. Furthermore, if the cross couplings $\boldsymbol{\xi}$ and $\boldsymbol{\zeta}$ vanish, the model is isotropic if $\boldsymbol{\epsilon} = \epsilon\mathbf{I}$ and $\boldsymbol{\mu} = \mu\mathbf{I}$, and anisotropic otherwise.

2.3 Characterization of passive models

A material is called passive (P) if the net energy flux through the boundary of all sufficiently smooth regions Ω contained in the material is non-positive, *i.e.*,

$$\int_0^t \int_{\partial\Omega} \boldsymbol{E} \times \boldsymbol{H} \cdot \boldsymbol{n} \, \mathrm{dS} \, \mathrm{d}\tau \leq 0 \quad \text{for all } t \geq 0, \tag{2.18}$$

for all possible fields, $\boldsymbol{E}$ and $\boldsymbol{H}$, at the boundary that are quiescent before time $t = 0$. Using the source-free Poynting's theorem, (5.2), we see that this is equivalent to the energy condition $\mathcal{E}(t) \geq 0$ for all possible fields at the boundary and all regions. Stated differently, the medium does not produce energy.

In this section, we give three different characterizations of the passivity for linear, homogeneous, stationary materials, satisfying the requirements in Section 2.2. We also show that they are equivalent in the case of constitutive relations with a symmetric, positive definite instantaneous response, and that they imply that the material is passive in the sense above. The three classes are:

The time-domain type (T):

$$\int_0^t \boldsymbol{e}^{\mathrm{T}} \cdot \partial_\tau[\boldsymbol{\varepsilon}\boldsymbol{e}] \, \mathrm{d}\tau \geq 0 \quad \text{for all } t \geq 0 \tag{2.19}$$

for all continuously differentiable fields $\boldsymbol{e}$ that are quiescent before time $t = 0$.

The Laplace-domain type (L):

$$\begin{gathered} \mathrm{Re}\{s\boldsymbol{\varepsilon}(s)\} \geq 0 \quad \text{for all complex valued } s \in \mathbb{C}_+ \\ \text{or} \\ \int_0^\infty \mathrm{e}^{-2\eta\tau} \boldsymbol{e}^{\mathrm{T}} \cdot \partial_\tau[\boldsymbol{\varepsilon}\boldsymbol{e}] \, \mathrm{d}\tau \geq 0 \quad \text{for all} \quad \eta \geq 0 \end{gathered} \tag{2.20}$$

for all continuously differentiable fields $\boldsymbol{e}$ that are quiescent before time $t = 0$.

The Fourier-domain type (F):

$$\begin{gathered} \mathrm{Re}\{\mathrm{i}\omega\boldsymbol{\varepsilon}(\mathrm{i}\omega)\} \geq 0 \quad \text{for all real valued} \quad \omega \\ \text{or} \\ \int_{-\infty}^{\infty} \boldsymbol{e}^{\mathrm{T}} \cdot \partial_\tau[\boldsymbol{\varepsilon}\boldsymbol{e}]\,\mathrm{d}\tau \geq 0 \end{gathered} \tag{2.21}$$

for all continuously differentiable fields $\boldsymbol{e}$ that are compactly supported.

The reason for using three different types of passivity is that they occur naturally in different applications. The time-domain formulation, (T), is most natural from a physical point of view, but in this case it is hard to derive sufficient conditions for an arbitrary constitutive relation, see Ref. [139]. The Laplace-domain method is powerful for the analysis of the constitutive relation as well as for solving initial-boundary value problems [154]. Finally, the Fourier-domain characterization is widely used in the time harmonic case, and it also provides an easy analytical characterization whether a given constitutive relation is passive or not.

We proceed by proving the following equalities:

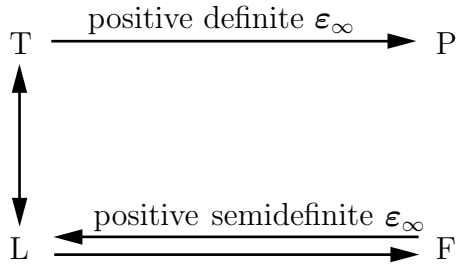

and the statements in (L) and (F). Observe that all conditions (T), (L), and (F) imply passivity (P) for the constitutive relations considered in this thesis.

Before the equalities above are considered the statements in (L) and (F) are shown. The equalities are shown in the following manner: (T)→(L), (L)→(F), (F)→(T), (L)→(T), and (T)→(P). In the proof of (T)→(L)→(F) no additional assumptions on the instantaneous response are made. For the parts (F)→(T) and (T)→(P), we need to assume that the instantaneous response is positive semi-definite and positive definite, respectively. Notice that the assumption of a positive semi-definite instantaneous response is slightly more general then the previously used assumptions on $\boldsymbol{\varepsilon}_\infty$. However, this generalization is in practice vacuous, since in general existence of a solution cannot be guaranteed in this case.

We start with the equivalence of the different statements in (L) and (F). The (F) statement follows from the Plancherel relation [84] for real-valued functions, *i.e.*,

$$\int_{-\infty}^{\infty} f(\tau)g(\tau)\,\mathrm{d}\tau = \frac{1}{2\pi}\int_{-\infty}^{\infty} \mathrm{Re}\{\hat{f}^*(\mathrm{i}\omega)\hat{g}(\mathrm{i}\omega)\}\,\mathrm{d}\omega.$$

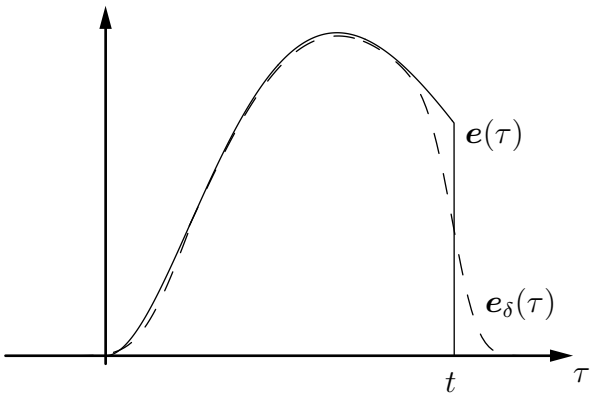

Figure 2.1: Smoothed function in the proof of F→T.

We get

$$\int_{-\infty}^{\infty} \boldsymbol{e}^{\mathrm{T}} \cdot \partial_\tau[\boldsymbol{\varepsilon e}]\,\mathrm{d}\tau = \frac{1}{2\pi}\int_{-\infty}^{\infty} \hat{\boldsymbol{e}}^{\mathrm{H}}(\mathrm{i}\omega)\cdot \mathrm{Re}\{\mathrm{i}\omega\boldsymbol{\varepsilon}(\mathrm{i}\omega)\}\hat{\boldsymbol{e}}(\mathrm{i}\omega)\,\mathrm{d}\omega$$

and hence the medium is passive if and only if $\mathrm{Re}\{\mathrm{i}\omega\boldsymbol{\varepsilon}(\mathrm{i}\omega)\} = -\omega\,\mathrm{Im}\{\boldsymbol{\varepsilon}(\mathrm{i}\omega)\} \geq 0$ for all real-valued ω. The (L) statement follows from the Plancherel relation and the shift property of the Fourier transform

$$\int_0^{\infty} \mathrm{e}^{-2\eta t}\boldsymbol{e}^{\mathrm{T}} \cdot \partial_t[\boldsymbol{\varepsilon e}]\,\mathrm{d}t = \frac{1}{2\pi}\int_{-\infty}^{\infty} \hat{\boldsymbol{e}}^{\mathrm{H}}(\eta+\mathrm{i}\omega)\cdot \mathrm{Re}\{(\eta+\mathrm{i}\omega)\boldsymbol{\varepsilon}(\eta+\mathrm{i}\omega)\}\hat{\boldsymbol{e}}(\eta+\mathrm{i}\omega)\,\mathrm{d}\omega$$

for all real-valued $\boldsymbol{e}$. Hence the characterization $\mathrm{Re}\{s\boldsymbol{\varepsilon}(s)\} \geq 0$ holds for all s with $\mathrm{Re}\{s\} \geq 0$. Observe that since $\boldsymbol{\chi}(t)$ is causal, *i.e.*, $\boldsymbol{\chi}(t) = 0$ for $t < 0$, its Laplace-domain restricted to the imaginary axis coincide with the Fourier transform.

To show the implication (T)→(L) we use integration by parts

$$\begin{aligned}\int_0^t \mathrm{e}^{-2\eta\tau}\boldsymbol{e}^{\mathrm{T}} \cdot \partial_\tau[\boldsymbol{\varepsilon e}]\,\mathrm{d}\tau \\ = \mathrm{e}^{-2\eta t}\int_0^t \boldsymbol{e}^{\mathrm{T}} \cdot \partial_\tau[\boldsymbol{\varepsilon e}]\,\mathrm{d}\tau + \int_0^t \left\{2\eta\mathrm{e}^{-2\eta\tau}\int_0^\tau \boldsymbol{e}^{\mathrm{T}} \cdot \partial_{\tau_1}[\boldsymbol{\varepsilon e}]\,\mathrm{d}\tau_1\right\}\mathrm{d}\tau\end{aligned}$$

which is positive if $\int_0^t(\boldsymbol{e}^{\mathrm{T}} \cdot \partial_t[\boldsymbol{\varepsilon e}])(\tau)\,\mathrm{d}\tau \geq 0$.

The implication (L)→(F) is obtained if we use the compact support of the fields in (F) and shift the time scale, or consider the restriction of the Laplace characterization to the imaginary axis.

To show the implication (F)→(T), we start by showing that the instantaneous response is symmetric. We then use that $\boldsymbol{\varepsilon}(\mathrm{i}\omega) \sim \boldsymbol{\varepsilon}_\infty$ for large ω and observe that $-\omega\,\mathrm{Im}\{\boldsymbol{\varepsilon}_\infty\}$ changes sign with ω and hence $\boldsymbol{\varepsilon}_\infty$ is symmetric. Now use the positive (semi-)definiteness of $\boldsymbol{\varepsilon}_\infty$ and choose an arbitrary field $\boldsymbol{e} \in \mathrm{C}^1[0,t]$ such that $\boldsymbol{e}(0) = 0$ and extend $\boldsymbol{e}$ smoothly to zero outside $[0,t]$ with a mollifier technique, *i.e.*, set $\boldsymbol{e}_\delta = \boldsymbol{e} * \psi_\delta$ where $\psi_\delta(t) = \psi(t/\delta)$ and ψ is a positive smooth function with

unit integral and compact support such that $\psi(t) = 0$ for $t \leq 0$, see Figure 2.1. The instantaneous reaction part vanishes due to non-contributing limits and in the limit $\delta \to 0$ we get the time-domain characterization (T)

$$\int_{-\infty}^{\infty} \boldsymbol{e}_\delta^{\mathrm{T}} \cdot \partial_t[\boldsymbol{\varepsilon}\boldsymbol{e}_\delta]\,\mathrm{d}\tau = \int_{-\infty}^{\infty} \boldsymbol{e}_\delta^{\mathrm{T}} \cdot \partial_t[\boldsymbol{\chi} * \boldsymbol{e}_\delta]\,\mathrm{d}\tau \xrightarrow{\delta\to 0} \int_0^t \boldsymbol{e}^{\mathrm{T}} \cdot \partial_\tau[\boldsymbol{\chi} * \boldsymbol{e}]\,\mathrm{d}\tau \leq \int_0^t \boldsymbol{e}^{\mathrm{T}} \cdot \partial_\tau[\boldsymbol{\varepsilon}\boldsymbol{e}]\,\mathrm{d}\tau.$$

These calculations are made under the smoothing assumption that, *e.g.*, $\boldsymbol{\chi}' \in \mathrm{L}^1$ or $\boldsymbol{\chi}$ is piecewise C^1.

(L)→(T) follows from (L)→(F)→(T) the fact that the Laplace-domain characterization (L) implies that the instantaneous response is positive semidefinite, *viz.* choose a real $s \to \infty$ in (L) to get the result $\mathrm{Re}\{\boldsymbol{\varepsilon}_\infty\} \geq 0$ and hence that positive semidefiniteness of the instantaneous response is a necessary condition for Laplace type passivity [90].

Finally, we observe that to get passivity (P) it is necessary that there exists a sufficiently smooth solution to the Maxwell equations, see Chapter 5. From the observation that a symmetric, positive definite instantaneous response gives existence we notice that all characterizations (T), (L) and (F) together with a positive definite instantaneous response imply dissipation (P). This gives the following sufficient conditions for a model to be passive

$$\mathrm{Re}\{s\boldsymbol{\varepsilon}(\boldsymbol{x}, s)\} \geq 0 \text{ for all } s \in \mathbb{C}_+ \quad \text{and} \quad \boldsymbol{\varepsilon}_\infty(\boldsymbol{x}) = \boldsymbol{\varepsilon}_\infty^{\mathrm{T}}(\boldsymbol{x}) > \delta \text{ for some } \delta > 0$$

This condition is rather easy to check for a specific set of constitutive relation, both on their integral form, $\boldsymbol{\varepsilon} = \boldsymbol{\varepsilon}_\infty + \boldsymbol{\chi}*$, and on a local form of Equation (2.42), see Section 2.7.

In a time-domain identification of the susceptibility kernel it is natural to measure the reflection operator and to calculate the susceptibility kernel by the solution of an inverse scattering problem [91, 119, 93]. The typical result is a sampling of the susceptibility kernel in an interval $[0, t]$, and hence, it is not straightforward to use the frequency characterization above. Instead, one can use the time-domain characterization of passivity (T) directly [104].

2.4 Instantaneous response

The instantaneous (or high-frequency or optical) response models the rapid part of the interaction between the electromagnetic fields and the material. It is given by the matrix $\boldsymbol{\varepsilon}_\infty$ in the high-frequency asymptotic expansion (2.14) or equivalently as the small time approximation of (2.13). $\boldsymbol{\varepsilon}_\infty$ is assumed to be a symmetric, positive definite 6×6 matrix. From a mathematical as well as a computational point of view, the instantaneous response is of considerable importance. Together with the curl operators it constitutes the principal part of the Maxwell equations and hence controls much of the mathematical properties of the solution, *i.e.*, existence, uniqueness, and continuity. The instantaneous response is also of considerable importance

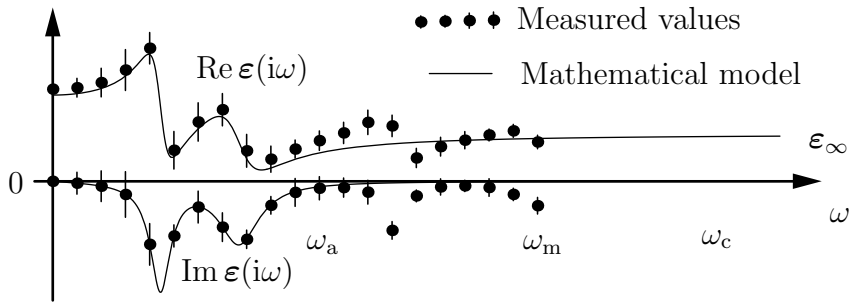

Figure 2.2: Illustration of the range of validity of the constitutive relations. The measured values of the constitutive map $\boldsymbol{\varepsilon}$ are known up to frequency ω_{m}, the mathematical model is used for frequencies up to ω_{a}, and ω_{c} is the upper limit for the use of a continuum model of the medium, respectively.

in numerical approximations, *e.g.*, in the stability conditions of finite difference schemes (FDTD). Due to the theoretical as well as the practical importance of the instantaneous response, it is interesting to study the uniqueness of the instantaneous response.

The macroscopic description of the interaction between electromagnetic fields and materials is modeled with constitutive relations. The constitutive relations are based on a continuum model of the material, *i.e.*, the interaction at a microscopic level (molecules, atoms, nucleus, ...) is replaced by a set of effective material parameters. At a microscopic level, the electromagnetic interaction is much more accurately modeled with theories such as quantum electrodynamics (QED), see Refs [72, 73]. Hence, the macroscopic continuum model of a material is only accurate up to a specific frequency, typically somewhere between visual light and X-rays, see Figure 1.1 and Figure 2.2. Above this frequency the macroscopic Maxwell equations do not give an accurate description of electromagnetic phenomena.

Consider an electromagnetic application in the frequency range $[\omega_{\min}, \omega_{\max}]$. The values of the constitutive map are given in the same frequency range, *i.e.*,

$$\boldsymbol{\varepsilon}(\mathrm{i}\omega) \quad \text{for} \quad \omega \in [\omega_{\min}, \omega_{\max}]$$

are provided. The question is: How can the map $\boldsymbol{\varepsilon}$ be continuated outside the frequency range $[\omega_{\min}, \omega_{\max}]$? In this section we focus on the high-frequency value of $\boldsymbol{\varepsilon}$, *i.e.*,

$$\boldsymbol{\varepsilon}_\infty = \lim_{\omega \to \infty} \boldsymbol{\varepsilon}(\mathrm{i}\omega).$$

To start, from analytic function theory it is known that an analytic function is determined from its values in a neighborhood of a point [100]. Either the values of $\boldsymbol{\varepsilon}$ together with the values of the derivatives of $\boldsymbol{\varepsilon}$ at a single frequency or the values of $\boldsymbol{\varepsilon}$ in an interval determine the complete map $\boldsymbol{\varepsilon}$ (to avoid technicalities, we assume that the imaginary axis is in the region of analyticity, see Section 2.5). However, measured (physical) values are always contaminated with errors, and moreover, the

Maxwell equations do only constitute an approximate description of the phenomena called electromagnetics.

By an explicit construction below, it is shown that the instantaneous response is non-unique. Let the original constitutive relations be given by a bi-anisotropic model with the instantaneous response $\boldsymbol{\varepsilon}_\infty$. This model is assumed to be accurate in the frequency range $[\omega_{\min}, \omega_{\max}]$. The goal is to construct an approximate set of constitutive relations that resembles the material properties in the frequency range $[\omega_{\min}, \omega_{\max}]$ and has the high-frequency response $\boldsymbol{\varepsilon}'_\infty \neq \boldsymbol{\varepsilon}_\infty$. An admissible approximate constitutive map $\boldsymbol{\varepsilon}'$ is given by

$$\begin{aligned}\boldsymbol{\varepsilon}'(s) &= \boldsymbol{\varepsilon}(s) + \left(\frac{\omega_0^2}{s^2 + \nu s + \omega_0^2} - 1\right)(\boldsymbol{\varepsilon}_\infty - \boldsymbol{\varepsilon}'_\infty) \\ &= \boldsymbol{\varepsilon}(s) - \frac{s^2 + \nu s}{s^2 + \nu s + \omega_0^2}(\boldsymbol{\varepsilon}_\infty - \boldsymbol{\varepsilon}'_\infty)\end{aligned} \tag{2.22}$$

where $\boldsymbol{\varepsilon}'_\infty$ is the new high-frequency response and $\nu \geq 0$ and ω_0 are model parameters. The model is passive if $0 < \boldsymbol{\varepsilon}'_\infty < \boldsymbol{\varepsilon}_\infty$, *i.e.*,

$$\operatorname{Re} s\boldsymbol{\varepsilon}' \geq \operatorname{Re}\left\{s\boldsymbol{\varepsilon}'_\infty + \frac{s\omega_0^2}{s^2 + \nu s + \omega_0^2}(\boldsymbol{\varepsilon}_\infty - \boldsymbol{\varepsilon}'_\infty)\right\} \geq \boldsymbol{\varepsilon}'_\infty \operatorname{Re} s \tag{2.23}$$

where we also have used the inequality (2.43) on page 34 and that $\boldsymbol{\varepsilon}$ is a passive constitutive map. The 'error' in the approximation is

$$\sup_{\omega \in [\omega_{\min}, \omega_{\max}]} \|\boldsymbol{\varepsilon}'(\mathrm{i}\omega) - \boldsymbol{\varepsilon}(\mathrm{i}\omega)\| \leq \frac{\omega_{\max}^2 + \nu\omega_{\max}}{\omega_0^2 - \omega_{\max}^2} \sup_{\boldsymbol{x} \in \mathbb{R}^3} |\boldsymbol{\varepsilon}'_\infty - \boldsymbol{\varepsilon}_\infty| \to 0 \quad \text{as} \quad \omega_0 \to \infty.$$

This shows that it is possible to construct arbitrarily good approximations of a constitutive relations with a prescribed instantaneous response as long as the size of the instantaneous response decreases. The requirement to decrease the instantaneous response can be interpreted as a requirement to increase the wave-front speed.

In the next subsection, we show that the approximation (2.22) also is sufficient to get good approximations of the solution of the Maxwell equations.

2.4.1 Convergence estimates

The approximation (2.22) is only meaningful if the fields $\boldsymbol{e}'$ associated with the approximate constitutive map $\boldsymbol{\varepsilon}'$ constitute a good approximation of the set of fields $\boldsymbol{e}$ associated with the original constitutive map $\boldsymbol{\varepsilon}$. We use the Laplace-domain representation to get an error estimate of the approximate fields. Let $\hat{\boldsymbol{e}}(\boldsymbol{x}, s)$ be the solution of the Maxwell equations together with the constitutive map $\boldsymbol{\varepsilon}$, *i.e.*, $\hat{\boldsymbol{e}}$ solves

$$s\boldsymbol{\varepsilon}(\boldsymbol{x}, s)\hat{\boldsymbol{e}} - \nabla \times \mathrm{J}\hat{\boldsymbol{e}} = -\hat{\boldsymbol{\jmath}}(\boldsymbol{x}, s) \quad \text{for} \quad \boldsymbol{x} \in \mathbb{R}^3$$

together with appropriate radiation (or boundary) conditions. The approximate field satisfies

$$s\boldsymbol{\varepsilon}'(\boldsymbol{x}, s)\hat{\boldsymbol{e}}' - \nabla \times \mathrm{J}\hat{\boldsymbol{e}}' = -\hat{\boldsymbol{\jmath}}(\boldsymbol{x}, s) \quad \text{for} \quad \boldsymbol{x} \in \mathbb{R}^3 \tag{2.24}$$

together with similar radiation conditions. The error $\hat{\boldsymbol{e}}' - \hat{\boldsymbol{e}}$ satisfies

$$s\boldsymbol{\varepsilon}(\boldsymbol{x},s)(\hat{\boldsymbol{e}}' - \hat{\boldsymbol{e}}) - \nabla \times \mathrm{J}(\hat{\boldsymbol{e}}' - \hat{\boldsymbol{e}}) = s(\boldsymbol{\varepsilon}'(\boldsymbol{x},s) - \boldsymbol{\varepsilon}(\boldsymbol{x},s))\hat{\boldsymbol{e}}' \quad \text{for} \quad \boldsymbol{x} \in \mathbb{R}^3. \tag{2.25}$$

We start with an energy estimate on the approximate fields (2.24). Multiply (2.24) from the left with $\hat{\boldsymbol{e}}'^{\mathrm{T}}\cdot$ to get

$$s\hat{\boldsymbol{e}}'^{\mathrm{T}} \cdot \boldsymbol{\varepsilon}'\hat{\boldsymbol{e}}' - \hat{\boldsymbol{e}}'^{\mathrm{T}} \cdot \nabla \times \mathrm{J}\hat{\boldsymbol{e}}' = -\hat{\boldsymbol{e}}'^{\mathrm{T}} \cdot \hat{\boldsymbol{\jmath}}.$$

Integrate over $\mathbb{R}^3$ and estimate the terms. The first term is estimated with (2.23), *i.e.*,

$$\operatorname{Re} s\hat{\boldsymbol{e}}'^{\mathrm{T}} \cdot \boldsymbol{\varepsilon}'\hat{\boldsymbol{e}}' \geq \eta\hat{\boldsymbol{e}}'^{\mathrm{T}} \cdot \boldsymbol{\varepsilon}'_\infty\hat{\boldsymbol{e}}' \geq \eta C|\hat{\boldsymbol{e}}'|^2,$$

where $\eta = \operatorname{Re} s$ is positive. The second term vanishes due to the radiation condition and the third term is estimated with the Schwartz' inequality. This gives

$$\eta C\|\hat{\boldsymbol{e}}'\|_3^2 \leq \frac{\delta}{2}\|\hat{\boldsymbol{e}}'\|_3^2 + \frac{1}{2\delta}\|\hat{\boldsymbol{\jmath}}\|_3^2 \quad \text{for} \quad \delta > 0$$

or equivalently

$$\|\hat{\boldsymbol{e}}'\|_3^2 \leq \frac{\|\hat{\boldsymbol{\jmath}}\|_3^2}{\delta(2\eta C - \delta)}.$$

Choose the constant δ such that $\delta(2\eta C - \delta) > 0$. The above estimate is repeated for the error equation (2.25). This gives a similar estimate for the error field $\hat{\boldsymbol{e}}'$, *i.e.*,

$$\|\hat{\boldsymbol{e}}' - \hat{\boldsymbol{e}}\|_3 \leq \frac{|s(s^2 + \nu s)|\,\|\hat{\boldsymbol{\jmath}}\|_3}{|s^2 + \nu s + \omega_0^2|\,\delta(2\eta C - \delta)} \sup_{\boldsymbol{x}\in\mathbb{R}^3} |\boldsymbol{\varepsilon}'_\infty - \boldsymbol{\varepsilon}_\infty|.$$

This estimate shows that the Laplace-domain error fields approach zero for fixed values of the Laplace parameter s as the approximation constant ω_0 increases, *i.e.*,

$$\|\hat{\boldsymbol{e}}'(\cdot,s) - \hat{\boldsymbol{e}}(\cdot,s)\|_3 \to 0 \quad \text{as} \quad \omega_0 \to \infty.$$

In general, the approximate fields do not approach the original fields in the time domain, due to the lack of approximation in the high-frequency part of the constitutive relations, *i.e.*, the wave-front sets of the solutions do not agree. However, the approximation was only designed to be valid in the frequency range $[\omega_{\min}, \omega_{\max}]$. This frequency range is transformed to the time domain by a smoothing procedure. Introduce a set of smoothed fields as

$$\tilde{\boldsymbol{e}}(\boldsymbol{x},t) = \int_0^t \boldsymbol{e}(\boldsymbol{x},t-t')\psi_\tau(t')\,\mathrm{d}t' = (\boldsymbol{e} * \psi_\tau)(\boldsymbol{x},t)$$

and similarly for the approximate fields $\tilde{\boldsymbol{e}}'$. The weight function $\psi_\tau(t)$ is a smooth and positive function with unit integral that is supported in $[0,\tau]$, *i.e.*, a mollifier. The smoothed fields have the Laplace-domain representation

$$\tilde{\boldsymbol{e}}(\boldsymbol{x},t) = \frac{1}{2\pi}\int_{\mathbb{R}} \mathrm{e}^{(\eta+\mathrm{i}\omega)t}\hat{\boldsymbol{e}}(\boldsymbol{x},\eta+\mathrm{i}\omega)\hat{\psi}_\tau(\eta+\mathrm{i}\omega)\,\mathrm{d}\omega.$$

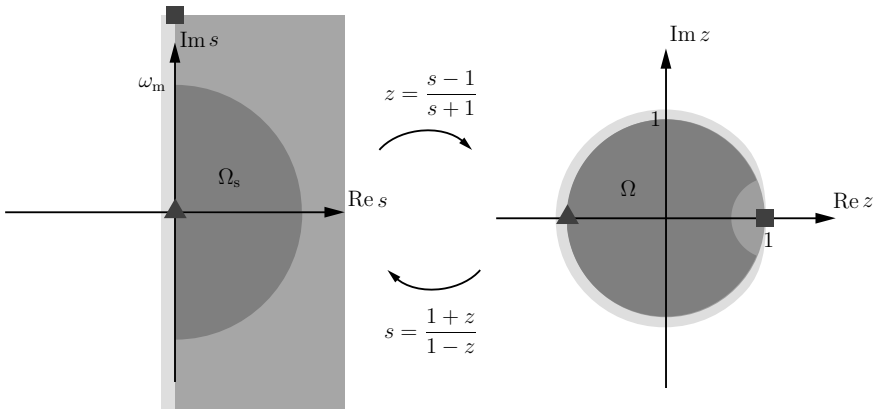

Figure 2.3: Cayley transformation.

The Laplace transformed version of the weight function $\hat{\psi}_\tau(s)$ is analytic for $\operatorname{Re} s > -\infty$ and decays exponentially, *i.e.*, there are numbers C_M such that

$$|\hat{\psi}_\tau(s)| \leq C_M(1+|s|)^{-M} \quad \text{for} \quad s \in \mathbb{C}_+ \quad \text{and} \quad M = 0, 1, \ldots \tag{2.26}$$

Observe that the weight function approaches the Dirac delta distribution $\delta(t)$ for small times τ, *i.e.*, $\psi_\tau(t) \to \delta(t)$ as $\tau \to 0$, and hence the frequency filtered fields resemble the original fields for small times τ.

We use the above estimates to show convergence of the constitutive approximation in the time domain, *i.e.*,

$$\int_0^T \int_{\mathbb{R}^3} |\tilde{\boldsymbol{e}}'(\boldsymbol{x},t) - \tilde{\boldsymbol{e}}(\boldsymbol{x},t)|^2 \,\mathrm{dV}\,\mathrm{d}t \to 0 \quad \text{as} \quad \omega_0 \to \infty$$

for fixed τ and T. In fact, the integral is estimated as

$$\begin{aligned}\int_0^T \mathrm{e}^{2\eta t}\mathrm{e}^{-2\eta t}\|\tilde{\boldsymbol{e}}'(\cdot,t) - \tilde{\boldsymbol{e}}(\cdot,t)\|_3^2 \,\mathrm{d}t &\leq \mathrm{e}^{2\eta T}\int_0^\infty \mathrm{e}^{-2\eta t}\|\tilde{\boldsymbol{e}}'(\cdot,t) - \tilde{\boldsymbol{e}}(\cdot,t)\|_3^2 \,\mathrm{d}t \\ &\leq \frac{\mathrm{e}^{2\eta T}}{2\pi}\int_{\mathbb{R}} \|\hat{\boldsymbol{e}}'(\cdot,\eta+\mathrm{i}\omega) - \hat{\boldsymbol{e}}(\cdot,\eta+\mathrm{i}\omega)\|_3^2 \,|\hat{\psi}_\tau(\eta+\mathrm{i}\omega)|^2 \,\mathrm{d}\omega \leq \frac{C\mathrm{e}^{2\eta T}}{\omega_0^2}\end{aligned}$$

for a constant C. The estimate shows that the smoothed approximate fields approach the smoothed original fields as the model parameter ω_0 increases.

2.4.2 Active medium models

Above, it was shown that it is possible to construct arbitrary good approximations of a constitutive map as long as the instantaneous response decreases. To understand more about the properties of the constitutive relations we discuss a few properties of the approximation of analytic functions. We start with a general approximation of analytic functions on bounded regions.

As before, let $\boldsymbol{\varepsilon}$ denote the 'exact' constitutive map and let $\boldsymbol{\varepsilon}'$ denote a constitutive map that approximates $\boldsymbol{\varepsilon}$ in the frequency interval $[\omega_{\min}, \omega_{\max}]$. To show that

it is possible to chose an arbitrary high-frequency response in the approximation, we construct an approximation with the desired properties. The goal is to find a function $\boldsymbol{\varepsilon}'(s)$ such that

$$\sup_{\omega_{\min}\leq\omega\leq\omega_{\max}} |\boldsymbol{\varepsilon}'(\mathrm{i}\omega)-\boldsymbol{\varepsilon}(\mathrm{i}\omega)|\leq\delta \quad \text{and} \quad \lim_{\omega\to\infty}\boldsymbol{\varepsilon}'(\mathrm{i}\omega)=\boldsymbol{\varepsilon}'_\infty. \tag{2.27}$$

Use the Cayley transformation

$$z=\frac{s-1}{s+1} \quad \text{with the inverse} \quad s=\frac{1+z}{1-z} \tag{2.28}$$

to map $\mathbb{C}_+$ to the unit circle, see Figure 2.3. The elements of the matrix

$$(z-1)^{-1}(\boldsymbol{\varepsilon}(z)-\boldsymbol{\varepsilon}'_\infty)$$

are analytic in a region Ω_z, see Figure 2.3. Let $\mathbf{Q}(z)$ be a polynomial approximation of $(z-1)^{-1}(\boldsymbol{\varepsilon}(z)-\boldsymbol{\varepsilon}'_\infty)$ in Ω_z, *i.e.*,

$$\sup_{z\in\Omega_z}|\mathbf{Q}(z)-\frac{\boldsymbol{\varepsilon}(z)-\boldsymbol{\varepsilon}'_\infty}{z-1}|<\delta_z$$

where $\mathbf{Q}(z)$ is a matrix of polynomials with real-valued coefficients, see "Runge's theorem" for details [100]. Set

$$\boldsymbol{\varepsilon}'(z)=\boldsymbol{\varepsilon}'_\infty+(z-1)\mathbf{Q}(z)$$

then

$$|\boldsymbol{\varepsilon}'(z)-\boldsymbol{\varepsilon}(z)|=|\boldsymbol{\varepsilon}'_\infty+(z-1)\mathbf{Q}(z)-\boldsymbol{\varepsilon}(z)|\leq|z-1|\,|\mathbf{Q}(z)-\frac{\boldsymbol{\varepsilon}(z)-\boldsymbol{\varepsilon}'_\infty}{z-1}|.$$

Use the Cayley transform (2.28) to get back to the Laplace domain. The function $\boldsymbol{\varepsilon}'(s)$ is then a rational approximation of $\boldsymbol{\varepsilon}(s)$ such that

$$\sup_{\omega_{\min}\leq\omega\leq\omega_{\max}}|\boldsymbol{\varepsilon}'(\mathrm{i}\omega)-\boldsymbol{\varepsilon}(\mathrm{i}\omega)|\leq\frac{2\delta_z}{\sqrt{\omega_{\min}^2+1}}\leq 2\delta_z.$$

The approximate constitutive map is the rational function

$$\boldsymbol{\varepsilon}'(s)=\boldsymbol{\varepsilon}'_\infty-\frac{2}{s+1}\mathbf{Q}(\frac{s-1}{s+1})$$

with an arbitrary small error $2\delta_z$. Observe that the construction above is independent of the choice of the high-frequency response $\boldsymbol{\varepsilon}'_\infty$.

However, in general, the fields associated with $\boldsymbol{\varepsilon}'$ do not resemble the original fields. For a bad choice of $\boldsymbol{\varepsilon}'_\infty$ the good properties, *i.e.*, well-posedness, might be lost. Although the approximate problem is well-posed, it can be shown that the associated fields do not necessarily resemble the original fields. To see this, consider an approximate map $\boldsymbol{\varepsilon}'$ with an isotropic high-frequency response $\boldsymbol{\varepsilon}'_\infty$. The wave-front speed of the approximate problem is $c'_\infty=(\epsilon'_\infty\mu'_\infty)^{-1/2}$. For a sufficiently small value of the wave-front speed c'_∞, the fields of the approximate problem cannot reach the location of the original fields. The failure of the approximation can be understood from the lack of passivity, *i.e.*, the approximate model is not passive for sufficiently large values of $\boldsymbol{\varepsilon}'_\infty$. Hence, the solution can have an exponential growth rate.

2.4.3 Nevanlinna-Pick problem

To construct an approximation that ensures passive models, we consider the theory of Nevanlinna functions [6, 56]. A function f is in the Nevanlinna class if $\operatorname{Re} f(s) \geq 0$ and $f(s)$ is analytic for $\operatorname{Re} s > 0$, *i.e.*,

$$f : \ \mathbb{C}_+ \to \bar{\mathbb{C}}_+.$$

The generic representation of these functions is[6]

$$f(s) = s\mu - \mathrm{i}\nu + \int_{\mathbb{R}} \frac{\alpha s - \mathrm{i}}{\alpha + \mathrm{i}s} \, \mathrm{d}\tau(\alpha)$$

where $0 \leq \mu \in \mathbb{R}$, $\nu \in \mathbb{R}$, and $\tau(\alpha)$ is a non-decreasing function of bounded variation.

The Nevanlinna-Pick problem concerns the possibility to construct a function f in the Nevanlinna class with prescribed values at a given set of points. For our purpose it is sufficient to consider the following version: Construct a function f in the Nevanlinna class such that

$$f(s_i) = f_i \quad \text{for} \quad i = 1, 2, \ldots$$

where $\operatorname{Re} s_i > 0$. The interpolation problem is soluble if and only if the Nevanlinna matrices

$$\mathbf{N} = \left[\frac{f_i + f_j^*}{s_i + s_j^*}, \ i, j = 1, 2, \ldots , \right] \tag{2.29}$$

are non-negative definite, see Theorem 3.3.3 in Ref. [6]. Moreover, if any of the matrices are singular, the function $f(s)$ is unique and equal to a real-valued rational function.

The Nevanlinna-Pick problem is used to get insight into the high-frequency behavior of the constitutive map. Let $\boldsymbol{\varepsilon}$ be a passive constitutive map, *i.e.*, $\operatorname{Re} s\boldsymbol{\varepsilon}(s) \geq 0$. Construct a set of functions

$$f_u(s) = \boldsymbol{u}^{\mathrm{H}} s\boldsymbol{\varepsilon}(s)\boldsymbol{u} \quad \text{with} \quad \boldsymbol{u} \in \mathbb{C}^6 \quad \text{and} \quad |\boldsymbol{u}| = 1.$$

These functions are in the Nevanlinna class and for sufficiently many column matrices $\boldsymbol{u}$ the map $\boldsymbol{\varepsilon}$ is uniquely determined by the values of f_u, *e.g.*,

$$\boldsymbol{u}_1 = \begin{pmatrix} 1 \\ 0 \\ 0 \\ 0 \\ 0 \\ 0 \end{pmatrix}, \quad \boldsymbol{u}_2 = \begin{pmatrix} 0 \\ 1 \\ 0 \\ 0 \\ 0 \\ 0 \end{pmatrix}, \quad \boldsymbol{u}_3 = \frac{1}{\sqrt{2}} \begin{pmatrix} 1 \\ 1 \\ 0 \\ 0 \\ 0 \\ 0 \end{pmatrix}, \quad \text{and} \quad \boldsymbol{u}_4 = \frac{1}{\sqrt{2}} \begin{pmatrix} 1 \\ \mathrm{i} \\ 0 \\ 0 \\ 0 \\ 0 \end{pmatrix}$$

determines the four elements $\epsilon_{1,1}$, $\epsilon_{2,2}$, $\epsilon_{2,1}$, and $\epsilon_{1,2}$. The general bi-anisotropic model (2.17) is determined by 36 column matrices. Let us construct a constitutive map $\boldsymbol{\varepsilon}'(s)$ with high-frequency response $\boldsymbol{\varepsilon}'_\infty$ such that

$$\boldsymbol{\varepsilon}'(s_i) = \boldsymbol{\varepsilon}(s_i) \quad \text{for} \quad i = 1, 2, \ldots$$

with $\operatorname{Re} s_i > 0$. Instead of interpolating the values of $\boldsymbol{\varepsilon}(s_i)$, we interpolate the values of

$$\boldsymbol{u}^{\mathrm{H}}(s_i\boldsymbol{\varepsilon}(s_i) - s_i\boldsymbol{\varepsilon}'_\infty)\boldsymbol{u} \quad \text{for} \quad i = 1, 2, \ldots$$

and add $\boldsymbol{u}^{\mathrm{H}} s\boldsymbol{\varepsilon}'_\infty \boldsymbol{u}$ to the interpolation function to obtain the correct $\boldsymbol{\varepsilon}'(s)$. The elements of the Nevanlinna matrix are

$$\mathbf{N}_{i,j} = \frac{f_u(s_i) - s_i\boldsymbol{u}^{\mathrm{H}}\boldsymbol{\varepsilon}'_\infty\boldsymbol{u} + f_u^*(s_j) - s_j^*\boldsymbol{u}^{\mathrm{H}}\boldsymbol{\varepsilon}'_\infty\boldsymbol{u}}{s_i + s_j^*} = \frac{f_u(s_i) + f_u^*(s_j)}{s_i + s_j^*} - \boldsymbol{u}^{\mathrm{H}}\boldsymbol{\varepsilon}'_\infty\boldsymbol{u}.$$

To satisfy the non-negative requirement we get an upper bound on the high-frequency response, *i.e.*,

$$\boldsymbol{u}^{\mathrm{H}}\boldsymbol{\varepsilon}'_\infty\boldsymbol{u} \leq \left[\frac{f_u(s_i) + f_u^*(s_j)}{s_i + s_j^*},\ i, j = 1, 2, \ldots\right].$$

2.5 Long-time response

The time-domain representation of the constitutive relations (2.8) suggests that it is essential to have detailed information about the history of the electromagnetic fields to determine the flux densities. However, a priori knowledge about the past field values are seldom (or never) given in an electromagnetic application. This apparent contradiction is resolved by the long-time response of the constitutive relations. The long-time response of the constitutive relations is given by the behavior of the susceptibility kernel for large times or equivalently the behavior of the constitutive map at the imaginary axis.

The importance of the long-time response of the constitutive relations is shown by substitution of the convolution integral (2.8) into the Maxwell equations, *i.e.*,

$$\partial_t\boldsymbol{\varepsilon}_\infty\boldsymbol{e}(\boldsymbol{x}, t) + \partial_t\int_{-\infty}^{t}\boldsymbol{\chi}(\boldsymbol{x}, t - t')\boldsymbol{e}(\boldsymbol{x}, t')\,\mathrm{d}t' - \nabla\times\mathrm{J}\boldsymbol{e}(\boldsymbol{x}, t) = -\boldsymbol{j}(\boldsymbol{x}, t).$$

To determine the fields for times $t > 0$, the convolution integral is divided into two parts, *i.e.*,

$$\begin{aligned}\partial_t\boldsymbol{\varepsilon}_\infty\boldsymbol{e}(\boldsymbol{x}, t) + \partial_t\int_{0-}^{t}\boldsymbol{\chi}(\boldsymbol{x}, t - t')\boldsymbol{e}(\boldsymbol{x}, t')\,\mathrm{d}t' - \nabla\times\mathrm{J}\boldsymbol{e}(\boldsymbol{x}, t)& \\ = -\boldsymbol{j}(\boldsymbol{x}, t) - \partial_t\int_{-\infty}^{0-}\boldsymbol{\chi}(\boldsymbol{x}, t - t')\boldsymbol{e}(\boldsymbol{x}, t')\,\mathrm{d}t'.&\end{aligned}$$

The terms on the left-hand side depend only on the field values at positive times and at the right-hand side the (induced) current and the past field values are collected. Even if the past field values, $\boldsymbol{e}(\boldsymbol{x}, t)$ for $t < 0$, are not a priori known, it is possible to determine the field values $\boldsymbol{e}(\boldsymbol{x}, t)$ for large times if the influence of the past field values is small.

The convolution term of the past field values is estimated as

$$|\partial_t \int_{-\infty}^{0} \boldsymbol{\chi}(\boldsymbol{x}, t-t')\boldsymbol{e}(\boldsymbol{x}, t')\,\mathrm{d}t'| \leq \sup_{t<0} |\boldsymbol{e}(\boldsymbol{x}, t)| \int_{t}^{\infty} |\partial_{t'}\boldsymbol{\chi}(\boldsymbol{x}, t')|\,\mathrm{d}t'. \tag{2.30}$$

The influence of the past field values vanishes for large times if the above term (2.30) decays as $t \to \infty$. This decay is satisfied by condition (2.15), *i.e.*,

$$\int_{0+}^{\infty} |\partial_t \boldsymbol{\chi}(\boldsymbol{x}, t)|\,\mathrm{d}t \leq \infty$$

and $\boldsymbol{\chi}(\boldsymbol{x}, t)$ is a continuous function of the temporal coordinate t in $[0, \infty]$ and has a finite discontinuity at $t = 0$.

The conductivity is given by the long-time limit

$$\boldsymbol{\varsigma}(\boldsymbol{x}) = \lim_{t\to\infty} \boldsymbol{\chi}(\boldsymbol{x}, t) < \infty.$$

Observe that although the conductivity is the infinite long tail of the susceptibility kernel it acts as a direct term in the Maxwell equations.

The Laplace-domain representation of the constitutive map is

$$\begin{aligned} s\boldsymbol{\varepsilon}(\boldsymbol{x}, s) &= s \int_{0-}^{\infty} \mathrm{e}^{-st} \left(\boldsymbol{\varepsilon}_\infty(\boldsymbol{x})\delta(t) + \boldsymbol{\chi}(\boldsymbol{x}, t)\right) \mathrm{d}t \\ &= s\boldsymbol{\varepsilon}_\infty(\boldsymbol{x}) + \boldsymbol{\chi}(\boldsymbol{x}, 0) + \int_{0+}^{\infty} \mathrm{e}^{-st}\partial_t\boldsymbol{\chi}(\boldsymbol{x}, t)\,\mathrm{d}t. \end{aligned} \tag{2.31}$$

The integral is well-defined in the limit $\operatorname{Re} s = 0$ and the constitutive map is a continuous function of the angular frequency at the imaginary axis, *i.e.*,

$$\mathrm{i}\omega\boldsymbol{\varepsilon}(\mathrm{i}\omega) = \lim_{\eta\searrow 0} (\eta + \mathrm{i}\omega)\boldsymbol{\varepsilon}(\eta + \mathrm{i}\omega)$$

is continuous. A low-frequency asymptotic expansion of (2.31) gives the conductivity, *i.e.*,

$$s\boldsymbol{\varepsilon}(\boldsymbol{x}, s) \to \boldsymbol{\chi}(\boldsymbol{x}, \infty) = \boldsymbol{\varsigma}(\boldsymbol{x}) \quad \text{as} \quad s \to 0.$$

Analogous to the instantaneous response, the long-time response is undetermined from a physics point of view. This is simply seen by comparing the constitutive maps

$$\boldsymbol{\varepsilon}(\boldsymbol{x}, s) \quad \text{and} \quad \boldsymbol{\varepsilon}'(\boldsymbol{x}, s) = \frac{s + \eta_0}{s}\boldsymbol{\varepsilon}(\boldsymbol{x}, s + \eta_0)$$

where $\boldsymbol{\varepsilon}$ is analytic in $\mathbb{C}_+$ and passive. The error of the approximate constitutive map is

$$|\boldsymbol{\varepsilon}'(\boldsymbol{x}, s) - \boldsymbol{\varepsilon}(\boldsymbol{x}, s)| = |\frac{\eta_0}{s}|\,|\frac{(s + \eta_0)\boldsymbol{\varepsilon}(\boldsymbol{x}, \eta_0 + s) - s\boldsymbol{\varepsilon}(\boldsymbol{x}, s)}{\eta_0}| = \mathrm{O}(\eta_0)$$

uniformly in ω for $\operatorname{Re} s = \eta > 0$. The convergence estimate in Section 2.4.1 shows that the fields associated with $\boldsymbol{\varepsilon}'$ approach the fields associated with $\boldsymbol{\varepsilon}$ for finite times

as the approximate parameter η_0 decreases to zero. The approximate constitutive map is analytic for $\operatorname{Re} s > -\eta_0$ except for a simple pole at $s = 0$, *i.e.*,

$$\boldsymbol{\varepsilon}'(\boldsymbol{x}, s) = \frac{\boldsymbol{\varsigma}'(\boldsymbol{x})}{s} + \mathrm{O}(1) \quad \text{as} \quad s \to 0$$

where the conductivity $\boldsymbol{\varsigma}'$ is given by

$$\boldsymbol{\varsigma}'(\boldsymbol{x}) = \eta_0 \boldsymbol{\varepsilon}(\boldsymbol{x}, \eta_0).$$

It is interesting to observe that it is always possible to remove the conductivity from the constitutive map. This is illustrated by comparing the conductivity model and the Debye model, *i.e.*, compare

$$\boldsymbol{\varepsilon}(\boldsymbol{x}, s) = \boldsymbol{\varepsilon}_\infty(\boldsymbol{x}) + \frac{\boldsymbol{\varsigma}(\boldsymbol{x})}{s} \quad \text{and} \quad \boldsymbol{\varepsilon}'(\boldsymbol{x}, s) = \boldsymbol{\varepsilon}_\infty(\boldsymbol{x}) + \frac{\boldsymbol{\varsigma}(\boldsymbol{x})}{\tau^{-1} + s}.$$

Both models are passive and the error $|\boldsymbol{\varepsilon}(s) - \boldsymbol{\varepsilon}'(s)|$ is small if the relaxation time τ is large. It is illustrative to compare the approximation in the time domain. The susceptibility kernel of the conductivity and Debye models are

$$\boldsymbol{\chi}(\boldsymbol{x}, t) = \boldsymbol{\varsigma}(\boldsymbol{x})\mathrm{H}(t) \quad \text{and} \quad \boldsymbol{\chi}'(\boldsymbol{x}, t) = \boldsymbol{\varsigma}(\boldsymbol{x})\mathrm{H}(t)\mathrm{e}^{-t/\tau},$$

respectively. For a fixed time $T < \infty$ the error is

$$\sup_{0<t<T} |\boldsymbol{\chi}(\boldsymbol{x}, t) - \boldsymbol{\chi}'(\boldsymbol{x}, t)| = \mathrm{O}(T/\tau) \quad \text{as} \quad \tau \to \infty.$$

Observe that the long-time response of the conductivity and Debye susceptibility kernels are $\boldsymbol{\varsigma}$ and $\mathbf{0}$, respectively.

2.6 Statics

Solutions of the Maxwell equations that do not change with time are called static solutions. In reality, one often uses a static (or quasi static) approximation when the wavelength of the electromagnetic field is much larger then the spatial domain of interest. We start with a general discussion about potentials in Section 2.6.1 and in Section 2.6.2 the static limit is discussed.

2.6.1 Potentials

For some problems it is convenient to express the electromagnetic fields with potentials. Two scalar and two vector potentials are used to determine the electromagnetic fields

$$\begin{pmatrix} \widehat{\boldsymbol{E}} \\ \widehat{\boldsymbol{H}} \end{pmatrix} = \begin{pmatrix} -\nabla\hat{\phi} \\ -\nabla\hat{\phi}^{(\mathrm{M})} \end{pmatrix} + \begin{pmatrix} \boldsymbol{\epsilon} & \boldsymbol{\xi} \\ \boldsymbol{\zeta} & \boldsymbol{\mu} \end{pmatrix}^{-1} \begin{pmatrix} \nabla \times \widehat{\boldsymbol{A}}^{(\mathrm{E})} \\ \nabla \times \widehat{\boldsymbol{A}} \end{pmatrix}.$$

The vector potentials are restricted with the gauge requirement

$$\nabla \cdot \widehat{\boldsymbol{A}}^{(\mathrm{E})} = \nabla \cdot \widehat{\boldsymbol{A}} = 0.$$

To show that the potentials are well-defined, the passivity (2.20) is used, *i.e.*, the constitutive map is bounded as

$$C(1 + \operatorname{Re} s) \geq \operatorname{Re}\{s\boldsymbol{\varepsilon}(\boldsymbol{x}, s)\} \geq \delta \operatorname{Re} s \tag{2.32}$$

where (2.43) on page 34 has been used. The potential representation follows from the passivity of $s\boldsymbol{\varepsilon}(\boldsymbol{x}, s)$ in $\mathbb{C}_+$, *i.e.*, together with the solubility of two elliptic systems. The idea with the potential representation is more clearly revolved with the short-hand notation

$$\hat{\boldsymbol{e}} = -\nabla\hat{\varphi} + \boldsymbol{\varepsilon}^{-1}\nabla \times \hat{\boldsymbol{a}},$$

see Appendix A.2 for a discussion about this notation. Substitution of the potentials into the Maxwell equations gives the equation

$$-s\boldsymbol{\varepsilon}\nabla\hat{\varphi} + s\nabla \times \hat{\boldsymbol{a}} - \nabla \times (\mathrm{J}\boldsymbol{\varepsilon}^{-1}\nabla \times \hat{\boldsymbol{a}}) = -\hat{\boldsymbol{j}}$$

for the potentials. The vector potentials are eliminated with the divergence operator. This gives a set of second order equations in the scalar potentials, *i.e.*,

$$-\nabla \cdot (s\boldsymbol{\varepsilon}\nabla\hat{\varphi}) = -\nabla \cdot \hat{\boldsymbol{j}} \tag{2.33}$$

or written as a system

$$\begin{cases} -\nabla \cdot (s\boldsymbol{\epsilon}\nabla\hat{\phi}) - \nabla \cdot (s\boldsymbol{\xi}\nabla\hat{\phi}^{(\mathrm{M})}) = -\nabla \cdot \widehat{\boldsymbol{J}}, \\ -\nabla \cdot (s\boldsymbol{\zeta}\nabla\hat{\phi}) - \nabla \cdot (s\boldsymbol{\mu}\nabla\hat{\phi}^{(\mathrm{M})}) = -\nabla \cdot \widehat{\boldsymbol{J}}_{\mathrm{M}}. \end{cases}$$

This is a 2×2 system of elliptic equations for $s \in \mathbb{C}_+$. For the full space problem we add a set of radiation conditions.

It is natural to consider weak solutions for the potentials, *i.e.*, multiply the equation (2.33) with a test function $\tilde{\varphi}$ and integrate over space. This gives a sesquilinear form in the potential $\hat{\varphi}$ and the test function $\tilde{\varphi}$, *i.e.*,

$$\int_\Omega \nabla\tilde{\varphi}^{\mathrm{H}} \cdot s\boldsymbol{\varepsilon}\nabla\hat{\varphi}\,\mathrm{dV} - \int_\Omega \nabla \cdot (\tilde{\varphi}^{\mathrm{H}} s\boldsymbol{\varepsilon}\nabla\hat{\varphi})\,\mathrm{dV} = -\int_\Omega \tilde{\varphi}^{\mathrm{H}}\nabla \cdot \hat{\boldsymbol{j}}\,\mathrm{dV}\,. \tag{2.34}$$

With appropriate radiation or boundary conditions it is possible to focus on the first term on the left-hand side. The form

$$\mathrm{L_s}(\tilde{\varphi}, \hat{\varphi}) = \int_\Omega \nabla\tilde{\varphi}^{\mathrm{H}} \cdot s\boldsymbol{\varepsilon}\nabla\hat{\varphi}\,\mathrm{dV} \tag{2.35}$$

is sesquilinear and bounded as

$$C_{\mathrm{s}}\|\nabla\tilde{\varphi}\|^2 \geq \operatorname{Re}\mathrm{L_s}(\tilde{\varphi}, \tilde{\varphi}) \geq \operatorname{Re} s \int_\Omega \nabla\tilde{\varphi}^{\mathrm{H}} \cdot \boldsymbol{\varepsilon}_\infty\nabla\tilde{\varphi}\,\mathrm{dV} \geq \delta \operatorname{Re} s\|\nabla\tilde{\varphi}\|^2$$

where we also used (2.43) on page 34. The Lax-Milgram lemma [50, 67] can be used to show the existence and the uniqueness of the scalar potential if suitable boundary conditions are imposed for the potentials.

The knowledge of the scalar potentials is used to get a set of equations for the vector potentials, *i.e.*, the vector potentials satisfy

$$s\nabla \times \hat{\boldsymbol{a}} - \nabla \times (\mathrm{J}\boldsymbol{\varepsilon}^{-1}\nabla \times \hat{\boldsymbol{a}}) = -\hat{\boldsymbol{j}} + s\boldsymbol{\varepsilon}\nabla\hat{\varphi} \tag{2.36}$$

together with the gauge requirement $\nabla \cdot \hat{\boldsymbol{a}} = 0$. The left-hand side of (2.36) is a short-hand notation for

$$\begin{pmatrix} s\nabla \times \widehat{\boldsymbol{A}}^{(\mathrm{E})} \\ s\nabla \times \widehat{\boldsymbol{A}} \end{pmatrix} - \begin{pmatrix} \boldsymbol{0} & \nabla\times \\ -\nabla\times & \boldsymbol{0} \end{pmatrix} \begin{pmatrix} \boldsymbol{\epsilon} & \boldsymbol{\xi} \\ \boldsymbol{\zeta} & \boldsymbol{\mu} \end{pmatrix}^{-1} \begin{pmatrix} \nabla \times \widehat{\boldsymbol{A}}^{(\mathrm{E})} \\ \nabla \times \widehat{\boldsymbol{A}} \end{pmatrix}. \tag{2.37}$$

From the passivity there is a uniform bound $\operatorname{Re}\boldsymbol{\varepsilon}^{-1} \geq \eta\delta'$ on the constitutive map. The left-hand side of (2.36) is

$$s\nabla \times \hat{\boldsymbol{a}} - \nabla \times (\mathrm{J}(\boldsymbol{\varepsilon}^{-1} - \eta\delta')\nabla \times \hat{\boldsymbol{a}}) + \eta\delta'\nabla^2\mathrm{J}\hat{\boldsymbol{a}}.$$

Multiply with $(\mathrm{J}\tilde{\boldsymbol{a}})^{\mathrm{H}}\cdot$ from the left where $\tilde{\boldsymbol{a}}$ are vector-valued test functions, *i.e.*, the first three equations (2.37) are scalar multiplied with $\widetilde{\boldsymbol{A}}$ and the fourth to sixth equation of (2.37) with $-\widetilde{\boldsymbol{A}}^{(\mathrm{E})}$, *i.e.*,

$$s(\mathrm{J}\tilde{\boldsymbol{a}})^{\mathrm{H}} \cdot \nabla \times \hat{\boldsymbol{a}} - (\mathrm{J}\tilde{\boldsymbol{a}})^{\mathrm{H}} \cdot \nabla \times (\mathrm{J}(\boldsymbol{\varepsilon}^{-1} - \eta\delta')\nabla \times \hat{\boldsymbol{a}}) + (\mathrm{J}\tilde{\boldsymbol{a}})^{\mathrm{H}} \cdot \eta\delta'\nabla^2\mathrm{J}\hat{\boldsymbol{a}}. \tag{2.38}$$

Analogous to the scalar potential we neglect the boundary terms, *i.e.*, we assume that the fields vanish at the boundary. To get coercivity estimates, we rewrite the terms of (2.38) in the following manner. The first term is rewritten as

$$\operatorname{Re}\{s(\mathrm{J}\tilde{\boldsymbol{a}})^{\mathrm{H}} \cdot \nabla \times \tilde{\boldsymbol{a}}\} = \nabla \cdot \operatorname{Re}\{s\widetilde{\boldsymbol{A}}^{(\mathrm{E})} \times \widetilde{\boldsymbol{A}}\},$$

the second term is

$$-(\nabla \times \tilde{\boldsymbol{a}})^{\mathrm{H}} \cdot \operatorname{Re}(\boldsymbol{\varepsilon}^{-1} - \eta\delta')\nabla \times \tilde{\boldsymbol{a}} + \nabla \cdot \operatorname{Re}\{\tilde{\boldsymbol{a}}^{\mathrm{H}} \times (\boldsymbol{\varepsilon}^{-1} - \eta\delta')\nabla \times \tilde{\boldsymbol{a}}\},$$

and finally the third term is

$$\nabla \cdot \operatorname{Re}\{\eta\delta' \sum_{i=1}^{3} (\widehat{A}_i^{(\mathrm{E})})^* \nabla \widehat{A}_i^{(\mathrm{E})} + \widehat{A}_i^* \nabla \widehat{A}_i\} - \eta\delta'|\nabla\tilde{\boldsymbol{a}}|^2. \tag{2.39}$$

where the shorthand notation

$$|\nabla\tilde{\boldsymbol{a}}|^2 = \sum_{i=1}^{3} |\nabla\widehat{A}_i^{(\mathrm{E})}|^2 + |\nabla\widehat{A}_i|^2.$$

have been used in the right-hand side of (2.39). With appropriate boundary conditions (or radiation conditions) one can focus on the form

$$\mathrm{L_v}(\tilde{\boldsymbol{a}}, \tilde{\boldsymbol{a}}) = \int_\Omega (\nabla \times \tilde{\boldsymbol{a}})^{\mathrm{H}} \cdot \operatorname{Re}\{\boldsymbol{\varepsilon}^{-1} - \eta\delta'\}(\nabla \times \tilde{\boldsymbol{a}}) + \eta\delta'|\nabla\tilde{\boldsymbol{a}}|^2 \,\mathrm{dV}\,. \tag{2.40}$$

This form is bounded as

$$C_{\mathrm{v}}\|\nabla\tilde{\boldsymbol{a}}\|^2 \geq \operatorname{Re} \mathrm{L}_{\mathrm{v}}(\tilde{\boldsymbol{a}},\tilde{\boldsymbol{a}}) \geq \eta\delta'\|\nabla\tilde{\boldsymbol{a}}\|^2.$$

This form is coercive and hence the vector potentials are well-behaved for suitable boundary conditions.

Notice that the potential representation reduces to the commonly used scalar and vector potentials in an isotropic medium with no magnetic currents and sources, *i.e.*,

$$\nabla\cdot\widehat{\boldsymbol{B}} = 0 \quad \text{implies} \quad \hat{\phi}^{(\mathrm{M})} = 0$$

and

$$s\mu\widehat{\boldsymbol{H}} - \nabla\times\widehat{\boldsymbol{E}} = \boldsymbol{0} \quad \text{implies} \quad \widehat{\boldsymbol{A}}^{(\mathrm{E})} = \boldsymbol{0}.$$

2.6.2 Static limit

Static fields are fields that do not depend on the temporal coordinate. In the statics of electromagnetics, we assume that the field intensities are independent of time. The flux densities are static in non-conducting regions (regions where $\boldsymbol{\varsigma} = \boldsymbol{0}$), but in general not well-defined in conducting regions (regions where $\boldsymbol{\varsigma} \neq \boldsymbol{0}$).

There are two essentially similar approaches to statics. In the first, statics is the longtime limit of the electromagnetic fields for static currents and charges, *i.e.*,

$$\lim_{t\to\infty} \boldsymbol{e}(\boldsymbol{x},t)$$

where $\boldsymbol{e}(\boldsymbol{x},t)$ solves the Maxwell equations with static currents $\boldsymbol{j}(\boldsymbol{x},t) = \boldsymbol{j}(\boldsymbol{x})$ and static charge densities $\varrho(\boldsymbol{x},t) = \varrho(\boldsymbol{x})$ for $t > 0$. In the second approach the static fields can be interpreted as a low frequency limit of time harmonic fields, *i.e.*,

$$\operatorname{Re}\{\boldsymbol{e}(\boldsymbol{x},\mathrm{i}\omega)\mathrm{e}^{\mathrm{i}\omega t}\} \quad \text{as} \quad \omega\to 0.$$

Both these approaches can be considered as limits of solutions of the Maxwell equations $\boldsymbol{e}(\boldsymbol{x},s)$ as $s\to 0$. However, here we are mainly interested in the behavior of the constitutive relations in the limit $s\to 0$ and not the mathematical assumptions of the above approaches. It is not possible to use the sesquilinear forms in the static limit since the constitutive map vanishes in non-conducting regions, *i.e.*,

$$\nabla\tilde{\varphi}^{\mathrm{H}}\cdot s\boldsymbol{\varepsilon}(\boldsymbol{x},s)\nabla\tilde{\varphi} \to 0 \quad \text{as} \quad s\to 0 \quad \text{if} \quad \nabla\tilde{\varphi}^{\mathrm{H}}\cdot\boldsymbol{\varsigma}(\boldsymbol{x})\nabla\tilde{\varphi} = 0.$$

It is also well-known that the charge density $\varrho(\boldsymbol{x})$ is the origin of static fields in non-conducting regions. The charge density is related to the divergence of the current density by the continuity equation

$$s\hat{\varrho}(\boldsymbol{x},s) = -\nabla\cdot\hat{\boldsymbol{j}}(s,\boldsymbol{x}) \quad \text{for} \quad s\in\mathbb{C}_+.$$

Let's start with an assumption on the asymptotic expansion of the constitutive map in the neighborhood of $s=0$, *i.e.*,

$$s\boldsymbol{\varepsilon}(\boldsymbol{x},s) = \boldsymbol{\varsigma}(\boldsymbol{x}) + s\boldsymbol{\varepsilon}_{\mathrm{s}}(\boldsymbol{x}) + \mathrm{o}(s) \quad \text{as} \quad \mathbb{C}_+ \ni s\to 0$$

where the conductivity $\boldsymbol{\varsigma}$ and the static limit $\boldsymbol{\varepsilon}_\mathrm{s}$ are assumed to be symmetric. The asymptotic expansion is for example valid if $\boldsymbol{\chi}(t) - \boldsymbol{\chi}(\infty) \in \mathrm{L}^1[0,\infty]$, see (2.16). The requirement of passivity, see (2.43) on page 34, gives

$$\operatorname{Re}\{s\boldsymbol{\varepsilon}(\boldsymbol{x},s)\} = \boldsymbol{\varsigma}(\boldsymbol{x}) + \operatorname{Re} s\boldsymbol{\varepsilon}_\mathrm{s}(\boldsymbol{x}) + \mathrm{o}(s) \geq \operatorname{Re} s\boldsymbol{\varepsilon}_\infty(\boldsymbol{x}).$$

It is sufficient to use the estimate (2.32) for the scalar potentials. However, for the vector potentials, a bound in the inverse of the constitutive map is required. In the limit $\eta \to 0$, the constitutive map is bounded as

$$\frac{1}{\delta'} \geq \operatorname{Re}\{\eta\boldsymbol{\varepsilon}(\boldsymbol{x},\eta)\} \geq \eta\delta$$

and hence there is a similar bound on the inverse, *i.e.*,

$$\frac{1+\mathrm{o}(1)}{\delta} \geq \operatorname{Re}\{\boldsymbol{\varepsilon}^{-1}(\boldsymbol{x},\eta)\} \geq \eta\delta'(1+\mathrm{o}(1)) \quad \text{as} \quad \eta \to 0,$$

where the symmetry of $\boldsymbol{\varsigma}$ and $\boldsymbol{\varepsilon}_\mathrm{s}$ has been used.

The sesquilinear form (2.35) is normalized to give a well-behaved static limit. Let

$$\tilde{\mathrm{L}}_\mathrm{s}(\tilde{\varphi},\hat{\varphi}) = \frac{\mathrm{L}_\mathrm{s}(\tilde{\varphi},\hat{\varphi})}{\operatorname{Re}\mathrm{L}_\mathrm{s}(\tilde{\varphi},\tilde{\varphi})/|\nabla\tilde{\varphi}|^2}$$

be the normalized sesquilinear form. This form is coercive

$$\operatorname{Re}\tilde{\mathrm{L}}_\mathrm{s}(\tilde{\varphi},\tilde{\varphi}) = |\nabla\tilde{\varphi}|^2.$$

and the normalization is bounded as

$$\frac{1}{\delta'} \geq \frac{\operatorname{Re}\mathrm{L}_\mathrm{s}(\tilde{\varphi},\tilde{\varphi})}{|\nabla\tilde{\varphi}|^2} \geq \delta\eta \quad \text{as} \quad s = \eta \to 0.$$

Define the static limit as the solution of the normalized version of (2.34) as the Laplace parameter s approaches 0, *i.e.*,

$$\tilde{\mathrm{L}}_\mathrm{s}(\tilde{\varphi},\hat{\varphi}) = \frac{-\int_\Omega \tilde{\varphi}^\mathrm{H}\nabla\cdot\hat{\boldsymbol{\jmath}}\,\mathrm{dV}}{\operatorname{Re}\mathrm{L}_\mathrm{s}(\tilde{\varphi},\tilde{\varphi})/|\nabla\tilde{\varphi}|^2} \quad \text{as} \quad s = \eta \to 0 \tag{2.41}$$

where the boundary term have been neglected for simplicity. In a conducting region the normalization is bounded for all values of η and the limit is well-defined. In non-conducting regions the weight is of the order of $\eta\boldsymbol{\varepsilon}(\boldsymbol{x},\eta)$ and to make the right-hand side of (2.41) well-defined, the current must have zero divergence. Notice that in a non-conducting region the limit (2.41) retrieves the divergence equations (2.2), *i.e.*, equation (2.41) reduces to the weak form of (2.2) in the static limit

$$\int_\Omega (\nabla\tilde{\varphi})^\mathrm{H}\cdot\boldsymbol{\varepsilon}_\mathrm{s}\nabla\hat{\varphi}\,\mathrm{dV} = \int_\Omega \tilde{\varphi}^\mathrm{H}\varrho\,\mathrm{dV}\,.$$

A similar procedure is performed for the vector potentials. The normalized sesquilinear form is

$$\tilde{\mathrm{L}}_{\mathrm{v}}(\tilde{\boldsymbol{a}}, \hat{\boldsymbol{a}}) = \frac{\mathrm{L}_{\mathrm{v}}(\tilde{\boldsymbol{a}}, \hat{\boldsymbol{a}})}{\mathrm{Re}\,\mathrm{L}_{\mathrm{v}}(\tilde{\boldsymbol{a}}, \tilde{\boldsymbol{a}})/|\nabla\tilde{\boldsymbol{a}}|^2}.$$

This form is coercive and the normalization is bounded as

$$\frac{1+\mathrm{o}(1)}{\delta} \geq \frac{\mathrm{Re}\,\mathrm{L}_{\mathrm{v}}(\tilde{\boldsymbol{a}}, \tilde{\boldsymbol{a}})}{|\nabla\tilde{\boldsymbol{a}}|^2} \geq \delta'\eta(1+\mathrm{o}(1)) \quad \text{as} \quad s = \eta \to 0.$$

Define the static limit as the weak scaled version of (2.36) as $\eta \to 0$, *i.e.*,

$$\tilde{\mathrm{L}}_{\mathrm{v}}(\tilde{\boldsymbol{a}}, \hat{\boldsymbol{a}}) = \frac{-\int_\Omega \tilde{\boldsymbol{a}}^{\mathrm{H}} \cdot (\hat{\boldsymbol{j}} - s\boldsymbol{\varepsilon}\nabla\hat{\varphi})\,\mathrm{dV}}{\mathrm{Re}\,\mathrm{L}_{\mathrm{v}}(\tilde{\boldsymbol{a}}, \tilde{\boldsymbol{a}})/|\nabla\tilde{\boldsymbol{a}}|^2} \quad \text{as} \quad s = \eta \to 0$$

where the boundary terms have been neglected.

2.7 State variables and polarization

The temporal convolution (2.8) is the generic representation of dispersion in the time domain. In this representation, the material remembers the history of the electromagnetic fields and the interaction between the material and the electromagnetic fields depends on this memory. Even if the temporal convolution is frequently used, it has some drawbacks. First, from a physics point of view, it is not clear how the mechanics of the memory works. Secondly, the model is not computationally efficient, *i.e.*, the temporal integration is time and memory consuming, and finally it is rather difficult to extend the temporal convolution to non-linear constitutive relations.

To surmount the difficulties outlined above, we consider the class of local constitutive relations. In this class of constitutive relations, the values of the flux densities do only depend on the values of the field intensities and a fixed number of state variables in a neighborhood of t. The generic representation of a local constitutive relation is as an ordinary differential equation in the state variables. Here, we choose to use a second order formulation as an illustration, *i.e.*,

$$\begin{cases} \boldsymbol{d} = \boldsymbol{\varepsilon}_\infty \boldsymbol{e} + \boldsymbol{\alpha}\boldsymbol{p} \\ \boldsymbol{\gamma}\partial_t^2\boldsymbol{p} + \boldsymbol{\nu}\partial_t\boldsymbol{p} + \boldsymbol{\omega}\boldsymbol{p} = \boldsymbol{\beta}\boldsymbol{e} \end{cases} \tag{2.42}$$

where the instantaneous response $\boldsymbol{\varepsilon}_\infty = \boldsymbol{\varepsilon}_\infty(\boldsymbol{x})$ is a symmetric and positive definite 6×6 matrix, $\boldsymbol{p} = \boldsymbol{p}(\boldsymbol{x}, t)$ an $m \times 1$ matrix, $\boldsymbol{\alpha} = \boldsymbol{\alpha}(\boldsymbol{x})$ a $6 \times m$ matrix, $\boldsymbol{\gamma} = \boldsymbol{\gamma}(\boldsymbol{x})$ an $m \times m$ matrix, $\boldsymbol{\nu} = \boldsymbol{\nu}(\boldsymbol{x})$ an $m \times m$ matrix, $\boldsymbol{\omega} = \boldsymbol{\omega}(\boldsymbol{x})$ an $m \times m$ matrix, and $\boldsymbol{\beta} = \boldsymbol{\beta}(\boldsymbol{x})$ an $m \times 6$ matrix. Observe, that the second order system (2.42) is reduced to an equivalent first order system by the substitution $\partial_t\boldsymbol{p} = \dot{\boldsymbol{p}}$. In the state variable representation, the material do not remember the history of the fields instead the electromagnetic field intensities affect the state of the material. The

dispersive effects are due to the dynamics of the state variables. Moreover, the state variable representation is computationally efficient, see Section 5.5.

The Laplace-domain representation of (2.42) is

$$\hat{\boldsymbol{d}} = (\boldsymbol{\varepsilon}_\infty + \boldsymbol{\alpha}(\boldsymbol{\gamma} s^2 + \boldsymbol{\nu} s + \boldsymbol{\omega})^{-1}\boldsymbol{\beta})\hat{\boldsymbol{e}}$$

where it is assumed that the inverse is well-defined and vanish for large frequencies. The constitutive map $\boldsymbol{\varepsilon}(s)$ is in the form of a rational function in s, *i.e.*, the elements of $\boldsymbol{\varepsilon}(s)$ are rational functions. The good approximation properties of the rational functions are seen in the general approximation in Section 2.4.2 and more appropriately in the explicit solution algorithm of the Nevanlinna-Pick problem, see Refs [100, 56, 6, 95]. It is also common to use least-squares minimization to determine a rational approximation from frequency-domain data [174].

The most frequently used form of the state variables are the Debye (or relaxation) model and the Lorentz (or resonance) model, *i.e.*, in a isotropic setting

$$\epsilon(\boldsymbol{x}, s) = \epsilon_\infty(\boldsymbol{x}) + \sum_{n=1}^{N_{\mathrm{D}}} \frac{\alpha_n(\boldsymbol{x})}{1 + \tau_n s} + \sum_{n=1}^{N_{\mathrm{L}}} \frac{\beta_n(\boldsymbol{x})}{\omega_n^2 + s\nu_n + s^2}$$

where N_{D} is the number of the Debye states and N_{L} is the number of Lorentz states. A single Debye and Lorentz model is passive if $\alpha(\boldsymbol{x}) \geq 0$ and $\beta(\boldsymbol{x}) \geq 0$, respectively. The model is stable if $\tau > 0$ and $\nu > 0$. In the time domain, the electric field $\boldsymbol{E}(\boldsymbol{x}, t)$ and magnetic field $\boldsymbol{H}(\boldsymbol{x}, t)$ satisfy the Maxwell equations (2.1) with the substitutions

$$\boldsymbol{D}(\boldsymbol{x}, t) = \epsilon_\infty(\boldsymbol{x})\boldsymbol{E}(\boldsymbol{x}, t) + \sum_{n=1}^{N_{\mathrm{D}}} \boldsymbol{P}_n^{(\mathrm{D})}(\boldsymbol{x}, t) + \sum_{n=1}^{N_{\mathrm{L}}} \boldsymbol{P}_n^{(\mathrm{L})}(\boldsymbol{x}, t)$$

and $\boldsymbol{B}(\boldsymbol{x}, t) = \mu \boldsymbol{H}(\boldsymbol{x}, t)$. The Debye states $\boldsymbol{P}_n^{(\mathrm{D})}$ and Lorentz states $\boldsymbol{P}_n^{(\mathrm{L})}$ are updated with the ordinary differential equations

$$\tau_n \partial_t \boldsymbol{P}_n^{(\mathrm{D})} + \boldsymbol{P}_n^{(\mathrm{D})} = \alpha_n(\boldsymbol{x})\boldsymbol{E} \quad \text{for} \quad n = 1, \ldots, N_{\mathrm{D}}$$

and

$$\partial_t^2 \boldsymbol{P}_n^{(\mathrm{L})} + \nu_n \partial_t \boldsymbol{P}_n^{(\mathrm{L})} + \omega_n^2 \boldsymbol{P}_n^{(\mathrm{L})} = \beta_n(\boldsymbol{x})\boldsymbol{E} \quad \text{for} \quad n = 1, \ldots, N_{\mathrm{L}},$$

respectively.

Additional advantages with the state-space representation is the simple extension to non-stationary and non-linear medium models. The model becomes non-stationary by the extension

$$\boldsymbol{\varepsilon}_\infty = \boldsymbol{\varepsilon}_\infty(\boldsymbol{x}, t), \quad \boldsymbol{\phi} = \boldsymbol{\phi}(\boldsymbol{x}, t), \quad \text{and} \quad \boldsymbol{\psi} = \boldsymbol{\psi}(\boldsymbol{x}, t),$$

see Refs [4, 2, 3, 1] for a general discussions about non-stationary models. Non-linear models are, *e.g.*,

$$\begin{cases} \boldsymbol{d} = \boldsymbol{\varepsilon}_\infty \boldsymbol{e} + \boldsymbol{\beta}^{\mathrm{T}} \boldsymbol{p} \\ \partial_t^2 \boldsymbol{p} + \boldsymbol{\nu}(\boldsymbol{p})\partial_t \boldsymbol{p} + \boldsymbol{\omega}_0^2(\boldsymbol{p}) = \boldsymbol{\beta} \boldsymbol{e} \end{cases}$$

where $\boldsymbol{\nu}(\boldsymbol{p})$ is positive definite, *i.e.*, $\dot{\boldsymbol{p}}^{\mathrm{T}} \boldsymbol{\nu}(\boldsymbol{p}) \dot{\boldsymbol{p}} \geq C|\dot{\boldsymbol{p}}|^2$ and $\dot{\boldsymbol{p}}^{\mathrm{T}} \boldsymbol{\omega}_0^2(\boldsymbol{p})$ is assumed to be a differential.

2.8 Alternative forms of the constitutive relations

The preferred form of the constitutive relations depends on the specific application. In this thesis, the emphasis is on energy analysis and computations. In these applications it is natural to consider the field intensities as fundamental fields and the flux densities as derived quantities, *i.e.*, the map $(\boldsymbol{E}, \boldsymbol{H}) \to (\boldsymbol{D}, \boldsymbol{B})$. However, in applications related to the relativistic behavior of matter, such as moving objects, it is natural to consider the electric field intensity and the magnetic flux density as the fundamental field quantities, *i.e.*, the map $(\boldsymbol{E}, \boldsymbol{B}) \to (\boldsymbol{D}, \boldsymbol{H})$. The generic bi-anisotropic model is written

$$\begin{pmatrix} \widehat{\boldsymbol{D}} \\ \widehat{\boldsymbol{H}} \end{pmatrix} = \begin{pmatrix} \mathbf{P} & \mathbf{L} \\ \mathbf{M} & \mathbf{Q} \end{pmatrix} \begin{pmatrix} \widehat{\boldsymbol{E}} \\ \widehat{\boldsymbol{B}} \end{pmatrix}$$

in the (EB-DH) formulation, see Refs [153, 177]. Formal inversion of the (EH-DB) model (2.17) and identification with the (EB-DH) model gives the relation

$$\begin{pmatrix} \widehat{\boldsymbol{D}} \\ \widehat{\boldsymbol{H}} \end{pmatrix} = \begin{pmatrix} \boldsymbol{\epsilon} - \boldsymbol{\xi}\boldsymbol{\mu}^{-1}\boldsymbol{\zeta} & \boldsymbol{\xi}\boldsymbol{\mu}^{-1} \\ -\boldsymbol{\mu}^{-1}\boldsymbol{\zeta} & \boldsymbol{\mu}^{-1} \end{pmatrix} \begin{pmatrix} \widehat{\boldsymbol{E}} \\ \widehat{\boldsymbol{B}} \end{pmatrix}.$$

The constitutive tensors (dyadics) $\boldsymbol{\epsilon}, \boldsymbol{\mu}, \boldsymbol{\xi}$, and $\boldsymbol{\zeta}$ are analytic in $\mathbb{C}_+$. Moreover, the two tensors $\boldsymbol{\epsilon}$ and $\boldsymbol{\mu}$ are non-zero in $\mathbb{C}_+$. Hence, the inverse $\boldsymbol{\mu}^{-1}$ is analytic and non-zero in $\mathbb{C}_+$. This shows that the tensors $\mathbf{P}$, $\mathbf{Q}$, $\mathbf{L}$, and $\mathbf{M}$ in the (EB-DH) formulation are analytic in $\mathbb{C}_+$.

2.9 Inequalities

Above and below we use a few inequalities based on the analytic properties of the constitutive map $\boldsymbol{\varepsilon}(s)$. Let $\boldsymbol{\varepsilon}(s)$ be a passive constitutive map with high-frequency response $\boldsymbol{\varepsilon}_\infty$, *i.e.*,

$$\operatorname{Re}\{s\boldsymbol{\varepsilon}(s)\} \geq 0 \quad \text{for} \quad s \in \mathbb{C}_+ \quad \text{and} \quad \boldsymbol{\varepsilon}(s) = \boldsymbol{\varepsilon}_\infty + \mathrm{O}(s^{-1}) \quad \text{as} \quad |s| \to \infty.$$

Then we have the estimate

$$\operatorname{Re}\{s\boldsymbol{\varepsilon}(s)\} \geq \boldsymbol{\varepsilon}_\infty \operatorname{Re} s. \tag{2.43}$$

To show this estimate we use

$$\operatorname{Re}\{s\boldsymbol{\varepsilon}(s)\} = \operatorname{Re}\{s(\boldsymbol{\varepsilon}(s) - \boldsymbol{\varepsilon}_\infty)\} + \operatorname{Re}\{s\boldsymbol{\varepsilon}_\infty\}.$$

The first term on the right hand side is bounded by the minimum principle for harmonic functions [100], *i.e.*, transform $\mathbb{C}_+$ to the unit disc $|z| < 1$ with the Cayley transform (2.28) and use the fact that the real-valued part of the high-frequency response ($\operatorname{Re}\{\boldsymbol{\varepsilon}_\infty\}$) vanishes at the boundary. We get

$$\operatorname{Re}\{s(\boldsymbol{\varepsilon}(s) - \boldsymbol{\varepsilon}_\infty)\} \geq \operatorname{Re}\{\mathrm{i}\omega(\boldsymbol{\varepsilon}(\mathrm{i}\omega) - \boldsymbol{\varepsilon}_\infty)\} = \operatorname{Re}\{\mathrm{i}\omega\boldsymbol{\varepsilon}(\mathrm{i}\omega)\} \geq 0.$$

In the wave splitting and the Bremmer series, see Chapters 4 and 6, respectively, we need an estimate on the square-root symbol (the branch $\operatorname{Re}\sqrt{z} \geq 0$ is chosen)

$$\sqrt{s\epsilon(s)s\mu(s) + \xi^2}$$

where the scalars $\epsilon(s)$ and $\mu(s)$ are passive and have well-defined high-frequency values, *i.e.*,

$$\operatorname{Re}\{s\epsilon(s)\} \geq 0 \quad \text{and} \quad \epsilon(s) = \epsilon_\infty + \mathrm{O}(s^{-1}) \quad \text{as} \quad |s| \to \infty$$

and similarly for the permeability μ. The real-valued part of the square-root symbol can be estimated as

$$\operatorname{Re}\sqrt{s\epsilon(s)s\mu(s) + \xi^2} \geq \sqrt{\epsilon_\infty \mu_\infty}\, \operatorname{Re} s \tag{2.44}$$

for all real-valued ξ. We show this is in two steps. The case $\xi = 0$ follows from: Any complex-valued numbers $z_1 = a + \mathrm{i}b \in \mathbb{C}_+$ and $z_2 = c + \mathrm{i}d \in \mathbb{C}_+$ satisfy

$$\begin{aligned}
\operatorname{Re}\sqrt{z_1 z_2} &= \operatorname{Re}\sqrt{(a+\mathrm{i}b)(c+\mathrm{i}d)} = (\sqrt{(ac-bd)^2 + (ad+bc)^2} + ac - bd)^{1/2}/\sqrt{2} \\
&= (\sqrt{(ac)^2 + (bd)^2 + (ad)^2 + (bc)^2} + ac - bd)^{1/2}/\sqrt{2} \\
&\geq (\sqrt{(ac+bd)^2} + ac - bd)^{1/2}/\sqrt{2} = \sqrt{ac} = \sqrt{\operatorname{Re} z_1 \operatorname{Re} z_2}\ .
\end{aligned}$$

The second part of (2.44) is given by: A complex-valued number $z \in \mathbb{C}_+$ and a real-valued number ξ satisfy

$$\operatorname{Re}\sqrt{z^2 + \xi^2} \geq \operatorname{Re} z.$$

The stationary point is given of

$$\partial_\xi \operatorname{Re}\sqrt{z^2 + \xi^2} = \xi \operatorname{Re}(z^2 + \xi^2)^{-1/2} = 0.$$

This point $\xi = 0$ is the minimum.

Chapter 3

Acoustics

The motivation to include a discussion of the acoustic wave equation in this thesis is twofold. First, it is motivated by the many acoustic wave propagation problems, *e.g.*, in exploration geophysics and underwater acoustics. Secondly, it is motivated by the mathematical similarities between the Maxwell equations and the acoustic wave equation, *e.g.*, the Maxwell equations reduce to a acoustic wave equation in two spatial dimensions.

We start with a brief discussion of the acoustic wave equation in Section 3.1. In Sections 3.2 and 3.3 the formal similarities between the Maxwell equations and the acoustic wave equation are outlined in two and one spatial dimensions, respectively.

3.1 Acoustic wave equation

The acoustic wave equation models the evolution of sound, *i.e.*, pressure waves. It can be written either as a scalar second order equation in the pressure p

$$\partial_t^2 p - \frac{1}{\kappa}\nabla\cdot(\rho^{-1}\nabla p) = \frac{1}{\kappa}\partial_t q - \frac{1}{\kappa}\nabla\cdot(\frac{1}{\rho}\boldsymbol{f})$$

or as a symmetric first order hyperbolic system in the pressure $p(\boldsymbol{x},t)$ and the particle velocity $\boldsymbol{v}(\boldsymbol{x},t)$, *i.e.*,

$$\begin{cases} \kappa(\boldsymbol{x})\partial_t p + \nabla\cdot\boldsymbol{v} = q(\boldsymbol{x},t), \\ \rho(\boldsymbol{x})\partial_t \boldsymbol{v} + \nabla p = \boldsymbol{f}(\boldsymbol{x},t). \end{cases} \tag{3.1}$$

The medium properties are described by the compressibility κ and the density ρ. The acoustic wave field is generated by the sources $\boldsymbol{f}(\boldsymbol{x},t)$ and $q(\boldsymbol{x},t)$, see Table 3.1. In the scattering problem, we assume that the sources are quiescent and that the fields vanish before time $t=0$. This gives the initial conditions

$$p(\boldsymbol{x},0) = \partial_t p(\boldsymbol{x},0) = 0$$

or

$$p(\boldsymbol{x},0) = 0 \quad \text{and} \quad \boldsymbol{v}(\boldsymbol{x},0) = \boldsymbol{0},$$

Description	Symbol	SI units	Scaled units
Pressure	p	Pa	$(\mathrm{Ws/m^3})^{1/2}$
Particle velocity	$\boldsymbol{v}$	m/s	$(\mathrm{Ws/m^3})^{1/2}$
Compressibility	κ	Pa^{-1}	$(\mathrm{Ws/m^3})^{1/2}$
Density	ρ	$\mathrm{Kg/m^3}$	$(\mathrm{Ws/m^3})^{1/2}$
Force density	$\boldsymbol{f}$	$\mathrm{N/m^3}$	$(\mathrm{Ws/m^5})^{1/2}$
Injection rate	q	s^{-1}	$(\mathrm{Ws/m^5})^{1/2}$

Table 3.1: The acoustic fields

for the second order and first order versions of the acoustic wave equation, respectively. The Laplace transformed version of the acoustic equation (3.1) is

$$\begin{cases} s\kappa(\boldsymbol{x},s)\hat{p} + \nabla\cdot\hat{\boldsymbol{v}} = \hat{q}(\boldsymbol{x},s), \\ s\rho(\boldsymbol{x},s)\hat{\boldsymbol{v}} + \nabla\hat{p} = \hat{\boldsymbol{f}}(\boldsymbol{x},s), \end{cases} \tag{3.2}$$

together with the radiation condition

$$\sqrt{\rho_0}\hat{v}_r - \sqrt{\kappa_0}\hat{p} = \mathrm{o}(|\boldsymbol{x}|^{-1}) = \mathrm{o}(r^{-1}) \quad \text{as} \quad r\to\infty, \tag{3.3}$$

where $\hat{v}_r$ stands for the radial component of the particle velocity. To ensure causality, the compressibility $\kappa(\boldsymbol{x},s)$ (and density $\rho(\boldsymbol{x},s)$) is an analytic function of s in the right complex half-plane. Furthermore, we restrict the analysis to passive dispersive models such that

$$\mathrm{Re}\{s\kappa(\boldsymbol{x},s)\} \geq 0, \tag{3.4}$$

and

$$\kappa(\boldsymbol{x},s) - \kappa_0 = \mathrm{O}(s^{-2}) \quad \text{as } s\to\infty. \tag{3.5}$$

3.2 The Maxwell equations in two spatial dimensions

In some situations, it is natural to consider the Maxwell equations in two spatial dimensions. Let the field intensities and flux densities be independent of the x_3 coordinate, *i.e.*, the fields depend only on the transverse, $x = (x_1, x_2)$, part of the spatial coordinates. Furthermore, we assume that the constitutive relations are isotropic. In this case, the Maxwell equations separate into a transverse electric (TE) equation and a transverse magnetic (TM) equation.

Let D denote the transverse gradient operator and J the transverse rotation matrix, *i.e.*,

$$\mathrm{D} = \begin{pmatrix} \partial_1 \\ \partial_2 \end{pmatrix} \quad \text{and} \quad \mathrm{J} = \begin{pmatrix} 0 & 1 \\ -1 & 0 \end{pmatrix}.$$

The curl operator has the transverse components and vertical component

$$\mathrm{J}\,\mathrm{D}\,E_3 \quad \text{and} \quad \mathrm{D}\cdot\mathrm{J}E, \tag{3.6}$$

respectively, where also the vector field is decomposed into its transverse and vertical components, see also Section 4.1 and Appendix A.

In the (TE) case, the electric field is orthogonal to the x-plane. The (TE) equations are

$$\begin{cases} s\epsilon(x,s)\widehat{E}_3 - \mathrm{D}\cdot\mathrm{J}\widehat{H} + \widehat{J}_3(x,s) = 0, \\ s\mu(x,s)\mathrm{J}\widehat{H} - \mathrm{D}\,\widehat{E}_3 + \mathrm{J}\widehat{J}^{(\mathrm{M})}(x,s) = 0. \end{cases} \tag{3.7}$$

In the corresponding (TM) case, the magnetic field intensity is orthogonal to the x-plane, *i.e.*,

$$\begin{cases} s\mu(x,s)\widehat{H}_3 + \mathrm{D}\cdot\mathrm{J}\widehat{E} + \widehat{J}^{(\mathrm{M})}(x,s) = 0, \\ s\epsilon(x,s)\mathrm{J}\widehat{E} + \mathrm{D}\,\widehat{H}_3 + \mathrm{J}\widehat{J}(x,s) = 0. \end{cases} \tag{3.8}$$

The analogous acoustic wave equations are

$$\begin{cases} s\kappa(x,s)\hat{p} + \mathrm{D}\cdot\hat{v} = \hat{q}(x,s), \\ s\rho(x,s)\hat{v} + \mathrm{D}\,\hat{p} = \hat{f}(x,s), \end{cases} \tag{3.9}$$

if the fields are independent of the vertical coordinate.

We can identify the (TE) and (TM) equations with the acoustic equations. In the (TE) case, the pressure field corresponds to the vertical component of the electric field and the particle velocity to the transverse part of the magnetic field, *i.e.*,

$$p \leftrightarrow E_3, \quad v \leftrightarrow -\mathrm{J}H, \quad \kappa \leftrightarrow \epsilon, \quad \text{and} \quad \rho \leftrightarrow \mu.$$

In the (TM) case, we identify the pressure field with the vertical component of the magnetic field intensity, the particle velocity with the transverse electric field intensity, *i.e.*,

$$p \leftrightarrow H_3, \quad v \leftrightarrow \mathrm{J}E, \quad \kappa \leftrightarrow \mu, \quad \text{and} \quad \rho \leftrightarrow \epsilon.$$

3.3 The Maxwell equations in one spatial dimension

Assume that the electromagnetic fields are independent of the transverse directions $x = (x_1, x_2)$, *e.g.*, $\boldsymbol{E} = E(x_3)$. The curl operator has the transverse part

$$-\partial_3 \mathrm{J}E. \tag{3.10}$$

The Maxwell equations reduce to

$$\begin{cases} s\epsilon(x_3,s)\widehat{E} + \partial_3\mathrm{J}\widehat{H} = -\widehat{J}(x_3,s) \\ s\mu(x_3,s)\mathrm{J}\widehat{H} + \partial_3\widehat{E} = -\mathrm{J}\widehat{J}^{(\mathrm{M})}(x_3,s) \end{cases} \tag{3.11}$$

where the second equation have been multiplied with the rotation matrix J. The corresponding one-dimensional acoustic wave equation is

$$\begin{cases} s\kappa\hat{p} + \partial_3\hat{v}_3 = \hat{q}, \\ s\rho\hat{v}_3 + \partial_3\hat{p} = \hat{f}_3. \end{cases} \tag{3.12}$$

The acoustic and electromagnetic equations are identified as

$$\widehat{E} \leftrightarrow \hat{p}, \quad \mathrm{J}\widehat{H} \leftrightarrow \hat{v}_3, \quad \epsilon \leftrightarrow \kappa, \quad \text{and} \quad \mu \leftrightarrow \rho.$$

Chapter 4

Wave splitting

With wave splitting (or directional decomposition) of a wave field we mean a full or partial decomposition of the wave field into wave constituents propagating in opposite directions. Wave splitting of electromagnetic and acoustic wave fields appear as a natural concept in many problems, *e.g.*, wave guide theory, Bremmer series, radiation conditions, absorbing boundary conditions, parabolic approximations, and inverse scattering.

We start with a brief introduction to wave-field decomposition in Section 4.1. In Section 4.2, we discuss different one-dimensional wave splittings. Section 4.3 treats energy flux wave splittings. Multi-dimensional wave splittings of acoustic and electromagnetic wave fields are considered in Sections 4.4 and 4.5, respectively.

4.1 Introduction

There are several alternative possibilities to split (or decompose) a wave field with respect to a direction. In this chapter, we discuss some aspects of the wave splitting. One of the most obvious motivations for wave splitting are in one-way wave propagation, *i.e.*, a wave field that evolves in one direction, *e.g.*, wave fields in guided structures [35]. It is also common to approximate numerically large problems with one-way problems. Typical electromagnetic applications are long range radio wave propagation, propagation of laser beams, and integrated optics [242, 57, 221, 126]. For the acoustic (and elastodynamic) wave fields there are applications in exploration geophysics [22, 34] and underwater acoustics [146, 76]. The Bremmer series accounts for the backscattered field that the one-way approximation neglects, see Refs [28, 39, 52, 242]. In the analysis of partial differential equations, wave splitting appears naturally in the analysis of boundary conditions [154], radiation conditions [193, 48] , and absorbing boundary conditions [63, 187, 66, 228]. Wave splitting is also a natural ingredient in inverse scattering problems, see [116] and Chapters 7 and 8.

To split a wave field with respect to a preferred direction $\boldsymbol{i}$ ($|\boldsymbol{i}| = 1$), it is natural to start with a decomposition of the spatial coordinate $\boldsymbol{x}$ into its component parallel to $\boldsymbol{i}$ and its components perpendicular to $\boldsymbol{i}$. The component in the direction $\boldsymbol{i}$ is

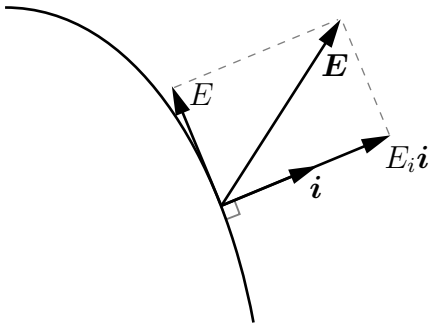

Figure 4.1: Decomposition of a vector field $\boldsymbol{E}$ into its tangential components E and normal component E_i with respect to the direction $\boldsymbol{i}$.

given by

$$x_i = \boldsymbol{i} \cdot \boldsymbol{x}$$

and the components perpendicular to $\boldsymbol{i}$ by

$$x = -\boldsymbol{i} \times (\boldsymbol{i} \times \boldsymbol{x}) = \boldsymbol{x} - \boldsymbol{i} x_i.$$

Observe that the transverse part x is a vector. In this thesis, we denote vector fields in $\mathbb{R}^3$ with bold face italics, *e.g.*, $\boldsymbol{x}$, and the corresponding transverse components by the symbol x, see Appendix A. In this notation the electric field is written

$$E_i = \boldsymbol{i} \cdot \boldsymbol{E} \quad \text{and} \quad E = -\boldsymbol{i} \times (\boldsymbol{i} \times \boldsymbol{E}) = \boldsymbol{E} - E_i \boldsymbol{i}, \tag{4.1}$$

see Figure 4.1.

It is not sufficient to decompose the vector fields into their components parallel and perpendicular to $\boldsymbol{i}$, it is also necessary to decompose the spatial differential operator into its component parallel to the direction $\boldsymbol{i}$ and its components perpendicular to $\boldsymbol{i}$, *i.e.*,

$$\partial_i = \boldsymbol{i} \cdot \nabla \quad \text{and} \quad \mathrm{D} = -\boldsymbol{i} \times (\boldsymbol{i} \times \nabla) = \nabla - \boldsymbol{i} \partial_i,$$

respectively. The cross product between a vector field and the preferred direction $\boldsymbol{i}$ is given by the rotation operator J (a rotation of $-\pi/2$ around i), *i.e.*,

$$\boldsymbol{i} \times \boldsymbol{E} = -\mathrm{J}E. \tag{4.2}$$

In many problems, the preferred direction is fixed. We choose this direction to be the vertical direction, *i.e.*, $\boldsymbol{i} = \boldsymbol{i}_3$. In this case the transverse part of the spatial differentiation operator ∇ and the transverse part of a vector field $\boldsymbol{E}$ are

$$\mathrm{D} = \begin{pmatrix} \partial_1 \\ \partial_2 \end{pmatrix} \quad \text{and} \quad E = \begin{pmatrix} E_1 \\ E_2 \end{pmatrix}, \tag{4.3}$$

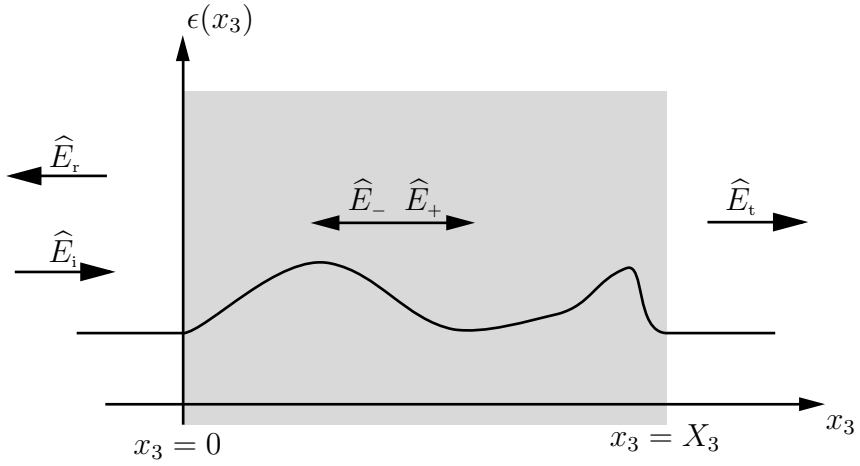

Figure 4.2: The scattering problem for a dielectric slab.

respectively, see also Sections 3.2 and 3.3. With the notation above, the Maxwell equations (2.1) are written

$$\begin{cases} \partial_t D + \partial_3 \mathrm{J} H - \mathrm{J}\,\mathrm{D}\,H_3 = -J(x, x_3, t), \\ \partial_t D_3 - \mathrm{D}^{\mathrm{T}}\,\mathrm{J} H = -J_3(x, x_3, t), \\ \partial_t B - \partial_3 \mathrm{J} E + \mathrm{J}\,\mathrm{D}\,E_3 = 0, \\ \partial_t B_3 + \mathrm{D}^{\mathrm{T}}\,\mathrm{J} E = 0, \end{cases} \tag{4.4}$$

where the rotation matrix J has the matrix representation

$$\mathrm{J} = \begin{pmatrix} 0 & 1 \\ -1 & 0 \end{pmatrix}. \tag{4.5}$$

4.2 One-dimensional wave splitting

The wave splitting concept is illustrated with electromagnetic scattering by a slab. Consider an incident plane wave impinging normally at the slab depicted in Figure 4.2. We assume that the fields are generated by sources to the left of the slab. Outside the slab, the wave field is decomposed into an incoming wave field $\widehat{E}_{\mathrm{i}}$ and a reflected wave field $\widehat{E}_{\mathrm{r}}$ to the left of the slab and a transmitted wave field $\widehat{E}_{\mathrm{t}}$ to the right of the slab. Here, $\hat{\cdot}$ denotes the Laplace transformed quantity. The wave fields outside the slab are hence decomposed into wave constituents propagating in the positive and negative directions. The wave splitting generalizes this directional decomposition to the wave fields in the interior of the slab.

Let the slab be modeled by a passive and isotropic medium, *i.e.*,

$$\widehat{\boldsymbol{D}}(\boldsymbol{x}, s) = \epsilon(x_3, s)\widehat{\boldsymbol{E}}(\boldsymbol{x}, s) \quad \text{and} \quad \widehat{\boldsymbol{B}}(\boldsymbol{x}, s) = \mu(x_3, s)\widehat{\boldsymbol{H}}(\boldsymbol{x}, s) \tag{4.6}$$

with scalar ϵ and μ. Outside the slab, the permittivity and permeability reduce to their free-space values, *i.e.*, $\epsilon(x_3, s) = 1$ and $\mu(x_3, s) = 1$, respectively. The wave

field is polarized in the $x = (x_1, x_2)$ plane, *i.e.*,

$$\widehat{\boldsymbol{E}}(\boldsymbol{x}, s) = \begin{pmatrix} \widehat{E}_1(x_3, s) \\ \widehat{E}_2(x_3, s) \\ 0 \end{pmatrix} \quad \text{and} \quad \widehat{\boldsymbol{H}}(\boldsymbol{x}, s) = \begin{pmatrix} \widehat{H}_1(x_3, s) \\ \widehat{H}_2(x_3, s) \\ 0 \end{pmatrix},$$

where $\widehat{E}$ and $\widehat{H}$ are the tangential parts of the electromagnetic fields (4.3). In this case, the Maxwell equations (4.4) reduce to a one-dimensional wave equation. The tangential components of the electric and magnetic fields satisfy the equations

$$\begin{cases} s\epsilon(x_3, s)\widehat{E} + \partial_3 \mathrm{J}\widehat{H} = 0, \\ s\mu(x_3, s)\mathrm{J}\widehat{H} + \partial_3 \widehat{E} = 0, \end{cases} \tag{4.7}$$

in a source-free environment. To decompose the wave field with respect to the vertical direction x_3, it is natural to rewrite the system (4.7) in the form of an evolution equation in x_3, *i.e.*,

$$\partial_3 \begin{pmatrix} \widehat{E} \\ \mathrm{J}\widehat{H} \end{pmatrix} + \begin{pmatrix} 0 & s\mu(x_3, s) \\ s\epsilon(x_3, s) & 0 \end{pmatrix} \begin{pmatrix} \widehat{E} \\ \mathrm{J}\widehat{H} \end{pmatrix} = \begin{pmatrix} 0 \\ 0 \end{pmatrix}. \tag{4.8}$$

We decompose the electromagnetic wave field into wave constituents propagating in the positive x_3-direction and negative x_3-direction, respectively. There are several different wave splittings. We start with a locally exact wave splitting in Section 4.2.1. Here, the wave field is decomposed at a point x_3 as if the medium parameters are independent of x_3, *i.e.*, we freeze the coordinate dependence and perform the wave splitting. The locally exact wave splitting decouples the wave fields in a homogeneous medium. In Section 4.2.2, the wave splitting is generalized to an approximate decomposition, *i.e.*, a wave splitting performed with respect to a reference medium. This splitting is not 'locally exact', however a proper choice of the reference medium reduces the coupling between the two wave constituents. Wave splitting in the time-domain is considered in Section 4.2.3. In the time-domain, it is advantageous to perform the splitting with respect to the instantaneous response of the medium, *i.e.*, the principal part of the partial differential equation.

4.2.1 Locally exact wave splitting

In the locally exact wave splitting, the wave field is decomposed as if the medium is independent of the spatial coordinates. The wave field is decomposed by a diagonalization of the system matrix of (4.8), *i.e.*, diagonalization of the matrix

$$\mathcal{A} = \begin{pmatrix} 0 & s\mu(x_3, s) \\ s\epsilon(x_3, s) & 0 \end{pmatrix}.$$

The eigenvalues of $\mathcal{A}$ are the square roots of the characteristic operator $A = s^2\epsilon\mu$, *i.e.*,

$$\pm\Gamma \quad \text{where} \quad \Gamma = \sqrt{s^2\epsilon\mu},$$

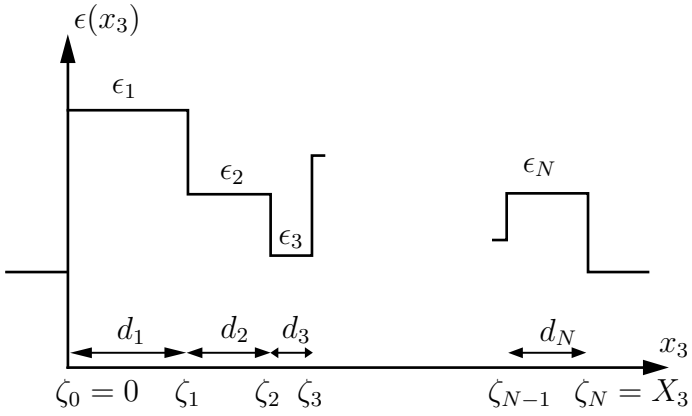

Figure 4.3: The geometry of a layered dielectric slab.

where we introduced the vertical-propagation operator Γ. We also use the vertical-propagation coefficient (symbol) $\gamma = \sqrt{s^2\epsilon\mu}$. The corresponding eigenvectors are given by

$$\alpha_1 \begin{pmatrix} \sqrt{\mu} \\ \sqrt{\epsilon} \end{pmatrix} \quad \text{and} \quad \alpha_2 \begin{pmatrix} \sqrt{\mu} \\ -\sqrt{\epsilon} \end{pmatrix}.$$

The eigenvectors are only determined up to a normalization. Depending on the choice of the normalization parameters α_1 and α_2 one gets different wave splittings. Three common normalizations are:

1. the electric-field normalization

$$\alpha_1 = \alpha_2 = \mu^{-1/2},$$

2. the magnetic-field normalization

$$\alpha_1 = \alpha_2 = \epsilon^{-1/2},$$

3. the energy-flux normalization

$$\alpha_1 = \alpha_2 = 1,$$

respectively, see Refs [52, 242]. In this thesis, we use the electric-field normalization. In the electric-field normalization, the down- and up-going wave constituents are given by

$$\begin{pmatrix} \widehat{E}_+ \\ \widehat{E}_- \end{pmatrix} = \frac{1}{2} \begin{pmatrix} 1 & \mathrm{Z} \\ 1 & -\mathrm{Z} \end{pmatrix} \begin{pmatrix} \widehat{E} \\ \mathrm{J}\widehat{H} \end{pmatrix}, \tag{4.9}$$

where $\mathrm{Z} = \sqrt{\mu/\epsilon}$ is the impedance, $\widehat{E}_+$ is the down-going wave constituent, and $\widehat{E}_-$ is the up-going wave constituent. The electric and magnetic fields are retrieved with the inverse of (4.9), *i.e.*,

$$\begin{pmatrix} \widehat{E} \\ \mathrm{J}\widehat{H} \end{pmatrix} = \begin{pmatrix} 1 & 1 \\ \mathrm{Y} & -\mathrm{Y} \end{pmatrix} \begin{pmatrix} \widehat{E}_+ \\ \widehat{E}_- \end{pmatrix}, \tag{4.10}$$

where $\mathrm{Y} = \mathrm{Z}^{-1}$ is the admittance. Substitution of (4.10) into the one-dimensional wave equation (4.8) gives a system of one-way wave equations. The split fields $\widehat{E}_\pm$ satisfy

$$\partial_3 \begin{pmatrix} \widehat{E}_+ \\ \widehat{E}_- \end{pmatrix} + \begin{pmatrix} \Gamma & 0 \\ 0 & -\Gamma \end{pmatrix} \begin{pmatrix} \widehat{E}_+ \\ \widehat{E}_- \end{pmatrix} = \mathrm{R} \begin{pmatrix} 1 & -1 \\ -1 & 1 \end{pmatrix} \begin{pmatrix} \widehat{E}_+ \\ \widehat{E}_- \end{pmatrix} \tag{4.11}$$

in a source-free region. In a homogeneous background, the reflection operator $\mathrm{R} = -\mathrm{Y}^{-1}\partial_3\mathrm{Y}/2$ vanishes and the system decouples. This is especially convenient for wave propagation in a layered medium. Let the permittivity and permeability be given by

$$\epsilon(x_3, s) = \epsilon_j(s) \quad \text{and} \quad \mu(x_3, s) = \mu_j(s) \quad \text{for} \quad \zeta_{j-1} \leq x_3 < \zeta_j,$$

where $0 = \zeta_0 < \zeta_1 < \cdots < \zeta_N = X_3$, see Figure 4.3. In each layer, the one-way system is decoupled. The solution of the one-way system (4.11) is given by

$$\begin{cases} \widehat{E}_+(\zeta_j-, s) = \widehat{E}_+(\zeta_{j-1}+, s)\mathrm{e}^{-\gamma_j d_j}, \\ \widehat{E}_-(\zeta_{j-1}+, s) = \widehat{E}_-(\zeta_j-, s)\mathrm{e}^{-\gamma_j d_j}, \end{cases}$$

where $d_j = \zeta_j - \zeta_{j-1}$ is the thickness of the layers, γ_j the vertical-propagation coefficient (symbol) in the layers, and $j = 1, \ldots, N$. The split fields are coupled at the interfaces between the layers. The coupling between the down- and up-going wave fields follows from the continuity of the tangential components of the electromagnetic field intensities. The coupling is given by

$$\begin{cases} \widehat{E}_+(\zeta_j+, s) = (1 + \mathrm{R}_j)\widehat{E}_+(\zeta_j-, s) - \mathrm{R}_j\widehat{E}_-(\zeta_j+, s), \\ \widehat{E}_-(\zeta_j-, s) = \mathrm{R}_j\widehat{E}_+(\zeta_j-, s) + (1 - \mathrm{R}_j)\widehat{E}_-(\zeta_j+, s), \end{cases}$$

where the reflection operator is

$$\mathrm{R}_j = (\mathrm{Y}_{j+1} + \mathrm{Y}_j)^{-1}(\mathrm{Y}_j - \mathrm{Y}_{j+1}) = (\mathrm{Z}_{j+1} + \mathrm{Z}_j)^{-1}(\mathrm{Z}_{j+1} - \mathrm{Z}_j), \tag{4.12}$$

see Figure 4.4.

4.2.2 Reference medium wave splitting

In Section 4.2.1, the wave splitting was performed with respect to the actual medium model. In some cases, it is advantageous to perform the splitting with respect to

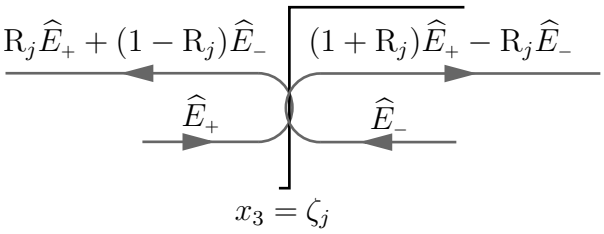

Figure 4.4: The boundary coupling between the split fields.

a reference medium, *e.g.*, a smooth background, a layered media, or free space. To simplify the notation, we consider materials with a homogeneous permeability. Decompose the wave field with respect to a permittivity $\epsilon'(x_3)$ (and permeability μ). The vertical propagation operator is given by $\Gamma = (s^2\epsilon'\mu)^{1/2}$. Following Section 4.2.1, we get a coupled set of one-way wave equations

$$\partial_3 \begin{pmatrix} \widehat{E}_+ \\ \widehat{E}_- \end{pmatrix} + \begin{pmatrix} \Gamma & 0 \\ 0 & -\Gamma \end{pmatrix} \begin{pmatrix} \widehat{E}_+ \\ \widehat{E}_- \end{pmatrix} = \begin{pmatrix} \mathrm{R}+\Xi & -\mathrm{R}+\Xi \\ -\mathrm{R}-\Xi & \mathrm{R}-\Xi \end{pmatrix} \begin{pmatrix} \widehat{E}_+ \\ \widehat{E}_- \end{pmatrix} \tag{4.13}$$

where R is the reflection operator and Ξ is the error in the approximation of the square root of A, *i.e.*,

$$\mathrm{R} = -\frac{\mathrm{Y}^{-1}\partial_3\mathrm{Y}}{2} = -\frac{\partial_3\epsilon'}{4\epsilon'} \quad \text{and} \quad \Xi = \frac{\Gamma - \Gamma^{-1}A}{2} = s\sqrt{\mu}\frac{\epsilon'-\epsilon}{2\sqrt{\epsilon'}},$$

respectively. Notice that the coupling is decomposed into the reflection part R and the error part Ξ. The error part contains the Laplace parameter s (the frequency). Hence, it is possible to reduce the size of the coupling by a proper choice of the reference medium, see Section 6.2.

4.2.3 Time-domain wave splitting

Time-domain wave splitting and its connection to one-dimensional inverse scattering have been extensively studied, see Section 7.2. Here, we outline a few properties of the time-domain wave splitting. Let the slab be modeled by an isotropic, passive, and non-magnetic model, *i.e.*,

$$\boldsymbol{D}(\boldsymbol{x},t) = \epsilon_\infty(\boldsymbol{x})\boldsymbol{E}(\boldsymbol{x},t) + \int_{-\infty}^{t} \chi(\boldsymbol{x},t-t')\boldsymbol{E}(\boldsymbol{x},t')\,\mathrm{d}t' \quad \text{and} \quad \boldsymbol{B}(\boldsymbol{x},t) = \mu\boldsymbol{H}(\boldsymbol{x},t).$$

In the time-domain, it is preferable to perform the wave splitting with respect to the instantaneous response $\epsilon_\infty(\boldsymbol{x})$ (and μ). Following Section 4.2.1, we get the time-domain counterpart of (4.9), *i.e.*, the down- and up-going wave constituents are defined as

$$\begin{pmatrix} E_+ \\ E_- \end{pmatrix} = \frac{1}{2}\begin{pmatrix} 1 & \mathrm{Z}_\infty \\ 1 & -\mathrm{Z}_\infty \end{pmatrix} \begin{pmatrix} E \\ JH \end{pmatrix} \tag{4.14}$$

where $\mathrm{Z}_\infty = \sqrt{\mu/\epsilon_\infty}$ is the wave-front impedance. The split fields satisfy the following system of coupled one-way equations

$$\partial_3 \begin{pmatrix} E_+ \\ E_- \end{pmatrix} + \partial_t \begin{pmatrix} c_\infty^{-1} & 0 \\ 0 & -c_\infty^{-1} \end{pmatrix} \begin{pmatrix} E_+ \\ E_- \end{pmatrix} = \frac{\partial_3 \epsilon_\infty}{4\epsilon_\infty} \begin{pmatrix} -1 & 1 \\ 1 & -1 \end{pmatrix} \begin{pmatrix} E_+ \\ E_- \end{pmatrix} - \frac{\sqrt{\mu}\partial_t \chi*}{2\sqrt{\epsilon_\infty}} \begin{pmatrix} 1 & 1 \\ -1 & -1 \end{pmatrix} \begin{pmatrix} E_+ \\ E_- \end{pmatrix} \quad (4.15)$$

where $c_\infty^{-1} = \sqrt{\epsilon_\infty \mu}$ is the wave-front slowness. Observe that the principal part of the one-way system is decoupled. The coupling is divided into a reflection part and a dispersive part due to the approximate wave splitting.

In numerical implementations it is convenient to scale the coordinates to travel-time coordinates and to use a state-variable representation of the dispersion, see Sections 7.2 and 2.7, respectively. The travel-time coordinates offer a good description of the wave front for calculation of the impulse response of a slab. The time-domain wave splitting appears natural in the invariant imbedding and Green function approaches to one-dimensional inverse scattering problems, see Sections 7.2.1 and 7.2.2, respectively.

The wave splitting concept has been generalized to several complex medium models, see the end of Section 7.2.2. It is also possible to perform a locally exact wave splitting (dispersive wave splitting) in the time-domain [61, 206]. This decomposition is practical for inverse scattering by a spatially homogeneous and temporally dispersive slab as well as for a time-domain theory of precursors [62, 141, 60]. Notice, that a locally exact time-domain wave splitting can give non-local operators even though the dispersive term has a local representation.

4.3 Energy-flux splitting

There are several generalizations of the one-dimensional wave splitting to multi-dimensions. In this section, we consider a generalization to bounded regions Ω where the energy flux through the surface $\partial\Omega$ is decomposed, see Figure 4.5. This decomposition is performed by a one-dimensional wave splitting with respect to the inward unit normal $\boldsymbol{i} = -\boldsymbol{n}$. The choice of inward normal implies that the input (output) energy corresponds to the positive (negative) $\boldsymbol{i}$-direction.

In Section 4.3.1, we consider frequency-domain wave splitting and in Section 4.3.2 the time-domain case is discussed.

4.3.1 Frequency-domain energy-flux wave splitting

The energy-flux wave splitting can be obtained from an energy analysis of the Maxwell equations. We get the energy balance from the Poynting's theorem [128, 176]

$$\nabla \cdot \widehat{\boldsymbol{E}} \times \widehat{\boldsymbol{H}}^* + s^* \widehat{\boldsymbol{E}} \cdot \widehat{\boldsymbol{D}}^* + s \widehat{\boldsymbol{H}}^* \cdot \widehat{\boldsymbol{B}} + \widehat{\boldsymbol{E}} \cdot \widehat{\boldsymbol{J}}^* = 0. \quad (4.16)$$

Integrate over the region Ω to get

$$\int_{\partial\Omega} \widehat{\boldsymbol{E}} \times \widehat{\boldsymbol{H}}^* \cdot \boldsymbol{n} \, \mathrm{dS} + \int_\Omega s^* \widehat{\boldsymbol{E}} \cdot \widehat{\boldsymbol{D}}^* + s \widehat{\boldsymbol{H}}^* \cdot \widehat{\boldsymbol{B}} \, \mathrm{dV} + \int_\Omega \widehat{\boldsymbol{E}} \cdot \widehat{\boldsymbol{J}}^* \, \mathrm{dV} = 0.$$

The energy flux through the surface $\partial\Omega$ is given by the real-valued part of the normal component of the Poynting vector, *i.e.*,

$$\frac{1}{2} \operatorname{Re}\{\widehat{\boldsymbol{E}} \times \widehat{\boldsymbol{H}}^* \cdot \boldsymbol{n}\} = -\frac{1}{2} \operatorname{Re} \widehat{E} \cdot \mathrm{J}\widehat{H}^*,$$

where J is the rotation operator (4.2) and the tangential fields are defined with respect to the direction $\boldsymbol{i} = -\boldsymbol{n}$. To get the energy-flux wave splitting, the energy flux is decomposed into two parts with definite signs. Let the impedance Z be real-valued and positive, and use the polarization identity to get

$$\frac{1}{2} \operatorname{Re} \widehat{E} \cdot \mathrm{J}\widehat{H}^* = \frac{1}{2\mathrm{Z}} \left| \frac{\widehat{E} + \mathrm{Z}\mathrm{J}\widehat{H}}{2} \right|^2 - \frac{1}{2\mathrm{Z}} \left| \frac{\widehat{E} - \mathrm{Z}\mathrm{J}\widehat{H}}{2} \right|^2 .$$

The positive and negative terms can be interpreted as the energy-flux input and energy-flux output of the region, respectively. Define the in-going $\widehat{E}_+$ and out-going $\widehat{E}_-$ wave constituents as

$$\begin{pmatrix} \widehat{E}_+ \\ \widehat{E}_- \end{pmatrix} = \frac{1}{2} \begin{pmatrix} 1 & \mathrm{Z} \\ 1 & -\mathrm{Z} \end{pmatrix} \begin{pmatrix} \widehat{E} \\ \mathrm{J}\widehat{H} \end{pmatrix} . \tag{4.17}$$

The energy balance is

$$\widehat{\mathcal{E}}(s) + \widehat{\mathcal{E}}_-(s) = \widehat{\mathcal{E}}_+(s) - \operatorname{Re} \frac{1}{2} \int_\Omega \widehat{\boldsymbol{E}}(\boldsymbol{x}, s) \cdot \widehat{\boldsymbol{J}}^*(\boldsymbol{x}, s) \, \mathrm{dV} \tag{4.18}$$

where $\widehat{\mathcal{E}}$ is the energy in the region Ω, *i.e.*,

$$\widehat{\mathcal{E}}(s) = \operatorname{Re} \frac{1}{2} \int_\Omega \widehat{\boldsymbol{E}}^*(\boldsymbol{x}, s) \cdot s\widehat{\boldsymbol{D}}(\boldsymbol{x}, s) + \widehat{\boldsymbol{H}}^*(\boldsymbol{x}, s) \cdot s\widehat{\boldsymbol{B}}(\boldsymbol{x}, s) \, \mathrm{dV} \tag{4.19}$$

and $\widehat{\mathcal{E}}_\pm(s)$ are the inward and outward energy flux

$$\widehat{\mathcal{E}}_\pm(s) = \frac{1}{2} \int_{\partial\Omega} \frac{1}{\mathrm{Z}} |\widehat{E}_\pm(\boldsymbol{x}, s)|^2 \, \mathrm{dS} \, .$$

First, we observe that the energy-flux wave splitting (4.17) reduces to the one-dimensional wave splitting (4.9) if $\boldsymbol{i} = \boldsymbol{i}_3$. This lets us interpret the energy-flux wave splitting as a locally exact wave splitting with respect to the inward unit normal in one dimension. Secondly, we observe that in the case of a spherical region $\Omega = \{\boldsymbol{x} : |\boldsymbol{x}| \leq r\}$ and a vacuum background, the wave splitting reduces to the (Silver-Müller) radiation condition, *i.e.*,

$$\widehat{\mathcal{E}}_+(s) \to 0 \quad \text{as} \quad r \to \infty$$

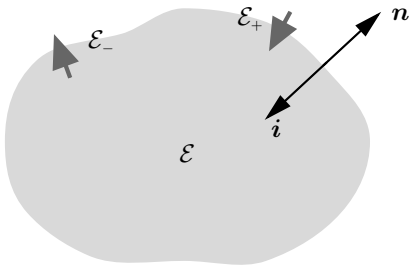

Figure 4.5: The energy-flux splitting.

or equivalently (with $\boldsymbol{i} = -\boldsymbol{r}$)

$$\widehat{E}_+(r,s) = \frac{\widehat{E}(r,s) + \mathrm{Z}_0 \mathrm{J}\widehat{H}(r,s)}{2} = \frac{\widehat{E}(r,s) + \boldsymbol{r} \times \mathrm{Z}_0 \widehat{H}(r,s)}{2} = \mathrm{o}(r^{-1}) \quad \text{as} \quad r \to \infty,$$

where $r = |\boldsymbol{x}|$ and $\boldsymbol{r} = \boldsymbol{x}/r$.

Notice that the energy balance (4.18) is valid for arbitrary bi-anisotropic medium models (2.17). Finally, the requirement of passive medium models gives an L^2-bound on the map

$$\widehat{E}_+ \longrightarrow \widehat{E}_-,$$

e.g., for a source-free region the output energy is bounded by the input energy

$$\int_{\partial\Omega} |\widehat{E}_-(\boldsymbol{x},s)|^2 \,\mathrm{dS} \leq \int_{\partial\Omega} |\widehat{E}_+(\boldsymbol{x},s)|^2 \,\mathrm{dS}\,.$$

4.3.2 Time-domain energy-flux wave splitting

It is straightforward to generalize the energy-flux wave splitting (4.17) to the time-domain. As in the one-dimensional wave splitting in Section 4.2.3 it is natural to decompose the wave field with respect to the instantaneous response. Let $\boldsymbol{E}(\boldsymbol{x},t)$ and $\boldsymbol{H}(\boldsymbol{x},t)$ be given at the surface $\partial\Omega$ and assume that the medium is isotropic with the instantaneous permittivity $\epsilon_\infty(\boldsymbol{x})$ and the permeability $\mu_\infty(\boldsymbol{x})$. We define the tangential split fields with respect to the inward unit normal $\boldsymbol{i} = -\boldsymbol{n}$ as

$$E_\pm(\boldsymbol{x},t) = \frac{-\boldsymbol{n} \times (\boldsymbol{n} \times \boldsymbol{E}) \mp \mathrm{Z}_\infty \boldsymbol{n} \times \boldsymbol{H}}{2} = \frac{E \pm \mathrm{Z}_\infty \mathrm{J} H}{2}, \tag{4.20}$$

where $\mathrm{Z}_\infty(\boldsymbol{x})$ is the instantaneous part of the impedance, *i.e.*, $\mathrm{Z}_\infty = \sqrt{\mu_\infty/\epsilon_\infty}$ and the tangential fields E and H are defined in (4.1). As in the frequency domain (4.17), the time-domain wave splitting (4.20) is a natural component in energy estimates. The Poynting vector in the forward direction can be decomposed as

$$\boldsymbol{n} \cdot (\boldsymbol{E} \times \boldsymbol{H}) = \frac{1}{\mathrm{Z}_\infty} \left| \frac{E - \mathrm{Z}_\infty \mathrm{J} H}{2} \right|^2 - \frac{1}{\mathrm{Z}_\infty} \left| \frac{E + \mathrm{Z}_\infty \mathrm{J} H}{2} \right|^2 = \frac{E_-^2 - E_+^2}{\mathrm{Z}_\infty} \tag{4.21}$$

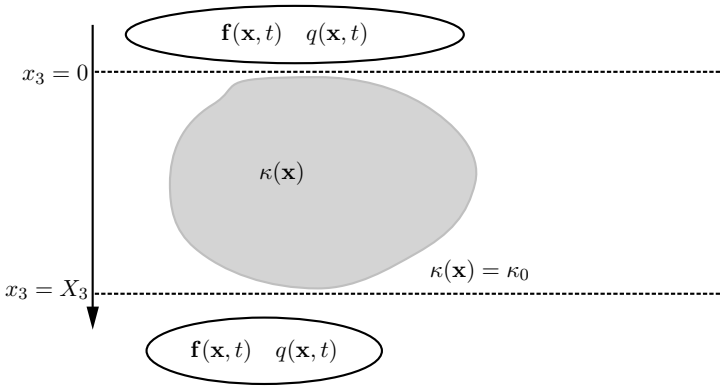

Figure 4.6: The acoustic scattering geometry.

This gives the energy balance

$$\mathcal{E}(T) + \mathcal{E}_-(T) = \mathcal{E}(0) + \mathcal{E}_+(T) - \int_0^T \int_\Omega \boldsymbol{E}(\boldsymbol{x},t) \cdot \boldsymbol{J}(\boldsymbol{x},t) \,\mathrm{dV}\,\mathrm{d}t. \tag{4.22}$$

Where the energy $\mathcal{E}$ in the region Ω is defined as

$$\mathcal{E}(T) = \mathcal{E}(0) + \int_0^T \int_\Omega \boldsymbol{E}(\boldsymbol{x},t) \cdot \partial_\tau \boldsymbol{D}(\boldsymbol{x},t) + \boldsymbol{H}(\boldsymbol{x},t) \cdot \partial_\tau \boldsymbol{B}(\boldsymbol{x},t) \,\mathrm{dV}\,\mathrm{d}t$$

and the energy input and output through the surface $\partial\Omega$ as

$$\mathcal{E}_\pm(T) = \int_0^T \int_{\partial\Omega} |E_\pm(\boldsymbol{x},t)|^2 \mathrm{Y}_\infty \,\mathrm{dS}\,\mathrm{d}t$$

with the instantaneous admittance $\mathrm{Y}_\infty = \mathrm{Z}_\infty^{-1}$. The time-domain energy-flux wave splitting (4.20) appears natural in the study of the boundary conditions for symmetric hyperbolic systems of partial differential equations [154]. Furthermore, it offers a simple FDTD implementation of the boundary conditions, see Section 5.5.1. In this thesis, the time-domain wave splitting (4.20) is used in the formulation of the multi-dimensional inverse scattering problems, see Chapter 8.

4.4 Acoustic equation

In this section, we consider multi-dimensional wave splittings of an acoustic wave field with respect to the depth direction x_3. Let the medium be modeled by a temporally dispersive compressibility $\kappa(\boldsymbol{x}, s)$ and a homogeneous and non-dispersive density $\rho = \rho_0$. The Laplace transformed version of the acoustic equation (3.1) is

$$\begin{cases} s\kappa(\boldsymbol{x},s)\hat{p}(\boldsymbol{x},s) + \nabla \cdot \hat{\boldsymbol{v}}(\boldsymbol{x},s) = \hat{q}(\boldsymbol{x},s), \\ s\rho_0\hat{\boldsymbol{v}}(\boldsymbol{x},s) \;+\; \nabla\hat{p}(\boldsymbol{x},s) \;= \hat{\boldsymbol{f}}(\boldsymbol{x},s). \end{cases} \tag{4.23}$$

To ensure causality, the compressibility $\kappa(\boldsymbol{x}, s)$ is an analytic function of s in the right complex half plane. Furthermore, we restrict the analysis to passive dispersive models, *i.e.*,

$$\operatorname{Re}\{s\kappa(\boldsymbol{x}, s)\} \geq \kappa_0 \operatorname{Re} s = \kappa_0 \eta, \tag{4.24}$$

see Section 2.3 and (2.43). For simplicity, we assume that $\kappa(\boldsymbol{x}, s)$ depends smoothly on the spatial coordinate $\boldsymbol{x}$. Observe that the first order system (4.23) corresponds to a second order wave equation in the pressure, *i.e.*,

$$s^2\hat{p} - c^2(\boldsymbol{x}, s)\nabla^2\hat{p} = s\rho_0 c^2\hat{q} - c^2\nabla\cdot\hat{\boldsymbol{f}}, \tag{4.25}$$

where c is the speed $c(\boldsymbol{x}, s) = (\kappa(\boldsymbol{x}, s)\rho_0)^{-1/2}$.

In Section 4.4.1, a formal wave splitting of the acoustic wave field is introduced. An exact wave splitting is performed for the case of layered media in Section 4.4.2. Approximate wave splittings are discussed in Sections 4.4.3 to 4.4.5 with a local approximation, pseudo-differential calculus, and a paraxial approximation, respectively. In Section 4.4.6, a time-domain wave splitting is outlined.

4.4.1 Acoustic multi-dimensional wave splitting

Write the Laplace transformed system (4.23) as an evolution equation in the preferred direction x_3

$$(\partial_3 + \mathcal{A})\hat{w} = \hat{g}. \tag{4.26}$$

The system matrix $\mathcal{A}$ is

$$\mathcal{A} = \begin{pmatrix} 0 & s\rho_0 \\ -\mathrm{D}^{\mathrm{T}}(s^{-1}\rho_0^{-1}\mathrm{D}) + s\kappa(x, x_3, s) & 0 \end{pmatrix}, \tag{4.27}$$

and the field vector $\hat{w}$ and source vector $\hat{g}$ are

$$\hat{w} = \begin{pmatrix} \hat{p} \\ \hat{v}_3 \end{pmatrix} \quad \text{and} \quad \hat{g} = \begin{pmatrix} \hat{f}_3 \\ \hat{q} + \mathrm{D}^{\mathrm{T}}(\rho_0^{-1}s^{-1}\hat{f}) \end{pmatrix},$$

respectively. The problem (4.26) is not well-posed for marching in the x_3 direction, but it is possible to decompose the system (4.26) into two parts, one propagating in the positive x_3-direction and the other propagation in the negative x_3-direction. We decompose the system by formally diagonalizing the system matrix (4.27). The diagonalization operator is only determined up to a normalization. Here we use the acoustic-pressure normalization [52]. The diagonal elements are the square roots of the characteristic operator

$$\mathrm{A} = -\partial_1^2 - \partial_2^2 + s^2\kappa(x, x_3, s)\rho_0 = -\mathrm{D}^2 + s^2 c^{-2}(x, x_3, s). \tag{4.28}$$

In general, it is difficult to determine an exact square root, so instead, we determine an approximate square root of A.

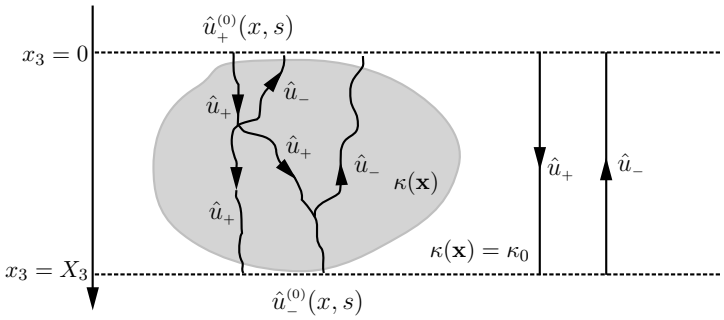

Figure 4.7: The one-way acoustic scattering geometry.

Let Γ be an operator such that the difference $\mathrm{A} - \Gamma^2$ is small. We call Γ the vertical-propagation operator for the acoustic wave equation. Let Ξ denote the error in the approximation of the square-root operator, *i.e.*,

$$\Xi = (\Gamma - \Gamma^{-1}\mathrm{A})/2. \tag{4.29}$$

We construct approximations of $\mathrm{A}^{1/2}$, such that Ξ is small in a general medium and vanishes identically in a homogeneous medium. In the acoustic-pressure normalization, the composition operator L and the decomposition operator L^{-1} are defined as

$$\mathrm{L} = \begin{pmatrix} 1 & 1 \\ (s\rho_0)^{-1}\Gamma & -(s\rho_0)^{-1}\Gamma \end{pmatrix} \quad \text{and} \quad \mathrm{L}^{-1} = \frac{1}{2}\begin{pmatrix} 1 & s\rho_0\Gamma^{-1} \\ 1 & -s\rho_0\Gamma^{-1} \end{pmatrix},$$

respectively. The decomposition operator L^{-1} defines the down- and up-going components $\hat{u} = (\hat{u}_+, \hat{u}_-)^{\mathrm{T}}$ of the wave field, *i.e.*,

$$\begin{pmatrix} \hat{u}_+ \\ \hat{u}_- \end{pmatrix} = \frac{1}{2}\begin{pmatrix} 1 & s\rho_0\Gamma^{-1} \\ 1 & -s\rho_0\Gamma^{-1} \end{pmatrix}\begin{pmatrix} \hat{p} \\ \hat{v}_3 \end{pmatrix},$$

see also Figure 4.7. We substitute $\hat{w} = \mathrm{L}\hat{u}$ into the dynamics (4.26) to get

$$(\partial_3 \mathrm{L} + \mathcal{A}\mathrm{L})\hat{u} = \hat{g}.$$

A multiplication with the decomposition operator and the use of the relation $\partial_3 \mathrm{L} = (\partial_3 \mathrm{L}) + \mathrm{L}\partial_3$ give

$$(\partial_3 + \mathrm{L}^{-1}\mathcal{A}\mathrm{L})\hat{u} = -\mathrm{L}^{-1}(\partial_3 \mathrm{L})\hat{u} + \mathrm{L}^{-1}\hat{g}.$$

The principal part of the equation is now decomposed as

$$\mathrm{L}^{-1}\mathcal{A}\mathrm{L} = \frac{1}{2}\begin{pmatrix} \Gamma + \Gamma^{-1}\mathrm{A} & -\Gamma + \Gamma^{-1}\mathrm{A} \\ \Gamma - \Gamma^{-1}\mathrm{A} & -\Gamma - \Gamma^{-1}\mathrm{A} \end{pmatrix} = \begin{pmatrix} \Gamma & 0 \\ 0 & -\Gamma \end{pmatrix} + \begin{pmatrix} -\Xi & -\Xi \\ \Xi & \Xi \end{pmatrix},$$

and we see that the principle part decouples if Ξ is of lower order than Γ. In the region $0 \le x_3 \le X_3$, the decomposed fields $\hat{u}$ satisfy the source free one-way system of equations

$$\partial_3 \begin{pmatrix} \hat{u}_+ \\ \hat{u}_- \end{pmatrix} + \begin{pmatrix} \Gamma & 0 \\ 0 & -\Gamma \end{pmatrix}\begin{pmatrix} \hat{u}_+ \\ \hat{u}_- \end{pmatrix} = \begin{pmatrix} \mathrm{R} + \Xi & -\mathrm{R} + \Xi \\ -\mathrm{R} - \Xi & \mathrm{R} - \Xi \end{pmatrix}\begin{pmatrix} \hat{u}_+ \\ \hat{u}_- \end{pmatrix}, \tag{4.30}$$

where $\mathrm{R} = -\Gamma^{-1}\partial_3\Gamma/2$. We also use the matrix-valued interaction operator $\mathcal{R}$ defined as

$$\mathcal{R} = \begin{pmatrix} \mathrm{R}_{1,1} & \mathrm{R}_{1,2} \\ \mathrm{R}_{2,1} & \mathrm{R}_{2,2} \end{pmatrix} = \mathrm{R} \begin{pmatrix} 1 & -1 \\ -1 & 1 \end{pmatrix} + \Xi \begin{pmatrix} 1 & 1 \\ -1 & -1 \end{pmatrix}. \tag{4.31}$$

The boundary conditions for the one-way wave equation (4.30) are

$$\hat{u}_+(x,0) = \hat{u}_+^{(0)}(x) \quad \text{and} \quad \hat{u}_-(x,X_3) = \hat{u}_-^{(0)}(x), \tag{4.32}$$

where the boundary terms are obtained from the solution of the one-way problem (4.30) in free space. In free space, the vertical-propagation operator Γ reduces to multiplication with the free space vertical-propagation symbol

$$\gamma_0(\xi, s) = \sqrt{c_0^{-2}s^2 + \xi^2},$$

in the spatial Fourier domain, *i.e.*,

$$\Gamma_0\hat{u}(x) = \frac{1}{4\pi^2}\int_{y\in\mathbb{R}^2}\int_{\xi\in\mathbb{R}^2} \gamma_0(\xi,s)\mathrm{e}^{\mathrm{i}\xi\cdot(x-y)}\hat{u}(y)\,\mathrm{d}y\,\mathrm{d}\xi. \tag{4.33}$$

The solution is

$$\begin{cases} \hat{u}_+^{(0)}(x) = \dfrac{1}{4\pi^2}\displaystyle\int_{x_3=-\infty}^{0}\int_{\xi\in\mathbb{R}^2}\int_{y\in\mathbb{R}^2} \mathrm{e}^{\mathrm{i}\xi\cdot(x-y)}\mathrm{e}^{\gamma_0 x_3}\hat{h}_+(y)\,\mathrm{d}y\,\mathrm{d}\xi\,\mathrm{d}x_3, \\ \hat{u}_-^{(0)}(x) = \dfrac{1}{4\pi^2}\displaystyle\int_{x_3=X_3}^{\infty}\int_{\xi\in\mathbb{R}^2}\int_{y\in\mathbb{R}^2} \mathrm{e}^{\mathrm{i}\xi\cdot(x-y)}\mathrm{e}^{-\gamma_0 x_3}\hat{h}_-(y)\,\mathrm{d}y\,\mathrm{d}\xi\,\mathrm{d}x_3, \end{cases}$$

where $\hat{h}_\pm$ are the down- and up-going part of the source, *i.e.*,

$$\hat{h}_+ = (\hat{g}_1 + s\rho_0\Gamma_0^{-1}\hat{g}_2)/2 \quad \text{and} \quad \hat{h}_- = (\hat{g}_1 - s\rho_0\Gamma_0^{-1}\hat{g}_2)/2,$$

respectively.

4.4.2 Layered media

Before we try to determine an appropriate representation of the vertical-propagation operator in a general medium, we consider a layered structure. Let the compressibility be given by

$$\kappa(x, x_3, s) = \kappa_j(s) \quad \text{for} \quad \zeta_{j-1} \le x_3 < \zeta_j$$

where $0 = \zeta_0 < \ldots < \zeta_N = X_3$. In each layer, the vertical-propagation operator Γ_j reduces to a multiplication with the vertical-propagation symbol

$$\gamma_j(\xi, s) = \sqrt{\rho_0\kappa_j(s)s^2 + \xi^2},$$

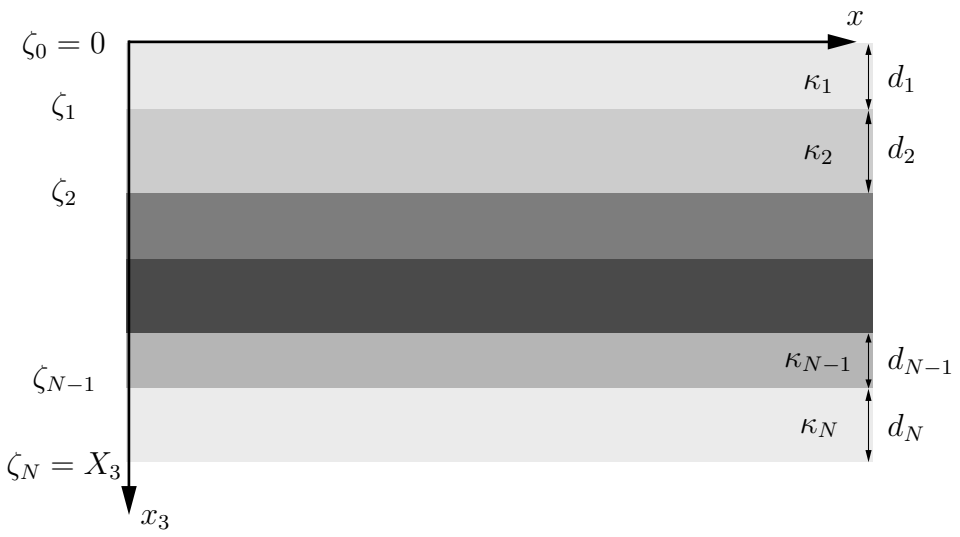

Figure 4.8: The acoustic scattering geometry for a layered medium.

in the spatial Fourier domain, *i.e.*,

$$\Gamma_j \hat{u}(x, x_3, s) = \frac{1}{4\pi^2} \int_{y\in\mathbb{R}^2} \int_{\xi\in\mathbb{R}^2} \gamma_j(\xi, s) \mathrm{e}^{\mathrm{i}\xi\cdot(x-y)} \hat{u}(y, x_3, s) \, \mathrm{d}y \, \mathrm{d}\xi. \tag{4.34}$$

In the interior of a layer, the one-way wave equation (4.30) decouples. The solution of the one-way wave equation in a layer is

$$\begin{cases} \hat{u}_+(x, \zeta_j-, s) &= \dfrac{1}{4\pi^2} \displaystyle\int_{\xi\in\mathbb{R}^2} \int_{y\in\mathbb{R}^2} \mathrm{e}^{\mathrm{i}\xi\cdot(x-y)} \mathrm{e}^{-\gamma_j(\xi,s)d_j} \hat{u}_+(y, \zeta_{j-1}+, s) \, \mathrm{d}y \, \mathrm{d}\xi, \\ \hat{u}_-(x, \zeta_{j-1}+, s) &= \dfrac{1}{4\pi^2} \displaystyle\int_{\xi\in\mathbb{R}^2} \int_{y\in\mathbb{R}^2} \mathrm{e}^{\mathrm{i}\xi\cdot(x-y)} \mathrm{e}^{-\gamma_j(\xi,s)d_j} \hat{u}_-(y, \zeta_j-, s) \, \mathrm{d}y \, \mathrm{d}\xi, \end{cases}$$

where $d_j = \zeta_j - \zeta_{j-1}$, $j = 1, \ldots, N$ is the thickness of the layers, see Figure 4.8. The down- and up-going wave constituents are coupled at the interfaces of the layers. The coupling is given by

$$\begin{cases} \hat{u}_+(x, \zeta_j+, s) = (1 + \mathrm{R}_j)\hat{u}_+(x, \zeta_j-, s) - \mathrm{R}_j \hat{u}_-(x, \zeta_j+, s) \\ \hat{u}_-(x, \zeta_j-, s) = \mathrm{R}_j \hat{u}_+(x, \zeta_j-, s) + (1 - \mathrm{R}_j)\hat{u}_-(x, \zeta_j+, s) \end{cases}$$

where the reflection operator is

$$\mathrm{R}_j = (\Gamma_j + \Gamma_{j+1})^{-1}(\Gamma_j - \Gamma_{j+1}). \tag{4.35}$$

The transmission part is given by the familiar $1 + \mathrm{R}_j = (\Gamma_j + \Gamma_{j+1})^{-1} 2\Gamma_j$, see also Figure 4.4. Just as the one-dimensional reflection operator (4.12), the reflection operator (4.35) is bounded.

4.4.3 Local approximation

In this section, we consider a local approximation of the square-root operator. We restrict the analysis to passive medium models (4.24) with a homogeneous instantaneous response, *i.e.*,

$$\kappa(\boldsymbol{x}, s) - \kappa_0 = \mathrm{O}(s^{-2}) \quad \text{as } s \to \infty. \tag{4.36}$$

It is convenient to write the compressibility (4.36) as a perturbation of free space

$$\kappa(\boldsymbol{x}, s) = \kappa_0 + \delta\psi(\boldsymbol{x}, s)s^{-2}$$

where $\psi(\boldsymbol{x}, s)$ is uniformly bounded in $\boldsymbol{x}$ and s for $\operatorname{Re} s \geq \beta_0 > 0$. The parameter δ determines the size of the perturbation.

The local approximation of the square-root operator is determined as the square root of a locally homogeneous medium, *i.e.*, freeze the coordinate dependence and define the square root with Fourier calculus. This gives a left-symbol representation of the vertical-propagation operator, *i.e.*, the operator is defined as the action of the integral

$$(\Gamma_{\mathrm{L}}\hat{u})(x, s) = \frac{1}{4\pi^2}\int_{\xi\in\mathbb{R}^2}\int_{y\in\mathbb{R}^2} \gamma_{\mathrm{L}}(x, \xi, s)\mathrm{e}^{\mathrm{i}(x-y)\cdot\xi}\hat{u}(y, s)\,\mathrm{d}y\,\mathrm{d}\xi,$$

where $\gamma_{\mathrm{L}}(x, \xi, s)$ is the local vertical-propagation symbol (or coefficient)

$$\gamma_{\mathrm{L}}(x, \xi, s) = \sqrt{c^{-2}(x, s)s^2 + \xi^2} = \sqrt{c_0^{-2}s^2 + \xi^2 + \delta\psi(x, s)}\,. \tag{4.37}$$

Here and in the following, the dependence of the vertical coordinate x_3 is suppressed. The local vertical-propagation operator Γ_{L} is a classical pseudo-differential operator for fixed s, see Section 4.4.4. Here, we use the dispersive property (4.36) to analyze the vertical propagation operator and to get uniform estimates for s in a half-plane $\operatorname{Re} s \geq \eta_0 > 0$.

We start with some properties of the free-space vertical-propagation operator defined in (4.33). The real-valued part of s is a lower bound of the real-valued part of γ_0, *i.e.*, $\operatorname{Re}\gamma_0 \geq c_0^{-1}\eta$. Fourier calculus gives a similar lower bound on the symmetric part of the free-space vertical-propagation operator

$$\operatorname{Re}\Gamma_0 \geq c_0^{-1}\eta, \tag{4.38}$$

and an upper bound on the inverse

$$\|\Gamma_0^{-1}\| \leq c_0\eta^{-1}.$$

We expand the vertical-propagation operator Γ_{L} in the free space vertical-propagation operator Γ_0. Extract the free-space symbol $\gamma_0(\xi, s)$ from the symbol (4.37)

$$\gamma_{\mathrm{L}}(x, \xi, s) = \gamma_0(\xi, s)\sqrt{1 + \delta\gamma_0^{-2}(\xi, s)\psi(x, s)}\,.$$

The symbol ψ contains all inhomogeneous and dispersive parts and it is uniformly bounded in x, x_3, and s. For sufficiently large values of η, we can expand the symbol in the binomial series

$$\gamma_{\mathrm{L}}(x,\xi,s) = \gamma_0(\xi,s) + \sum_{n=1}^{\infty} \binom{1/2}{n} \delta^n \psi^n(x,s) \gamma_0^{1-2n}(\xi,s).$$

Use the linearity of the left symbol and the left-symbol composition rule

$$(\Psi\Gamma_0\hat{u})(x,s) = \frac{1}{4\pi^2} \int_{\xi\in\mathbb{R}^2} \int_{y\in\mathbb{R}^2} \mathrm{e}^{\mathrm{i}\xi\cdot(x-y)} \psi(x,s)\gamma_0(\xi,s)\hat{u}(y,s)\,\mathrm{d}y\,\mathrm{d}\xi,$$

where Ψ is the multiplicative operator associated with the symbol ψ, *i.e.*, $\Psi = \psi$. The vertical-propagation operator is

$$\Gamma_{\mathrm{L}} = \Gamma_0 + \sum_{n=1}^{\infty} \binom{1/2}{n} \delta^n \Psi^n \Gamma_0^{1-2n} = \Gamma_0 + \frac{\delta}{2}\Psi\Gamma_0^{-1} + \mathrm{O}(\delta^2/\eta^3) \tag{4.39}$$

where $\mathrm{O}(\delta^k/\eta^l)$ denotes an operator of the size $\delta^k\Psi^k\Gamma_0^{-l}$, *i.e.*, there is a constant C' such that

$$\|\,\mathrm{O}(\delta^k/\eta^l)\| \le C'\delta^k\eta^{-l}.$$

Use (4.39) and the coercivity, (4.38), to get the estimate

$$\mathrm{Re}\,\Gamma_{\mathrm{L}} \ge c_0^{-1}\eta/2 \tag{4.40}$$

for sufficiently large values of η. The inverse of the vertical propagation operator Γ_{L}^{-1} is

$$\begin{aligned} \Gamma_{\mathrm{L}}^{-1} &= \left(1 + \Gamma_0^{-1}\Psi\Gamma_0^{-1}\delta/2 + \mathrm{O}(\delta^2/\eta^4)\right)^{-1}\Gamma_0^{-1} \\ &= \Gamma_0^{-1} - \Gamma_0^{-1}\Psi\Gamma_0^{-2}\delta/2 + \mathrm{O}(\delta^2/\eta^5). \end{aligned} \tag{4.41}$$

Notice that the vertical-propagation operator is a perturbation of the free-space vertical-propagation operator, *i.e.*, $\Gamma_{\mathrm{L}} \sim \Gamma_0$ for large η.

The representations (4.39) and (4.41) are used to derive uniform estimates on the operators in Section 4.4.1. The error term Ξ of the square-root approximation (4.29) is

$$\Xi_{\mathrm{L}} = (\Gamma_{\mathrm{L}} - \Gamma_{\mathrm{L}}^{-1}\mathcal{A})/2 = \delta(\Psi\Gamma_0^{-1} - \Gamma_0^{-1}\Psi)/4 + \mathrm{O}(\delta^2/\eta^3).$$

The reflection operator (4.31) is estimated as

$$\begin{aligned} \Gamma_{\mathrm{L}}^{-1}\partial_3\Gamma_{\mathrm{L}} &= \left(\Gamma_0^{-1} - \Gamma_0^{-1}\Psi\Gamma_0^{-2}\delta/2 + \mathrm{O}(\delta^2/\eta^4)\right)\left(\partial_3\Psi\Gamma_0\delta + \mathrm{O}(\delta^2/\eta^3)\right) \\ &= \delta\Gamma_0^{-1}\partial_3\Psi\Gamma_0^{-1} + \mathrm{O}(\delta^2/\eta^3). \end{aligned}$$

Finally, we get a uniform bound on the interaction operator $\mathcal{R}_{\mathrm{L}}$, *i.e.*, there is a constant C such that

$$\|\mathcal{R}_{\mathrm{L}}\| \le C\delta\eta^{-1} \quad \text{for all } x_3 \text{ and } s \text{ such that } \mathrm{Re}\,s \ge \eta_0 \tag{4.42}$$

with η_0 sufficiently large. Notice that it would be sufficient to use the free-space vertical-propagation operator in the approximate wave decomposition to get estimates (4.40) and (4.42).

4.4.4 Pseudo-differential calculus

Pseudo-differential calculus offers a mathematical technique that can be used to represent and analyze the operators in the one-way wave equation (4.30) and to define an asymptotic expansion of the square-root operator. For a general discussion of pseudo-differential operators see *e.g.*, Refs [125, 214, 101, 5, 233, 235].

Pseudo-differential analysis of the square-root operator for fixed frequencies have been discussed by Fishman *et al.*, in a number of papers [75, 76, 80, 82, 81, 79]. A recent approach to improve the square-root approximation is the uniform asymptotic expansion [78, 54]. For a few special structures it is possible to find an analytical representation of the square-root operator [77, 76]. In [52], de Hoop used pseudo-differential calculus to analyze the square-root operator $\mathrm{A}^{1/2}$ and its applications in Bremmer series for the case of real-valued values of the Laplace parameter, *i.e.*, $s = \eta \geq \eta_0 > 0$. A generalization to anisotropic material is discussed by Jonsson and de Hoop in Ref. [131].

We start with a brief discussion of approximations of the square-root operator for a fixed value of the Laplace parameter s and a fixed depth x_3. In the following we often suppress the s and x_3 parameters.

We consider left-symbol representations of the pseudo-differential operators, *i.e.*, the operators are defined by the integral

$$\mathrm{Q}u = q(x, -\mathrm{i}\,\mathrm{D})u = \frac{1}{4\pi^2} \int_{\xi\in\mathbb{R}^2} \int_{y\in\mathbb{R}^2} q(x,\xi)\mathrm{e}^{\mathrm{i}\xi\cdot(x-y)}u(y)\,\mathrm{d}y\,\mathrm{d}\xi$$

where $q(x,\xi)$ is the symbol associated with the operator Q. The symbol class $\mathrm{S}^m(\mathbb{R}^2\times\mathbb{R}^2)$ consists of smooth functions $q(x,\xi)$ such that

$$|\,\mathrm{D}_x^\beta\,\mathrm{D}_\xi^\alpha\, q(x,\xi)| \leq C_{\alpha,\beta}(1+|\xi|)^{m-|\alpha|} \tag{4.43}$$

for all multi-indices α, β, and numbers $x, \xi \in \mathbb{R}^2$, and has the property

$$q(x,\xi) \sim \sum_{n=0}^{\infty} q_n(x,\xi),$$

where $q_j(x,\xi)$ is positively homogeneous in ξ of degree $m-j$, *i.e.*,

$$q_j(x,\tau\xi) = \tau^{m-j} q(x,\xi).$$

The index m is the order of the symbol. With $\Psi^m(\mathbb{R}^2\times\mathbb{R}^2)$, we denote the class of pseudo-differential operators, associated with the symbols in $\mathrm{S}^m(\mathbb{R}^2\times\mathbb{R}^2)$. Observe that D denotes the spatial differential operator in the x-plane.

The dynamics of the one-way system (4.30) is determined by the vertical-propagation operator Γ. The vertical-propagation operator is defined implicitly through (4.29) as an approximation to the square root of the characteristic operator A. The symbol of the characteristic operator (4.28) is

$$\mathrm{a}(x,\xi) = \mathrm{a}(x,\xi,x_3,s) = s^2 c^{-2}(x,x_3,s) + \xi^2 \in \mathrm{S}^2(\mathbb{R}^2\times\mathbb{R}^2). \tag{4.44}$$

The space coordinates x and ξ are the actual pseudo-differential parameters whereas the Laplace coordinate s is a fixed complex-valued parameter and x_3 is a fixed real-valued parameter. The characteristic operator is an elliptic operator of order two, *i.e.*,

$$|c^2 a(x, \xi, \eta + \mathrm{i}\omega)|^2 = (\eta^2 + \omega^2)^2 + 2(\eta^2 - \omega^2)|c\xi|^2 + |c\xi|^4 \geq |c\xi|^4/2 \tag{4.45}$$

for sufficiently large values of ξ.

One can define a pseudo-differential approximation of the square root of the characteristic operator in an iterative fashion. Let Γ_0 be a first order approximation of the square-root operator, *i.e.*,

$$\Gamma_0^2 - \mathrm{A} \in \Psi^1(\mathbb{R}^2 \times \mathbb{R}^2).$$

Examples of valid first order approximation are given by the symbols $\gamma_0 = |\xi|$ or $\gamma_0 = (s^2 c^{-2}(x) + \xi^2)^{1/2}$. The pseudo-differential operator approximation of $\mathrm{A}^{1/2}$ is improved by addition of the operator

$$\Gamma_1 = (\Gamma_0^{-1}\mathrm{A} - \Gamma_0)/2 \in \Psi^0(\mathbb{R}^2 \times \mathbb{R}^2) \tag{4.46}$$

to Γ_0, *i.e.*,

$$(\Gamma_0 + \Gamma_1)^2 - \mathrm{A} \in \Psi^0(\mathbb{R}^2 \times \mathbb{R}^2). \tag{4.47}$$

Iteration of the algorithm above gives a pseudo-differential operator approximation of $\mathrm{A}^{1/2}$, *i.e.*,

$$\left(\sum_{k=0}^{\infty} \Gamma_k\right)^2 - \mathrm{A} \in \Psi^{-\infty}(\mathbb{R}^2 \times \mathbb{R}^2).$$

Observe that a good choice of the initial approximation Γ_0 can improve the level of approximation of the succeeding terms.

There is a formal problem in the symbol calculus of the local approximation $\gamma = \gamma_{\mathrm{L}} = (s^2 c^{-2}(x) + \xi^2)^{1/2}$. Differentiation of the symbol gives a problem at the zeros of the square root, *i.e.*, $\xi^2 = c^{-2}\omega^2$ (assuming fixed frequency $s = \mathrm{i}\omega$ and a lossless medium $\operatorname{Im} c = 0$). A zero corresponds to the underlying wave propagation, *i.e.*, the characteristics of the 'hyperbolic' operator. However, in the pseudo-differential calculus, the emphasis is on the asymptotic properties as $|\xi| \to \infty$. The small values of ξ can be collected in a smoothing operator. In the analysis this is accomplished by a cut-off function. Let $\chi = \chi(\xi)$ be a smooth function such that

$$\chi(\xi) = \begin{cases} 1 & |\xi| < 2|s/c|, \\ 0 & |\xi| > 3|s/c|. \end{cases}$$

Decompose γ_{L} in a low wave number part and a high wave number part

$$\gamma_{\mathrm{L}} = \chi\gamma_{\mathrm{L}} + (1 - \chi)\gamma_{\mathrm{L}}.$$

The low wave number part corresponds to the smoothing operator and the high frequency is a classical symbol (4.43).

Although the asymptotic expansion above appears to be a good representation for the vertical-propagation operator Γ, the approximation is not very good. The basic problem is that the pseudo-differential calculus emphasizes the approximation for large values of the ξ parameter which corresponds to the evanescent regime of the wave field.

To be able to incorporate time-domain results it is natural to consider uniform estimates in the Laplace parameter s. We include the Laplace parameter in the pseudo-differential calculus with the theory of pseudo-differential operators with a parameter [214, 101, 5]. We consider the symbol class $\mathrm{S}^m(\mathbb{R}^2 \times \mathbb{R}^2 \times \Lambda)$ consisting of smooth functions $q(x, \xi, s)$ such that

$$|\,\mathrm{D}_x^\beta\,\mathrm{D}_\xi^\alpha\,\partial_s^j q(x,\xi,s)| \le C_{\alpha,\beta}(1+|\xi|+|s|)^{m-|\alpha|-j} \tag{4.48}$$

for all multi-indices α, β, integers j, and numbers $x, \xi \in \mathbb{R}^2$ and $s \in \Lambda$, and has the property

$$q(x,\xi,s) \sim \sum_{n=0}^{\infty} q_n(x,\xi,s),$$

where $q_j(x, \xi, s)$ is positively homogeneous in (ξ, s) of degree $m - j$, *i.e.*,

$$q_j(x,\tau\xi,\tau s) = \tau^{m-j} q(x,\xi,s).$$

The domain $\Lambda \subset \mathbb{C}_+$ will be specified below. The index m is the order of the symbol. Observe that the parameter dependent symbol classes often are denoted by $\mathrm{S}^{m,\nu}(\mathbb{R}^2 \times \mathbb{R}^2 \times \Lambda)$ where ν is the regularity. The symbol class considered here has an infinite regularity. With $\Psi^n(\mathbb{R}^2 \times \mathbb{R}^2 \times \Lambda)$, we denote the class of pseudo-differential operators, associated with the symbols in $\mathrm{S}^n(\mathbb{R}^2 \times \mathbb{R}^2 \times \Lambda)$. In the left-symbol calculus, the operators are defined by the integral

$$q(x,-\mathrm{i}\,\mathrm{D},s)u = \frac{1}{4\pi^2}\int_{\xi\in\mathbb{R}^2}\int_{y\in\mathbb{R}^2} q(x,\xi,s)\mathrm{e}^{\mathrm{i}\xi\cdot(x-y)}u(y)\,\mathrm{d}y\,\mathrm{d}\xi.$$

The space coordinates x and ξ are the actual pseudo-differential parameters whereas the Laplace coordinate s is a complex-valued parameter (the vertical coordinate x_3 is fixed and real-valued). An operator $q(x, -\mathrm{i}\,\mathrm{D}, s)$ is elliptic of order n if for some $r < \infty$

$$|q(x,\xi,s)| \ge C|\xi|^n \quad \text{for } |\xi| \ge r \quad \text{and } s \in \Lambda. \tag{4.49}$$

The symbol of the characteristic operator (4.28) is

$$\mathrm{a}(x,\xi,s) = s^2 c^{-2}(x) + \xi^2 \in \mathrm{S}^2(\mathbb{R}^2 \times \mathbb{R}^2 \times \Lambda)$$

for all regions Λ. Furthermore, $\mathrm{a}(x, \xi, s)$ is elliptic, of order 1, if $\Lambda \cap \{s : \mathrm{Re}\, s = 0\}$ is bounded, *e.g.*, if Λ is a right half-plane $\Lambda = \{s : \mathrm{Re}\, s \ge \eta_0 > 0\}$. It is elliptic, of

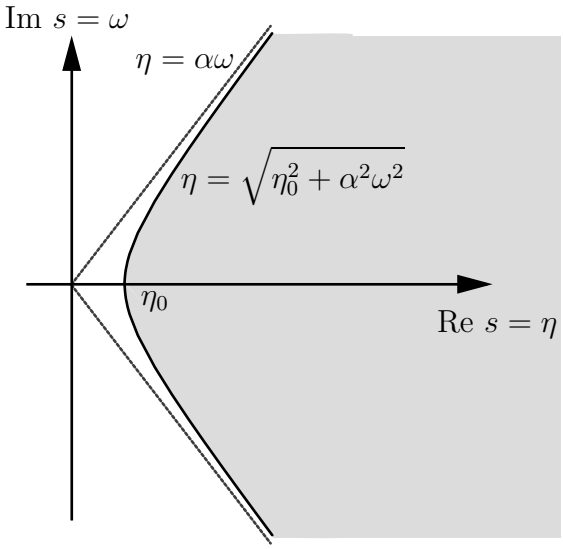

Figure 4.9: Region of definition for uniform pseudo-differential estimates of the vertical-propagation operator $\gamma(x, -\mathrm{i}\,\mathrm{D}, s)$.

order 2, if $\Lambda \cap \{s : |\operatorname{Re}(s)| \le \eta_0\}$ is bounded for all η_0, *e.g.*, if Λ is a region such that $\eta \ge \alpha|\omega|$ for some $\alpha \ge \alpha_0 > 0$, *i.e.*, $\Lambda = \{s : |\arg s| < \pi/2 - \delta\}$ for some fixed $\delta > 0$. The first statement follows from the estimate

$$|c^2\mathrm{a}(x,\xi,\eta_0+\mathrm{i}\omega)|^2 = (\eta_0^2 - \omega^2 + c^2|\xi|^2)^2 + 4\omega^2\eta_0^2 \ge \eta_0^4 + 2\eta_0^2(\omega^2 + c^2|\xi|^2) \tag{4.50}$$

with equality for $\omega = c|\xi|$. For the second estimate, we consider the region described by

$$\Lambda_{\eta_0,\alpha} = \{\eta + \mathrm{i}\omega : \eta \ge \sqrt{\eta_0^2 + \alpha^2\omega^2}\,\},$$

see Figure 4.9. The absolute value of $c^2\mathrm{a}(x,\xi,s)$ is

$$\begin{aligned}
&|c^2\mathrm{a}(x,\xi,\sqrt{\eta_0+\alpha^2\omega^2}+\mathrm{i}\omega)|^2 = (\eta_0^2 + c^2\xi^2 + \omega^2(\alpha^2-1))^2 + 4\omega^2(\eta_0^2+\alpha^2\omega^2)\\
&= (\eta_0^2 + c^2|\xi|^2)^2 - (1-\alpha^2)2\omega^2(\eta_0^2 + c^2|\xi|^2) + \omega^4(\alpha^2+1)^2 + 4\omega^2\eta_0^2\\
&= \left(\frac{\eta_0^2 + c^2|\xi|^2}{\sqrt{1+\alpha^2}} - \omega^2\sqrt{1+\alpha^2}\right)^2 + \frac{\alpha^2}{1+\alpha^2}(\eta_0^2 + c^2|\xi|^2)^2\\
&\qquad + (\alpha^4+\alpha^2)\omega^4 + 2\alpha^2\omega^2(\eta_0^2 + c^2|\xi|^2) + 4\omega^2\eta_0^2\\
&\ge \frac{\alpha^2}{1+\alpha^2}\left((\eta_0^2 + c^2|\xi|^2)^2 + \omega^4 + 2\omega^2(\eta_0^2 + c^2|\xi|^2)\right)\\
&= \frac{\alpha^2}{1+\alpha^2}\left(\eta_0^2 + c^2|\xi|^2 + \omega^2\right)^2
\end{aligned} \tag{4.51}$$

However, our focus is on the square root of A. Here, we use estimate (4.51) to show that we can construct a well-defined approximation of the square root. The principal part of the square root of A is

$$\gamma_{\mathrm{L}}(x,\xi,s) = \sqrt{c^{-2}(x)s^2 + \xi^2}. \tag{4.52}$$

Formal differentiation and the use of estimate (4.51) show that the symbol is in the symbol class $\mathrm{S}^1(\mathbb{R}^2 \times \mathbb{R}^2 \times \Lambda_{\eta_0,\alpha})$ for $\alpha > 0$ and $\eta_0 \geq 0$.

If we try to increase the region $\Lambda_{\eta_0,\alpha}$ to include a half-plane, *i.e.*, $\alpha \to 0$, the nice properties of the symbol class vanish. The first order approximation (4.52) is the local wave splitting of Section 4.4.3. The iterative scheme (4.46)—(4.47) can be used to construct higher order approximations of the square-root operator.

The square root can also defined with a resolvent method, see *e.g.*, Refs [**?**, 52, 214].

4.4.5 Paraxial approximations

The paraxial (or parabolic) approximation was introduced by Leontovich and Fock in the 40's. Since then, the paraxial approximation has been applied to various wave propagation problems, *e.g.*, exploration geophysics, underwater acoustics, radiowave propagation, random media, and laser beam propagation. The paraxial approximations are typically rational approximations of the vertical-propagation operator, *e.g.*, Pade approximations and Thiele approximations, see Refs [30, 170, 57, 173, 53, 36, 255, 98]. Here, we restrict the analysis to the first order approximation given by the Taylor series approximation

$$\sqrt{s^2c^{-2} + \xi^2} \approx sc^{-1} + \frac{\xi^2}{2sc^{-1}}.$$

The approximation is accurate if $|c\xi/s| \ll 1$, *i.e.*, waves propagation in the vertical direction. The spatial differentiation operator is not appropriately treated in the Taylor series approximation above. We define the parabolic approximation as the operator

$$\Gamma_{\mathrm{p}} = sc^{-1}(x,x_3,s) - \frac{1}{2s}\,\mathrm{D}^{\mathrm{T}}(c(x,x_3,s)\,\mathrm{D}\,). \tag{4.53}$$

The error in the parabolic approximation $\Xi = (\Gamma_{\mathrm{p}}^{-1}\mathrm{A} - \Gamma_{\mathrm{p}})/2$ has the principal part symbol

$$-\frac{\xi^4}{4sc^{-1}(2s^2c^{-2} + \xi^2)}.$$

The error is small in the vertical direction, *i.e.*, for small $|\xi|$, but the error is unbounded in the transverse directions [183]. We use this parabolic approximation in the time-reversal mirror analysis in Section 9.2.

4.4.6 Time-domain multi-dimensional wave splitting

In a sequence of papers Weston *et al.*, have studied a generalization of the one-dimensional time-domain wave splitting to multi-dimensions. We give a brief description of the analysis, for more details we refer to the literature [117, 114, 118, 253, 249, 250, 251, 116].

Consider the non-dispersive second order wave equation (4.25)

$$\partial_t^2 p - c^2(x, x_3)\nabla^2 p = 0 \tag{4.54}$$

in the pressure p. The wave field is decomposed with respect to the depth direction. At a depth $x_3 = x_3'$ the wave field is decomposed by freezing the $x_3 = \alpha$ variable and performing the splitting for a speed $c(x, \alpha)$ — compare with the locally exact wave splitting in Section 4.2.1.

The decomposition is defined by the solution of two initial-boundary value problems. The problems are given by the acoustic equation

$$\partial_t^2 u - c^2(x, \alpha)\nabla^2 u = 0 \quad \text{for} \quad x_3 \geq x_3' \quad \text{and} \quad t \in [0, T] \tag{4.55}$$

together with zero initial values, *i.e.*, $u(x, x_3, 0) = \partial_t u(x, x_3, 0) = 0$. The boundary conditions are of Neumann or Dirichlet type, *i.e.*,

$$\partial_{x_3} u(x, x_3, t)|_{x_3 = x_3'} = u_{\mathrm{N}}(x, t) \tag{4.56}$$

or

$$u(x, x_3', t) = u_{\mathrm{D}}(x, t), \tag{4.57}$$

respectively. The solution u of the wave equation (4.55) together with the Neumann data (4.56) is used to define the Neumann operator K_α by

$$\lim_{x_3 \searrow x_3'} u(x, x_3, t) = -\mathrm{K}_\alpha u_{\mathrm{N}}.$$

The Neumann operator maps the Neumann data to the Dirichlet data on the plane $x_3 = x_3'$. Similarly, the Dirichlet problem (4.57) defines an operator K_α^{-1} by

$$\lim_{x_3 \searrow x_3'} \partial_3 u(x, x_3, t) = -\mathrm{K}_\alpha^{-1} u_{\mathrm{D}}.$$

The above Dirichlet and Neumann relations are valid for all depth x_3 and all fields u_{D} and u_{N}. This permits us to define down-going waves from the condition

$$u + \mathrm{K}_\alpha \partial_3 u = 0 \quad \text{or} \quad \mathrm{K}_\alpha^{-1} u + \partial_3 u = 0.$$

The corresponding up-going condition is given by

$$u - \mathrm{K}_\alpha \partial_3 u = 0 \quad \text{or} \quad \mathrm{K}_\alpha^{-1} u - \partial_3 u = 0.$$

It can be shown [252] that the Neumann operator is the inverse of the square root of wave equation (4.54), *i.e.*,

$$\mathrm{K}_\alpha^{-2} = c(x, \alpha)^{-2}\partial_t^2 - \mathrm{D}^2 = c(x, \alpha)^{-2}\partial_t^2 - \partial_1^2 - \partial_2^2.$$

For the depth dependent problem, the Neumann operator K is defined as

$$\mathrm{K} u(x, x_3, t) = \mathrm{K}_\alpha u(x, \alpha, t)|_{\alpha = x_3}.$$

The down- and up-going wave fields are defined by the Neumann operator as

$$\begin{pmatrix} u_+ \\ u_- \end{pmatrix} = \frac{1}{2} \begin{pmatrix} 1 & \mathrm{K} \\ 1 & -\mathrm{K} \end{pmatrix} \begin{pmatrix} p \\ \partial_3 p \end{pmatrix},$$

where the split fields satisfy the one-way wave equations[116]

$$\partial_3 \begin{pmatrix} u_+ \\ u_- \end{pmatrix} + \begin{pmatrix} \mathrm{K}^{-1} & 0 \\ 0 & -\mathrm{K}^{-1} \end{pmatrix} \begin{pmatrix} u_+ \\ u_- \end{pmatrix} = \frac{\mathrm{K}\partial_3 \mathrm{K}^{-1}}{2} \begin{pmatrix} -1 & 1 \\ 1 & -1 \end{pmatrix} \begin{pmatrix} u_+ \\ u_- \end{pmatrix}.$$

Observe that the Neumann operator K is the inverse of the time-domain version of a locally exact vertical-propagation operator $\Gamma = \mathrm{A}^{1/2}$, *i.e.*, formally

$$\mathrm{K}^{-1} = \mathcal{L}^{-1} \mathrm{A}^{1/2}$$

where $\mathcal{L}^{-1}$ is the inverse Laplace transform. For further discussion of this time-domain wave splitting and its applications on inverse scattering see Refs [117, 114, 118, 253, 249, 250, 251, 116].

4.5 Electromagnetic wave splitting

The analysis of the acoustic wave splitting in Section 4.4 can be generalized to the Maxwell equations. For the Maxwell equations one gets a system of four equations in contrast to a system of two equations in the acoustic case.

The Laplace domain version of the Maxwell equations (4.4) for an isotropic medium are

$$\begin{cases} s\epsilon \widehat{E} + \partial_3 \mathrm{J} \widehat{H} - \mathrm{J}\,\mathrm{D}\,\widehat{H}_3 = -\widehat{J}, \\ s\epsilon \widehat{E}_3 - \mathrm{D}^{\mathrm{T}}\,\mathrm{J} \widehat{H} = -\widehat{J}_3, \\ s\mu \widehat{H} - \partial_3 \mathrm{J} \widehat{E} + \mathrm{J}\,\mathrm{D}\,\widehat{E}_3 = 0, \\ s\mu \widehat{H}_3 + \mathrm{D}^{\mathrm{T}}\,\mathrm{J} \widehat{E} = 0. \end{cases} \tag{4.58}$$

The medium is assumed to be passive and the permeability μ is assumed to be homogeneous. To obtain an evolution problem in the preferred direction, we eliminate the vertical components of the electric and magnetic field intensities. Notice that vertical differential operator ∂_3 only operates on the transverse components of the electromagnetic field intensities. The Maxwell equations reduce to the system

$$\begin{cases} s\epsilon \widehat{E} + \partial_3 \mathrm{J} \widehat{H} + \mathrm{J}\,\mathrm{D} \left(s^{-1} \mu^{-1}\, \mathrm{D}^{\mathrm{T}}\, \mathrm{J} \widehat{E} \right) = -\widehat{J}, \\ s\mu \widehat{H} - \partial_3 \mathrm{J} \widehat{E} + \mathrm{J}\,\mathrm{D} \left(s^{-1} \epsilon^{-1}\, \mathrm{D}^{\mathrm{T}}\, \mathrm{J} \widehat{H} \right) = \mathrm{J}\,\mathrm{D}\, s^{-1} \epsilon^{-1} \widehat{J}_3. \end{cases} \tag{4.59}$$

This system of four equations is rewritten as an evolution problem in the vertical direction, *i.e.*,

$$\begin{aligned} \partial_3 \begin{pmatrix} \widehat{E} \\ \mathrm{J}\widehat{H} \end{pmatrix} + \begin{pmatrix} 0 & s\mu - s^{-1}\,\mathrm{D}(\epsilon^{-1}\,\mathrm{D}^{\mathrm{T}}\,) \\ s\epsilon + s^{-1}\mathrm{J}\,\mathrm{D}(\mu^{-1}\,\mathrm{D}^{\mathrm{T}}\,)\mathrm{J} & 0 \end{pmatrix} \begin{pmatrix} \widehat{E} \\ \mathrm{J}\widehat{H} \end{pmatrix} \\ = \begin{pmatrix} -s^{-1}\,\mathrm{D}(\epsilon^{-1} \widehat{J}_3) \\ -\widehat{J} \end{pmatrix}. \end{aligned} \tag{4.60}$$

In Section 4.5.1, a formal wave splitting is outlined and in Section 4.5.2 wave splitting in a layered medium is considered. For further discussion about wave splitting of the Maxwell equations we refer to the literature, see *e.g.*, [242, 116].

4.5.1 Formal wave splitting

Following the formal wave splitting of the acoustic wave equation in Section 4.4.1, the system (4.60) is written as

$$(\partial_3 + \mathcal{A})\hat{w} = \hat{g}. \tag{4.61}$$

The system matrix A is

$$\mathcal{A} = \begin{pmatrix} 0 & \mathcal{A}_{1,2} \\ \mathcal{A}_{2,1} & 0 \end{pmatrix} = \begin{pmatrix} 0 & s\mu - s^{-1}\,\mathrm{D}(\epsilon^{-1}\,\mathrm{D}^{\mathrm{T}}\,) \\ s\epsilon + s^{-1}\mathrm{J}\,\mathrm{D}(\mu^{-1}\,\mathrm{D}^{\mathrm{T}}\,)\mathrm{J} & 0 \end{pmatrix}, \tag{4.62}$$

and the field vector $\hat{w}$ and source vector $\hat{g}$ are

$$\hat{w} = \begin{pmatrix} \widehat{E} \\ \mathrm{J}\widehat{H} \end{pmatrix} = \begin{pmatrix} \widehat{E}_1 \\ \widehat{E}_2 \\ \widehat{H}_2 \\ -\widehat{H}_1 \end{pmatrix} \quad \text{and} \quad \hat{g} = \begin{pmatrix} -s^{-1}\,\mathrm{D}(\epsilon^{-1}\widehat{J}_3) \\ -\widehat{J} \end{pmatrix},$$

respectively. Observe that $\mathcal{A}$ is a 2×2 matrix of 2×2 matrix elements. We decompose the system by formally diagonalizing the system matrix (4.62). The diagonalization operator is only determined up to a normalization; here we use the electric-field normalization [242]. The diagonal elements are the square root of the characteristic operator

$$\mathrm{A} = \mathcal{A}_{1,2}\mathcal{A}_{2,1} = s^2\epsilon\mu - \epsilon\,\mathrm{D}(\epsilon^{-1}\,\mathrm{D}^{\mathrm{T}}\,) + \mathrm{J}\,\mathrm{D}(\mathrm{D}^{\mathrm{T}}\,)\mathrm{J}.$$

In general, it is difficult to define an exact square root, so instead, we determine an approximate square root of A. Let Γ be an operator such that the difference $\mathrm{A} - \Gamma^2$ is small. We call Γ the vertical-propagation operator for the Maxwell equations. Let Ξ denote the degree of accuracy in the approximation, *i.e.*,

$$\Xi = (\Gamma - \Gamma^{-1}\mathrm{A})/2. \tag{4.63}$$

In the electric field normalization, we use the impedance Z and admittance Y, defined as

$$\mathrm{Z} = \Gamma^{-1}\mathcal{A}_{1,2} \quad \text{and} \quad \mathrm{Y} = \mathrm{Z}^{-1} = \mathcal{A}_{1,2}^{-1}\Gamma. \tag{4.64}$$

These operators connect the electric and magnetic field to each other. The composition operator L and the decomposition operator L^{-1} are defined as

$$\mathrm{L} = \begin{pmatrix} 1 & 1 \\ \mathrm{Z}^{-1} & -\mathrm{Z}^{-1} \end{pmatrix} \quad \text{and} \quad \mathrm{L}^{-1} = \frac{1}{2}\begin{pmatrix} 1 & \mathrm{Z} \\ 1 & -\mathrm{Z} \end{pmatrix}, \tag{4.65}$$

respectively. The decomposition operator L^{-1} defines the down- and up-going components $\hat{u} = (\hat{u}_+, \hat{u}_-)$ of the wave-field, *i.e.*,

$$\begin{pmatrix} \hat{u}_+ \\ \hat{u}_- \end{pmatrix} = \mathrm{L}^{-1} \begin{pmatrix} \widehat{E} \\ \mathrm{J}\widehat{H} \end{pmatrix} \quad \text{and} \quad \begin{pmatrix} \widehat{E} \\ \mathrm{J}\widehat{H} \end{pmatrix} = \mathrm{L} \begin{pmatrix} \hat{u}_+ \\ \hat{u}_- \end{pmatrix}.$$

Substitute $\hat{w} = \mathrm{L}\hat{u}$ into the dynamics (4.26) and we get

$$(\partial_3 \mathrm{L} + \mathcal{A}\mathrm{L})\hat{u} = \hat{g}.$$

Multiply with the decomposition operator and use the relation $\partial_3 \mathrm{L} = (\partial_3 \mathrm{L}) + \mathrm{L}\partial_3$. This gives

$$(\partial_3 + \mathrm{L}^{-1}\mathcal{A}\mathrm{L})\hat{u} = -\mathrm{L}^{-1}(\partial_3 \mathrm{L})\hat{u} + \mathrm{L}^{-1}\hat{g}.$$

The principal part of the equation decouples which is given by the following calculation:

$$\begin{aligned} \mathrm{L}^{-1}\mathcal{A}\mathrm{L} =& \frac{1}{2} \begin{pmatrix} 1 & \mathrm{Z} \\ 1 & -\mathrm{Z} \end{pmatrix} \begin{pmatrix} 0 & \mathcal{A}_{1,2} \\ \mathcal{A}_{2,1} & 0 \end{pmatrix} \begin{pmatrix} 1 & 1 \\ \mathrm{Z}^{-1} & -\mathrm{Z}^{-1} \end{pmatrix} \\ =& \frac{1}{2} \begin{pmatrix} 1 & \mathrm{Z} \\ 1 & -\mathrm{Z} \end{pmatrix} \begin{pmatrix} \Gamma & -\Gamma \\ \mathcal{A}_{2,1} & \mathcal{A}_{2,1} \end{pmatrix} \\ =& \frac{1}{2} \begin{pmatrix} \Gamma + \Gamma^{-1}\mathrm{A} & -\Gamma + \Gamma^{-1}\mathrm{A} \\ \Gamma - \Gamma^{-1}\mathrm{A} & -\Gamma - \Gamma^{-1}\mathrm{A} \end{pmatrix} = \begin{pmatrix} \Gamma & 0 \\ 0 & -\Gamma \end{pmatrix} + \begin{pmatrix} -\Xi & -\Xi \\ \Xi & \Xi \end{pmatrix}. \end{aligned}$$

We see that the equations decouple provided Ξ is of lower order than Γ.

In the region $0 \leq x_3 \leq X_3$, the decomposed fields $\hat{u}$ satisfy the source free one-way system of equations

$$\begin{pmatrix} \partial_3 + \Gamma & 0 \\ 0 & \partial_3 - \Gamma \end{pmatrix} \begin{pmatrix} \hat{u}_+ \\ \hat{u}_- \end{pmatrix} = \begin{pmatrix} \mathrm{R} + \Xi & -\mathrm{R} + \Xi \\ -\mathrm{R} - \Xi & \mathrm{R} - \Xi \end{pmatrix} \begin{pmatrix} \hat{u}_+ \\ \hat{u}_- \end{pmatrix}, \tag{4.66}$$

where $\mathrm{R} = -\mathrm{Y}^{-1}\partial_3 \mathrm{Y}/2$.

4.5.2 Layered media

In a isotropic layered medium the vertical-propagation operator, impedance operator and admittance operator have explicit representations. The symbol of the system matrix $\mathcal{A}$ is composed of the 2×2 matrices

$$\mathrm{a}_{1,2} = s\mu + \xi\xi^{\mathrm{T}}/s\epsilon$$

and

$$\mathrm{a}_{2,1} = s\epsilon + \mathrm{J}\xi(\mathrm{J}\xi)^{\mathrm{T}}/s\mu.$$

The symbols $\mathrm{a}_{1,2}$ and $\mathrm{a}_{2,1}$ have the same set of eigenvectors ξ and $\mathrm{J}\xi$, *i.e.*,

$$\mathrm{a}_{1,2}\xi = (s\mu + \xi^2/s\epsilon)\xi, \quad \mathrm{a}_{2,1}\xi = s\epsilon\xi$$

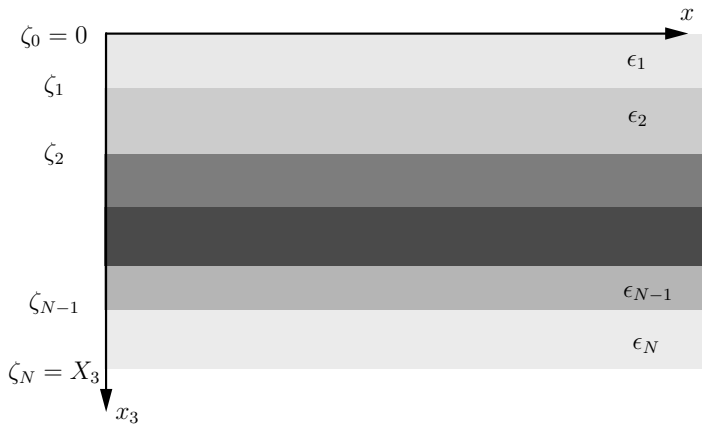

Figure 4.10: The layered media.

and

$$\mathrm{a}_{2,1}\mathrm{J}\xi = (s\epsilon + \xi^2/s\mu)\mathrm{J}\xi, \quad \mathrm{a}_{1,2}\mathrm{J}\xi = s\mu\mathrm{J}\xi.$$

The first set is the TM case, *i.e.*, the magnetic field $\mathrm{J}\xi$ is orthogonal to the direction ξ. The second set is the TE case, *i.e.*, the electric field $\mathrm{J}\xi$ is orthogonal to the direction ξ. The symbol of the characteristic operator $\mathrm{A} = \mathcal{A}_{1,2}\mathcal{A}_{2,1}$ is

$$\mathrm{a} = \mathrm{a}_{1,2}\mathrm{a}_{2,1} = s^2\epsilon\mu + \xi\xi^{\mathrm{T}} + \mathrm{J}\xi(\mathrm{J}\xi)^{\mathrm{T}}.$$

The TE and TM polarizations are

$$\mathrm{a}_{1,2}\mathrm{a}_{2,1}\xi = \left(s^2\epsilon\mu + \xi^2\right)\xi$$

and

$$\mathrm{a}_{1,2}\mathrm{a}_{2,1}\mathrm{J}\xi = \left(s^2\epsilon\mu + \xi^2\right)\mathrm{J}\xi,$$

respectively.

The vertical-propagation symbol is

$$\gamma = \gamma^{(\mathrm{TE})} = \gamma^{(\mathrm{TM})} = \sqrt{s^2\epsilon\mu + \xi^2}.$$

Observe that the TE and TM vertical-propagation operators are identical in an isotropic medium. The symbol of the impedance operator $\mathrm{Z} = \Gamma^{-1}\mathcal{A}_{1,2}$ is

$$\mathrm{z}^{(\mathrm{TE})} = \frac{s\mu}{\gamma^{(\mathrm{TE})}} \quad \text{and} \quad \mathrm{z}^{(\mathrm{TM})} = \frac{\gamma^{(\mathrm{TM})}}{s\epsilon}.$$

The symbol of the admittance operator $\mathrm{Y} = \mathcal{A}_{1,2}^{-1}\Gamma$ is

$$\mathrm{y}^{(\mathrm{TE})} = \frac{\gamma^{(\mathrm{TE})}}{s\mu} \quad \text{and} \quad \mathrm{y}^{(\mathrm{TM})} = \frac{s\epsilon}{\gamma^{(\mathrm{TM})}}.$$

Wave propagation in a layered medium reduces to propagation of the TE- and TM-modes. To see this, let the permittivity be given by

$$\epsilon(x, x_3, s) = \epsilon_j(s) \quad \text{for} \quad \zeta_{j-1} \leq x_3 < \zeta_j$$

where $0 = \zeta_0 < \ldots < \zeta_N = X_3$. In each layer, the vertical-propagation operator Γ_j reduces to multiplication with the vertical-propagation symbol

$$\gamma_j(\xi, s) = \sqrt{\epsilon_j(s)\mu s^2 + \xi^2},$$

in the spatial Fourier domain, *i.e.*,

$$\Gamma_j \hat{u}(x, x_3, s) = \frac{1}{4\pi^2} \int_{y\in\mathbb{R}^2} \int_{\xi\in\mathbb{R}^2} \gamma_j(\xi, s) \mathrm{e}^{\mathrm{i}\xi\cdot(x-y)} \hat{u}(y, x_3, s)\, \mathrm{d}y\, \mathrm{d}\xi. \tag{4.67}$$

In the interior of a layer, the one-way wave equations (4.66) decouple. The solution of the one-way wave equation in a layer is

$$\begin{cases} \hat{u}_+(x, \zeta_j-, s) = \dfrac{1}{4\pi^2} \displaystyle\int_{\xi\in\mathbb{R}^2} \int_{y\in\mathbb{R}^2} \mathrm{e}^{\mathrm{i}\xi\cdot(x-y)} \mathrm{e}^{-\gamma_j(\xi,s)d_j} \hat{u}_+(y, \zeta_{j-1}+, s)\, \mathrm{d}y\, \mathrm{d}\xi, \\ \hat{u}_-(x, \zeta_{j-1}+, s) = \dfrac{1}{4\pi^2} \displaystyle\int_{\xi\in\mathbb{R}^2} \int_{y\in\mathbb{R}^2} \mathrm{e}^{\mathrm{i}\xi\cdot(x-y)} \mathrm{e}^{-\gamma_j(\xi,s)d_j} \hat{u}_-(y, \zeta_j-, s)\, \mathrm{d}y\, \mathrm{d}\xi, \end{cases}$$

where $d_j = \zeta_j - \zeta_{j-1}$, $j = 1, \ldots, N$ is the thickness of each layer, see Figure 4.10. The down- and up-going wave constituents are coupled at the interfaces of the layers. The coupling is given by

$$\begin{cases} \hat{u}_+(x, \zeta_j+, s) = (1 + \mathrm{R}_j)\hat{u}_+(x, \zeta_j-, s) - \mathrm{R}_j \hat{u}_-(x, \zeta_j+, s), \\ \hat{u}_-(x, \zeta_j-, s) = \mathrm{R}_j \hat{u}_+(x, \zeta_j-, s) + (1 - \mathrm{R}_j)\hat{u}_-(x, \zeta_j+, s), \end{cases}$$

where the reflection operator has the (TE) and (TM) modes

$$\mathrm{R}_j^{(\mathrm{TE})} = \frac{\gamma_j^{(\mathrm{TE})}\mu_j^{-1} - \gamma_{j+1}^{(\mathrm{TE})}\mu_{j+1}^{-1}}{\gamma_j^{(\mathrm{TE})}\mu_j^{-1} + \gamma_{j+1}^{(\mathrm{TE})}\mu_{j+1}^{-1}}$$

and

$$\mathrm{R}_j^{(\mathrm{TM})} = \frac{\gamma_j^{(\mathrm{TM})}\epsilon_j^{-1} - \gamma_{j+1}^{(\mathrm{TM})}\epsilon_{j+1}^{-1}}{\gamma_j^{(\mathrm{TM})}\epsilon_j^{-1} + \gamma_{j+1}^{(\mathrm{TM})}\epsilon_{j+1}^{-1}},$$

respectively.

Chapter 5

Direct problem

The direct electromagnetic problem is to determine the electromagnetic fields from given sources and material parameters (constitutive relations). Typical applications are found in antenna theory, wave guides, and integrated optics. The direct problem has been extensively studied and its mathematical properties are well understood.

In Section 5.1, the direct problem is outlined and in Section 5.2, an energy analysis of a initial boundary value problem is given. Section 5.4 contains a discussion of the local energy decay of the Maxwell equations. Two finite difference schemes are reviewed in Section 5.5.

5.1 Formulation

In a majority of electromagnetic problems we know the source, typically the currents on an antenna, and we want to determine the fields generated by the source, see Figures 1.2 and 5.1.

There are a few important properties to analyze when one wants to solve this kind of problems. They are:

Existence: Does there exist a solution to problem? Even if we know that there exists a solution to the original physical problem, we have to be sure that there exists a solution to the mathematical model of problem.

Uniqueness: If the solution exists, is it unique?

Continuous dependence on the data: What happens if we only have data corrupted with errors (*i.e.*, the field values are measured, and there are always errors in actual measurements). Here we want the error in the solution to be small if the error in the data is small.

The problem is well-posed if all these conditions hold [110, 154]. There are several numerical methods that can be used to solve electromagnetic problems, *e.g.*,

FDTD: The finite difference time-domain methods. Here the electromagnetic problem is restricted to a bounded region and the differential operators in the

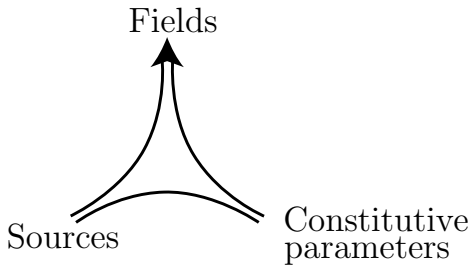

Figure 5.1: The direct problem. One determines the field from given currents, sources, and material properties.

Maxwell equations are approximated with finite differences. The resulting system is solved in a time-stepping manner, see *e.g.*, Refs [51, 102, 154, 220, 228] and Section 5.5.

FEM & FD: The finite element and the finite difference methods. The spatial differential operators of the frequency-domain Maxwell equations are approximated with local operators. This gives sparse linear systems of equations, see *e.g.*, Refs [220, 211].

MoM: The method of moments. The Maxwell equations are transformed to an integral equation. This integral equation is approximated with a finite dimensional linear system. The system is solved with a time-stepping algorithm in the time-domain and a linear system solver in the frequency-domain [112]. A recent approach is the fast multipole method, that reduces the computational complexity and hence have made it possible to solve 'relatively large' 3D problems [208, 201].

All the above methods can be used to solve the Maxwell equations in an arbitrary region, *i.e.*, in theory one can solve all direct problems! However, it might be too time- and memory consuming to perform the actual computations.

Some direct problems have a geometry that admit a more efficient numerical method, *e.g.*, eigenfunction expansions [128, 219, 191, 192]. In other cases, it is necessary to perform additional approximations. A well known approach is the high-frequency expansions, *e.g.*, ray tracing, Geometrical Optics (GO), Geometrical Theory of Diffraction (GDT), Physical Optics (PO), and Physical Theory of Diffraction (PTD), see *e.g.*, Refs [129, 180, 152, 144, 236, 19, 69]. There are also asymptotic expansions with respect to a direction, *e.g.*, the paraxial approximation and the general wave splitting algorithms, see Chapter 4. These directional approximations give one-way wave problems. In Chapter 6, we consider the Bremmer series as a method to include back-scattered wave constituents in the one-way wave formulation.

5.2 Energy

It is natural to consider energy quantities in the analysis of the Maxwell equations. The electromagnetic energy has already been used in the analysis of the constitutive relations in Chapter 2 and in the energy-flux wave splitting in Section 4.3.1. Observe that the energy is not uniquely defined [74], the definition given here is the usually accepted one.

The increase of energy $\mathcal{E}(t)$ in a region Ω from time $t = 0$ to time $t = T > 0$ is defined by

$$\begin{aligned}\mathcal{E}(T) - \mathcal{E}(0) &= \int_0^T \int_\Omega \boldsymbol{e}(\boldsymbol{x},t)^{\mathrm{T}} \cdot \partial_t \boldsymbol{d}(\boldsymbol{x},t)\,\mathrm{dV}\,\mathrm{d}t \\ &= \int_0^T \int_\Omega \boldsymbol{E}(\boldsymbol{x},t)\cdot\partial_t\boldsymbol{D}(\boldsymbol{x},t) + \boldsymbol{H}(\boldsymbol{x},t)\cdot\partial_t\boldsymbol{B}(\boldsymbol{x},t)\,\mathrm{dV}\,\mathrm{d}t.\end{aligned} \tag{5.1}$$

Observe that we are only interested in the energy difference $\mathcal{E}(T) - \mathcal{E}(0)$ and not in the total value of the energy.

The Poynting's theorem relates the increase of energy in Ω to the energy flux though the boundary $\partial\Omega$ and the electric currents in Ω, *i.e.*,

$$\begin{aligned}\mathcal{E}(T) - \mathcal{E}(0) = &-\int_0^T \int_{\partial\Omega} \boldsymbol{E}(\boldsymbol{x},t)\times\boldsymbol{H}(\boldsymbol{x},t)\cdot\boldsymbol{n}(\boldsymbol{x})\,\mathrm{dS}\,\mathrm{d}t \\ &- \int_0^T \int_\Omega \boldsymbol{E}(\boldsymbol{x},t)\cdot\boldsymbol{J}(\boldsymbol{x},t)\,\mathrm{dV}\,\mathrm{d}t.\end{aligned} \tag{5.2}$$

To get an understanding of the energy quantity $\mathcal{E}$, we consider the energy in a homogeneous isotropic source-free Lorentz medium. The constitutive relations are described by an ordinary differential equation in the polarization $\boldsymbol{P}$, *i.e.*,

$$\boldsymbol{D}(\boldsymbol{x},t) = \epsilon_\infty(\boldsymbol{x})\boldsymbol{E}(\boldsymbol{x},t) + \boldsymbol{P}(\boldsymbol{x},t) \tag{5.3}$$

where the polarization $\boldsymbol{P}(\boldsymbol{x},t)$ satisfies

$$\partial_t^2\boldsymbol{P} + \nu\partial_t\boldsymbol{P} + \omega_0^2\boldsymbol{P} = \alpha\boldsymbol{E}(\boldsymbol{x},t). \tag{5.4}$$

The permeability is assumed to be isotropic and non-dispersive, *i.e.*, $\boldsymbol{B} = \mu\boldsymbol{H}$. The material parameter ν is the collision frequency, ω_0 is the harmonic frequency, and α is proportional to the density of the inclusions, see Section 2.7. Multiply the second equation with the time derivative of the polarization $\dot{\boldsymbol{P}} = \partial_t\boldsymbol{P}$ and collect terms to get

$$\frac{1}{2}\partial_t|\dot{\boldsymbol{P}}|^2 + \nu|\dot{\boldsymbol{P}}|^2 + \frac{1}{2}\omega_0^2\partial_t|\boldsymbol{P}|^2 = \alpha\dot{\boldsymbol{P}}\cdot\boldsymbol{E}.$$

From the first equation in (5.3) we get the power density

$$\begin{aligned}\boldsymbol{E}\cdot\partial_t\boldsymbol{D} + \boldsymbol{H}\cdot\partial_t\boldsymbol{B} &= \frac{1}{2}\partial_t\left(\epsilon_\infty|\boldsymbol{E}|^2 + \mu|\boldsymbol{H}|^2\right) + \boldsymbol{E}\cdot\dot{\boldsymbol{P}} \\ &= \frac{1}{2}\partial_t\left(\epsilon_\infty|\boldsymbol{E}|^2 + \mu|\boldsymbol{H}|^2 + \alpha^{-1}\omega_0^2|\boldsymbol{P}|^2 + \alpha^{-1}|\dot{\boldsymbol{P}}|^2\right) + \alpha^{-1}\nu|\dot{\boldsymbol{P}}|^2.\end{aligned}$$

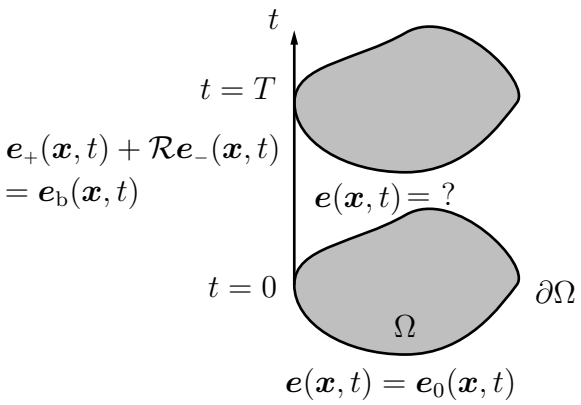

Figure 5.2: Geometry for the initial-boundary value problem.

The increase of energy in the region Ω from time $t = 0$ to $t = T$ is

$$\mathcal{E}(T) = \mathcal{E}(0) + \int_0^T \int_\Omega \frac{\nu}{\alpha} |\dot{\boldsymbol{P}}(\boldsymbol{x}, t)|^2 \,\mathrm{dV}\,\mathrm{d}t + \frac{1}{2} \int_\Omega \epsilon_\infty |\boldsymbol{E}(\boldsymbol{x}, t)|^2 + \mu |\boldsymbol{H}(\boldsymbol{x}, t)|^2 + \frac{\omega_0^2}{\alpha} |\boldsymbol{P}(\boldsymbol{x}, t)|^2 + \frac{|\dot{\boldsymbol{P}}(\boldsymbol{x}, t)|^2}{\alpha} \,\mathrm{dV} \Bigg|_{t=0}^{T}.$$

Here it is convenient to make a separation of the energy density in a rapid part given by the field intensities

$$\mathcal{E}_\infty(t) = \frac{1}{2} \int_\Omega \epsilon_\infty |\boldsymbol{E}(\boldsymbol{x}, t)|^2 + \mu |\boldsymbol{H}(\boldsymbol{x}, t)|^2 \,\mathrm{dV},$$

a slower material part given by

$$\frac{1}{2} \int_\Omega \frac{\omega_0^2}{\alpha} |\boldsymbol{P}(\boldsymbol{x}, t)|^2 + \frac{|\dot{\boldsymbol{P}}(\boldsymbol{x}, t)|^2}{\alpha} \,\mathrm{dV},$$

and one part due to losses

$$\int_0^T \int_\Omega \frac{\nu}{\alpha} |\dot{\boldsymbol{P}}(\boldsymbol{x}, t)|^2 \,\mathrm{dV}\,\mathrm{d}t.$$

The loss part constitutes the energy change from electromagnetic energy to heat, whereas the other material part merely represents the electromagnetic energy stored in the material.

5.3 Initial-boundary value problem

Many electromagnetic problems can be formulated as an initial-boundary value problem, *i.e.*, field values are given in Ω for $t \leq 0$, boundary values are given at $\partial\Omega$ for

$0 \leq t \leq T$, and currents are given in Ω for $0 \leq t \leq T$. The mathematical formulation is as follows. The fields $\boldsymbol{e}(\boldsymbol{x}, t)$ satisfy the Maxwell equations in the region Ω, *i.e.*,

$$\partial_t[\boldsymbol{\varepsilon}\boldsymbol{e}] - \nabla \times \mathrm{J}\boldsymbol{e} = -\boldsymbol{j}(\boldsymbol{x}, t) \qquad \text{for } \boldsymbol{x} \in \Omega \text{ and } t \in [0, T].$$

The initial values consists of the all previous field values in a convolution formulation of dispersion, *i.e.*,

$$\boldsymbol{e}(\boldsymbol{x}, t) = \boldsymbol{e}_0(\boldsymbol{x}, t) \quad \text{for} \quad t \leq 0 \tag{5.5}$$

are given. In the state-variable representation, the initial values reduce to the field values in Ω at $t = 0$ together with the values of the states in Ω at $t = 0$ and in the case of second order formulations the values of the temporal derivatives of the states in Ω at $t = 0$. At the boundary $\partial\Omega$, a set of tangential fields are prescribed, *e.g.*, the tangential electric, the tangential magnetic, or a linear combination of them are given at the boundary. It is natural to formulate the boundary conditions in the energy-flux split fields (4.20), *i.e.*,

$$\boldsymbol{e}_+(\boldsymbol{x}, t) + \mathcal{R}\boldsymbol{e}_-(\boldsymbol{x}, t) = \boldsymbol{e}_\mathrm{b}(\boldsymbol{x}, t) \quad \text{at } \partial\Omega \text{ for } t \geq 0, \tag{5.6}$$

where $\mathcal{R}$ is a matrix-valued operator, *i.e.*,

$$\mathcal{R} : \ (\mathrm{L}^2(\partial\Omega \times [0, T]))^2 \mapsto (\mathrm{L}^2(\partial\Omega \times [0, T]))^2.$$

Use the energy-flux split fields to rewrite the Poynting's theorem as, see Section 4.3.2

$$\mathcal{E}(T) + \mathcal{E}_-(T) = \mathcal{E}(0) + \mathcal{E}_+(T) - \int_0^T \int_\Omega \boldsymbol{E}(\boldsymbol{x}, t) \cdot \boldsymbol{J}(\boldsymbol{x}, t) \, \mathrm{dV} \, \mathrm{d}t. \tag{5.7}$$

where $\mathcal{E}_\pm$ is the energy-flux input and output through the boundary, *i.e.*,

$$\mathcal{E}_\pm(T) = \int_0^t \int_{\partial\Omega} |E_\pm(\boldsymbol{x}, t)|^2 \mathrm{Y}_\infty \, \mathrm{dS} \, \mathrm{d}t.$$

Energy methods can be used to get a bound on the fields in the region and the tangential components at the boundary $\partial\Omega$ [154, 103]. For the inverse problem in Chapter 8 it is sufficient to consider a source-free region with passive medium and $\mathcal{R} = 0$. In this case the energy balance (5.7) gives a bound on the fields.

5.4 Local energy decay

It is natural to assume that the influence of the pre-history of electromagnetic field is weak, *i.e.*, the influence of the fields decays as time evolves. We used this decay property in the motivation of the constitutive relations in Chapter 2 and it is a fundamental part of the time-reversal cavity in Chapter 9, see *e.g.*, Refs [257, 24, 11, 190, 189] for a discussion about local energy decay for wave equations.

To state the local energy decay property, we consider the Maxwell equations in $\mathbb{R}^3$ together with a set of constitutive relations and initial values. The question is what happens with the electromagnetic fields in a region Ω as time evolves?

Before we discuss the mathematical analysis, we motivate the analysis from a physical point of view. Typically a field is decomposed into a static constituent and a (radiating) wave field. The static constituent is independent of time and, by definition, does not decay in time.

So what is the static field constituent? From electrostatics , we have the classical potential solution satisfying $\nabla \times \boldsymbol{E} = \boldsymbol{0}$. That is, the static field belongs to the nullspace (or kernel) of the curl operators of the Maxwell equations. The divergence equations (2.2) relate the static fields to the source densities, and therefore the static field vanishes in a charge- and current-free space.

A mathematical formulation is: consider $\mathcal{E}_\infty(t)$ as $t \to \infty$, where $\mathcal{E}_\infty(t)$ is the instantaneous part of the energy, *i.e.*,

$$\mathcal{E}_\infty(t) = \int_\Omega \begin{pmatrix} \boldsymbol{E}(\boldsymbol{x},t) \\ \boldsymbol{H}(\boldsymbol{x},t) \end{pmatrix}^{\mathrm{T}} \cdot \begin{pmatrix} \boldsymbol{\epsilon}_\infty(\boldsymbol{x}) & \boldsymbol{\xi}_\infty(\boldsymbol{x}) \\ \boldsymbol{\zeta}_\infty(\boldsymbol{x}) & \boldsymbol{\mu}_\infty(\boldsymbol{x}) \end{pmatrix} \begin{pmatrix} \boldsymbol{E}(\boldsymbol{x},t) \\ \boldsymbol{H}(\boldsymbol{x},t) \end{pmatrix} \mathrm{dV}\,.$$

The fields $\boldsymbol{E}, \boldsymbol{H}, \boldsymbol{D}$, and $\boldsymbol{B}$ satisfy the Maxwell equations (2.1) together with a set of constitutive relations (2.4) and the initial values

$$\boldsymbol{E}(\boldsymbol{x},t) = \boldsymbol{E}_0(\boldsymbol{x},t) \quad \text{and} \quad \boldsymbol{H}(\boldsymbol{x},t) = \boldsymbol{H}_0(\boldsymbol{x},t) \tag{5.8}$$

for $\boldsymbol{x} \in \mathbb{R}^3$ and $t \leq 0$.

The local decay result of Avila and Costa in [11] shows that the non-static part of the field decays, *i.e.*,

$$\mathcal{E}_\infty(t) \to 0 \quad \text{as} \quad t \to \infty \tag{5.9}$$

if the medium is non-dispersive and depends smoothly on $\boldsymbol{x}$ such that

$$|\boldsymbol{\varepsilon}_\infty(\boldsymbol{x}) - 1| = \mathrm{O}(|\boldsymbol{x}|^{-1-\delta}) \quad \text{as} \quad |\boldsymbol{x}| \to \infty \quad \text{for some} \quad \delta > 0.$$

The static part is connected to the charge density by the divergence equations (2.2).

The local energy decay for general constitutive relations, *e.g.*, the requirements on the longtime response is a subject for future research.

5.5 Finite-difference approximations

A natural way to solve the electromagnetic and acoustic initial boundary value problems is to use a finite-difference approximation. In the time-domain, this numerical method is referred to as the finite difference time-domain (FDTD) method. The popularity of the method has followed with the development of the computers. Several FDTD schemes were developed in the 50's, *e.g.*, the leapfrog scheme, the Lax-Wendroff scheme, and the Lax-Fredrich scheme. A good understanding of the schemes is given by the von Neumann analysis and the Lax-Richtmyer equivalence theorem [51, 102, 154, 220, 228].

In the 60's, Yee introduced the Yee-cell for electromagnetic problems. The Yee-cell utilizes a leapfrog (central differences) approximation on a shifted grid. In this thesis, we do not use the Yee-cell in the solution of the Maxwell equations. Instead, we use a standard leapfrog scheme and a Lax-Wendroff scheme. This is motivated by the treatment of the boundary conditions.

Before we describe the different FDTD schemes, the basic analysis of FDTD schemes is reviewed. The Lax-Richtmyer equivalence theorem states that an FDTD scheme converges to the true solution as the discretization parameters approach zero if and only if the scheme is consistent and stable. Consistency means that the difference between difference scheme and the partialdifferential operator is small for a fine discretization, *e.g.*, the difference scheme is accurate for smooth fields. The stability condition states that the difference between two fields is not allowed to grow too fast [220].

It is interesting to compare the Lax-Richtmyer equivalence theorem with the construction of the constitutive relations in Chapter 2. In the treatment of the instantaneous response in Section 2.4, the passivity enters as a stability condition, *i.e.*, to get an approximate constitutive map, it is necessary that the constitutive relations are consistent, *i.e.*, give a good approximation of the interaction between the fields and the material for the desired set of fields, and that the approximation is stable, *i.e.*, passivity gives a bound on the growth of the fields.

5.5.1 The leapfrog scheme

We start with the leapfrog scheme for the acoustic wave equation in two spatial dimensions, see Section 3.2. The pressure field $p(x_1, x_2, t)$ and the velocity field $\boldsymbol{v}(x_1, x_2, t)$ are approximated by the fields

$$p|_{i,j}^n \approx p(i\Delta x, j\Delta x, n\Delta t) \quad \text{and} \quad \boldsymbol{v}|_{i,j}^n \approx \boldsymbol{v}(i\Delta x, j\Delta x, n\Delta t).$$

The leapfrog scheme is based on a central difference approximation of both the spatial and temporal differential operators. This gives the internal scheme

$$\begin{cases} p|_{i,j}^{n+1} = p|_{i,j}^{n-1} - \kappa_{i,j}^{-1} 2\Delta t \, \mathrm{D}_0 \cdot \boldsymbol{v}|_{i,j}^n \\ \boldsymbol{v}|_{i,j}^{n+1} = \boldsymbol{v}|_{i,j}^{n-1} - \rho_{i,j}^{-1} 2\Delta t \, \mathrm{D}_0 \, p|_{i,j}^n \end{cases} \tag{5.10}$$

where D_0 is the central difference operator in two spatial dimensions, *i.e.*,

$$\mathrm{D}_0 \, f|_{i,j} = \frac{1}{2\Delta x} \begin{pmatrix} f|_{i+1,j} - f|_{i-1,j} \\ f|_{i,j+1} - f|_{i,j-1} \end{pmatrix}.$$

The scheme has to be modified at the boundary. We consider the case when the boundary conditions are given by the energy-flux split fields. For a finite inhomogeneous object located in a square area $(x_1, x_2) \in [0, 1] \times [0, 1]$, the fields at the boundary are computed with a one-way propagation type of scheme. For example, at the boundary $x_1 = 0$, the acoustic wave equations are equivalent to the following

system of differential equations (for simplicity, it is assumed that $\rho_0 = c_0 = 1$)

$$\begin{cases} \partial_t p_\pm \pm \partial_1 p_\pm + \dfrac{1}{2}\,\mathrm{D}\cdot\boldsymbol{v} = 0, \\ \partial_t \boldsymbol{v} + \mathrm{D}\,p = 0, \end{cases}$$

where we have used the energy flux split fields in Section 4.3.2, *i.e.*,

$$p_\pm = \frac{p \mp v_n}{2} = \frac{p \pm v_1}{2}$$

at the boundary $x_1 = 0$. If the incoming part of the split fields is prescribed at the boundary, *i.e.*, $p_+(x,t) = p_+^{(\mathrm{m})}(x,t)$, we get the system

$$\begin{cases} p_+|_{0,j}^{n+1} = p_+^{(\mathrm{m})}|_{0,j}^{n+1}, \\ p_-|_{0,j}^{n+1} = p_-|_{0,j}^{n} + \dfrac{\Delta t}{\Delta x}\left(p_-|_{1,j}^{n} - p_-|_{0,j}^{n}\right) - \dfrac{\Delta t}{2}\,\mathrm{D}_0\cdot\boldsymbol{v}|_{0,j}^{n}. \end{cases}$$

Use the definition of the split fields to update the pressure field and the normal component of the particle velocity, *i.e.*,

$$\begin{cases} p|_{0,j}^{n+1} = p_+|_{0,j}^{n+1} + p_-|_{0,j}^{n+1}, \\ v_1|_{0,j}^{n+1} = p_+|_{0,j}^{n+1} - p_-|_{0,j}^{n+1}. \end{cases}$$

The transverse part of the particle velocity is updated as

$$v_2|_{0,j}^{n+1} = v_2|_{0,j}^{n-1} - 2\Delta t\,\mathrm{D}_0\,p|_{0,j}^{n}. \tag{5.11}$$

The boundary conditions at the other boundaries are treated similarly.

5.5.2 Leapfrog scheme for the Maxwell equations

To simplify the notation, we only consider a single Debye polarization and a single Lorentz polarization. The electromagnetic field intensities satisfy

$$\begin{cases} \epsilon_\infty \partial_t \boldsymbol{E} - \nabla\times\boldsymbol{H} + \partial_t \boldsymbol{P}^{(\mathrm{D})} + \partial_t \boldsymbol{P}^{(\mathrm{L})} = \boldsymbol{0}, \\ \mu_\infty \partial_t \boldsymbol{H} + \nabla\times\boldsymbol{E} = \boldsymbol{0}, \\ \tau \partial_t \boldsymbol{P}^{(\mathrm{D})} + \boldsymbol{P}^{(\mathrm{D})} = \alpha \boldsymbol{E}, \\ \partial_t^2 \boldsymbol{P}^{(\mathrm{L})} + \nu \partial_t \boldsymbol{P}^{(\mathrm{L})} + \omega_0^2 \boldsymbol{P}^{(\mathrm{L})} = \beta \boldsymbol{E}, \end{cases} \tag{5.12}$$

rewrite the system as

$$\begin{cases} \epsilon_\infty \partial_t \boldsymbol{E} + \tau^{-1}\alpha \boldsymbol{E} = \nabla\times\boldsymbol{H} + \tau^{-1}\boldsymbol{P}^{(\mathrm{D})} - \dot{\boldsymbol{P}}^{(\mathrm{L})}, \\ \mu_\infty \partial_t \boldsymbol{H} = -\nabla\times\boldsymbol{E}, \\ \tau \partial_t \boldsymbol{P}^{(\mathrm{D})} + \boldsymbol{P}^{(\mathrm{D})} = \alpha \boldsymbol{E}, \\ \partial_t \dot{\boldsymbol{P}}^{(\mathrm{L})} + \nu \dot{\boldsymbol{P}}^{(\mathrm{L})} = -\omega_0^2 \boldsymbol{P}^{(\mathrm{L})} + \beta \boldsymbol{E}, \\ \partial_t \boldsymbol{P}^{(\mathrm{L})} = \dot{\boldsymbol{P}}^{(\mathrm{L})}. \end{cases} \tag{5.13}$$

Approximate the differential operators with central differences and the left-hand side quantities with temporal central averages. This gives the leapfrog scheme

$$\begin{cases} (\epsilon_\infty + \Delta t\tau^{-1}\alpha)\boldsymbol{E}|^{n+1} = (\epsilon_\infty - \Delta t\tau^{-1}\alpha)\boldsymbol{E}|^{n-1} + 2\Delta t(\nabla_0 \times \boldsymbol{H} + \tau^{-1}\boldsymbol{P}^{(\mathrm{D})} - \dot{\boldsymbol{P}}^{(\mathrm{L})})|^n, \\ \mu_\infty \boldsymbol{H}|^{n+1} = \mu_\infty \boldsymbol{H}|^{n-1} - 2\Delta t \nabla_0 \times \boldsymbol{E}|^n, \\ (\tau + \Delta t)\boldsymbol{P}^{(\mathrm{D})}|^{n+1} = (\tau - \Delta t)\boldsymbol{P}^{(\mathrm{D})}|^{n-1} + 2\Delta t\, \alpha \boldsymbol{E}|^n, \\ (1 + \Delta t\nu)\dot{\boldsymbol{P}}^{(\mathrm{L})}|^{n+1} = (1 - \Delta t\nu)\dot{\boldsymbol{P}}^{(\mathrm{L})}|^{n-1} - 2\Delta t\, (\omega_0^2 \boldsymbol{P}^{(\mathrm{L})}|^n + \beta \boldsymbol{E}|^n), \\ \boldsymbol{P}^{(\mathrm{L})}|^{n+1} = \dot{\boldsymbol{P}}^{(\mathrm{L})}|^{n-1} + 2\Delta t\, \dot{\boldsymbol{P}}^{(\mathrm{L})}|^n. \end{cases}$$

The leapfrog scheme is second order accurate and stable if [228, 220]

$$\frac{\Delta t}{\Delta x} \leq \frac{1}{c_\infty \sqrt{d}}$$

where d is the number of spatial dimensions and c_∞ is the wave-front speed. It is straightforward to generalize the leapfrog scheme to general bi-anisotropic medium models.

5.5.3 The Lax-Wendroff scheme

An alternative finite-difference scheme is given by the Lax-Wendroff scheme. The Lax-Wendroff scheme is based an a Taylor series approximation of the acoustic wave fields, *i.e.*,

$$\begin{cases} p|^{n+1} = p|^n + \Delta t\, \partial_t p|^n + \dfrac{\Delta t^2}{2} \partial_t^2 p|^n + \mathrm{O}(\Delta t^3), \\ \boldsymbol{v}|^{n+1} = \boldsymbol{v}|^n + \Delta t\, \partial_t \boldsymbol{v}|^n + \dfrac{\Delta t^2}{2} \partial_t^2 \boldsymbol{v}|^n + \mathrm{O}(\Delta t^3). \end{cases}$$

The acoustic wave equation is used to eliminate the temporal differentiations of the pressure and particle velocity. This gives the approximation

$$\begin{cases} p|^{n+1} = p^n - \dfrac{\Delta t}{\kappa} \nabla \cdot \boldsymbol{v}^n + \dfrac{\Delta t^2}{2\kappa} \nabla \cdot \left(\dfrac{1}{\rho} \nabla p|^n \right), \\ \boldsymbol{v}|^{n+1} = \boldsymbol{v}|^n - \dfrac{\Delta t}{\rho} \nabla p|^n + \dfrac{\Delta t^2}{2\rho} \nabla \left(\dfrac{1}{\kappa} \nabla \cdot \boldsymbol{v}|^n \right), \end{cases}$$

with the second order approximations for the spatial derivatives. The fields at the boundary are treated in a way that is similar to the one used in the leapfrog scheme, except that the tangential components are implemented with a Lax-type scheme, *e.g.*,

$$v_2|_{0,j}^{n+1} = \frac{v_2|_{0,j-1}^n + v_2|_{0,j+1}^n}{2} - \Delta t\, \mathrm{D}_0\, p|_{0,j}^n,$$

are used at the boundary $x_1 = 0$ instead of (5.11).

Chapter 6

Bremmer Series

The Bremmer series solves the coupled system of one-way wave equations in an iterative fashion. Hence, it accounts for the back scattered wave fields in the one-way wave approximation. The series was introduced by Bremmer to solve and analyze a one-dimensional scattering problem [28]. Convergence of the one-dimensional Bremmer series is considered in several papers, see *e.g.*, Refs [10, 143, 142]. In multi-dimensions, Corones [39] considered the Bremmer series as a correction to the paraxial approximation. The Bremmer series with a locally exact wave splitting is discussed by de Hoop [52], see also Stralen [242].

To illustrate the Bremmer series idea, we start with a discussion of scattering by a homogeneous slab in Section 6.1. The Bremmer series for a layered medium and an inhomogeneous slab is analyzed in Section 6.2. Acoustic scattering by an inhomogeneous slab is considered in Section 6.3.

6.1 Scattering by a homogeneous slab

We start with a very simple problem, *i.e.*, scattering by a homogeneous slab, see Figure 6.1. The slab and the surrounding medium are isotropic materials with a permittivity ϵ_i and permeability μ_i. Propagation of a plane wave in the medium is characterized by the vertical-propagation coefficient (symbol) γ_i, $i = 0, 1, 2$, see Section 4.2.1. A plain wave $\widehat{E}_{\rm i}\mathrm{e}^{-\gamma_0 x_3}$ impinges at the slab from the left. The incoming wave is reflected by the slab, *i.e.*, to the left of the slab we have the total electric field

$$\widehat{E}(x_3) = \widehat{E}_{\rm i}\mathrm{e}^{-\gamma_0 x_3} + \widehat{E}_{\rm r}\mathrm{e}^{\gamma_0 x_3} \quad \text{for} \quad x_3 < 0. \tag{6.1}$$

In the internal region of the slab, the total wave field can be written as a sum of a right- and left-going wave, *i.e.*,

$$\widehat{E}(x_3) = \widehat{E}_{+}\mathrm{e}^{-\gamma_1 x_3} + \widehat{E}_{-}\mathrm{e}^{\gamma_1 (x_3 - d)} \quad \text{for} \quad 0 < x_3 < d. \tag{6.2}$$

To the right of the slab, there is a single right-going wave

$$\widehat{E}(x_3) = \widehat{E}_{\rm t}\mathrm{e}^{-\gamma_2 (x_3 - d)} \quad \text{for} \quad x_3 > d. \tag{6.3}$$

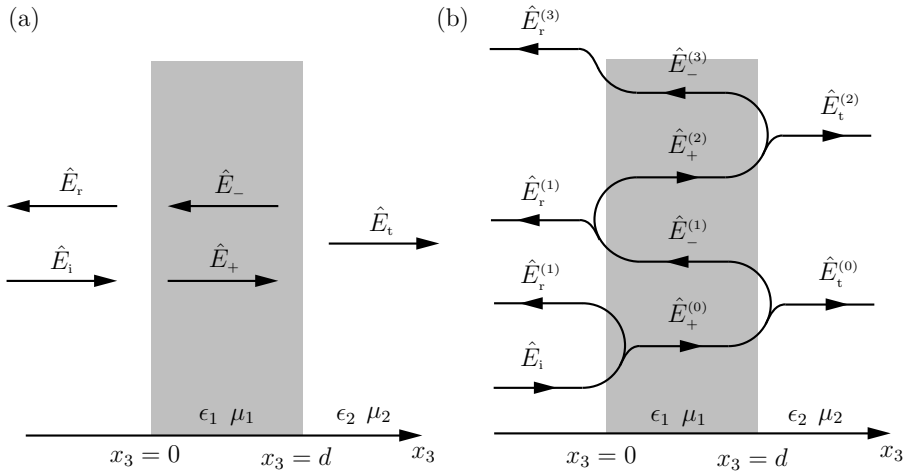

Figure 6.1: Scattering against a homogeneous slab: (a) the ansatz method, (b) the Bremmer series interpretation.

The corresponding magnetic fields are given by the impedance transformation (4.10). In (6.1), (6.2), and (6.3) we have the four unknowns $\widehat{E}_\mathrm{r}$, $\widehat{E}_+$, $\widehat{E}_-$, and $\widehat{E}_\mathrm{t}$. We can determine these parameters in several ways, *e.g.*, an ansatz followed by matching boundary conditions or as a sequence of single scattering problems, see Figure 6.1. In the ansatz method, we prescribe general fields inside as well as outside the slab and match the electric and magnetic fields at the boundaries $x_3 = 0$ and $x_3 = d$, respectively. We start with the ansatz method, *i.e.*, the tangential components of the electric and magnetic fields are continuous at the slab interfaces. This gives the system

$$\begin{pmatrix} 1 & -1 & -\mathrm{e}^{-\gamma_1 d} & 0 \\ \mathrm{Z}_0 & \mathrm{Z}_1 & -\mathrm{Z}_1\mathrm{e}^{-\gamma_1 d} & 0 \\ 0 & \mathrm{e}^{-\gamma_1 d} & 1 & -1 \\ 0 & \mathrm{Z}_1\mathrm{e}^{-\gamma_1 d} & -\mathrm{Z}_1 & -\mathrm{Z}_2 \end{pmatrix} \begin{pmatrix} \widehat{E}_\mathrm{r} \\ \widehat{E}_+ \\ \widehat{E}_- \\ \widehat{E}_\mathrm{t} \end{pmatrix} = \begin{pmatrix} -\widehat{E}_\mathrm{i} \\ \mathrm{Z}_0\widehat{E}_\mathrm{i} \\ 0 \\ 0 \end{pmatrix}. \tag{6.4}$$

The reflected and transmitted fields are determined as the solution of the system (6.4), *i.e.*,

$$\widehat{E}_\mathrm{r} = \frac{r_0 + r_1\mathrm{e}^{-2\gamma_1 d}}{1 + r_0 r_1 \mathrm{e}^{-2\gamma_1 d}}\widehat{E}_\mathrm{i}$$

and

$$\widehat{E}_\mathrm{t} = \frac{t_0 t_1 \mathrm{e}^{-2\gamma_1 d}}{1 + r_0 r_1 \mathrm{e}^{-2\gamma_1 d}}\widehat{E}_\mathrm{i},$$

respectively. Where the reflection coefficient r_j and the transmission coefficient t_j are

$$r_j = \frac{\mathrm{Z}_{j+1} - \mathrm{Z}_j}{\mathrm{Z}_{j+1} + \mathrm{Z}_j} \quad \text{and} \quad t_j = r_j + 1, \quad j = 0, 1,$$

respectively. The impedance Z_j is $\mathrm{Z}_j = \sqrt{\mu_j/\epsilon_j}$ for $j = 0, 1, 2$.

In the Bremmer series the problem is reduced to a sequence of single scattering problems. see Figure 6.1. First, the right going wave $\widehat{E}_{\mathrm{i}}(x_3)$ impinges at the interface $x_3 = 0$. One part is reflected by the interface and the rest is transmitted into the slab. The transmitted part propagates through the slab to the interface $x_3 = d$. Here one part is reflected back into the slab and the rest is transmitted through the interface. These arguments are then repeatedly applied to each of the reflected parts. The result is an infinite series of single scattering events. Summing all single scattering events gives the total wave field. The reflected field is

$$\begin{aligned}
\widehat{E}_{\mathrm{r}} &= \widehat{E}_{\mathrm{r}}^{(1)} + \widehat{E}_{\mathrm{r}}^{(3)} + \dots \\
&= \widehat{E}_{\mathrm{i}} \left(r_0 + (1-r_0)\mathrm{e}^{-\gamma_1 d} r_1 \mathrm{e}^{-\gamma_1 d}(1+r_0) \right. \\
&\quad \left. + (1-r_0)\mathrm{e}^{-\gamma_1 d} r_2 \mathrm{e}^{-\gamma_1 d}(-r_0)\mathrm{e}^{-\gamma_1 d} r_1 \mathrm{e}^{-\gamma_1 d}(1+r_0) \right) \\
&= \widehat{E}_{\mathrm{i}} \left(r_0 + r_1 \mathrm{e}^{-2\gamma_1 d} \right) \sum_{n=0}^{\infty} \left(-r_0 r_1 \mathrm{e}^{-2\gamma_1 d} \right)^n .
\end{aligned}$$

The corresponding transmitted field is

$$\begin{aligned}
\widehat{E}_{\mathrm{t}} &= \widehat{E}_{\mathrm{t}}^{(0)} + \widehat{E}_{\mathrm{t}}^{(2)} + \dots \\
&= \widehat{E}_{\mathrm{i}} \left((1-r_0)\mathrm{e}^{-\gamma_1 d}(1-r_1) + (1-r_0)\mathrm{e}^{-\gamma_1 d} r_2 \mathrm{e}^{-\gamma_1 d}(-r_0)\mathrm{e}^{-\gamma_1 d}(1-r_1) \right) \\
&= \widehat{E}_{\mathrm{i}} \, (1-r_0)(1-r_1)\mathrm{e}^{-\gamma_1 d} \sum_{n=0}^{\infty} \left(-r_0 r_1 \mathrm{e}^{-2\gamma_1 d} \right)^n .
\end{aligned}$$

The internal fields are determined in a similar fashion. The series converges if $|r_0 r_1 \mathrm{e}^{-2\gamma_1 d}| < 1$. Another interpretation of the Bremmer series is as an iterative solution of the system

$$\begin{pmatrix} 1 & 0 & -(1-r_0)\mathrm{e}^{-\gamma_1 d} & 0 \\ 0 & 1 & r_0 \mathrm{e}^{-\gamma_1 d} & 0 \\ 0 & -r_1 \mathrm{e}^{-\gamma_1 d} & 1 & 0 \\ 0 & -(1+r_1)\mathrm{e}^{-\gamma_1 d} & 0 & 1 \end{pmatrix} \begin{pmatrix} \widehat{E}_{\mathrm{r}} \\ \widehat{E}_{+} \\ \widehat{E}_{-} \\ \widehat{E}_{\mathrm{t}} \end{pmatrix} = \begin{pmatrix} r_0 \widehat{E}_{\mathrm{i}} \\ (1+r_0)\widehat{E}_{\mathrm{i}} \\ 0 \\ 0 \end{pmatrix}, \tag{6.5}$$

see also Figure 4.4.

6.2 Bremmer Series in one spatial dimension

The one-dimensional Bremmer series have been thoroughly investigated, see Refs [142, 10, 143, 99, 28]. The series converges in the Fourier domain for sufficiently small and smooth parameters and in general in the time domain.

Here, we give a rough convergence estimate of the series. We consider the system of one-way wave equations (4.13). The system is solved by a fixed point iteration,

i.e., the first and succeeding equations are

$$\begin{cases} (\partial_3 + \Gamma - \mathrm{R} - \Xi)\hat{u}_+^{(0)} = 0 \\ (\partial_3 - \Gamma - \mathrm{R} + \Xi)\hat{u}_-^{(0)} = 0 \\ \hat{u}_+^{(1)}(0) = \hat{u}_+^{(\mathrm{in})} \\ \hat{u}_-^{(1)}(X_3) = \hat{u}_-^{(\mathrm{in})}, \end{cases}$$

and

$$\begin{cases} (\partial_3 + \Gamma - \mathrm{R} - \Xi)\hat{u}_+^{(k)} = -(\mathrm{R} - \Xi)\hat{u}_-^{(k-1)} \\ (\partial_3 - \Gamma - \mathrm{R} + \Xi)\hat{u}_-^{(k)} = -(\mathrm{R} + \Xi)\hat{u}_+^{(k-1)} \\ \hat{u}_+^{(k)}(0) = 0 \\ \hat{u}_-^{(k)}(X_3) = 0, \end{cases} \quad \text{for} \quad k = 1, 2, \dots ,$$

respectively. Observe that we use the notation $\hat{u}_\pm = \widehat{E}_\pm$ for the down- and up-going wave constituents. The prescribed incoming wave fields are given by $\hat{u}_\pm^{(\mathrm{in})}$. The reflection operator and error term are given by

$$\mathrm{R} = -\frac{\partial_3 \epsilon'}{4\epsilon'} = -\partial_3 \ln(\epsilon')^{1/4} \quad \text{and} \quad \Xi = s\frac{\epsilon' - \epsilon}{2\sqrt{\epsilon'}},$$

respectively, see Section 4.2.2.

The total wave field is the sum of the Bremmer terms

$$\hat{u}_\pm = \sum_{k=0}^{\infty} \hat{u}_\pm^{(k)}. \tag{6.6}$$

The sequence converges, if the iteration is a contraction. We let the medium be non-magnetic and passive, *i.e.*, $\mu = 1$, and

$$\mathrm{Re}\{s\epsilon(x_3, s)\} \geq \eta\epsilon_\infty \quad \text{and} \quad \mathrm{Re}\{s\epsilon'(x_3, s)\} \geq \eta\epsilon'_\infty.$$

It is also assumed that $0 < \lim_{s\to\infty} \epsilon'(x_3, s) < \lim_{s\to\infty} \epsilon(x_3, s)$. We get a rough convergence estimate by an energy estimate type inequality, *i.e.*, multiply with $(\hat{u}_\pm^{(k)})^*$ from the left and we get

$$\begin{cases} \partial_3|\hat{u}_+^{(k)}(x_3)|^2 + 2(\Gamma - \mathrm{R} - \Xi)|\hat{u}_+^{(k)}(x_3)|^2 = -2(\hat{u}_+^{(k)})^*(\mathrm{R} - \Xi)\hat{u}_-^{(k-1)}(x_3), \\ \partial_3|\hat{u}_-^{(k)}(x_3)|^2 - 2(\Gamma + \mathrm{R} - \Xi)|\hat{u}_-^{(k)}(x_3)|^2 = -2(\hat{u}_-^{(k)})^*(\mathrm{R} + \Xi)\hat{u}_+^{(k-1)}(x_3). \end{cases} \tag{6.7}$$

Multiply with the factors of integration, *i.e.*,

$$\begin{cases} \exp(2\int_0^{x_3} \Gamma - \mathrm{R} - \Xi \,\mathrm{d}x_3') = \left(\dfrac{\epsilon'(x_3)}{\epsilon'(0)}\right)^{1/2} \exp(2\int_0^{x_3} \Gamma - \Xi \,\mathrm{d}x_3') \\ \exp(2\int_{x_3}^{X_3} \Gamma + \mathrm{R} - \Xi \,\mathrm{d}x_3') = \left(\dfrac{\epsilon'(x_3)}{\epsilon'(X_3)}\right)^{1/2} \exp(2\int_{x_3}^{X_3} \Gamma - \Xi \,\mathrm{d}x_3') \end{cases}$$

and integrate over $[0, x_3]$ and $[x_3, X_3]$, respectively, to get

$$\begin{cases} |\hat{u}_+^{(k)}(x_3)\sqrt[4]{\epsilon'}|^2 = -\displaystyle\int_0^{x_3} \exp(-2\int_{x_3'}^{x_3} \Gamma - \Xi \,\mathrm{d}x_3'')\, (\hat{u}_+^{(k)})^*(\mathrm{R} - \Xi)\hat{u}_-^{(k-1)}\sqrt{\epsilon'}\,\mathrm{d}x_3', \\ |\hat{u}_-^{(k)}(x_3)\sqrt[4]{\epsilon'}|^2 = -\displaystyle\int_{x_3}^{X_3} \exp(-2\int_{x_3}^{x_3'} \Gamma - \Xi \,\mathrm{d}x_3'')\, (\hat{u}_-^{(k)})^*(\mathrm{R} + \Xi)\hat{u}_+^{(k-1)}\sqrt{\epsilon'}\,\mathrm{d}x_3'. \end{cases} \tag{6.8}$$

Here, we use a supremum estimate on the terms, *i.e.*,

$$\begin{cases} |\hat{u}_+^{(k)}(x_3)\sqrt[4]{\epsilon'}|^2 \le 2 \sup\limits_{x_3'\in[0,x_3]} |\hat{u}_+^{(k)}(x_3')\sqrt[4]{\epsilon'}|\, |\hat{u}_-^{(k-1)}(x_3')\sqrt[4]{\epsilon'}| \\ \qquad\qquad \displaystyle\int_0^{x_3} \exp(-2\,\mathrm{Re}\int_{x_3'}^{x_3} \Gamma - \Xi \,\mathrm{d}x_3'')\, |\mathrm{R} - \Xi|\,\mathrm{d}x_3', \\ |\hat{u}_-^{(k)}(x_3)\sqrt[4]{\epsilon'}|^2 \le 2 \sup\limits_{x_3'\in[x_3,X_3]} |\hat{u}_-^{(k)}(x_3')\sqrt[4]{\epsilon'}|\, |\hat{u}_+^{(k-1)}(x_3')\sqrt[4]{\epsilon'}| \\ \qquad\qquad \displaystyle\int_{x_3}^{X_3} \exp(-2\,\mathrm{Re}\int_{x_3}^{x_3'} \Gamma - \Xi \,\mathrm{d}x_3'')\, |\mathrm{R} + \Xi|\,\mathrm{d}x_3'. \end{cases} \tag{6.9}$$

Use the passivity condition $\mathrm{Re}\{\Gamma - \Xi\} \ge \eta\epsilon_\infty'$ to get the estimate

$$\begin{cases} \sup\limits_{x_3'\in[0,X_3]} |\hat{u}_+^{(k)}\sqrt[4]{\epsilon'}| \le 2 \sup\limits_{x_3'\in[0,X_3]} |\hat{u}_-^{(k-1)}\sqrt[4]{\epsilon'}| \displaystyle\int_0^{X_3} \mathrm{e}^{-\eta(X_3-\zeta)}|\mathrm{R} - \Xi|\,\mathrm{d}\zeta, \\ \sup\limits_{x_3'\in[0,X_3]} |\hat{u}_-^{(k)}\sqrt[4]{\epsilon'}| \le 2 \sup\limits_{x_3'\in[0,X_3]} |\hat{u}_+^{(k-1)}\sqrt[4]{\epsilon'}| \displaystyle\int_0^{X_3} \mathrm{e}^{-\eta(X_3-\zeta)}|\mathrm{R} + \Xi|\,\mathrm{d}\zeta \end{cases} \tag{6.10}$$

for sufficiently large values of $\mathrm{Re}\, s = \eta$. The iteration is an contraction if η is sufficiently large or if the interaction is sufficiently small, *i.e.*, the series converges in the time domain but Fourier convergence ($s = \mathrm{i}\omega$) is only shown if (here, it is assumed that $\mathrm{Re}\{\Gamma - \Xi\} \ge 0$)

$$\int_0^{X_3} |\mathrm{R} \pm \Xi|\,\mathrm{d}x_3 = \int_0^{X_3} |-\frac{\partial_3\epsilon'}{4\epsilon'} \pm \mathrm{i}\omega\frac{\epsilon' - \epsilon}{2\sqrt{\epsilon'}}|\,\mathrm{d}x_3 \le \frac{1}{2}.$$

Atkinson [10] have shown that the series converge if and only if

$$\int_0^{\infty} |\frac{\partial_3\epsilon}{4\epsilon}|\,\mathrm{d}x_3 < \pi \tag{6.11}$$

and Kay [142] have shown that a reformulation of the Bremmer series converges if

$$\int_0^{\infty} |\frac{\partial_3\epsilon}{4\epsilon}|\,\mathrm{d}x_3 < \infty, \tag{6.12}$$

see also Refs [143, 99].

The coupling between the down- and up-going wave constituents is given by the reflection part R and the error part Ξ. It is interesting to minimize the total coupling, *i.e.*,

$$\min_{\epsilon'} \int_0^{X_3} |-\frac{\partial_3\epsilon'}{4\epsilon'} \pm \mathrm{i}\omega\frac{\epsilon'-\epsilon}{2\sqrt{\epsilon'}}|\,\mathrm{d}x_3.$$

This can be formulated as a variational problem with the solution of the corresponding Euler equation [247].

In the original formulation by Bremmer, the series was derived as a limiting case of a layered medium [28]. For a layered medium one gets a system similar to the slab system (6.5). The Bremmer series is a special iterative solution of this sparse linear system [211].

We also note the asymptotic property of the Bremmer series. Let the medium be a small perturbation of a homogeneous background, *i.e.*,

$$\epsilon(x_3, s) = \epsilon_{\mathrm{b}} + \delta\psi(x_3, s)$$

where δ is a real-valued parameter that determines the size of the perturbation. The reflection operator is

$$\mathrm{R} = -\delta\frac{\partial_3\psi}{4\epsilon_{\mathrm{b}}} + \mathrm{O}(\delta^2) \quad \text{and} \quad \mathrm{R}_j = \delta\frac{\psi_j - \psi_{j+1}}{4\epsilon_{\mathrm{b}}} + \mathrm{O}(\delta^2) \quad \text{as} \quad \delta \to 0$$

for a continuous and layered medium, respectively. The same estimates hold for the error estimate. Hence a reflection reduces the amplitude of the field one order in δ and the Bremmer series have the asymptotic convergence rate

$$\hat{u}_{\pm}^{(k)} = \mathrm{O}(\delta^{k-1}) \quad \text{as} \quad \delta \to 0.$$

6.3 The Bremmer series for the acoustic wave equation

In multi-dimensions, the Bremmer series was introduced by Corones as a correction to the paraxial approximation [39]. In Ref. [183], McMaken considered the convergence properties of the two-dimensional Bremmer series in the frequency domain. de Hoop have shown that the Bremmer series converges in the Laplace domain for a locally exact wave splitting provided that the Laplace parameter is real-valued and sufficiently large [52]. Here, we follow [105] to show time-domain convergence of the Bremmer series for passive medium models with a homogeneous high-frequency response. The non-homogeneous high-frequency response can be treated with an approximation procedure similar to the approximation in Section 2.4, see also Ref. [105].

We consider the one-way system (4.30), where the local approximation is used for the vertical-propagation operator and the interaction operator is bounded according to (4.42). In the Bremmer series, we solve the scattering problem (4.30)

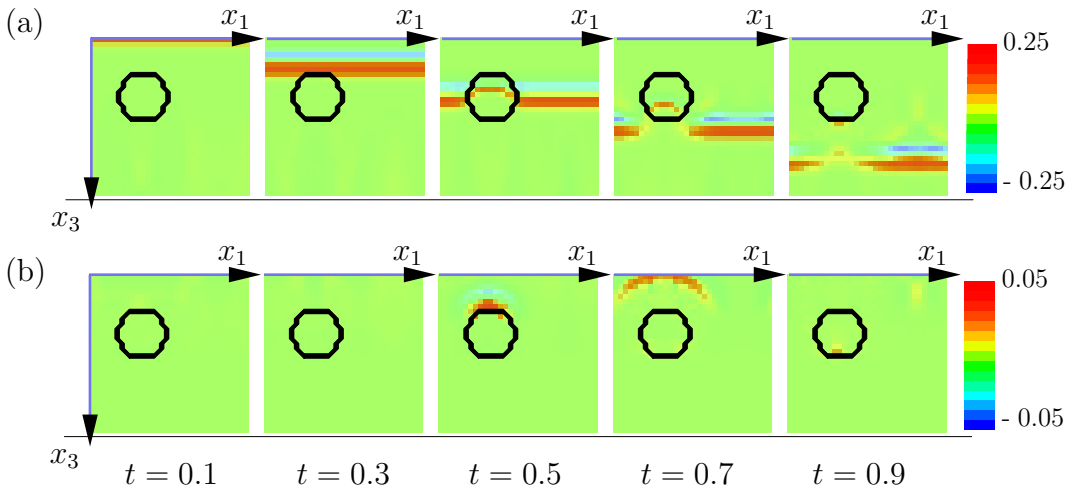

Figure 6.2: Numerical illustration of the Bremmer series. (a) The first down-going wave constituent. (b) The second up-going wave constituent. Time is evolving from the left to the right.

in an iterative fashion, *i.e.*, fixed point iterations, Neumann series or successive approximations. The initial step and the succeeding iterations are

$$\begin{cases} (\partial_3 + \Gamma_{\mathrm{L}} - \mathrm{R}_{\mathrm{L}} - \Xi_{\mathrm{L}})\hat{u}_+^{(0)} = 0 \\ (\partial_3 - \Gamma_{\mathrm{L}} - \mathrm{R}_{\mathrm{L}} + \Xi_{\mathrm{L}})\hat{u}_-^{(0)} = 0 \\ \hat{u}_+^{(1)}(x,0) = \hat{u}_+^{(\mathrm{in})}(x) \\ \hat{u}_-^{(1)}(x,X_3) = \hat{u}_-^{(\mathrm{in})}(x), \end{cases} \tag{6.13}$$

and

$$\begin{cases} (\partial_3 + \Gamma_{\mathrm{L}} - \mathrm{R}_{\mathrm{L}} - \Xi_{\mathrm{L}})\hat{u}_+^{(k)} = -(\mathrm{R}_{\mathrm{L}} + \Xi_{\mathrm{L}})\hat{u}_-^{(k-1)} \\ (\partial_3 - \Gamma_{\mathrm{L}} - \mathrm{R}_{\mathrm{L}} + \Xi_{\mathrm{L}})\hat{u}_-^{(k)} = -(\mathrm{R}_{\mathrm{L}} - \Xi_{\mathrm{L}})\hat{u}_+^{(k-1)} \\ \hat{u}_+^{(k)}(x,0) = 0 \\ \hat{u}_-^{(k)}(x,X_3) = 0, \end{cases} \quad \text{for} \quad k = 1,2,\dots, \tag{6.14}$$

respectively. The fields outside the strip $[0, X_3]$ are determined with the free space vertical-propagation operator Γ_0 defined in (4.33). Observe that there is an ambiguity in the definition of the Bremmer series regarding the position of the transmission part of the interaction $\mathrm{R}_{\mathrm{L}} \pm \Xi_{\mathrm{L}}$. In approaches based on integral equations it is common to include the transmission part in the right-hand side of the iteration [52]. Here, we choose to update the fields as much as possible and hence include the transmission part in the left-hand side. The convergence proof is essentially independent of this choice.

The total wave field is the sum of the Bremmer terms in (6.13) and (6.14)

$$\hat{u}_\pm = \sum_{k=0}^{\infty} \hat{u}_\pm^{(k)}.$$

The sequence converges, if the iteration is a contraction. We use energy estimates to get an L^2-bound, see Ref. [154, 68]. The equations (6.14) are multiplied with $\hat{u}_+^{(k)}$ and $\hat{u}_-^{(k)}$, respectively, and the estimates (4.40) and (4.42) are used to get

$$\begin{cases} \partial_3 \|\hat{u}_+^{(k)}(\cdot, x_3)\|_2^2 + (\eta c_0^{-1} - 3C\delta\eta^{-1})\|\hat{u}_+^{(k)}(\cdot, x_3)\|_2^2 \leq C\delta\eta^{-1}\|\hat{u}_-^{(k-1)}(\cdot, x_3)\|_2^2, \\ -\partial_3 \|\hat{u}_-^{(k)}(\cdot, x_3)\|_2^2 + (\eta c_0^{-1} - 3C\delta\eta^{-1})\|\hat{u}_-^{(k)}(\cdot, x_3)\|_2^2 \leq C\delta\eta^{-1}\|\hat{u}_+^{(k-1)}(\cdot, x_3)\|_2^2. \end{cases}$$

Next we integrate the inequalities over $[0, X_3]$. This gives the bounds

$$\begin{cases} \displaystyle\int_0^{X_3} \|\hat{u}_+^{(k)}(\cdot, x_3)\|_2^2 \,\mathrm{d}x_3 \leq \frac{C\delta}{\eta^2 c_0^{-1} - 3C\delta} \int_0^{X_3} \|\hat{u}_-^{(k-1)}(\cdot, x_3)\|_2^2 \,\mathrm{d}x_3, \\ \displaystyle\int_0^{X_3} \|\hat{u}_-^{(k)}(\cdot, x_3)\|_2^2 \,\mathrm{d}x_3 \leq \frac{C\delta}{\eta^2 c_0^{-1} - 3C\delta} \int_0^{X_3} \|\hat{u}_+^{(k-1)}(\cdot, x_3)\|_2^2 \,\mathrm{d}x_3. \end{cases}$$

The final bound is obtained by adding the two inequalities

$$\int_0^{X_3} \|\hat{u}^{(k)}(\cdot, x_3)\|_2^2 \,\mathrm{d}x_3 \leq \frac{C\delta}{\eta^2 c_0^{-1} - 3C\delta} \int_0^{X_3} \|\hat{u}^{(k-1)}(\cdot, x_3)\|_2^2 \,\mathrm{d}x_3.$$

For η sufficiently large, *i.e.*, $\eta^2 \geq 4C\delta c_0$, the map is a contraction and the Bremmer series (6.14) converges. The initial step in (6.13) gives in a similar way a bound on the first term

$$\int_0^{X_3} \|\hat{u}^{(0)}(\cdot, x_3)\|_2^2 \,\mathrm{d}x_3 \leq \|\hat{u}^{(\mathrm{in})}(\cdot)\|_2^2,$$

for $\eta^2 \geq 4C\delta c_0$.

To show that there exists a solution to the one-way systems (6.13) and (6.14), we can use the free space representations (4.39), (4.40), and (4.41). The one-way system is iterated with the free space solution (existence of the free space solution follows from Fourier calculus). The iteration converges for sufficiently large values of η_0.

A numerical example of the Bremmer series in shown in Figure 6.2. A plane wave in a homogeneous space, modeled by compressibility κ_0 and density ρ_0, impinges on a cylinder with compressibility $\kappa = 5\kappa_0$. The first down-going wave constituent is shown in Figure 6.2a, and the second order up-going wave constituent (the reflected field) is shown in Figure 6.2b.

6.3.1 Convergence rate

In the Bremmer series, the real-valued part of the Laplace parameter is fixed at the value, $\mathrm{Re}\, s = \eta$. We iterate the series N times and subsequently go back to the time-domain trough the inverse Laplace transform (2.10). If the parameter η is increased the series converges faster. However, the error has to be smaller due to multiplication with $\mathrm{e}^{\eta t}$ in the inverse Laplace transformation. For a fixed time $t = T$, the series can be iterated until the error is small enough (assume no numerical truncation errors) and the inverse Laplace transformation gives time-domain convergence.

A rough estimate of the error is

$$\begin{aligned}
&\int_0^T \int_0^{X_3} \| \sum_{k=1}^{N} u^{(k)}(\cdot, x_3, t) - u(\cdot, x_3, t)\|_2^2 \, \mathrm{d}x_3 \, \mathrm{d}t \\
&\leq \frac{\mathrm{e}^{2\eta T}}{2\pi} \int_{\mathbb{R}} \int_0^{X_3} \| \sum_{k=1}^{N} \hat{u}^{(k)}(\cdot, x_3, \eta + \mathrm{i}\omega) - \hat{u}(\cdot, x_3, \eta + \mathrm{i}\omega)\|_2^2 \, \mathrm{d}x_3 \, \mathrm{d}\omega \qquad (6.15) \\
&\leq \mathrm{e}^{2\eta T} \int_0^T \|u^{(0)}(\cdot, t)\|_2^2 \, \mathrm{d}t \sum_{k=N}^{\infty} \left(\frac{C\delta}{\eta^2 c_0^{-1} - 3C\delta} \right)^k .
\end{aligned}$$

The error estimate (6.15) gives the convergence rate

$$N \sim \eta T - \ln(\text{Error}) \qquad (6.16)$$

for large values of η. The number of iterations grows linearly in time, and the accuracy convergence is of exponential order, see Ref. [242] for corresponding numerical results in one spatial dimension. The error can be made arbitrary small by iterating the series enough number of times.

It is also interesting to consider the asymptotic convergence in weak scattering. Let the compressibility by a small perturbation of free space, *i.e.*, δ is small. We get the asymptotic convergence

$$\int_{t=0}^{T} \int_{x_3=0}^{X_3} \| \sum_{k=0}^{N} u^{(k)}(\cdot, x_3, t) - u(\cdot, x_3, t)\|_2^2 \, \mathrm{d}x_3 \, \mathrm{d}t = \mathrm{O}(\delta^N) \quad \text{as} \quad \delta \to 0. \qquad (6.17)$$

Chapter 7

Inverse problems

In this chapter and below we discuss inverse problems. The first question to ask is: what is an inverse problem? According to Keller two problems are each others inverses if the formulation of one of them require full or partial knowledge of the other [145]. This general description does not distinguish the two problems. In many cases it is desirable to consider one of the problems as a direct problem and the other as the inverse problem. Here, we define the direct and inverse problems from a cause and effect perspective. In the previous chapters, we studied how to determine the fields (effects) caused by given sources and constitutive relations. This is the direct problem. The inverse to this direct problem is to use the fields (effects) to infer information about the causes, *i.e.*, the sources and (or) the constitutive relations. Furthermore, the inverse problems are distinguished according to the amount of available information, *e.g.*, into inverse scattering, inverse source problems, imaging, and inverse spectral problems. There is an extensive literature on inverse problems, see *e.g.*, Refs [122, 124, 209, 234, 38, 23, 38, 25] for electromagnetic inverse problems and[169, 37, 127, 147, 18] for a general discussion about inverse problems in partial differential equations and integral equations.

In Section 7.1, we discuss inverse scattering and in Section 7.2 three algorithms for inverse scattering against a dielectric slab are outlined. In Chapter 8, the optimization approach of Section 7.2.3 is generalized to multidimensional inverse scattering problems.

7.1 Inverse scattering

To infer information about the electromagnetic structure of an object, we study the interaction between the object and electromagnetic fields. Typically, we illuminate the object with a known field and (part of) the scattered field is measured. To relate the scattered field to the electromagnetic properties of the object, we make a model of the object. In general, the electromagnetic properties of the object are modeled by the source-free Maxwell equations (2.1) together with a set of constitutive relations (2.4). We use our knowledge about the direct problem, *i.e.*, for a given set of constitutive relations we determine the interaction between the object and the electromagnetic field. Assuming that it is possible to determine the interaction

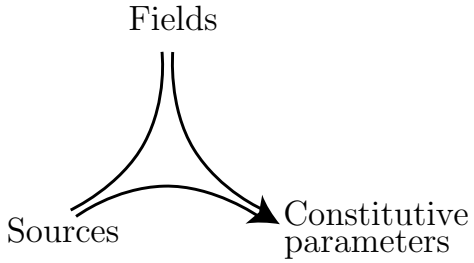

Figure 7.1: The inverse scattering problem. We infer information about the object from given scattering data.

between the electromagnetic field and all object models, one gets a set of admissible models of the object that resembles the interaction between the object and the field. The problem to determine the model from given scattering data is called the inverse scattering problem, see Figure 7.1.

A few important observations about the inverse scattering problem are:

Non-linear: The set of constitutive parameters does not depend linearly on the observed fields.

Uniqueness: To get a unique model, the set of admissible constitutive models might have to be restricted, *i.e.*, the scattering data might not contain sufficient information to uniquely determine the scatterer.

Existence: If the set of admissible models is restricted and (or) the observed fields are contaminated with noise, it is unlikely that there exists a model that fits the data.

Continuity: The identified set of models does not depend continuously on the observed fields, *i.e.*, there might be several different models that fit the data with high accuracy.

These observations are not very promising for solving the inverse scattering problem. The lack of continuous dependence of data (also the existence and uniqueness) is usually referred to as the ill-posedness of the inverse scattering problem. In general, we use additional information about the object to remedy these deficiencies to get a well-posed problem. The additional information is typically in the form of a priori knowledge about an accurate and simple model of the object, *e.g.*, an a priori given parameterization of the object. If the object model is sufficiently good and not too general, we get uniqueness (and existence) of the solution of the inverse scattering problem. The lack of continuous dependence of the data is typically resolved by additional assumptions about the spatial properties of the object, *e.g.*, the electromagnetic properties of the object are modeled by (piecewise) sufficiently smooth functions of the spatial coordinates. The assumption on the spatial structure is related to the fundamental limitation of the scattering problem, *i.e.*, we have a limited resolution, see Chapter 2.

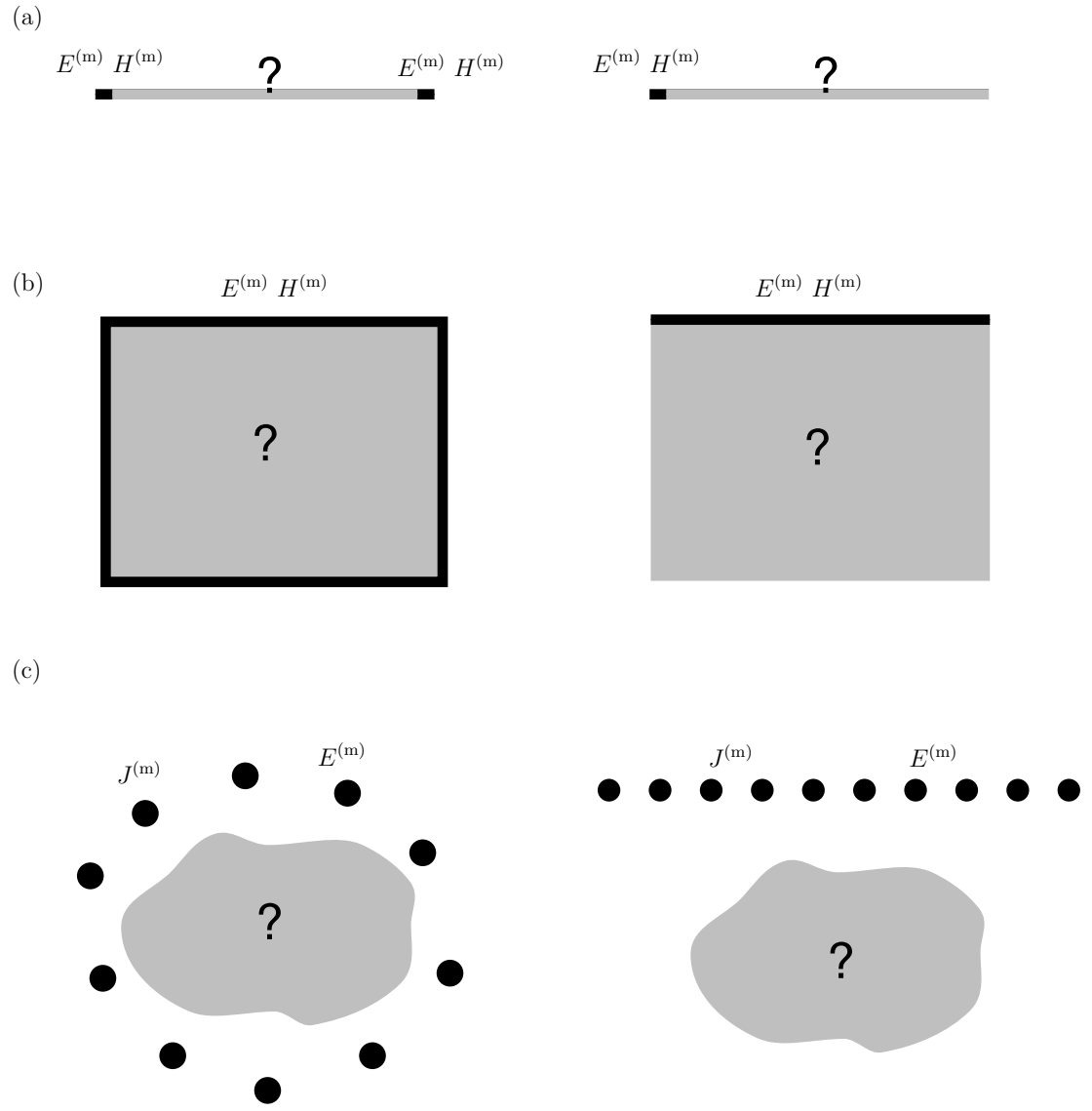

Figure 7.2: The measurement configuration of the inverse problem. The gray and black parts illustrate the unknown region and the region of field observation, respectively. From top to bottom: (a) The one-dimensional case. (b) The multi-dimensional case with a continuous set of field observations. (c) The multi-dimensional case with a discrete set of field observations.

Mathematically, we formulate the inverse scattering problem as a problem to identify parameters of the constitutive relations. The formulation depends on the amount of given data. A few typical measurement configurations are illustrated in Figure 7.2. Subfigures (a), (b), and (c) illustrate the one-dimensional case, the multi-dimensional case with a continuous set of observed data, and the multi-dimensional case with a discrete set of observed data, respectively. Furthermore, the data can be observed at a surface surrounding the object or only at part of the surface, *i.e.*, the left or right part of Figure 7.2, respectively. We also distinguish whether the data is given in the time domain or for a discrete set of frequencies. There are several other measurement configurations, *e.g.*, in many radar applications, where only the (backscattered) far-field (amplitude) is observed.

In medical imaging there are many applications where it is possible to get measurements at a surface surrounding the unknowing object. A well known example is X-ray tomography where a high frequency source is used to illuminate the object [123, 17]. A low frequency version is electrical impedance imaging where a current is induced at one spot on the bounding surface and the voltage is measured around the body [33]. Other medical applications are, *e.g.*, magnetic resonance imaging, ultrasound tomography, diffuse tomography, and biomagnetism, see Refs [7, 178, 151].

One-sided measurement configurations are of fundamental importance in geophysics. There is an extensive literature in this field, see *e.g.*, Refs [22, 213, 34]. Here, the problem is typically divided into determination of the smooth part of the speed (*e.g.*, travel time tomography) and detection of 'reflectors', *i.e.*, imaging. There are several approaches to these problems and we refer to the literature for a more detailed description of these geophysical applications. An example of an electromagnetic application with similar restrictions on the measured data is synthetic aperture radar [216, 25].

In the one-dimensional case, see Figure 7.2a, the fields are observed at one side of the object or at both sides, *i.e.*, one uses reflection and (or) transmission data. The one-dimensional case have been thoroughly studied in both the time- and frequency-domains, see *e.g.*, Refs [234, 45, 29, 172, 116] and Section 7.2. One fundamental problem in one-dimensional inverse scattering is that the set of admissible constitutive models have to be restricted, *i.e.*, typically it is only possible to identify two parameters from given reflection and transmission data. To understand this deficiency we consider the amount of data that is possible to observe for a linear and time-invariant model. The slab can be excited from either side of the slab with two orthogonal polarizations and the observed reflected and transmitted fields have two polarizations. This gives a total of $2^4 = 16$ observed functions of the temporal coordinate. Symmetries of the constitutive relations reduce the amount of independent data further. The uniqueness deficiency is resolved in multi-dimensions. Let the source and receivers have a spatial sampling Δx and temporal sampling Δt. For field observations in a unit box in d spatial dimensions, it is possible to get

$$\big(2(1/\Delta x)^{d-1}\, 2d\big)^2\ (T/\Delta t), \qquad d = 1, 2, 3$$

samples of data. The corresponding 'maximal' number of constitutive parameter

samples is roughly

$$36\,(1/\Delta x)^d\,(T/\Delta t), \qquad d = 1, 2, 3.$$

To conclude: in one spatial dimension, the inverse scattering problem is underdetermined. In two spatial dimensions, the amount of data and the model parameters are of the same order, and in three spatial dimensions, the observed amount of data is one order of magnitude larger then the amount of admissible model parameters. For uniqueness results we refer to the literature, see *e.g.*, Refs [194, 209, 195, 37, 127, 226, 150, 147, 148, 226, 227].

Frequency-domain techniques dominate the electromagnetic inverse literature. Among an extensive literature we have the Born approximations [186], least-squares optimization with conjugate gradient [111, 241, 202], contrast source inversion [237, 239, 240], equivalent source method [175], and global optimization methods [185, 94], see also Refs [168, 169, 238, 85, 197, 109, 230, 163, 149] for additional details and references.

In this thesis, we focus on time-domain methods. One-dimensional inverse problems are studied with layer-stripping algorithms in Refs [29, 158, 159, 160] and least-squares optimization in Refs [116, 234]. Two layer-stripping algorithms are briefly described in Sections 7.2.1 and 7.2.2 and a least squares approach in Section 7.2.3.

Among the multi-dimensional time-domain approaches there are the Born type inversion [188, 256, 184, 245], space-time integral equations [15], layer-stripping approaches [254], time-domain diffraction tomography [200, 49], physical optics approximation [210], and the singularity expansion method [59, 234].

In Chapter 8, we use a gradient based least-squares optimization approach for multi-dimensional inverse scattering problems. Multi-dimensional least-squares optimization was introduced for the acoustic equation in [231], where a discrete set of measurements is considered, see also Refs [70, 71, 232, 115, 96, 218, 246, 106, 108, 107].

7.2 One-dimensional inverse scattering

One-dimensional inverse scattering problem offers a natural introduction to parameter identification and wave splitting techniques. Following [158], we study the scattering of a plane wave impinging normally at a slab, see Figure 7.3. The reflected field is written as a temporal convolution between the incident field E_i and the reflection kernel R, *i.e.*,

$$E_\mathrm{r}(x_3, t + x_3/c_0) = \int_{-\infty}^{t} R(t - t' + x_3/c_0) E_\mathrm{i}(0, t')\,\mathrm{d}t'. \tag{7.1}$$

Notice that R is the impulse response of the slab, *i.e.*, if the incoming plane wave has the form of a Dirac delta pulse $E_\mathrm{i}(x_3, t) = \delta(t - x_3/c_0)$, the reflected field is $E_\mathrm{r}(x_3, t) = R(t + x_3/c_0)$. The reflected wave field is recorded for the time interval $[0, 2T]$, where T is the one-way travel time, see (7.2) below. Assume that the electromagnetic properties of the slab are accurately described by an instantaneous permittivity

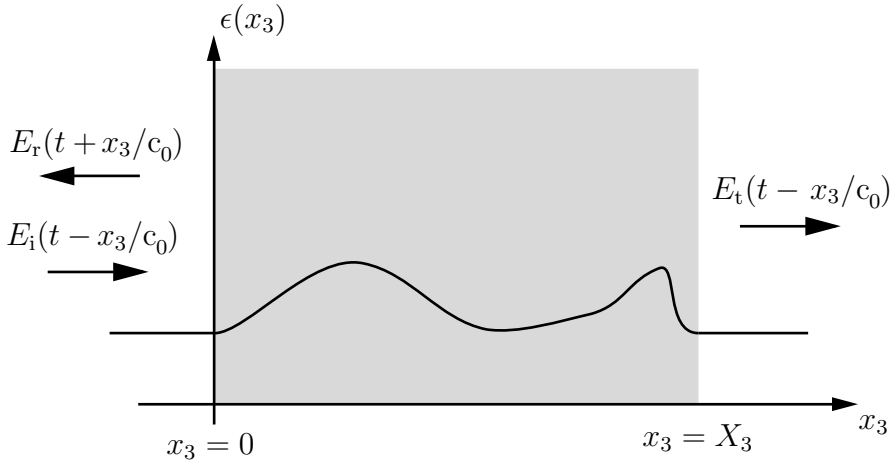

Figure 7.3: The scattering problem for a dielectric slab.

$\epsilon = \epsilon(x_3)$ and the free space permeability $\mu = 1$. The electric and magnetic fields satisfy the one-dimensional wave equation

$$\begin{cases} \epsilon(x_3)\partial_t E + \partial_3 \mathrm{J} H = 0, \\ \mu\partial_t \mathrm{J} H \quad + \partial_3 E \;\; = 0, \end{cases} \qquad x_3 \in [0, X_3].$$

It is convenient to transform the spatial and temporal coordinates to travel time coordinates. The spatial coordinate x_3 is transformed to ζ by

$$\zeta(x_3) = \frac{1}{T} \int_0^{x_3} c(x_3')^{-1} \, \mathrm{d}x_3', \quad \zeta \in [0, 1],$$

where T is the one-way travel time through the slab, *i.e.*,

$$T = \int_0^{X_3} c(x_3')^{-1} \, \mathrm{d}x_3'. \tag{7.2}$$

and $c = (\epsilon\mu)^{-1/2}$ is the wave-front speed. The temporal coordinate t is scaled by the one-way travel time as

$$\tau = t/T, \quad \tau \in [0, 2].$$

This transformation gives a homogeneous principal part of the wave equation, hence the characteristics are straight lines, see Figure 7.4. It is natural to separate the wave field into wave constituents propagating in opposite directions. The down- and up-going wave constituents u_+ and u_- are defined by the one-dimensional wave splitting (4.14). The split fields $u_\pm$ satisfy the coupled set of one-way wave equations

$$\partial_\zeta \begin{pmatrix} u_+ \\ u_- \end{pmatrix} + \partial_\tau \begin{pmatrix} 1 & 0 \\ 0 & -1 \end{pmatrix} \begin{pmatrix} u_+ \\ u_- \end{pmatrix} = \frac{A(\zeta)}{2} \begin{pmatrix} -1 & 1 \\ 1 & -1 \end{pmatrix} \begin{pmatrix} u_+ \\ u_- \end{pmatrix}, \tag{7.3}$$

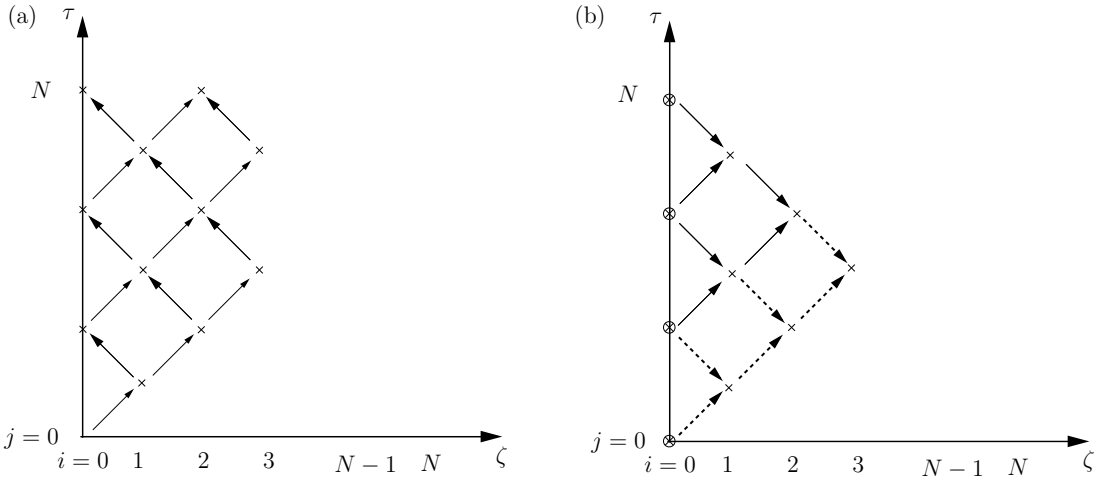

Figure 7.4: Information flow of the scattering problem and inverse scattering problem, respectively. The direct problem is solved forward in time τ whereas the inverse problem is solved forward in space ζ. The parameter identification in the inverse problem is performed at the dashed arrows. $\otimes$ indicates the location of the data.

where the permittivity is contained in

$$A(\zeta) = -\partial_\zeta \ln(c(\zeta)) = \partial_\zeta \ln(\epsilon(\zeta))/2, \quad \zeta \in [0, 1].$$

We start with a few essential properties of the system of the one-way wave equations (7.3). First, the system is hyperbolic in both the temporal coordinate τ and the spatial coordinate ζ. This offers a well-posed migration of the data, *i.e.*, it is a stable process to propagate the fields from $\zeta = \zeta_1$ to $\zeta = \zeta_2$, see Figure 7.4b. Secondly, the homogeneous principal part gives straight characteristics and hence a simple numerical implementation. Finally, an incident Dirac-delta field locates the identification problem, *i.e.*, the wave front can be used to identify one medium parameter.

The layer-stripping algorithms, in Section 7.2.1 and 7.2.2 are based on these three properties. The properties also pinpoint some of the fundamental problems encountered in multi-dimensional inverse scattering. In multi-dimensions, the migration of data is not well-posed, there are no simple coordinate transformations that describe the wavefront, and typically it is not sufficient to identify one medium parameter. This makes it very difficult to generalize the beauty of the one-dimensional layer-stripping algorithms to multi-dimensions. Instead, we pursue a least-squares algorithm in Section 7.2.3 that can be generalized to multi-dimensions.

There are several approaches to and an extensive literature on the one-dimensional inverse scattering problem, see *e.g.*, Refs [234, 45, 29, 172, 116] with references. Here we illustrate two different layer-stripping algorithms for the inversion. First, we have the imbedding algorithm [46, 40, 41, 42, 43, 47, 158, 159], and, secondly, the Green function algorithm [166].

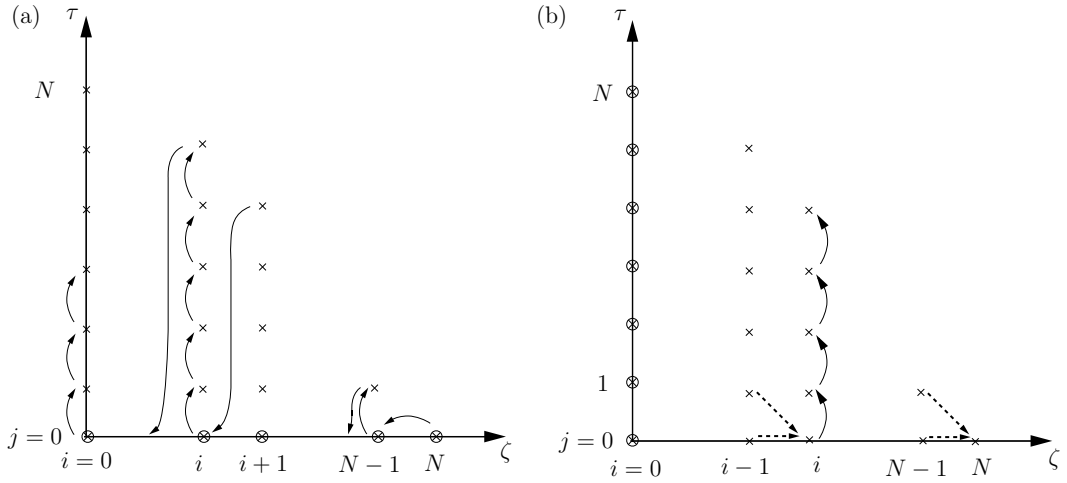

Figure 7.5: The flow chart of the imbedding algorithm: (a) The direct algorithm. (b) The inverse algorithm. The parameter identification in the inverse problem is performed at the dashed arrows. ⊗ indicates the location of the data.

7.2.1 Imbedding equation

The imbedding algorithm is based on a continuous imbedding of the slab. In the imbedding equation, the reflection kernel $R(\tau)$ in (7.1) is imbedded in a family of subproblems. Specifically, let $R(\zeta, \tau)$ denote the reflection kernel for the slab $[\zeta, 1]$. Notice that $R(\tau) = R(0, \tau)$ is the impulse response of the entire slab and that $R(1, \tau) = 0$ since the slab ends at $\zeta = 1$. The reflection kernel $R(\zeta, \tau)$ satisfies the imbedding equation [164]

$$\partial_\zeta R(\zeta, \tau) - 2\partial_\tau R(\zeta, \tau) = \frac{A(\zeta)}{2} \int_0^\tau R(\zeta, \tau - \tau') R(\zeta, \tau') \, \mathrm{d}\tau', \tag{7.4}$$

for $\tau > 0$ and $0 < \zeta < 1$. In the numerical implementation, the equation is discretized with the trapezoidal rule. The discetized reflection kernel satisfies

$$R_{i,j} = R_{i+1,j} + \frac{\Delta\zeta}{4} \left(A_{i+1}(R * R)_{i,j} + A_i (R * R)_{i,j} \right) + \mathrm{O}(\Delta\zeta^3),$$

where $R_{i,j} = R(i\Delta\zeta, 2j\Delta\zeta)$ and $\Delta\zeta$ is the spatial discretization step. In the direct problem, we determine the impulse response $R(0, \tau)$ of the slab. The medium parameter $A(\zeta)$ and the end condition $R(1, \tau) = 0$ and given. In addition to these two values we have the initial value

$$R(\zeta, 0) = -A(\zeta)/4, \quad 0 \le \zeta \le 1.$$

The direct problem is solved from $\zeta = 1$ to $\zeta = 0$, see Figure 7.5a.

In the inverse scattering problem, we determine the medium parameter $A(\zeta)$ from a given impulse response $R(0, \tau) = R(t/T)$. In this formulation of the inverse problem, the medium parameter $A_i = -4R_{i,0}$ is identified by the initial condition

$$-A_i = 4R_{i-1,1} - 2\Delta\zeta A_{i-1} R_{i-1,1} R_{i-1,0}$$

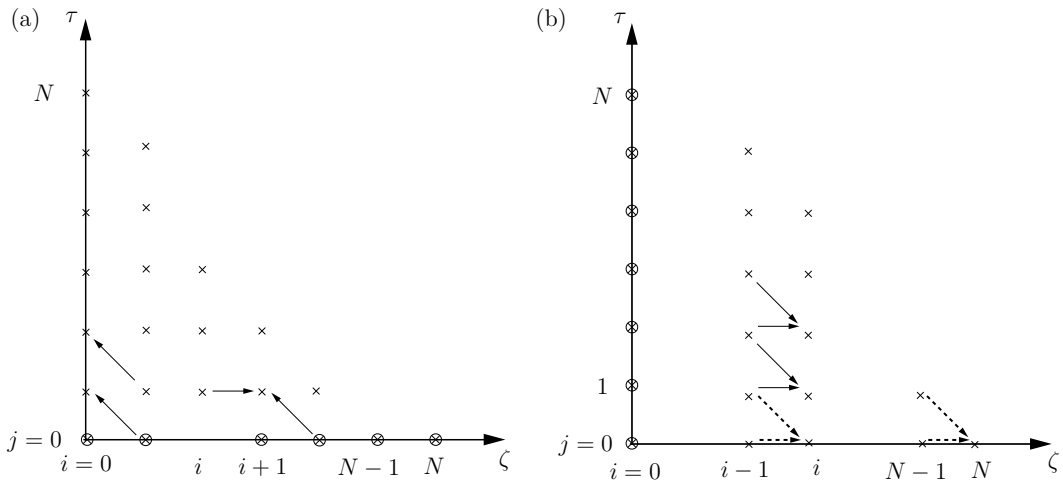

Figure 7.6: The Green functions algorithm: (a) The direct algorithm. (b) The inverse algorithm. The parameter identification in the inverse problem is performed at the dashed arrows. $\otimes$ indicates the location of the data.

and the reflection kernel $R_{i,j}$, $j \geq 1$ is updated at a new space position, see Figure 7.5b.

The algorithm above is restricted to identification of the permittivity, generalizations to simultaneous identification of the permittivity and conductivity are given by Kristensson and Krueger in [158, 159, 160, 161, 157], see also Refs [45, 14, 58, 116, 164].

The drawback of the imbedding algorithm is the extra computational cost due to the temporal convolution in (7.4). The convolution originates from the imbedding idea, where $R(\zeta, \tau)$ is the reflection kernel (or impulse response) of the subslab $[\zeta, 1]$. To determine this reflection kernel, the smooth tail of the incident wave field have to be deconvolved. The problem is solved by the Green function algorithm where the true wave fields are used.

7.2.2 Green functions approach

The Green function approach in this context was originally introduced by Krueger and Ochs [166]. In the Green functions approach, a set of kernels $G^{(+)}$ and $G^{(-)}$ represents the solution of (7.3), *i.e.*,

$$\begin{cases} u_+(\zeta, \tau+\zeta) = \mathrm{e}^{-\frac{1}{2}\int_0^\zeta A(\zeta')\,\mathrm{d}\zeta'} \left(u_+(0,\tau) + \displaystyle\int_{-\infty}^{\tau} G^{(+)}(\zeta, \tau-\tau') u_+(0,\tau')\,\mathrm{d}\tau' \right), \\ u_-(\zeta, \tau+\zeta) = \mathrm{e}^{-\frac{1}{2}\int_0^\zeta A(\zeta')\,\mathrm{d}\zeta'} \displaystyle\int_{-\infty}^{\tau} G^{(-)}(\zeta, \tau-\tau') u_+(0,\tau')\,\mathrm{d}\tau'. \end{cases}$$

The Green functions satisfy the coupled set of one-way equations

$$\begin{cases} \partial_\zeta G^{(+)} = \dfrac{1}{2} A G^{(-)}, \\ \partial_\zeta G^{(-)} - 2\partial_\tau G^{(-)} = \dfrac{1}{2} A G^{(+)}, \end{cases} \qquad \zeta \in [0,1], \quad \tau \geq 0. \tag{7.5}$$

The Green functions have the initial values

$$G^{(+)}(\zeta, 0) = \frac{-A(\zeta)}{4} \quad \text{and} \quad G^{(-)}(\zeta, 0) = \frac{-1}{8} \int_0^\zeta A(\zeta')^2 \, \mathrm{d}\zeta'$$

and the boundary conditions are

$$G^{(+)}(0, \tau) = 0 \quad \text{and} \quad G^{(-)}(0, \tau) = R(\tau).$$

We get a numerical approximation of $G^{(\pm)}$ by a trapezoidal rule discretization of the system (7.5). The result is

$$\begin{cases} G^{(+)}_{i,j} = G^{(+)}_{i-1,j} + \dfrac{\Delta\zeta}{4} \left(A_i G^{(-)}_{i,j} + A_{i-1} G^{(-)}_{i-1,j} \right), \\ G^{(-)}_{i,j} = G^{(-)}_{i+1,j-1} - \dfrac{\Delta\zeta}{4} \left(A_{i+1} G^{(+)}_{i+1,j-1} + A_i G^{(+)}_{i,j} \right). \end{cases}$$

The direct problem is updated with a stencil depicted in Figure 7.6a. In the inverse problem, the medium parameter A_i is first determined and subsequently, the Green functions are updated, see Figure 7.6b.

The imbedding and Green function approaches have been studied extensively. A compactly supported Green function was introduced by He in [113]. Karlsson unified the imbedding, Green function, and compact Green function approaches with the propagation method in [135, 136]. The methodology have been used to study inverse scattering for temporal dispersive medium [13, 134, 155, 91], temporal dispersive anisotropic medium [89, 88, 87, 86], temporal dispersive bi-isotropic medium [204, 162, 203, 205], non-linear medium [217, 165], non-stationary medium [4, 2, 3], waveguides [16, 156], heat waves [244], transmission lines [179], gyrotropic media [196, 140], non-reflecting medium [121, 120], spherically symmetric dispersive medium [138], source problems [222, 223, 224, 225], non-reflecting media [121, 120], periodic media [137], structural mechanics [21, 20, 83, 21], and viscoelastic medium [44, 133, 8]. Experimental results are found in [92, 91, 116]. Multi-dimensional generalizations are discussed by Weston in a sequence of papers [117, 114, 118, 253, 249, 250, 251, 116].

7.2.3 Least-squares optimization

In this subsection, we describe a gradient based least-squares optimization approach to one-dimensional inverse scattering by the slab depicted in Figure 7.3. The scattering data are given at the boundary of the slab. Here it is convenient to work with the electromagnetic fields, *i.e.*,

$$E^{(\mathrm{m})}(0,t), \quad H^{(\mathrm{m})}(0,t), \quad E^{(\mathrm{m})}(X_3,t), \quad \text{and} \quad H^{(\mathrm{m})}(X_3,t),$$

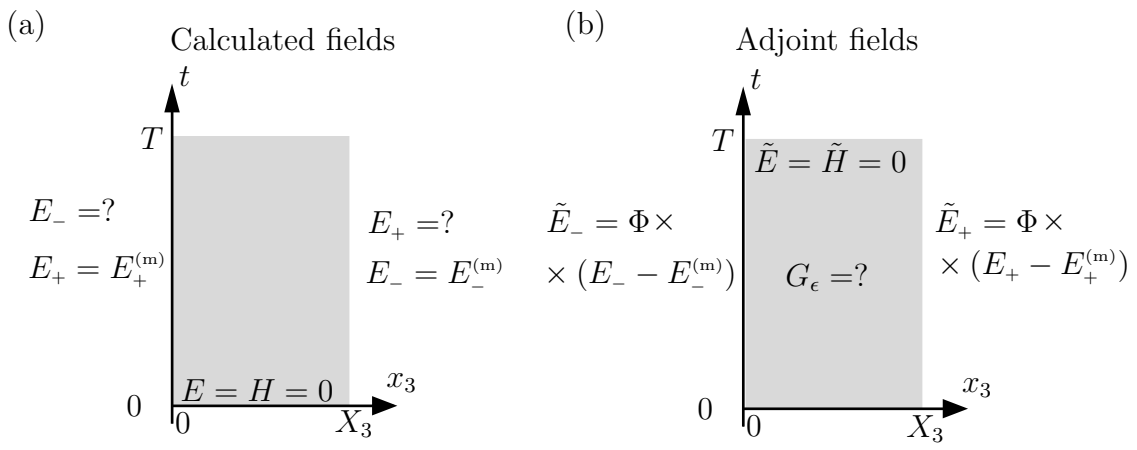

Figure 7.7: The direct and dual problems for the inverse scattering at a dielectric slab.

are given at the boundary of the slab. To identify the permittivity ϵ inside the slab, we minimize the misfit between a set of calculated fields E and H and the given fields at the boundary. We use the least-squares functional to determine the error of a permittivity ϵ

$$\mathcal{J}[\epsilon] = \sum_{\zeta=0,X_3} \int_0^T \Phi(t)\big(|E(\zeta,t) - E^{(m)}(\zeta,t)|^2 + |H(\zeta,t) - H^{(m)}(\zeta,t)|^2\big)\,\mathrm{d}t. \qquad (7.6)$$

The calculated fields satisfy the one-dimensional wave equation

$$\begin{cases} \epsilon(x_3)\partial_t E + \partial_3 \mathrm{J} H = 0, \\ \mu\partial_t \mathrm{J} H \;\; + \partial_3 E \;\; = 0, \end{cases} \quad \text{for} \quad x_3 \in [0, X_3],$$

together with the initial values $E(x_3,0) = H(x_3,0) = 0$ in the slab. We can choose appropriate boundary values of the calculated fields to get a simple and efficient algorithm. Here, we prescribe the split fields (4.14) at the boundary, *i.e.*,

$$E_+(0,t) = E_+^{(m)}(0,t) \quad \text{and} \quad E_-(X_3,t) = E_-^{(m)}(X_3,t).$$

Observe that it is the incoming fields that are prescribed at the boundary, *e.g.*, $E_+^{(m)}(0,t) = E_i(t)$ in Figure 7.3. With this choice, the misfit functional (7.6) reduces to the difference between the output fields

$$\mathcal{J}[\epsilon] = 2\int_0^T \Phi(t)\left(|E_-(0,t) - E_-^{(m)}(0,t)|^2 + |E_+(X_3,t) - E_+^{(m)}(X_3,t)|^2\right)\mathrm{d}t. \qquad (7.7)$$

We update the permittivity ϵ with a gradient based optimization algorithm. Perturb the permittivity an amount δ in the direction ϵ', *i.e.*,

$$\epsilon(x_3) \to \epsilon(x_3) + \delta\epsilon'(x_3).$$

The corresponding electric and magnetic fields are perturbed as

$$E \to E + \delta E' + \mathrm{O}(\delta^2) \quad \text{and} \quad H \to H + \delta H' + \mathrm{O}(\delta^2),$$

where $\mathrm{O}(\delta^2)$ is a term of the size δ^2. The first order perturbation satisfies the wave equation

$$\begin{cases} \epsilon(x_3)\partial_t E' + \partial_3 \mathrm{J} H' = -\epsilon'(x_3)\partial_t E(x_3,t), \\ \mu\partial_t \mathrm{J} H' \ + \ \partial_3 E' \ = 0, \end{cases} \qquad \text{for} \quad x_3 \in [0, X_3],$$

together with zero initial values $E'(x_3, 0) = H'(x_3, 0) = 0$ in the slab and zero input fields at the boundary

$$E'_+(0,t) = E'_-(X_3,t) = 0.$$

The misfit functional is perturbed as $\mathcal{J} \to \mathcal{J} + \delta\mathcal{J}' + \mathrm{O}(\delta^2)$ where the first order perturbation is given by

$$\mathcal{J}'[\epsilon] = 4\int_0^T \Phi(t)\, E'_-(0,t) \cdot (E_-(0,t) - E^{(\mathrm{m})}_-(0,t)) \\ + \Phi(t)\, E'_+(X_3,t) \cdot (E_+(X_3,t) - E^{(\mathrm{m})}_+(X_3,t))\,\mathrm{d}t.$$

To relate the perturbation of the misfit functional to the perturbation of the permittivity ϵ, we use the adjoint fields $\widetilde{E}$ and $\widetilde{H}$. The adjoint fields satisfy the wave equation

$$\begin{cases} \epsilon(x_3)\partial_t \widetilde{E} + \partial_3 \mathrm{J}\widetilde{H} = 0, \\ \mu\partial_t \mathrm{J}\widetilde{H} \ + \ \partial_3 \widetilde{E} \ = 0, \end{cases} \qquad \text{for} \quad x_3 \in [0, X_3].$$

This adjoint equation is solved backwards in time, from $t = T$ to $t = 0$, with zero initial values, *i.e.*, $\widetilde{E}(x_3, T) = \widetilde{H}(x_3, T) = 0$. At the boundary the difference between the output fields are used, *i.e.*,

$$\widetilde{E}_-(0,t) = \Phi(t)\ \big(E_-(0,t) - E^{(\mathrm{m})}_-(0,t)\big)$$

and

$$\widetilde{E}_+(X_3,t) = \Phi(t)\ \big(E_+(X_3,t) - E^{(\mathrm{m})}_+(X_3,t)\big)\,.$$

Cross multiply the perturbed fields and the adjoint field and collect terms to get

$$\partial_t \left(\epsilon E' \cdot \widetilde{E} + \mu H' \cdot \widetilde{H}\right) + \partial_3 \left(\widetilde{E} \cdot \mathrm{J}H' + E' \cdot \mathrm{J}\widetilde{H}\right) = -\epsilon' \widetilde{E} \cdot \partial_t E.$$

Integrate over the slab $[0, X_3]$, the time interval $[0, T]$, and use the identity

$$\widetilde{E} \cdot \mathrm{J}H' + E' \cdot \mathrm{J}\widetilde{H} = 2\left(E'_+ \cdot \widetilde{E}_+ - E'_- \cdot \widetilde{E}_-\right)$$

to get an expression of the perturbed misfit functional. The first order perturbation (Fréchet differential) of the misfit functional is

$$\mathcal{J}'[\epsilon] = -2 \int_0^{X_3} \int_0^T \epsilon'(x_3) \widetilde{E}(x_3, t) \cdot \partial_t E(x_3, t) \, \mathrm{d}t \, \mathrm{d}x_3 = \langle G_\epsilon, \epsilon' \rangle,$$

where $\langle \cdot, \cdot \rangle$ is the inner product in $\mathrm{L}^2([0, X_3])$. The gradient is identified as

$$G_\epsilon(x_3) = -2 \int_0^T \widetilde{E}(x_3, t) \cdot \partial_t E(x_3, t) \, \mathrm{d}t.$$

One-dimensional gradient based optimization is considered in Refs [234, 229, 171, 119]. Compared with the Green function algorithm the optimization algorithm is computationally more demanding. One evaluation of the misfit functional (7.7) is roughly identical to the total cost of the Green function algorithm. Furthermore, local optimization algorithms (*e.g.*, the conjugate gradient) might be trapped in a local minimum if the misfit functional is not convex. However, the least-squares algorithm has the advantage of great generality and simplicity. It can be used to solve different inverse problems related to many ordinary and partial differential equations as long as there are fast direct solvers. In contrast to the layer-stripping algorithms it is straightforward to generalize the least-squares algorithm to multi-dimensions. In the next chapter, we use a least-squares conjugate-gradient algorithm to solve multi-dimensional time-domain inverse scattering problems.

Chapter 8

Multi-dimensional time-domain least-squares inversion

In this chapter, we describe a gradient based optimization approach to a multi-dimensional inverse scattering problem.

The least-squares formulation and the use of an adjoint problem is outlined in Section 8.1. The adjoint problem and the gradients are derived for a permittivity, permeability, and conductivity medium in Section 8.2. Regularization and the usages of a priori information are discussed in Section 8.3. A parameter scaling is introduced in Section 8.4. The identification algorithm is given in pseudo-code in Section 8.5. A numerical example of the identification of the permittivity, permeability, and conductivity medium parameters is presented in Section 8.6. In Section 8.7, a motivation for the use of energy-flux split fields is given. Section 8.8 generalizes the adjoint problem and the gradients to Debye and Lorentz models. Numerical identifications of two Debye parameters and moisture are performed in Sections 8.9 and 8.10, respectively. The use of inverse scattering to find effective medium parameters are considered in Section 8.11. The chapter ends with a discussion of inverse scattering for bi-anisotropic material in Section 8.12.

8.1 Least-squares formulation

We determine the electromagnetic properties in a region $\Omega \subset \mathbb{R}^3$ (or $\mathbb{R}^2$) from a set of given electric and magnetic fields at the boundary of the region, *i.e.*,

$$E^{(\mathrm{m})}(x,t;m) \quad \text{and} \quad H^{(\mathrm{m})}(x,t;m) \tag{8.1}$$

are given for $x \in \partial\Omega$, $t \in [0,T]$, and $m = 1,2,..,M$. It is assumed that these fields are generated by sources outside the region Ω and that the fields are quiescent at $t \leq 0$ in Ω.

The inverse scattering problem is to identify N parameters (or functions of the spatial coordinate)

$$\boldsymbol{\alpha}(\boldsymbol{x}) = (\alpha_1(\boldsymbol{x}), \ldots, \alpha_N(\boldsymbol{x})),$$

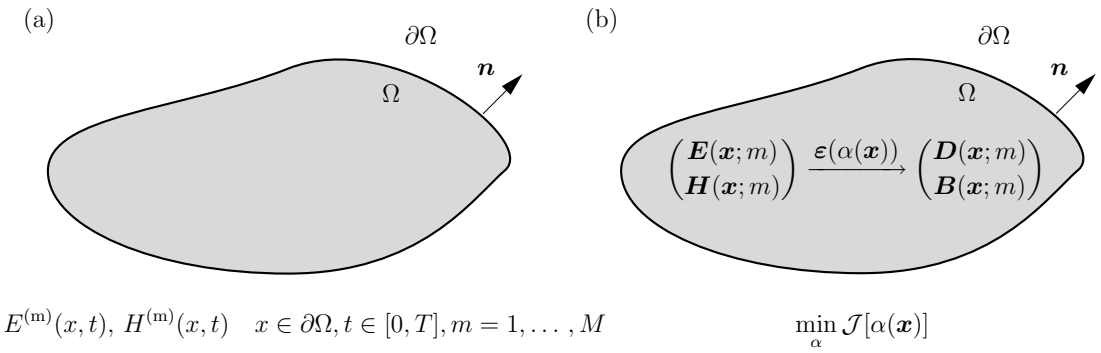

Figure 8.1: (a) The inverse scattering problem and (b) the optimization formulation of the parameter identification problem.

such that the corresponding calculated electromagnetic fields resemble the given fields at the boundary. The calculated fields $\boldsymbol{E}$, $\boldsymbol{H}$, $\boldsymbol{D}$, and $\boldsymbol{B}$ satisfy the source free Maxwell equations (2.1) in Ω together with a set of constitutive relations

$$\begin{pmatrix}\boldsymbol{E}(\boldsymbol{x};m)\\ \boldsymbol{H}(\boldsymbol{x};m)\end{pmatrix} \xrightarrow{\boldsymbol{\varepsilon}(\boldsymbol{\alpha}(\boldsymbol{x}))} \begin{pmatrix}\boldsymbol{D}(\boldsymbol{x};m)\\ \boldsymbol{B}(\boldsymbol{x};m)\end{pmatrix}$$

and quiescent initial fields

$$\boldsymbol{E}(\boldsymbol{x},t;m)=\boldsymbol{H}(\boldsymbol{x},t;m)=\boldsymbol{0} \quad \text{for} \quad t\leq 0. \tag{8.2}$$

We assume that the parameter values are known at the boundary of the region and that the constitutive map $\boldsymbol{\varepsilon}(\boldsymbol{\alpha}(\boldsymbol{x}))$ reduces to the free space map at the boundary.

The error of an identified set of parameters is measured by the least-squares functional

$$\begin{aligned}\mathcal{J}[\boldsymbol{\alpha}]=\sum_{m=1}^{M}\int_0^T\int_{\partial\Omega}\Phi(x,t;m)\big(&|E(x,t;m)-E^{(\mathrm{m})}(x,t;m)|^2\\ &+|H(x,t;m)-H^{(\mathrm{m})}(x,t;m)|^2\big)\,\mathrm{dS}\,\mathrm{d}t\end{aligned} \tag{8.3}$$

where a weight function $\Phi(x,t;m)$ is included for future convenience. Notice that the misfit in both the electric and magnetic fields are determined.

It is well known that either the electric field, magnetic field or a linear combination of the fields offers a well-posed direct problem, see Chapter 5. Therefore, there is a freedom in the choice of appropriate inputs to the algorithm, *e.g.*, the electric, magnetic, or a linear combination of them can be prescribed at the boundary. Here, we use the energy-flux split fields (4.20) with respect to the inward normal vector $-\boldsymbol{n}$ as the input to the algorithm, *i.e.*,

$$E_+(x,t;m)=E_+^{(\mathrm{m})}(x,t;m) \quad \text{for} \quad x\in\partial\Omega \tag{8.4}$$

where we use the a priori information about the constitutive map at the boundary to get

$$E_\pm=\frac{E\pm\mathrm{J}H}{2}=\frac{-\boldsymbol{n}\times(\boldsymbol{n}\times\boldsymbol{E})\pm\boldsymbol{n}\times\boldsymbol{H}}{2}. \tag{8.5}$$

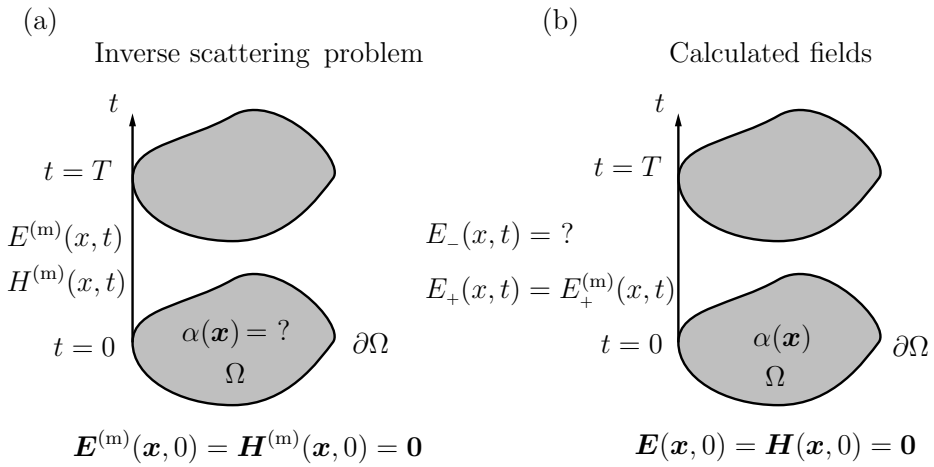

Figure 8.2: The inverse scattering problem and the direct problem for the calculated fields used in the misfit functional (8.6).

Here and in the following we use the dimensional scaling given by (2.5). The choice of the energy-flux split fields is motivated by an energy analysis in Section 8.7. For this choice, the misfit functional reduces to the L^2 difference of the output field

$$\mathcal{J}[\boldsymbol{\alpha}] = 2\sum_{k=1}^{M}\int_0^T\int_{\partial\Omega}\Phi(x,t;m)|E_-(x,t;m) - E_-^{(\mathrm{m})}(x,t;m)|^2\,\mathrm{dS}\,\mathrm{d}t. \tag{8.6}$$

To proceed, we need a strategy to find the set of parameters, α, that minimize the misfit. Here we use a gradient based optimization algorithm. The adjoint- or dual-problem gives an expression for the gradient. To illustrate the idea, we start with an abstract formulation. Let $\mathrm{P} = \mathrm{P}(y, \alpha(y), \partial)$ denote a linear differential operator. The differential operator P depends on the coordinate y, the differential operator $\partial = \partial_y$, and the parameter (function) $\alpha = \alpha(y)$. Assume that we can solve the equation

$$\mathrm{P}(y, \alpha(y), \partial)u = 0 \quad \text{for} \quad y \in \mathcal{D}$$

together with a set of boundary conditions. We want to relate the parameter α to the value of u at the boundary $\partial\mathcal{D}$. Perturb the parameter α an amount δ in the direction α', *i.e.*,

$$\alpha(y) \to \alpha(y) + \delta\alpha'(y).$$

The corresponding perturbed differential operator has the form

$$\mathrm{P}(y, \alpha(y), \partial) \to \mathrm{P}(y, \alpha(y), \partial) + \delta\alpha'(y)\mathrm{Q}(y, \partial).$$

Assume that the solution of the perturbed problem has an asymptotic expansion in δ, *i.e.*,

$$u(y) \to u(y) + \delta u'(y) + \mathrm{O}(\delta^2).$$

The first order perturbed term u' satisfies

$$\mathrm{P}(y, \alpha(y), \partial)u'(y) = -\alpha'(y)\mathrm{Q}(y, \partial)u(y)$$

together with vanishing boundary conditions. To relate the boundary term to the perturbation $\alpha'(y)$, we use the adjoint problem

$$\mathrm{P}^\dagger(y, \alpha(y), \partial)\tilde{u} = 0 \quad \text{for} \quad y \in \mathcal{D}$$

together with a set of adjoint boundary conditions. The adjoint operator is defined by the identity

$$\langle v, \mathrm{P}u\rangle = \langle \mathrm{P}^\dagger v, u\rangle = \text{boundary term}$$

where $\langle \cdot, \cdot \rangle$ is the inner product in $\mathcal{D}$

$$\langle v, u\rangle = \int_\Omega v^*(y)u(y)\,\mathrm{d}y. \tag{8.7}$$

This definition gives the identity

$$\text{boundary term} = \langle \tilde{u}, \mathrm{P}u'\rangle - \langle \mathrm{P}^\dagger\tilde{u}, u'\rangle = -\langle \tilde{u}, \alpha'\mathrm{Q}u\rangle.$$

Here, the boundary values of u are related to the perturbation α' in the region. For time-domain problems, the adjoint problem is typically solved backwards in time.

Least-squares inversion in the frequency domain is discussed in many papers, see Section 7. The time domain formulation was introduced by Tarantola in 1984 for a seismic problem, see Refs [232, 231, 96, 218]. In [188], a two dimensional electromagnetic inverse problem is discussed. Diffusive electromagnetic problems are considered in [246]. In [115, 116, 107] the acoustic inverse problem for data at a closed surface is considered. The present approach is found in [108, 106]. A mathematical analysis is found in [71, 70].

8.2 Permittivity, permeability, and conductivity models

We use the procedure with adjoint functions to derive the gradient for materials modeled with permittivity ϵ, permeability μ, and conductivity σ. The calculated electric and magnetic field intensities satisfy the source-free Maxwell equations

$$\begin{cases} \epsilon(\boldsymbol{x})\partial_t \boldsymbol{E} \ - \nabla \times \boldsymbol{H} + \sigma(\boldsymbol{x})\boldsymbol{E} = \boldsymbol{0}, \\ \mu(\boldsymbol{x})\partial_t \boldsymbol{H} + \nabla \times \boldsymbol{E} \ = \boldsymbol{0}, \end{cases} \tag{8.8}$$

for $\boldsymbol{x} \in \Omega$ and $t \in [0, T]$. The measurement starts at time $t = 0$. This gives the zero initial values

$$\boldsymbol{E}(\boldsymbol{x}, 0; m) = \boldsymbol{H}(\boldsymbol{x}, 0; m) = \boldsymbol{0}.$$

Following (8.4), the split fields, (8.5), are used as the input field, *i.e.*,

$$E_+(\boldsymbol{x}, t; m) = E_+^{(\mathrm{m})}(\boldsymbol{x}, t; m) \quad \text{for} \quad \boldsymbol{x} \in \partial\Omega.$$

To find the gradient with respect to the constitutive parameters ϵ, μ, and σ, the parameters are perturbed an amount δ, *i.e.*,

$$\begin{cases} \epsilon(\boldsymbol{x}) \to \epsilon(\boldsymbol{x}) + \delta\epsilon'(\boldsymbol{x}), \\ \mu(\boldsymbol{x}) \to \mu(\boldsymbol{x}) + \delta\mu'(\boldsymbol{x}), \\ \sigma(\boldsymbol{x}) \to \sigma(\boldsymbol{x}) + \delta\sigma'(\boldsymbol{x}). \end{cases}$$

The corresponding fields $\boldsymbol{E}$ and $\boldsymbol{H}$ in (8.8) are perturbed as

$$\begin{cases} \boldsymbol{E} \to \boldsymbol{E} + \delta\boldsymbol{E}' + \mathrm{O}(\delta^2), \\ \boldsymbol{H} \to \boldsymbol{H} + \delta\boldsymbol{H}' + \mathrm{O}(\delta^2), \end{cases} \tag{8.9}$$

where $\mathrm{O}(\delta^2)$ is a term of the size δ^2, *i.e.*, $\|\mathrm{O}(\delta^2)\| \leq C\delta^2$ as $\delta \to 0$, see Section 8.7 for details. We find the gradient of the misfit functional (8.3) with respect to the parameters ϵ, μ, and σ by calculating the increment of the misfit functional (8.6) to the first order, *i.e.*,

$$\begin{aligned} \mathcal{J}'[\epsilon, \mu, \sigma] &= \lim_{\delta \to 0} \frac{\mathcal{J}[\epsilon + \delta\epsilon', \mu + \delta\mu', \sigma + \delta\sigma'] - \mathcal{J}[\epsilon, \mu, \sigma]}{\delta} \\ &= 4 \sum_{m=1}^{M} \int_0^T \int_{\partial\Omega} \Phi E'_- \cdot (E_- - E_-^{(\mathrm{m})}) \, \mathrm{dS} \, \mathrm{d}t. \end{aligned} \tag{8.10}$$

The first order perturbations of the calculated fields $\boldsymbol{E}'$ and $\boldsymbol{H}'$ satisfy the Maxwell equations

$$\begin{cases} \epsilon\partial_t \boldsymbol{E}' - \nabla \times \boldsymbol{H}' + \sigma\boldsymbol{E}' = -\epsilon'\partial_t \boldsymbol{E} - \sigma'\boldsymbol{E}, \\ \mu\partial_t \boldsymbol{H}' + \nabla \times \boldsymbol{E}' = -\mu'\partial_t \boldsymbol{H}, \end{cases} \tag{8.11}$$

where the induced sources are given by the unperturbed fields in (8.8). The initial values and boundary values are

$$\boldsymbol{E}'(\boldsymbol{x}, 0) = \boldsymbol{H}'(\boldsymbol{x}, 0) = \boldsymbol{0}$$

and

$$E'_+(x, t) = 0 \quad \text{for} \quad x \in \partial\Omega, \tag{8.12}$$

respectively. The perturbation of the misfit functional (8.10) is related to the perturbed parameters (8.9) by a set of adjoint fields $\widetilde{\boldsymbol{E}}$ and $\widetilde{\boldsymbol{H}}$. The adjoint fields satisfy the equations

$$\begin{cases} \epsilon(\boldsymbol{x})\partial_t \widetilde{\boldsymbol{E}} - \nabla \times \widetilde{\boldsymbol{H}} - \sigma(\boldsymbol{x})\widetilde{\boldsymbol{E}} = \boldsymbol{0}, \\ \mu(\boldsymbol{x})\partial_t \widetilde{\boldsymbol{H}} + \nabla \times \widetilde{\boldsymbol{E}} = \boldsymbol{0}. \end{cases} \tag{8.13}$$

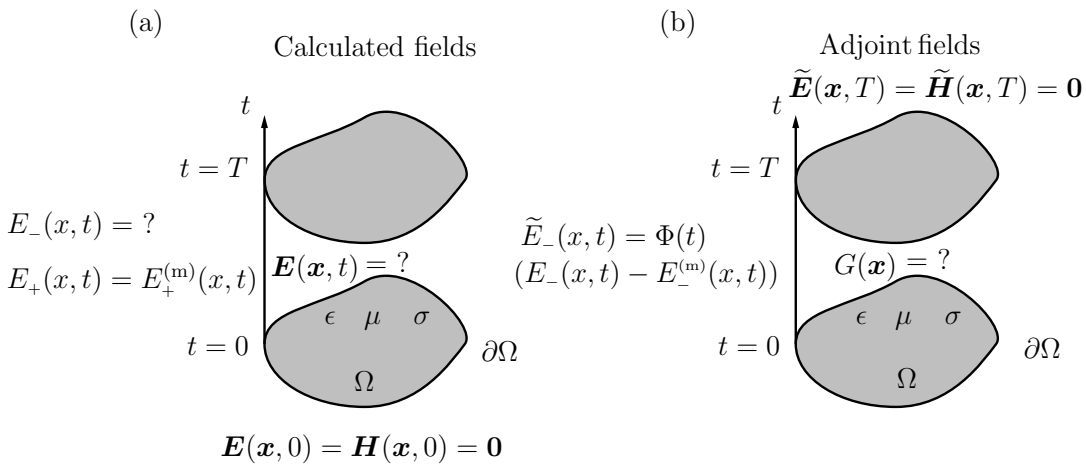

Figure 8.3: The forward problem of the calculated fields (8.8) and the problem of the adjoint fields (8.13) solved backward in time.

This adjoint equation is solved backwards in time, from $t = T$ to $t = 0$, with zero 'initial' values

$$\widetilde{\boldsymbol{E}}(\boldsymbol{x}, T) = \widetilde{\boldsymbol{H}}(\boldsymbol{x}, T) = \boldsymbol{0}.$$

At the boundary $\partial\Omega$, the adjoint field $\widetilde{E}_-$ is given by the difference between the calculated output field and the given output field, *i.e.*,

$$\widetilde{E}_-(x,t) = \Phi(t)\,\big(E_-(x,t) - E_-^{(\mathrm{m})}(x,t)\big) \quad \text{for} \quad x \in \partial\Omega, \tag{8.14}$$

where the weight function $\Phi(t)$ is a smooth function such that $\Phi(T) = 0$. The adjoint equation is essentially the original equation (8.8) (the conductivity changes sign) solved backwards in time with an input field ($\widetilde{E}_-$ is the natural input field when the equation is solved backwards in time) depending on the difference between the calculated output and the given output fields, see Figure 8.3.

Cross multiply the fields of the perturbed equation (8.11) with the fields of the adjoint problem (8.13), add and collect terms to get

$$\begin{aligned}\partial_t\,(\epsilon\boldsymbol{E}'\cdot\widetilde{\boldsymbol{E}} + \mu\boldsymbol{H}'\cdot\widetilde{\boldsymbol{H}}) + \nabla\cdot(\widetilde{\boldsymbol{E}}\times\boldsymbol{H}' + \boldsymbol{E}'\times\widetilde{\boldsymbol{H}}) \\ = -\epsilon'\widetilde{\boldsymbol{E}}\cdot\partial_t\boldsymbol{E} - \mu'\widetilde{\boldsymbol{H}}\cdot\partial_t\boldsymbol{H} - \sigma'\widetilde{\boldsymbol{E}}\cdot\boldsymbol{E}.\end{aligned}$$

Integrate this relation over time $[0, T]$ and space Ω. The first term vanishes according to the initial values of the perturbed and adjoint problems, and the second term gives an integral over the boundary, *i.e.*,

$$\begin{aligned}\int_0^T\int_{\partial\Omega}(\widetilde{\boldsymbol{E}}\times\boldsymbol{H}' + \boldsymbol{E}'\times\widetilde{\boldsymbol{H}})\cdot\boldsymbol{n}\,\mathrm{dS}\,\mathrm{d}t \\ = -\int_0^T\int_\Omega \epsilon'\widetilde{\boldsymbol{E}}\cdot\partial_t\boldsymbol{E} + \mu'\widetilde{\boldsymbol{H}}\cdot\partial_t\boldsymbol{H} + \sigma'\widetilde{\boldsymbol{E}}\cdot\boldsymbol{E}\,\mathrm{dV}\,\mathrm{d}t\end{aligned}$$

where $\boldsymbol{n}$ is the outward normal of the region Ω. Rewrite the boundary term in the input and output fields $E_{\pm}$

$$\begin{aligned}\boldsymbol{n}\cdot(\widetilde{\boldsymbol{E}}\times\boldsymbol{H}'+\boldsymbol{E}'\times\widetilde{\boldsymbol{H}}) &= -\widetilde{E}\cdot \mathrm{J}H' - E'\cdot \mathrm{J}\widetilde{H} \\ &= 2\left(\widetilde{E}_-\cdot E'_- - \widetilde{E}_+\cdot E'_+\right) = 2\Phi E'_-\cdot\left(E_- - E_-^{(\mathrm{m})}\right) \end{aligned} \tag{8.15}$$

where we have used (A.6) (observe that the split fields are defined with respect to the inward unit normal) and the boundary conditions (8.12) and (8.14). The first order perturbation of the misfit functional is

$$\begin{aligned}\mathcal{J}'[\epsilon,\mu,\sigma] &= -2\sum_{m=1}^{M}\int_0^T\int_\Omega \epsilon'\widetilde{\boldsymbol{E}}\cdot\partial_t\boldsymbol{E}+\mu'\widetilde{\boldsymbol{H}}\cdot\partial_t\boldsymbol{H}+\sigma'\widetilde{\boldsymbol{E}}\cdot\boldsymbol{E}\,\mathrm{dV}\,\mathrm{d}t \\ &= \langle G_\epsilon,\epsilon'\rangle + \langle G_\mu,\mu'\rangle + \langle G_{\sigma/\langle\sigma\rangle},\sigma'/\langle\sigma\rangle\rangle\end{aligned} \tag{8.16}$$

where $\langle\cdot,\cdot\rangle$ is the inner product in $\mathrm{L}^2(\Omega)$. In (8.16), we introduced a scaling $\langle\sigma\rangle$ of the conductivity. The scaling is used to average the different components of the gradient, see Section 8.4. The gradient is identified from (8.16), *i.e.*,

$$\boldsymbol{G}(\boldsymbol{x}) = (G_\epsilon(\boldsymbol{x}), G_{\sigma/\langle\sigma\rangle}(\boldsymbol{x}), G_\mu(\boldsymbol{x}))$$

where

$$\begin{cases} G_\epsilon(\boldsymbol{x}) &= -2\sum_{m=1}^{M}\int_0^T \widetilde{\boldsymbol{E}}(\boldsymbol{x},t,m)\cdot\partial_t\boldsymbol{E}(\boldsymbol{x},t,m)\,\mathrm{d}t, \\ G_{\sigma/\langle\sigma\rangle}(\boldsymbol{x}) &= -2\langle\sigma\rangle\sum_{m=1}^{M}\int_0^T \widetilde{\boldsymbol{E}}(\boldsymbol{x},t,m)\cdot\boldsymbol{E}(\boldsymbol{x},t,m)\,\mathrm{d}t, \\ G_\mu(\boldsymbol{x}) &= -2\sum_{m=1}^{M}\int_0^T \widetilde{\boldsymbol{H}}(\boldsymbol{x},t,m)\cdot\partial_t\boldsymbol{H}(\boldsymbol{x},t,m)\,\mathrm{d}t \\ &= \frac{2}{\mu}\sum_{m=1}^{M}\int_0^T \widetilde{\boldsymbol{H}}(\boldsymbol{x},t,m)\cdot\nabla\times\boldsymbol{E}(\boldsymbol{x},t,m)\,\mathrm{d}t. \end{cases} \tag{8.17}$$

Notice that equation (8.8) can be used to replace the magnetic field with the electric field in the permeability gradient. This is convenient from a computational point of view. The gradient points in the direction towards the fastest growth of the misfit functional. Hence, the parameters are updated in the opposite direction of the gradient.

8.3 Regularization and a priori information

The identification of the parameters are limited to a certain resolution. The resolution depends on the given amount of information, *e.g.*, the bandwidth of the given fields. This lack of information causes the identification algorithm to be ill-posed

in the sense that the parameters do not depend continuously on the given boundary fields. The identification algorithm is stabilized by increasing the amount of a priori information about the parameters—here we assume the parameters to be smooth. The smoothness assumption is included in the misfit functional $\mathcal{J}[\alpha]$ by a Tikhonov type of regularization that punish rapid spatial variations in the medium parameters, *i.e.*,

$$\nu_{\text{T}} \int_{\Omega} |\nabla \epsilon(\boldsymbol{x})|^2 + |\nabla \mu(\boldsymbol{x})|^2 + |\nabla \sigma(\boldsymbol{x})/\langle \sigma \rangle|^2 \, \mathrm{dV} \,. \tag{8.18}$$

The parameter values are known at the boundary of the region. We include this a priori information in the functional

$$\nu_{\text{B}} \int_{\Omega} \Psi_{\text{B}}(\boldsymbol{x}) \left(|\epsilon(\boldsymbol{x}) - 1|^2 + |\mu(\boldsymbol{x}) - 1|^2 + |\sigma(\boldsymbol{x})/\langle \sigma \rangle|^2 \right) \mathrm{dV} \,. \tag{8.19}$$

The function $\Psi_{\text{B}}(\boldsymbol{x})$ is small in the interior region. In the numerical identifications in this thesis we use

$$\Psi_{\text{B}}(\boldsymbol{x}) = \exp\left(\frac{-1}{2} \left(\frac{\operatorname{dist}(\boldsymbol{x}, \partial\Omega)}{\Delta x} \right)^2 \right)$$

where $\operatorname{dist}(\boldsymbol{x}, \partial\Omega)$ is the distance from the point $\boldsymbol{x}$ to the boundary $\partial\Omega$ and Δx the spatial discretization of the finite difference scheme, see Section 5.5.1.

With the Tikhonov regularization and the a priori boundary value information, the gradients are modified as

$$\begin{cases} G_{\epsilon} &= -2 \sum_{m=1}^{M} \int_0^T \widetilde{\boldsymbol{E}} \cdot \partial_t \boldsymbol{E} \, \mathrm{d}t - 2\nu_{\text{T}} \nabla^2 \epsilon + 2\nu_{\text{B}} \Psi_{\text{B}} (\epsilon - 1), \\ G_{\mu} &= -2 \sum_{m=1}^{M} \int_0^T \widetilde{\boldsymbol{H}} \cdot \partial_t \boldsymbol{H} \, \mathrm{d}t - 2\nu_{\text{T}} \nabla^2 \mu + 2\nu_{\text{B}} \Psi_{\text{B}} (\mu - 1), \\ G_{\sigma/\langle\sigma\rangle} &= -2\langle \sigma \rangle \sum_{m=1}^{M} \int_0^T \widetilde{\boldsymbol{E}} \cdot \boldsymbol{E} \, \mathrm{d}t - 2\nu_{\text{T}} \frac{\nabla^2 \sigma}{\langle \sigma \rangle} + 2\nu_{\text{B}} \Psi_{\text{B}} \frac{\sigma}{\langle \sigma \rangle}. \end{cases} \tag{8.20}$$

We also incorporate physical restrictions on the parameters into the identification algorithm. The restriction that the medium is passive implies that the conductivity σ is non-negative. The permittivity and permeability are assumed to be equal or greater to one. These type of restrictions could be included in an additional functional. However, we prefer to postulate the restrictions in the update of the parameters, *i.e.*, parameter values outside the domain of restrictions are set to the closest allowed value, *e.g.*,

$$\sigma(\boldsymbol{x}) \to \begin{cases} \sigma(\boldsymbol{x}) & \text{if} \quad \sigma(\boldsymbol{x}) \geq 0, \\ 0 & \text{if} \quad \sigma(\boldsymbol{x}) < 0. \end{cases} \tag{8.21}$$

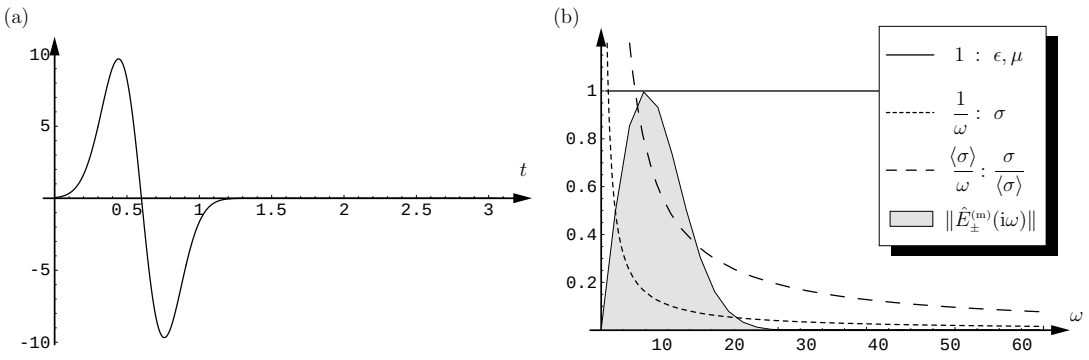

Figure 8.4: (a) The Gaussian input field. (b) The frequency spectrum on the given boundary field (8.23) and the frequency dependence of the constitutive parameters (8.22).

8.4 Parameter scaling

In the perturbed misfit functional, (8.16), we introduced a scaling $\langle\sigma\rangle$ to scale the conductivity. It is easy to understand the importance of the conductivity scaling from the different dimensions of the conductivity and permittivity. Both the permittivity ϵ and permeability μ are invariant under a time scaling $t \to t/\tau$ whereas the conductivity is scaled as $\sigma \to \sigma\tau$. Hence the gradient (8.20) depends on units used. If it was just a dimensional problem, it would be fairly easy to choose a scaling parameter. However, numerical tests indicate that the performance of the identification algorithm is very sensitive to the scaling parameter $\langle\sigma\rangle$.

To motivate the scaling, we consider the constitutive relations of the problem (8.8)

$$\widehat{D}(\mathrm{i}\omega) = \left(\epsilon + \frac{\sigma}{\mathrm{i}\omega}\right)\widehat{E}(\mathrm{i}\omega) \quad \text{and} \quad \widehat{B}(\mathrm{i}\omega) = \mu\widehat{H}(\mathrm{i}\omega) \tag{8.22}$$

where the hat denotes the frequency-domain electromagnetic fields (A.9). The parameters ϵ and μ are not weighted with respect to the frequency, and thus it is sufficient to use the scaling implied by the energy units (2.5). From the above relations one sees that the conductivity σ has a weight of $(\mathrm{i}\omega)^{-1}$. Let $\|\widehat{E}^{(\mathrm{m})}_{\pm}(\mathrm{i}\omega)\|$ denote the amplitude spectrum of the given boundary fields, *i.e.*,

$$\|\widehat{E}^{(\mathrm{m})}_{\pm}(\mathrm{i}\omega)\| = \left(\sum_{m=1}^{M}\int_{\partial\Omega} |\widehat{E}^{(\mathrm{m})}(x,\mathrm{i}\omega;m)|^2 + |\widehat{H}^{(\mathrm{m})}(x,\mathrm{i}\omega;m)|^2\,\mathrm{dS}\right)^{1/2}, \tag{8.23}$$

see the shaded region in Figure 8.4b. If we use a scaling $\langle\sigma\rangle$, the new parameter $\sigma(\boldsymbol{x})/\langle\sigma\rangle$ has a weight of $\langle\sigma\rangle/(\mathrm{i}\omega)$, see Figure 8.4b. We choose $\langle\sigma\rangle$ such that $\langle\sigma\rangle/(\mathrm{i}\omega)$ (the weight for $\sigma/\langle\sigma\rangle$) and 1 (the weight for ϵ and μ) have the same averaged values with respect to $\omega\|\widehat{E}^{(\mathrm{m})}_{\pm}(\mathrm{i}\omega)\|^2$, *i.e.*,

$$\int_0^\infty \left|\frac{\langle\sigma\rangle}{\mathrm{i}\omega}\right| \|\widehat{E}^{(\mathrm{m})}_{\pm}(\mathrm{i}\omega)\|^2\omega\,\mathrm{d}\omega = \int_0^\infty \|\widehat{E}^{(\mathrm{m})}_{\pm}(\mathrm{i}\omega)\|^2\omega\,\mathrm{d}\omega$$

or

$$\langle\sigma\rangle = \left(\int_0^\infty \|\widehat{E}_\pm^{(\mathrm{m})}(\mathrm{i}\omega)\|^2 \,\mathrm{d}\omega\right)^{-1} \int_0^\infty \|\widehat{E}_\pm^{(\mathrm{m})}(\mathrm{i}\omega)\|^2 \omega \,\mathrm{d}\omega.$$

Note that the choice for the scaling parameter $\langle\sigma\rangle$ is non-unique, *i.e.*, above we used a L^1 measure and a frequency weight ω.

Here, we motivate the scaling and generalize the scaling to general dispersion models. Let the constitutive relations depend on the n parameters $\alpha_1, \alpha_2, \ldots, \alpha_n$, *i.e.*,

$$\hat{\boldsymbol{d}}(\mathrm{i}\omega) = \boldsymbol{\varepsilon}(\mathrm{i}\omega; \alpha_1, \alpha_2, \ldots, \alpha_n)\hat{\boldsymbol{e}}(\mathrm{i}\omega),$$

where the six-vector notation (2.6) is used. In energy estimates, it is natural to consider the product

$$\hat{\boldsymbol{e}}(\boldsymbol{x}, \mathrm{i}\omega)^{\mathrm{H}} \cdot \mathrm{i}\omega\hat{\boldsymbol{d}}(\boldsymbol{x}, \mathrm{i}\omega) = \mathrm{i}\omega\hat{\boldsymbol{e}}(\boldsymbol{x}, \mathrm{i}\omega)^{\mathrm{H}} \cdot \boldsymbol{\varepsilon}(\mathrm{i}\omega; \alpha_1, \alpha_2, \ldots, \alpha_n)\hat{\boldsymbol{e}}(\boldsymbol{x}, \mathrm{i}\omega). \tag{8.24}$$

We get a measure of the sensitivity on a parameter α_k, by perturbing α_k and determine the change of the L^1 norm of (8.24). This give a scaling by forcing the expressions

$$\int_\Omega \int_0^\infty |\hat{\boldsymbol{e}}(\boldsymbol{x}, \mathrm{i}\omega)^{\mathrm{H}} \cdot \frac{\partial\boldsymbol{\varepsilon}(\mathrm{i}\omega; \alpha_1, \ldots, \alpha_n)}{\partial\alpha_i/\langle\alpha_i\rangle} \mathrm{i}\omega\hat{\boldsymbol{e}}(\boldsymbol{x}, \mathrm{i}\omega)| \,\mathrm{d}\omega \,\mathrm{dV}$$

to be equal. However, this is not an appropriate scaling, since the fields are not a priori known in the interior part of the region. For the parameter identification, we determine the a priori scaling by the expressions

$$\int_0^\infty |\frac{\partial\boldsymbol{\varepsilon}(\mathrm{i}\omega; \alpha_1, \ldots, \alpha_n)}{\partial\alpha_i/\langle\alpha_i\rangle}| \,\|\widehat{E}_\pm^{(\mathrm{m})}(\mathrm{i}\omega)\|^2 \omega \,\mathrm{d}\omega = \int_0^\infty \|\widehat{E}_\pm^{(\mathrm{m})}(\mathrm{i}\omega)\|^2 \omega \,\mathrm{d}\omega \tag{8.25}$$

where $\|\widehat{E}_\pm^{(\mathrm{m})}(\mathrm{i}\omega)\|$ is the amplitude spectra of the prescribed boundary fields (8.23). We also introduce a measure of distinguishing two parameters as

$$\langle\alpha_i - \alpha_j\rangle = \int_0^\infty |\frac{\partial\boldsymbol{\varepsilon}(\mathrm{i}\omega; \alpha_1, \ldots, \alpha_n)}{\partial\alpha_i/\langle\alpha_i\rangle} - \frac{\partial\boldsymbol{\varepsilon}(\mathrm{i}\omega; \alpha_1, \ldots, \alpha_n)}{\partial\alpha_j/\langle\alpha_j\rangle}| \,\|\widehat{E}_\pm^{(\mathrm{m})}(\mathrm{i}\omega)\|^2 \omega \,\mathrm{d}\omega. \tag{8.26}$$

We use two measures of the identification error. Let $\boldsymbol{\alpha}^{(i)}$ be a set of identified parameters. Firstly, we have the scaled difference of the identified parameters

$$\|\boldsymbol{\alpha}^{(i)} - \boldsymbol{\alpha}\|_{\langle\alpha\rangle} = \sum_{n=1}^{N} \frac{1}{\langle\alpha_n\rangle} \int_\Omega |\alpha_n^{(i)}(\boldsymbol{x}) - \alpha_n(\boldsymbol{x})| \,\mathrm{dV} \tag{8.27}$$

and secondly the error of the constitutive map

$$\begin{aligned}\|\boldsymbol{\varepsilon}(\boldsymbol{\alpha}^{(i)}(\boldsymbol{x})) - \boldsymbol{\varepsilon}(\boldsymbol{\alpha}(\boldsymbol{x}))\|_{\widehat{E}_\pm^{(\mathrm{m})}} \\ = \int_\Omega \int_0^\infty |\boldsymbol{\varepsilon}(\mathrm{i}\omega; \boldsymbol{\alpha}^{(i)}(\boldsymbol{x})) - \boldsymbol{\varepsilon}(\mathrm{i}\omega; \boldsymbol{\alpha}(\boldsymbol{x}))| \,\|\widehat{E}_\pm^{(\mathrm{m})}(\mathrm{i}\omega)\|^2 \omega \,\mathrm{d}\omega \,\mathrm{dV}\,.\end{aligned} \tag{8.28}$$

8.5 Identification algorithm

Once the gradient of the objective functional has been computed, one can use a conventional optimization method to minimize the objective functional in an iterative way. In this thesis we use a standard conjugate-gradient method (Polak-Ribiere algorithm [97, 198]) to minimize the objective functional and determine a sequence of parameters $\boldsymbol{\alpha}^{(i)}(\boldsymbol{x})$, $i = 0, \dots, I$. The iterative algorithm for the identification is as follows:

Parameterize the constitutive map, $\boldsymbol{\varepsilon}(s, \boldsymbol{\alpha})$, initialization of the parameters $\boldsymbol{\alpha}(\boldsymbol{x}) = \boldsymbol{\alpha}^{(0)}(\boldsymbol{x})$, and set $i = 0$.

Scale the identification parameters $\boldsymbol{\alpha}$, *i.e.*, Fourier transform (FFT) the boundary fields and determine the scaling parameters $\langle \alpha \rangle$ with (8.25).

Initiate the Tikhonov regularization parameter ν_{T} and the a priori boundary value parameter ν_{B}.

Initiate the discretization of the problem, *i.e.*, set $\Delta x = \Delta x^{(0)}$, $\Delta t = \Delta t^{(0)}$, and $j = 0$.

Iterate until final discretization, *i.e.*, $\Delta x = \Delta x^{(\mathrm{Final})}$ and $\Delta t = \Delta t^{(\mathrm{Final})}$.

- **Interpolate** the boundary fields and the parameters to the $(\Delta x, \Delta t)$ grid.
- **Iterate** until conjugate-gradient algorithm terminates, *e.g.*, the gradient $\boldsymbol{G}^{(i)}$ is sufficiently small or the parameter updates λ^i are sufficiently small.
  - **Iterate** over the measurements
    - **Calculate** the direct field (8.8) on the grid Δx, with the leapfrog scheme in Section 5.5.1. Save the values of the electric field $\boldsymbol{E}(\boldsymbol{x}, t)$ for $\boldsymbol{x} \in \Omega$ and $t \in [0, T]$.
    - **Gradient** Solve the adjoint problem (8.13) on the grid Δx, with the leapfrog scheme, and use (8.17) to determine the gradient.
  - **Regularize** the problem with the Tikhonov regularization (8.18) and a priori boundary values (8.19), *i.e.*, determine the gradients, $\boldsymbol{G}^{(i)}$, of the regularization and a priori boundary values (8.20).
  - **Search direction** with the conjugate-gradient algorithm

$$\widetilde{\boldsymbol{G}}^{(i)} = \boldsymbol{G}^{(i)} + \frac{\langle \boldsymbol{G}^{(i)} - \boldsymbol{G}^{(i-1)}, \boldsymbol{G}^{(i)} \rangle}{\langle \boldsymbol{G}^{(i-1)}, \boldsymbol{G}^{(i-1)} \rangle} \widetilde{\boldsymbol{G}}^{(i-1)}, \tag{8.29}$$

    if $i > 0$ and $\widetilde{\boldsymbol{G}}^{(i)} = \boldsymbol{G}^{(i)}$ if $i = 0$.
  - **Line search** along the $\widetilde{\boldsymbol{G}}^{(i)}$ direction

$$\mathcal{J}(\boldsymbol{\alpha}^{(i)} - \lambda_i \widetilde{\boldsymbol{G}}^{(i)}) = \min_{\lambda > 0} \mathcal{J}(\boldsymbol{\alpha}^{(i)} - \lambda \widetilde{\boldsymbol{G}}^{(i)}) \tag{8.30}$$

    Here a combination of a quadratic fit and golden section line search algorithm is used. Cut unallowed values in the parameter update (8.21).

Parameter update

$$\boldsymbol{\alpha}^{(i+1)} = \boldsymbol{\alpha}^{(i)} - \lambda_i \widetilde{\boldsymbol{G}}^{(i)}. \tag{8.31}$$

Cut unallowed values in the parameter update (8.21) and update $i \rightarrow i+1$.

End (Conjugate gradient).

Refine grid If Δx is small enough: break, else refine the discretization $\Delta x = \Delta x^{(j+1)}$, set $i = 0$, and update $j \rightarrow j+1$.

End (Identification).

The computational cost is contained in the determination of the gradient (8.17) and in the evaluation of the misfit functional (8.6). Each solution with the leap-frog scheme (5.10) is proportional to (spatial steps)^d(temporal steps) in two ($d = 2$) or three ($d = 3$) spatial dimensions. With M sets of measurements, I gradient iterations, and J evaluations of the misfit functional the total cost is proportional to

$$M\, J\, (1/\Delta x)^d\, (T/\Delta t)$$

for the evaluation of the misfit functional and

$$2\, M\, I\, (1/\Delta x)^d\, (T/\Delta t)$$

for the gradient calculation. The memory requirement is proportional to

$$(1/\Delta x)^d \quad \text{and} \quad (1/\Delta x)^d\, (T/\Delta t)$$

for the misfit evaluation and gradient evaluation, respectively. The memory requirement for the given data is roughly

$$M\, 2\; 2d\, (1/\Delta x)^{d-1}\, (T/\Delta t).$$

The total number of operations are reduced by a multi-grid technique, *i.e.*, perform as many of the iterations as possible at a coarse grid. In general, the memory requirements are severe. However, for lossless or low-loss media, the memory requirement of the gradient calculation can be reduced to

$$2d\, (T/\Delta t)\, (1/\Delta x)^{d-1}$$

at the cost of additional $M\, I\, (1/\Delta x)^d\, (T/\Delta t)$ operations.

The conjugate-gradient algorithm may be trapped at a local minimum if the cost function has some local minima other than the global minimum. In order to overcome this local minimum problem, a global optimization method can be used to obtain a rough initial guess before applying the conjugate-gradient algorithm.

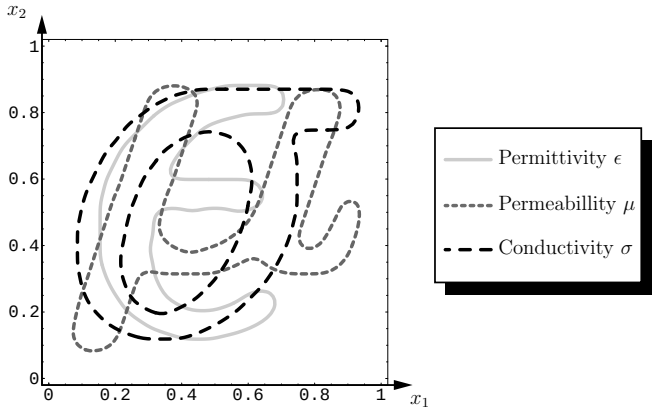

Figure 8.5: Contour plot of the permittivity $\epsilon(x)$, the permeability $\mu(x)$, and the conductivity $\sigma(x)$, respectively.

8.6 Numerical example in two spatial dimensions

As a numerical example of the permittivity, permeability, and conductivity identification, we consider an inhomogeneous object in the square region $(x_1, x_2) \in \Omega = [0,1] \times [0,1]$, see Figure 8.5. The permittivity $\epsilon(x)$ and the permeability $\mu(x)$ are in the range $[1, 1.4]$ whereas the conductivity $\sigma(x)$ is in the range $[0, 1.8]$, see Table 8.1.

Eight sets of boundary fields

$$E^{(\mathrm{m})}(x,t;m) \quad \text{and} \quad H^{(\mathrm{m})}(x,t;m) \quad \text{for} \quad m = 1, \ldots, 8 \tag{8.32}$$

are calculated for the model in Figure 8.5. In the simulations a spatially Gaussian shaped input field $E_{+}^{(\mathrm{m})}(x,t;m)$ are used to illuminate the region, *e.g.*, the first input field $m = 1$ is focused at the front side, see Figure 8.7a. The temporal character of the input fields is shown in Figure 8.4a. The corresponding output fields $E_{-}^{(\mathrm{m})}(x,t;m)$ are determined with the Lax-Wendroff scheme, see Section 5.5.3 on a 82×82 grid. The Lax-Wendroff scheme is used to avoid the problems of the inverse crime, *i.e.*, the use of the same algorithm both in the simulation of data as in the solution of the inverse problem [38].

Random 'white' noise $N(x,t;m)$ is added to the boundary field

$$E^{(\mathrm{m})} \to E^{(\mathrm{m})} + N \quad \text{and} \quad H^{(\mathrm{m})} \to H^{(\mathrm{m})} + N \tag{8.33}$$

where $N(x,t;m)$ has a Gaussian distribution. We use the quotient

$$\sigma_{\text{Noise}} = \frac{\left(\frac{1}{T} \int_0^T \frac{1}{M} \sum_{m=1}^{M} \frac{1}{|\partial\Omega|} \int_{\partial\Omega} N(\boldsymbol{x},t;m) \, \mathrm{dS} \, \mathrm{d}t \right)^{1/2}}{\left(\int_0^T \frac{1}{M} \sum_{m=1}^{M} \frac{1}{|\partial\Omega|} \int_{\partial\Omega} |E^{(\mathrm{m})}(\boldsymbol{x},t;m)|^2 + |H^{(\mathrm{m})}(\boldsymbol{x},t;m)|^2 \, \mathrm{dS} \, \mathrm{d}t \right)^{1/2}} \tag{8.34}$$

to denote the noise level. Notice that only the noise is normalized with $1/T$ in the noise level. After the noise is added, the fields are smoothed as

$$F|_{i,j}^{n} = (6F|_{i,j}^{n} + F|_{i,j}^{n+1} + F|_{i,j}^{n-1} + F|_{i+1,j}^{n} + F|_{i-1,j}^{n} + F|_{i,j+1}^{n} + F|_{i,j-1}^{n})/12$$

Description	Symbol	Scaled units	SI units
Spatial region	Ω	1×1	$1\,\mathrm{m} \times 1\,\mathrm{m}$
Temporal region	$[0, T]$	[0,3.1]	$[0, 10]$ ns
Central frequency	ω_0	10	0.5 GHz
$\text{Permittivity}_{\max}$	$\max\{\epsilon\}$	1.4	$1.4\epsilon_0$
$\text{Permeability}_{\max}$	$\max\{\mu\}$	1.4	$1.4\mu_0$
$\text{Conductivity}_{\max}$	$\max\{\sigma\}$	1.8	5 mS
Conductivity scaling	$\langle\sigma\rangle$	7.1	
Tikhonov regularization	ν_{T}	0.001	
A priori boundary value	ν_{B}	1.0	
Noise level	σ_{Noise}	0.02	

Table 8.1: Data for the permittivity, permeability, and conductivity identification in Section 8.6.

for $F = E^{(\mathrm{m})}$ and $F = H^{(\mathrm{m})}$. The noise level is shown in Figure 8.7e.

We follow the flow chart in Section 8.5. The parameterization of the constitutive map is given by

$$\epsilon(x, s) = \epsilon(x) + \frac{\sigma(x)}{s} \quad \text{and} \quad \mu(x, s) = \mu(x).$$

That is, we identify a permittivity $\epsilon(x)$, permeability $\mu(x)$, and a conductivity $\sigma(x)$. The initial values of the parameters are set to their free space values, *i.e.*,

$$\epsilon^{(0)}(x) - 1 = \mu^{(0)}(x) - 1 = \sigma^{(0)}(x) = 0$$

the corresponding initial error in the output field $E_{-}^{(0)} - E_{-}^{(\mathrm{m})}$ is shown in Figure 8.7.

The permittivity ϵ and permeability μ has a unit scale (assuming the energy units (2.5)), the conductivity scaling is determined by (8.25) to

$$\langle\sigma\rangle = 7.1,$$

see Figure 8.4b. The Tikhonov parameter was set to $\nu_{\mathrm{T}} = 0.001$ and the boundary parameter to $\nu_{\mathrm{B}} = 1$. The parameter identification was first performed on a 41×41 grid. The conjugate-gradient algorithm was used to update the parameters. In total 14 iterations together with 90 evaluations of the objective functional (8.6) were performed, see Figure 8.8. The fourteenth iteration was used to initiate the identification on the 82×82 grid. Here 7 iterations together with 60 evaluations of the objective functional were performed. The resulting parameters are shown next to the true parameters in Figure 8.6. The errors of the identified parameters (*e.g.*, $\epsilon^{(\mathrm{I})} - \epsilon$) are shown in Figure 8.10. The identification took approximately 2 hours on a SUN workstation Ultra 1, *i.e.*, 20 minutes on the courser grid and 80 minutes on the fine grid. The maximum memory requirement was about 50 Mb.

In the above identification, the regularization parameters were fixed, see Table 8.1. The sensitivity on the regularization parameters was tested in the range

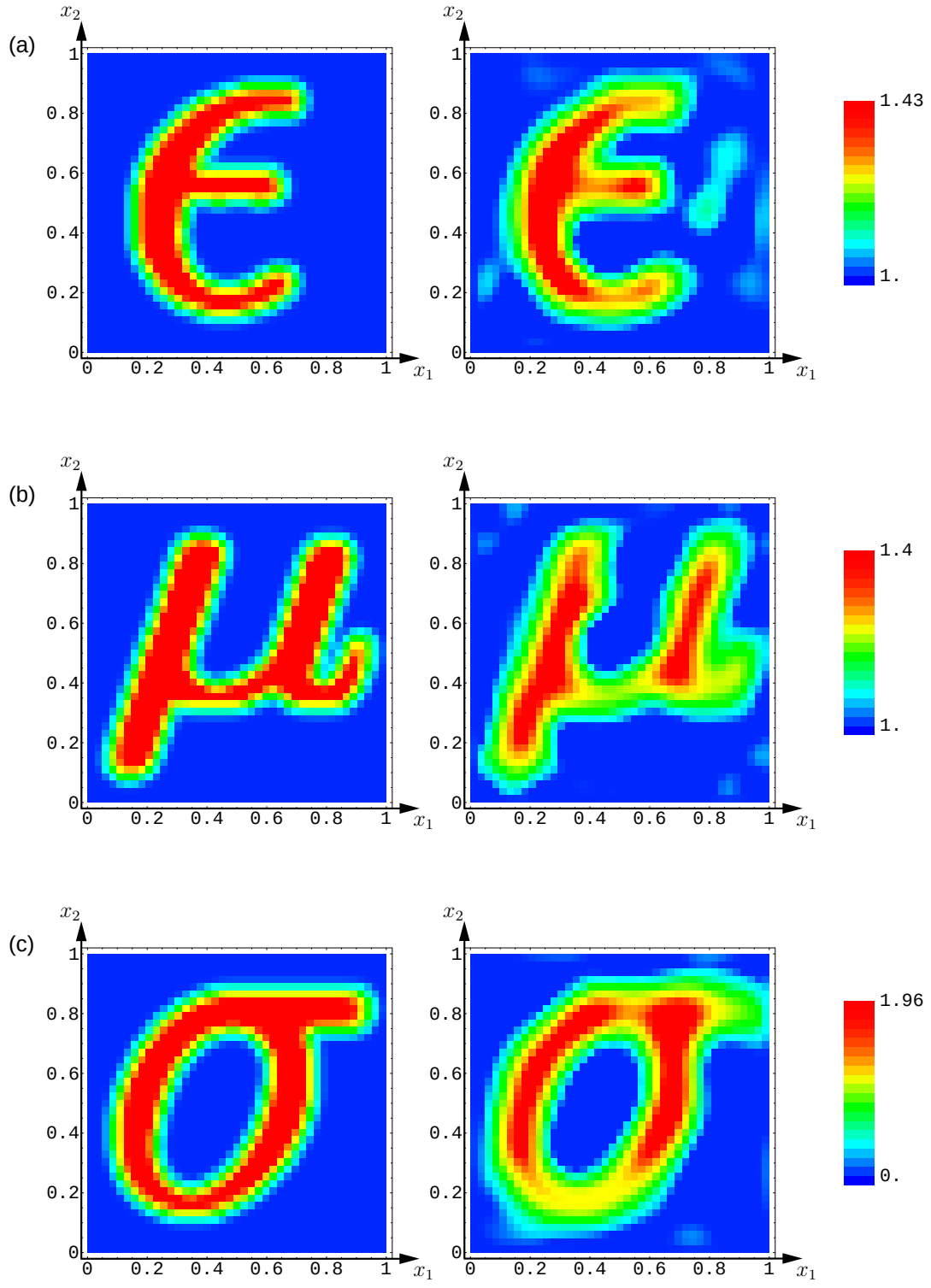

Figure 8.6: True (left) and identified (right) material parameters, (a) the permittivity, (b) the permeability, and (c) the conductivity, respectively.

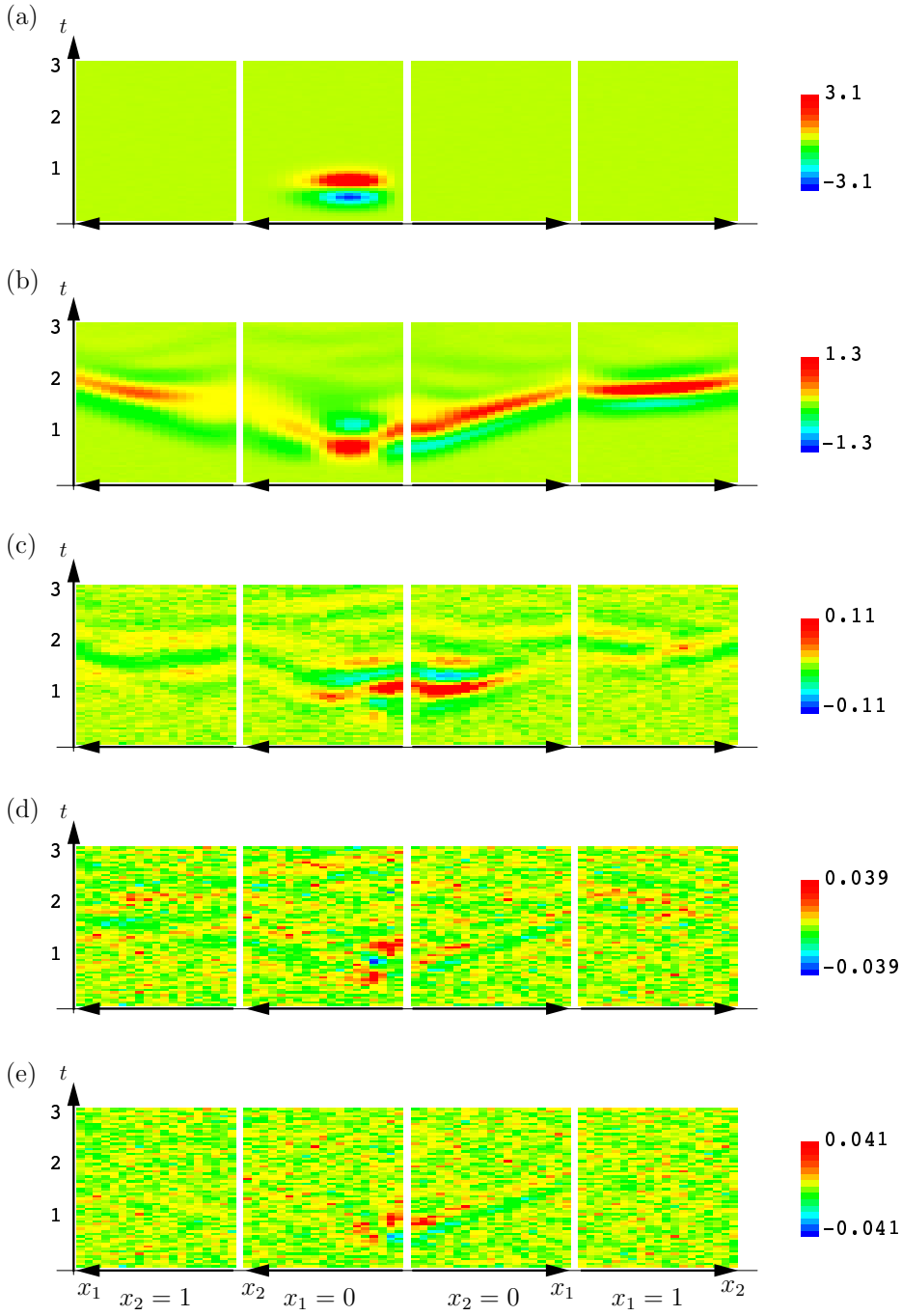

Figure 8.7: Space-time plots of the first of the eight in/output fields used in the reconstruction. From top to bottom: (a) the given input field $E_+^{(\mathrm{m})}(x,t;1)$, (b) the given output field $E_-^{(\mathrm{m})}(x,t;1)$, (c) the difference between a calculated output field with homogeneous parameters (the initial values in the optimization algorithm) and the given output field, $E_-^{(0)}(x,t;1) - E_-^{(\mathrm{m})}(x,t;1)$, (d) the difference between a calculated output field with the reconstructed parameters and the given output field, $E_-^{(I)}(x,t;1) - E_-^{(\mathrm{m})}(x,t;1)$, and (e) the difference between the calculated output with the true parameters and the given output, respectively.

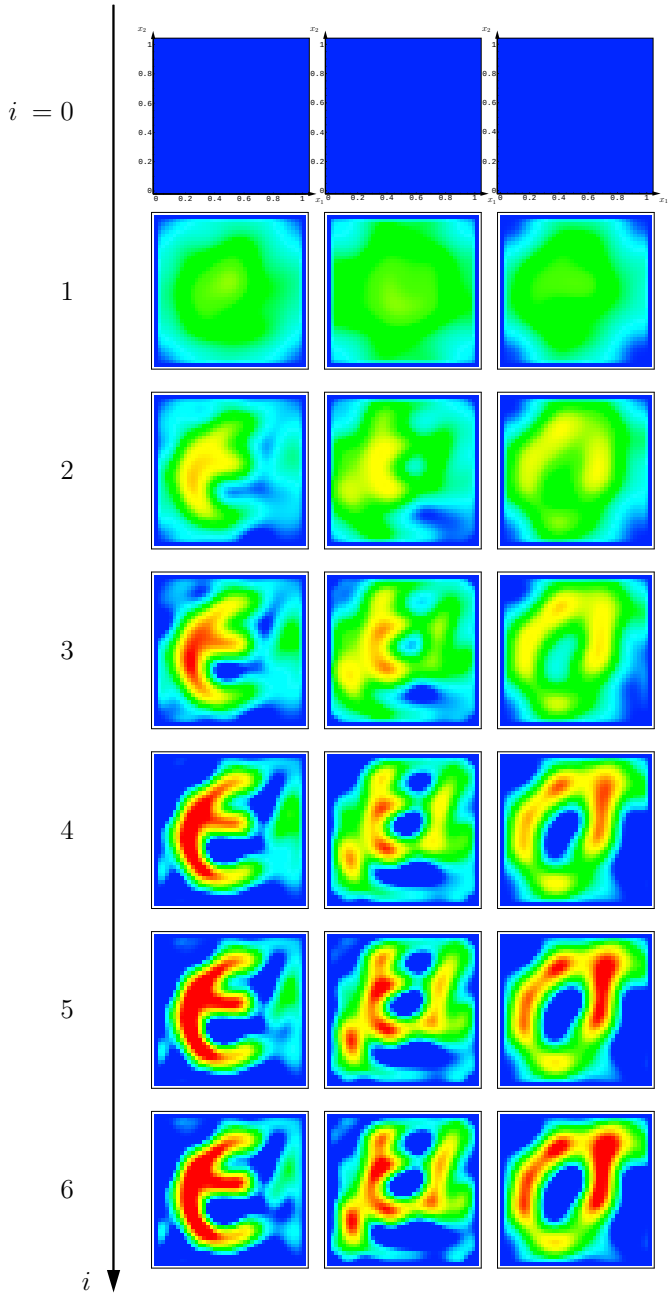

Figure 8.8: The $\epsilon^{(i)}(x)$, $\mu^{(i)}(x)$, and $\sigma^{(i)}(x)$ identifications as a function of the number of iterations i in the conjugate-gradient algorithm (8.31).

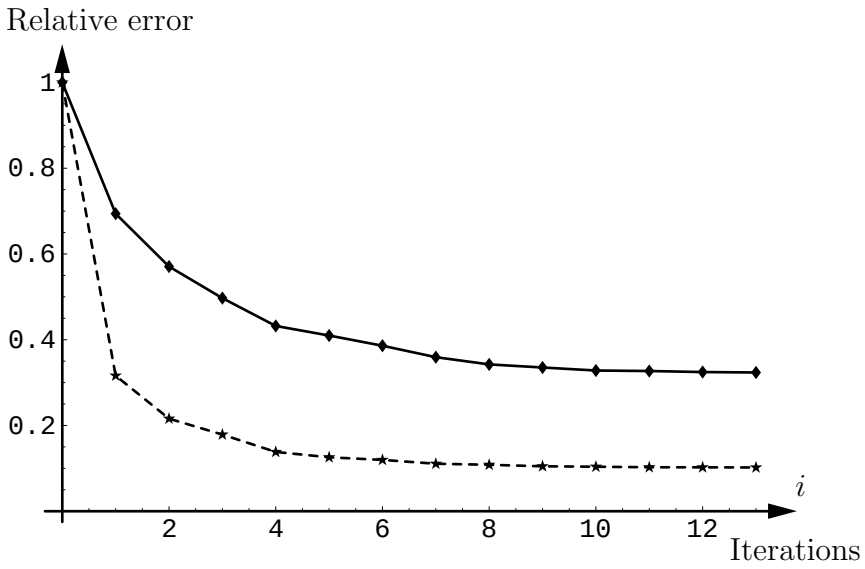

Figure 8.9: The error in the identification as function of the iterations. The solid line, the relative parameter error (8.27), and the dashed line the relative misfit $\mathcal{J}^{(i)}/\mathcal{J}^{(0)}$, respectively.

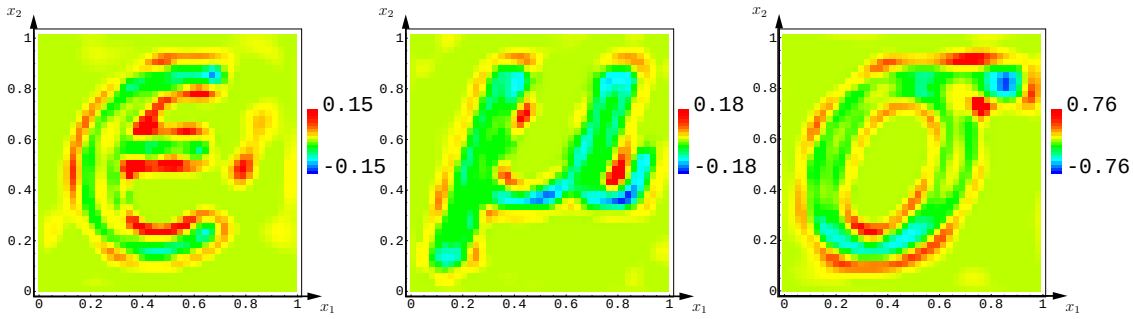

Figure 8.10: Error in the identified material parameters. From left to right: the permittivity, the permeability, and the conductivity, respectively.

$10^{-5} \leq \nu_{\mathrm{T}} \leq 10^{-1}$ and $10^{-2} \leq \nu_{\mathrm{B}} \leq 10^{2}$. As the Tikhonov regularization parameter ν_{T} increases, the reconstruction becomes smoother. However, in the range $10^{-4} \leq \nu_{\mathrm{T}} \leq 10^{-2}$, the effect is small. The sensitivity on ν_{B} is also quite weak, and the reconstruction deteriorates near the boundary for large values of ν_{B}. In fact, one can determine the optimal value of the regularization parameters with the generalized cross validation method [243]. The sensitivity on the conductivity scaling $\langle\sigma\rangle$ is comparatively much larger. In the range $5 \leq \langle\sigma\rangle \leq 10$, the reconstruction is good. For larger values of $\langle\sigma\rangle$ the conductivity gradient is exaggerated, and for smaller values of $\langle\sigma\rangle$ the conductivity diminishes. This is of particular importance since the scaling parameter is non-unique.

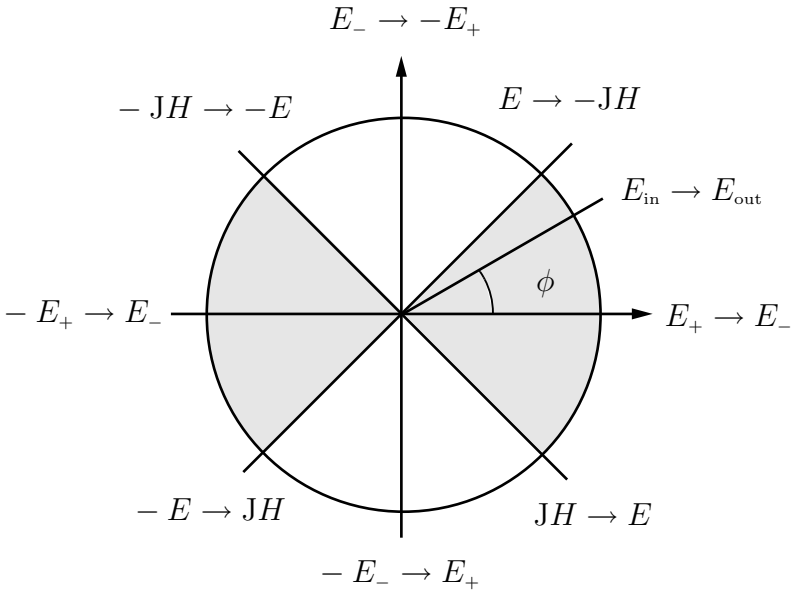

Figure 8.11: The input and output fields in (8.35). The 'allowed' input and output fields are in the shaded region.

8.7 Motivation for the input and output fields

In the inverse problem in Section 8.1, we know the tangential components of the electric and magnetic fields $E^{(\mathrm{m})}(x,t)$ and $H^{(\mathrm{m})}(x,t)$ at the boundary $\partial\Omega$. This gives us several possibilities to choose input and output fields in the optimization formulation (8.3). To motivate the use of the energy-flux split fields (8.4), we consider a general type of input and output fields. Define linear combinations of the tangential fields E_+ and E_-

$$\begin{cases} E_{\mathrm{in}}(x,t) &= \cos(\phi)\, E_+(x,t) \;+\sin(\phi)\, E_-(x,t), \\ E_{\mathrm{out}}(x,t) &= -\sin(\phi)\, E_+(x,t) + \cos(\phi)\, E_-(x,t), \end{cases} \tag{8.35}$$

where we treat E_{in} as the input to the optimization algorithm and E_{out} as the output. Notice that $\phi = 0$ gives the map $E_+ \mapsto E_-$, $\phi = \pi/4$ the map $E \mapsto -\mathrm{J}H$, and $\phi = -\pi/4$ the map $\mathrm{J}H \mapsto E$, see Figure 8.11. The inverse of the linear combination (8.35) is

$$\begin{cases} E_+(x,t) &= \cos(\phi)\, E_{\mathrm{in}}(x,t) - \sin(\phi)\, E_{\mathrm{out}}(x,t), \\ E_-(x,t) &= \sin(\phi)\, E_{\mathrm{in}}(x,t) + \cos(\phi)\, E_{\mathrm{out}}(x,t). \end{cases}$$

Let $\boldsymbol{E}$ and $\boldsymbol{H}$ be the solution of the Maxwell equations with $E_{\mathrm{in}} = E_{\mathrm{in}}^{(\mathrm{m})}$ prescribed at the boundary. Rewrite the misfit functional (8.3) in the input and output fields. To convey the ideas we simplify the notation and restrict the discussion to variations in the permittivity ϵ and a single excitation ($M = 1$). The misfit functional is

$$\mathcal{J}[\epsilon] = 2 \int_0^T \int_{\partial\Omega} \Phi(t)\, |E_{\mathrm{out}}(x,t) - E_{\mathrm{out}}^{(\mathrm{m})}(x,t)|^2 \,\mathrm{dS}\,\mathrm{d}t. \tag{8.36}$$

Perturb the permittivity an amount δ in the direction ϵ'

$$\epsilon(\boldsymbol{x}) \to \epsilon(\boldsymbol{x}) + \delta\epsilon'(\boldsymbol{x}).$$

We assume that $\epsilon'(\boldsymbol{x})$ is smooth and vanishes at the boundary $\partial\Omega$. The corresponding perturbations of the calculated fields are

$$\boldsymbol{E} \to \boldsymbol{E} + \delta\boldsymbol{E} \quad \text{and} \quad \boldsymbol{H} \to \boldsymbol{H} + \delta\boldsymbol{H}. \tag{8.37}$$

Observe that $\delta\boldsymbol{E}$ and $\delta\boldsymbol{H}$ denote the total perturbation. In this section, we show that $\delta\boldsymbol{E}$ and $\delta\boldsymbol{H}$ can be expanded asymptotically in the perturbation δ, see (8.44) on page 124. The perturbed fields satisfy the Maxwell equations

$$\begin{cases} (\epsilon + \delta\epsilon')\,\partial_t(\boldsymbol{E} + \delta\boldsymbol{E}) - \nabla \times (\boldsymbol{H} + \delta\boldsymbol{H}) + \sigma\,(\boldsymbol{E} + \delta\boldsymbol{E}) = \boldsymbol{0}, \\ \mu\partial_t(\boldsymbol{H} + \delta\boldsymbol{H}) + \nabla \times (\boldsymbol{E} + \delta\boldsymbol{E}) = \boldsymbol{0} \end{cases}$$

together with the boundary condition

$$E_{\text{in}}(x,t) + \delta E_{\text{in}}(x,t) = E_{\text{in}}^{(\text{m})}(x,t) \quad \text{for} \quad x \in \partial\Omega$$

and zero initial values $\boldsymbol{E} + \delta\boldsymbol{E} = \boldsymbol{H} + \delta\boldsymbol{H} = \boldsymbol{0}$ for $t = 0$. The increment in the misfit functional (8.36) is

$$\delta\mathcal{J}[\epsilon] = \mathcal{J}[\epsilon + \delta\epsilon'] - \mathcal{J}[\epsilon] = 4\int_0^T \int_{\partial\Omega} \Phi\,\left(\delta E_{\text{out}} \cdot (E_{\text{out}} - E_{\text{out}}^{(\text{m})}) + |\delta E_{\text{out}}|^2\right) \mathrm{dS}\,\mathrm{d}t,$$

where the perturbation of the calculated fields satisfies the Maxwell equations with an induced source

$$\begin{cases} (\epsilon(\boldsymbol{x}) + \delta\epsilon'(\boldsymbol{x}))\;\partial_t\delta\boldsymbol{E} - \nabla \times \delta\boldsymbol{H} + \sigma\delta\boldsymbol{E} = -\delta\epsilon'(\boldsymbol{x})\,\partial_t\boldsymbol{E}(\boldsymbol{x},t), \\ \mu\partial_t\delta\boldsymbol{H} + \nabla \times \delta\boldsymbol{E} = \boldsymbol{0}. \end{cases} \tag{8.38}$$

The boundary condition and initial values of $\delta\boldsymbol{E}$ and $\delta\boldsymbol{H}$ vanish, *i.e.*,

$$\delta E_{\text{in}}(x,t) = 0 \quad \text{for} \quad x \in \partial\Omega$$

and $\delta\boldsymbol{E}(\boldsymbol{x},0) = \delta\boldsymbol{H}(\boldsymbol{x},0) = \boldsymbol{0}$, respectively.

To show that the perturbed fields (8.37) have asymptotic expansions in the perturbation δ, we estimate the energy of the perturbed field. Apply the energy balance (4.22) to the perturbation of the calculated field (8.38). We get

$$\begin{aligned} \mathcal{E}[\delta\boldsymbol{E},\delta\boldsymbol{H}](t) + \int_0^t \|\cos(\phi)\delta E_{\text{out}}\|_{\partial\Omega}^2\,\mathrm{d}\tau \\ = \int_0^t \|\sin(\phi)\delta E_{\text{out}}\|_{\partial\Omega}^2\,\mathrm{d}\tau - \int_0^t \int_\Omega \delta\epsilon'\delta\boldsymbol{E}\cdot\dot{\boldsymbol{E}}\,\mathrm{dV}\,\mathrm{d}\tau \end{aligned}$$

where $\mathcal{E}[\delta\boldsymbol{E},\delta\boldsymbol{H}](t)$ is the energy of the field perturbation in the region Ω at time t, *i.e.*,

$$\mathcal{E}[\delta\boldsymbol{E},\delta\boldsymbol{H}](t) = \frac{1}{2}\int_\Omega (\epsilon + \delta\epsilon')|\delta\boldsymbol{E}|^2 + \mu|\delta\boldsymbol{H}|^2\,\mathrm{dV} + \int_0^t \int_\Omega \sigma|\delta\boldsymbol{E}|^2\,\mathrm{dV}\,\mathrm{d}\tau. \tag{8.39}$$

Observe that the perturbation of the permittivity is included in the energy. The right hand side of the energy balance is estimated with a Cauchy type inequality. We get

$$\begin{aligned}\int_0^t \int_\Omega \delta\epsilon'\, \delta\boldsymbol{E}\cdot\dot{\boldsymbol{E}}\,\mathrm{dV}\,\mathrm{d}\tau &\le \int_0^t \int_\Omega \frac{\epsilon+\delta\epsilon'}{2}|\delta\boldsymbol{E}|^2 + \frac{|\delta\epsilon'|^2}{|\epsilon+\delta\epsilon'|^2}\frac{\epsilon+\delta\epsilon'}{2}|\dot{\boldsymbol{E}}|^2\,\mathrm{dV}\,\mathrm{d}\tau \\ &\le \int_0^t \mathcal{E}[\delta\boldsymbol{E},\delta\boldsymbol{H}](t)\,\mathrm{d}\tau + \|\frac{\delta\epsilon'}{\epsilon+\delta\epsilon'}\|_\infty^2 \int_0^t \mathcal{E}[\dot{\boldsymbol{E}},\dot{\boldsymbol{H}}](\tau)\,\mathrm{d}\tau\end{aligned}$$

where $\mathcal{E}[\dot{\boldsymbol{E}},\dot{\boldsymbol{H}}](t)$ is the energy of the time differentiated fields. This estimate implies

$$\begin{aligned}\mathcal{E}[\delta\boldsymbol{E},\delta\boldsymbol{H}](t) + \cos(2\phi)\int_0^t \|\delta E_{\text{out}}\|^2\,\mathrm{d}\tau& \\ \le \int_0^t \mathcal{E}[\delta\boldsymbol{E},\delta\boldsymbol{H}](\tau)\,\mathrm{d}\tau + \|\frac{\delta\epsilon'}{\epsilon+\delta\epsilon'}\|_\infty^2 \int_0^t \mathcal{E}[\dot{\boldsymbol{E}},\dot{\boldsymbol{H}}](\tau)\,\mathrm{d}\tau.&\quad (8.40)\end{aligned}$$

For input and output fields with $\cos 2\phi \ge 0$ (*i.e.*, $|\phi| \le \pi/4$ or $|\phi-\pi| \le \pi/4$, see Figure 8.11), we can use the Grnwall lemma [154] to get a bound of the field perturbation. The energy of the perturbation is bounded by

$$\mathcal{E}[\delta\boldsymbol{E},\delta\boldsymbol{H}](t) \le \delta^2 \mathrm{e}^t \|\frac{\epsilon'}{\epsilon+\delta\epsilon'}\|_\infty^2 \int_0^t \mathcal{E}[\dot{\boldsymbol{E}},\dot{\boldsymbol{H}}](\tau)\,\mathrm{d}\tau \quad \text{if} \quad \cos 2\phi \ge 0. \tag{8.41}$$

The energy of the time differentiated field is estimated through differentiation of the Maxwell equations. This gives a bound

$$\mathcal{E}[\dot{\boldsymbol{E}},\dot{\boldsymbol{H}}](t) \le \int_0^t \|\partial_t E_+^{(\mathrm{m})}\|_{\partial\Omega}^2\,\mathrm{d}\tau.$$

Note that $\epsilon+\delta\epsilon' \ge \epsilon/2$ if the perturbation δ is small and hence, the perturbation of the calculated fields are of the same order as the perturbation, *i.e.*,

$$\|\delta\boldsymbol{E}\| + \|\delta\boldsymbol{H}\| = \mathrm{O}(\delta) \quad \text{if} \quad \cos 2\phi \ge 0.$$

Let $\boldsymbol{E}'$ and $\boldsymbol{H}'$ be the first order part of $\delta\boldsymbol{E}$ and $\delta\boldsymbol{H}$, respectively, *i.e.*,

$$\boldsymbol{E} \to \boldsymbol{E} + \delta\boldsymbol{E}' + \delta^2\boldsymbol{E} \quad \text{and} \quad \boldsymbol{H} \to \boldsymbol{H} + \delta\boldsymbol{H}' + \delta^2\boldsymbol{H}. \tag{8.42}$$

Observe that $\delta^2\boldsymbol{E}$ and $\delta^2\boldsymbol{H}$ denotes the part of the perturbation that is not of the first order. The first order perturbed fields $\boldsymbol{E}'$ and $\boldsymbol{H}'$ satisfy the first order part of (8.38), *i.e.*,

$$\begin{cases}\epsilon(\boldsymbol{x})\,\partial_t\boldsymbol{E}' - \nabla\times\boldsymbol{H}' + \sigma\boldsymbol{E}' = -\epsilon'(\boldsymbol{x})\,\dot{\boldsymbol{E}}(\boldsymbol{x},t),\\ \mu\partial_t\boldsymbol{H}' + \nabla\times\boldsymbol{E}' = \boldsymbol{0}\end{cases}$$

together with the boundary condition

$$E'_{\text{in}}(x,t) = 0 \quad \text{for} \quad x\in\partial\Omega$$

and the initial values $\boldsymbol{E}'(\boldsymbol{x},0) = \boldsymbol{H}'(\boldsymbol{x},0) = \boldsymbol{0}$.

To get the estimates of the succeeding terms of the asymptotic expansion (8.42), we repeat the arguments above. The second order perturbations $\delta^2\boldsymbol{E}$ and $\delta^2\boldsymbol{H}$ satisfy

$$\begin{cases} (\epsilon(\boldsymbol{x}) + \delta\epsilon'(\boldsymbol{x}))\ \partial_t\delta^2\boldsymbol{E} - \nabla\times\delta^2\boldsymbol{H} + \sigma\delta^2\boldsymbol{E} = -\delta\epsilon'(\boldsymbol{x})\,\dot{\boldsymbol{E}}'(\boldsymbol{x},t) \\ \mu\partial_t\delta^2\boldsymbol{H} + \nabla\times\delta^2\boldsymbol{E} = \boldsymbol{0} \end{cases} \tag{8.43}$$

together with the boundary condition

$$\delta^2 E_{\text{in}}(x,t) = 0 \quad \text{for} \quad x \in \partial\Omega$$

and the initial values $\delta^2\boldsymbol{E}(\boldsymbol{x},0) = \delta^2\boldsymbol{H}(\boldsymbol{x},0) = \boldsymbol{0}$. The estimate above gives

$$\mathcal{E}[\delta^2\boldsymbol{E},\delta^2\boldsymbol{H}](t) \leq \delta^2 \mathrm{e}^t \|\frac{\epsilon'}{\epsilon+\delta\epsilon'}\|_\infty^2 \int_0^t \mathcal{E}[\dot{\boldsymbol{E}}',\dot{\boldsymbol{H}}'](\tau)\,\mathrm{d}\tau \quad \text{if} \quad \cos 2\phi \geq 0,$$

where $\mathcal{E}[\delta^2\boldsymbol{E},\delta^2\boldsymbol{H}](t)$ is the energy of the second order perturbation. This shows that the fields $\delta^2\boldsymbol{E}$ and $\delta^2\boldsymbol{H}$ are of second order in the perturbation δ, *i.e.*,

$$\|\delta^2\boldsymbol{E}\| + \|\delta^2\boldsymbol{H}\| = \mathrm{O}(\delta^2) \quad \text{if} \quad \cos 2\phi \geq 0.$$

This justifies the notation

$$\boldsymbol{E} \to \boldsymbol{E} + \delta\boldsymbol{E}' + \mathrm{O}(\delta^2) \quad \text{and} \quad \boldsymbol{H} \to \boldsymbol{H} + \delta\boldsymbol{H}' + \mathrm{O}(\delta^2) \tag{8.44}$$

in (8.9).

In the increment of the misfit functional (8.36) we also need an estimate on the output field δE_{out}. Using the estimate of the energy (8.41) in (8.40), we get

$$\cos(2\phi)\int_0^t \|\delta E_{\text{out}}\|_{\partial\Omega}^2\,\mathrm{d}\tau \leq \delta^2\mathrm{e}^t\|\frac{\epsilon'}{\epsilon+\delta\epsilon'}\|_\infty^2\int_0^t \mathcal{E}[\dot{\boldsymbol{E}},\dot{\boldsymbol{H}}](\tau)\,\mathrm{d}\tau.$$

The output field is bounded if $\cos 2\phi > 0$, *i.e.*, $|\phi| < \pi/4$ or $|\phi-\pi| < \pi/4$, see Figure 8.11. For these values of ϕ the output field is of the order of the perturbation

$$\int_0^T \|\delta E_{\text{out}}\|_{\partial\Omega}^2\,\mathrm{d}t = \mathrm{O}(\delta^2) \quad \text{if} \quad \cos 2\phi > 0.$$

From this we conclude that we are able to perform the gradient calculation if $|\phi| < \pi/4$ or $|\phi-\pi| < \pi/4$. Observe that the best estimation is obtained with $\phi = 0$ (or $\phi = \pi$), *i.e.*, the split fields (8.5). This analysis motivates the reason for introducing the energy-flux split fields. Part of this section is found in Ref. [106].

8.8 Debye and Lorentz models

To get a more realistic model of the interaction between the electromagnetic fields and matter, we have to incorporate dispersive effects. Two common models of dispersion are given by the Debye and Lorentz models, see Section 2.7. The Debye

model depends on two parameters, the relaxation time τ and the concentration α (related to the alignment frequency), whereas the Lorentz model has three parameters, the collision frequency ν, the resonance frequency ω_0 and the concentration β (related to the plasma frequency). By superimposing several Debye and Lorentz models, we can get accurate models for many electromagnetic materials, see Section 2.7. However, the complexity of the identification problem increases with the number of unknown parameters. Hence, it is convenient to incorporate as much a priori information as possible into the identification problem. In this section, we assume a priori knowledge of the material parameters τ, ν, and ω_0 in the models and we try to identify the different Debye and Lorentz concentrations $\alpha_n(\boldsymbol{x})$ and $\beta_n(\boldsymbol{x})$. The permittivity is of the form

$$\epsilon(\boldsymbol{x}, s) = \epsilon_\infty(\boldsymbol{x}) + \sum_{n=1}^{N_\mathrm{D}} \frac{\alpha_n(\boldsymbol{x})}{1+\tau_n s} + \sum_{n=1}^{N_\mathrm{L}} \frac{\beta_n(\boldsymbol{x})}{\omega_n^2 + s\nu_n + s^2}$$

where N_D is the number of the Debye states and N_L is the number of Lorentz states. The media is assumed to be non-magnetic.

In the time domain, the electric field $\boldsymbol{E}(\boldsymbol{x}, t)$ and the magnetic field $\boldsymbol{H}(\boldsymbol{x}, t)$ satisfy the Maxwell equations (2.1) with the relations

$$\boldsymbol{D}(\boldsymbol{x}, t) = \epsilon_\infty(\boldsymbol{x})\boldsymbol{E}(\boldsymbol{x}, t) + \sum_{n=1}^{N_\mathrm{D}} \boldsymbol{P}_n^{(\mathrm{D})}(\boldsymbol{x}, t) + \sum_{n=1}^{N_\mathrm{L}} \boldsymbol{P}_n^{(\mathrm{L})}(\boldsymbol{x}, t) \tag{8.45}$$

and

$$\boldsymbol{B}(\boldsymbol{x}, t) = \mu \boldsymbol{H}(\boldsymbol{x}, t),$$

see Section 2.7. The Debye states $\boldsymbol{P}_n^{(\mathrm{D})}(\boldsymbol{x}, t)$ and Lorentz states $\boldsymbol{P}_n^{(\mathrm{L})}(\boldsymbol{x}, t)$ are updated with the ordinary differential equations

$$\tau_n \partial_t \boldsymbol{P}_n^{(\mathrm{D})} + \boldsymbol{P}_n^{(\mathrm{D})} = \alpha_n(\boldsymbol{x})\boldsymbol{E}(\boldsymbol{x}, t) \tag{8.46}$$

and

$$\partial_t^2 \boldsymbol{P}_n^{(\mathrm{L})} + \nu_n \partial_t \boldsymbol{P}_n^{(\mathrm{L})} + \omega_n^2 \boldsymbol{P}_n^{(\mathrm{L})} = \beta_n(\boldsymbol{x})\boldsymbol{E}(\boldsymbol{x}, t), \tag{8.47}$$

respectively. The experiment starts at time $t = 0$, this gives zero initial values of the electromagnetic fields and states

$$\boldsymbol{E}(\boldsymbol{x}, 0) = \boldsymbol{H}(\boldsymbol{x}, 0) = \boldsymbol{P}_n^{(\mathrm{D})}(\boldsymbol{x}, 0) = \boldsymbol{P}_n^{(\mathrm{L})}(\boldsymbol{x}, 0) = \partial_t \boldsymbol{P}_n^{(\mathrm{L})}(\boldsymbol{x}, 0) = \boldsymbol{0}.$$

At the boundary the input field is prescribed

$$E_+(\boldsymbol{x}, t; m) = E_+^{(\mathrm{m})}(\boldsymbol{x}, t; m) \quad \text{when} \quad \boldsymbol{x} \in \partial\Omega.$$

We find the gradient of the misfit functional (8.3) with respect to the parameters $\epsilon_\infty, \alpha_n$ and β_n by calculating the increment of the functional to the first order, *i.e.*,

$$\begin{aligned}\mathcal{J}'[\epsilon_\infty, \alpha_n, \beta_n] =& \lim_{\delta\to 0} \frac{\mathcal{J}[\epsilon_\infty + \delta\epsilon'_\infty, \alpha_n + \delta\alpha'_n, \beta_n + \delta\beta'_n] - \mathcal{J}[\epsilon_\infty, \alpha_n, \beta_n]}{\delta} \\ =& 4\sum_{m=1}^{M} \int_0^T \int_{\partial\Omega} \Phi E'_- \cdot (E_- - E_-^{(\mathrm{m})}) \,\mathrm{dS}\,\mathrm{d}t.\end{aligned}$$

To simplify the derivation, we observe that it is sufficient to consider a generalized Lorentz model, *i.e.*,

$$\boldsymbol{D}(\boldsymbol{x},t) = \epsilon_\infty(\boldsymbol{x})\boldsymbol{E}(\boldsymbol{x},t) + \boldsymbol{P}(\boldsymbol{x},t),$$

where the polarization $\boldsymbol{P}$ satisfies

$$\gamma\partial_t^2\boldsymbol{P} + \nu\partial_t\boldsymbol{P} + \omega_0^2\boldsymbol{P} - \beta(\boldsymbol{x})\boldsymbol{E} = \boldsymbol{0}.$$

The Debye polarization (8.46) is given by the case $\gamma = 0$, $\omega_0 = 1$, and $\nu = \tau$, whereas the Lorentz polarization (8.47) is given by $\gamma = 1$. The sum of many polarizations, follows from the linearity of the gradient. We perturb the instantaneous response ϵ_∞ an amount δ in the direction $\epsilon'_\infty(\boldsymbol{x})$

$$\epsilon_\infty(\boldsymbol{x}) \to \epsilon_\infty(\boldsymbol{x}) + \delta\epsilon'_\infty(\boldsymbol{x})$$

and the concentration β an amount δ in the direction $\beta'(\boldsymbol{x})$

$$\beta(\boldsymbol{x}) \to \beta(\boldsymbol{x}) + \delta\beta'(\boldsymbol{x}).$$

The electromagnetic field and polarization have the asymptotic expansions

$$\boldsymbol{E} \to \boldsymbol{E} + \delta\boldsymbol{E}' + \mathrm{O}(\delta^2), \quad \boldsymbol{H} \to \boldsymbol{H} + \delta\boldsymbol{H}' + \mathrm{O}(\delta^2)$$

and

$$\boldsymbol{P} \to \boldsymbol{P} + \delta\boldsymbol{P}' + \mathrm{O}(\delta^2),$$

respectively. The first order perturbations $\boldsymbol{E}'$, $\boldsymbol{H}'$, and $\boldsymbol{P}'$ satisfy the Maxwell equations and the Lorentz equation with induced sources, *i.e.*,

$$\begin{cases} \epsilon_\infty(\boldsymbol{x})\partial_t\boldsymbol{E}' - \nabla\times\boldsymbol{H}' + \partial_t\boldsymbol{P}' = -\epsilon'_\infty(\boldsymbol{x})\partial_t\boldsymbol{E}(\boldsymbol{x},t), \\ \mu\partial_t\boldsymbol{H}' + \nabla\times\boldsymbol{E}' = \boldsymbol{0} \end{cases} \tag{8.48}$$

and

$$\gamma\partial_t^2\boldsymbol{P}' + \nu\partial_t\boldsymbol{P}' + \omega^2\boldsymbol{P}' - \beta(\boldsymbol{x})\boldsymbol{E}' = \beta'(\boldsymbol{x})\boldsymbol{E}(\boldsymbol{x},t) \tag{8.49}$$

where $\boldsymbol{E}$, $\boldsymbol{H}$, and $\boldsymbol{P}$ are the fields of the unperturbed problem. The initial values of the perturbed fields are

$$\boldsymbol{E}'(\boldsymbol{x},0) = \boldsymbol{H}'(\boldsymbol{x},0) = \boldsymbol{P}'(\boldsymbol{x},0) = \gamma\partial_t\boldsymbol{P}'(\boldsymbol{x},0) = \boldsymbol{0}.$$

At the boundary the perturbed input field vanishes

$$E'_+(\boldsymbol{x},t) = 0, \quad \boldsymbol{x}\in\partial\Omega.$$

The first order perturbation of the misfit functional is

$$\begin{aligned}\mathcal{J}'[\epsilon_\infty,\beta] =& \lim_{\delta\to 0}\frac{\mathcal{J}[\epsilon_\infty+\delta\epsilon'_\infty,\beta+\delta\beta'] - \mathcal{J}[\epsilon_\infty,\beta']}{\delta} \\ =& 4\sum_{m=1}^{M}\int_0^T\int_{\partial\Omega}\Phi(t)\,E'_-(\boldsymbol{x},t;m)\cdot\left(E_-(\boldsymbol{x},t;m) - E_-^{(\mathrm{m})}(\boldsymbol{x},t;m)\right)\mathrm{dS}\,\mathrm{d}t.\end{aligned}$$

To find the gradient of the misfit functional, we introduce the adjoint fields $\widetilde{\boldsymbol{E}}$, $\widetilde{\boldsymbol{H}}$, and $\widetilde{\boldsymbol{P}}$. The adjoint fields satisfy the Maxwell equations

$$\begin{cases} \epsilon_\infty(\boldsymbol{x})\partial_t\widetilde{\boldsymbol{E}} - \nabla\times\widetilde{\boldsymbol{H}} + \beta(\boldsymbol{x})\partial_t\widetilde{\boldsymbol{P}} = \boldsymbol{0} \\ \mu\partial_t\widetilde{\boldsymbol{H}} + \nabla\times\widetilde{\boldsymbol{E}} = \boldsymbol{0} \end{cases} \tag{8.50}$$

together with the Lorentz type equation

$$\gamma\partial_t^2\widetilde{\boldsymbol{P}} - \nu\partial_t\widetilde{\boldsymbol{P}} + \omega^2\widetilde{\boldsymbol{P}} - \widetilde{\boldsymbol{E}} = \boldsymbol{0}. \tag{8.51}$$

The adjoint problem is solved backwards in time, from time $t = T$ to time $t = 0$. At time $t = T$, we have the zero 'initial' values

$$\widetilde{\boldsymbol{E}}(\boldsymbol{x},T) = \widetilde{\boldsymbol{H}}(\boldsymbol{x},T) = \widetilde{\boldsymbol{P}}(\boldsymbol{x},T) = \gamma\partial_t\widetilde{\boldsymbol{P}}(\boldsymbol{x},T) = \boldsymbol{0}.$$

At the boundary, the difference between the simulated and given output fields are used, *i.e.*,

$$E_-(\boldsymbol{x},t) = \Phi(t)\,\big(E_-(\boldsymbol{x},t) - E_-^{(\mathrm{m})}(\boldsymbol{x},t)\big) \quad \text{when} \quad \boldsymbol{x}\in\partial\Omega.$$

Observe, that the input field E_- is the natural input field when the equation is solved backwards in time.

Cross multiply the fields of the perturbed equations (8.48) and (8.49) with the fields of the adjoint problems (8.50) and (8.51). Integrate the result over time $[0,T]$ and space Ω. The first term vanishes due to the initial values of the perturbed and adjoint problems, and the second term gives an integral over the boundary, *i.e.*,

$$\int_0^T\int_{\partial\Omega}(\widetilde{\boldsymbol{E}}\times\boldsymbol{H}' + \boldsymbol{E}'\times\widetilde{\boldsymbol{H}})\cdot\boldsymbol{n}\,\mathrm{dS}\,\mathrm{d}t = -\int_0^T\int_\Omega \epsilon'_\infty\widetilde{\boldsymbol{E}}\cdot\partial_t\boldsymbol{E} - \beta'\boldsymbol{E}\cdot\partial_t\widetilde{\boldsymbol{P}}\,\mathrm{dV}\,\mathrm{d}t.$$

Rewrite the boundary term in the input and output fields $E_\pm$ and use the boundary condition for the adjoint fields to get an expression for the perturbation of the misfit functional, *i.e.*,

$$\begin{aligned}\mathcal{J}'[\epsilon_\infty,\beta] &= 2\sum_{m=1}^{M}\int_0^T\int_\Omega -\epsilon'_\infty\widetilde{\boldsymbol{E}}\cdot\partial_t\boldsymbol{E} + \beta'\partial_t\widetilde{\boldsymbol{P}}\cdot\boldsymbol{E}\,\mathrm{dV}\,\mathrm{d}t \\ &= \langle G_{\epsilon_\infty},\epsilon'_\infty\rangle + \langle G_{\beta/\langle\beta\rangle},\beta'/\langle\beta\rangle\rangle,\end{aligned}$$

where $\langle\beta\rangle$ is the parameter scaling (8.25). For the general case (8.45) we get the perturbed misfit functional

$$\begin{aligned}\mathcal{J}'[\epsilon_\infty,\alpha_n,\beta_n] &= 2\sum_{m=1}^{M}\int_0^T\int_\Omega -\epsilon'_\infty\widetilde{\boldsymbol{E}}\cdot\partial_t\boldsymbol{E} \\ &\qquad + \sum_{n=1}^{N_\mathrm{D}}\alpha'_n\partial_t\widetilde{\boldsymbol{P}}^{(\mathrm{D})}\cdot\boldsymbol{E} + \sum_{n=1}^{N_\mathrm{L}}\beta'_n\partial_t\widetilde{\boldsymbol{P}}^{(\mathrm{L})}\cdot\boldsymbol{E}\,\mathrm{dV}\,\mathrm{d}t \\ &= \langle G_{\epsilon_\infty},\epsilon'_\infty\rangle + \sum_{n=1}^{N_\mathrm{D}}\langle G_{\alpha_n/\langle\alpha_n\rangle},\alpha'_n/\langle\alpha_n\rangle\rangle + \sum_{n=1}^{N_\mathrm{L}}\langle G_{\beta_n/\langle\beta_n\rangle},\beta'_n/\langle\beta_n\rangle\rangle.\end{aligned}$$

	τ_{I}	τ_{II}	$\langle\alpha_{\text{I}}\rangle$	$\langle\alpha_{\text{II}}\rangle$	$\langle\alpha_{\text{I}}-\alpha_{\text{II}}\rangle$	$\frac{\mathcal{J}^{(I)}}{\mathcal{J}^{(0)}}$	$\frac{\|\alpha^{(I)}-\bar{\alpha}\|_{\langle\alpha\rangle}}{\|\alpha^{(0)}-\bar{\alpha}\|_{\langle\alpha\rangle}}$	$\frac{\|\epsilon(\alpha^{(N)})-\epsilon(\alpha)\|_{\widehat{E}_{\pm}^{(\text{m})}}}{\|\epsilon(\alpha^{(0)})-\epsilon(\alpha)\|_{\widehat{E}_{\pm}^{(\text{m})}}}$
(b)	0.05	0.18	1.2	2.3	0.59	0.26	0.34	0.27
(c)	0.05	0.10	1.2	1.6	0.33	0.21	0.38	0.21
(d)	0.05	0.07	1.2	1.3	0.16	0.19	0.84	0.22

Table 8.2: Data for the Debye model identification in Section 8.9.

The gradient is identified as

$$\boldsymbol{G} = \left(G_{\epsilon_\infty}, G_{\alpha_1/\langle\alpha_1\rangle}, \ldots, G_{\alpha_{N_{\text{D}}}/\langle\alpha_{N_{\text{D}}}\rangle}, G_{\beta_1/\langle\beta_1\rangle}, \ldots, G_{\beta_{N_{\text{L}}}/\langle\beta_{N_{\text{L}}}\rangle} \right),$$

where

$$\begin{cases} G_{\epsilon_\infty}(\boldsymbol{x}) &= -2 \sum_{m=1}^{M} \int_0^T \widetilde{\boldsymbol{E}}(\boldsymbol{x},t;m) \cdot \partial_t \boldsymbol{E}(\boldsymbol{x},t;m)\,\mathrm{d}t, \\ G_{\alpha_n/\langle\alpha_n\rangle}(\boldsymbol{x}) &= 2\langle\alpha_n\rangle \sum_{m=1}^{M} \int_0^T \partial_t \widetilde{\boldsymbol{P}}_n^{(\text{D})}(\boldsymbol{x},t;m) \cdot \boldsymbol{E}(\boldsymbol{x},t;m)\,\mathrm{d}t, \\ G_{\beta_n/\langle\beta_n\rangle}(\boldsymbol{x}) &= 2\langle\beta_n\rangle \sum_{m=1}^{M} \int_0^T \partial_t \widetilde{\boldsymbol{P}}_n^{(\text{L})}(\boldsymbol{x},t;m) \cdot \boldsymbol{E}(\boldsymbol{x},t;m)\,\mathrm{d}t. \end{cases}$$

8.9 Example: Identification of two Debye parameters

In this example, we consider the identification of the two Debye parameters $\alpha_{\text{I}}(x)$ and $\alpha_{\text{II}}(x)$ in two spatial dimensions. The unknown object is confined to the square $\Omega = [0,1] \times [1,0]$, see Figure 8.12a. The Laplace domain permittivity is given by

$$\epsilon(x,s) = 1 + \frac{\alpha_{\text{I}}(x)}{1+s\tau_{\text{I}}} + \frac{\alpha_{\text{II}}(x)}{1+s\tau_{\text{II}}} \quad \text{for} \quad x \in \Omega.$$

The $\alpha_{\text{I}}(x)$ and $\alpha_{\text{II}}(x)$ parameters have a spatial variation of a 'roman' I and II, respectively, see Figure 8.12a. A set of given fields $E^{(\text{m})}(x,t;m)$ and $H^{(\text{m})}(x,t;m)$ are simulated for eight different excitations and a small amount of noise is added to the fields.

In the first identification, Figure 8.12b, the relaxation times

$$\tau_{\text{I}} = 0.05 = 176\,\text{ps} \quad \text{and} \quad \tau_{\text{II}} = 0.18 = 600\,\text{ps}$$

are used. The SI values corresponds to the case of a $1\,\text{m}^2$ square region. The frequency characteristics of the parameters are given by the solid and dashed graphs to the left in Figure 8.12b. The scaling parameters are determined to

$$\langle\alpha_{\text{I}}\rangle = 1.2 \quad \text{and} \quad \langle\alpha_{\text{II}}\rangle = 2.3.$$

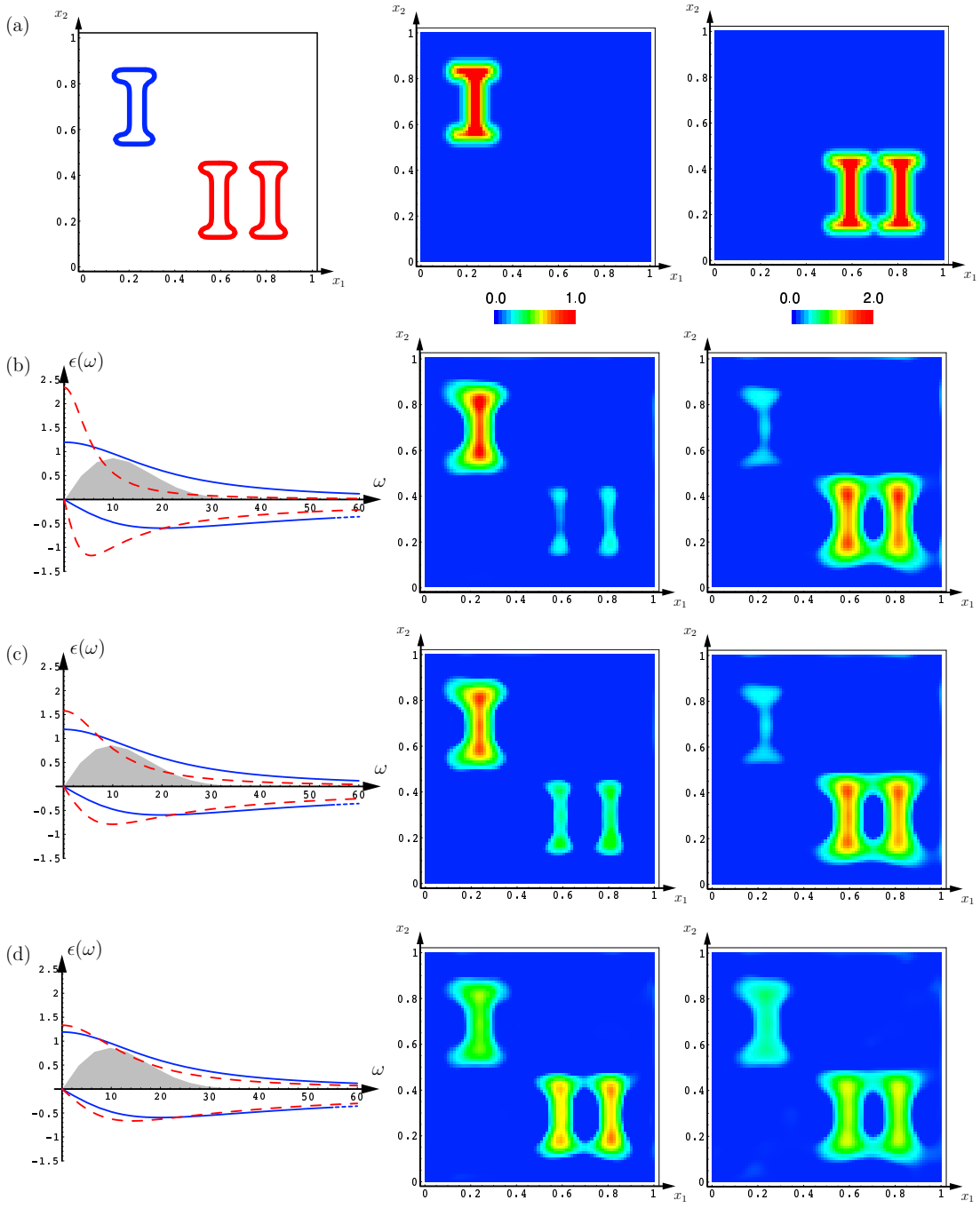

Figure 8.12: Identification of the two Debye parameters $\alpha_{\mathrm{I}}(x)$ and $\alpha_{\mathrm{II}}(x)$ in Section 8.9. The left column of (a) shows the geometry of the object. The frequency characteristic of material I and II are shown in to the left of (b), (c), and (d) for three different cases. Material I is given by the solid (blue) graphs and material II by the dashed (red) graphs. The center (right) plots show the spatial distribution of material I (material II) in (a), and the identified spatial distribution of material I (material II) in (b), (c), and (d) for the three cases.

In the center and to the right of Figure 8.12b, the identified parameters $\alpha_{\text{I}}^{(I)}$ and $\alpha_{\text{II}}^{(I)}$, are shown. Notice the ghost image in the identifications, *i.e.*, the algorithm does not succeed to fully distinguish the two Debye models. In Figure 8.12c, a similar identification is performed for the relaxation times

$$\tau_{\text{I}} = 0.05 = 176\,\text{ps} \quad \text{and} \quad \tau_{\text{II}} = 0.1 = 334\,\text{ps}.$$

In this case the scaling parameters are

$$\langle \alpha_{\text{I}} \rangle = 1.2 \quad \text{and} \quad \langle \alpha_{\text{II}} \rangle = 1.6.$$

In the final identification, Figure 8.12d, the relaxation times

$$\tau_{\text{I}} = 0.05 = 176\,\text{ps} \quad \text{and} \quad \tau_{\text{II}} = 0.07 = 233\,\text{ps}$$

are used.

In Table 8.2, the identification data is shown. We observe that the relative error of the identified parameters (8.27)

$$\|\alpha^{(I)} - \alpha\|_{\langle\alpha\rangle} / \|\alpha^{(0)} - \alpha\|_{\langle\alpha\rangle}$$

is smallest for the first identification. As the relaxation time τ_{II} approach τ_{I} in the second and third identification, the identification of the parameters deteriorates, see Figure 8.12bcd, *i.e.*, the algorithm does not succeed to separate the two Debye models unless the relaxation times are clearly separated. In Table 8.2, the separation of the parameters are measured by $\langle \alpha_{\text{I}} - \alpha_{\text{II}} \rangle$, see (8.26). As seen in Table 8.2, the relative misfit $\mathcal{J}^{(I)}/\mathcal{J}^{(0)}$ and the relative error of the permittivity $\|\epsilon(\alpha^{(I)}) - \epsilon(\alpha)\|_{\widehat{E}_{\pm}^{(m)}} / \|\epsilon(\alpha^{(0)}) - \epsilon(\alpha)\|_{\widehat{E}_{\pm}^{(m)}}$ are not very sensitive to the separation of the relaxation times τ_{I} and τ_{II}.

The boundary fields $E_{\pm}^{(\text{m})}(\boldsymbol{x}, t, m)$, $m = 1, 2, \ldots, 8$ were simulated on a 100×100-grid with a leapfrog scheme with discretization $\Delta t = \Delta x/2$ for 500 time steps. White noise with noise level 0.005 was added to the boundary fields. The scaling parameters were determined according to (8.25). The identification algorithm was initialized on a 41×41-grid with the initial parameter values $\alpha_{\text{I}}^0(x) = \alpha_{\text{II}}^0(x) = 0$. After 8–11 iterations, the parameters were interpolated to an 82×82-grid for an additional 4–6 iterations.

Observe that the inverse crime might have been committed, *i.e.*, the same numerical scheme was used for both the forward modeling and the solution of the inverse problem. However, the use of different discretizations and the addition of noise makes the crime less serious.

8.10 Moisture

In Sections 8.2 and 8.8, we derived the gradient with respect to the 'basic' isotropic models, *i.e.*, an instantaneous response, a conductivity, Debye models, and Lorentz models. Many isotropic materials are modeled with linear combinations of the above 'basic' models, *e.g.*, water, moisture, alcohol.

Water is usually modeled with a Debye polarization combined with an instantaneous response, *i.e.*,

$$\epsilon_{\mathrm{w}}(s) = \epsilon_{\mathrm{w}}(\infty) + \frac{\epsilon_{\mathrm{w}}(0) - \epsilon_{\mathrm{w}}(\infty)}{1 + \tau s},$$

where $\epsilon_{\mathrm{w}}(0)$ is the static value and $\epsilon_{\mathrm{w}}(\infty)$ is the high frequency value of the permittivity. More accurate models use several Debye models, see Ref. [132].

Moisture is a mixture between water and some other medium. Here we consider the case of water mixed with free space. In a volumetric mixture formula [132], the effective permittivity is given by

$$\epsilon_{\mathrm{eff}}(\boldsymbol{x}, s) = f_{\mathrm{w}}(\boldsymbol{x}) \left(\epsilon_{\mathrm{w}}(\infty) - 1 + \frac{\epsilon_{\mathrm{w}}(0) - \epsilon_{\mathrm{w}}(\infty)}{1 + \tau s} \right) + 1,$$

where $f_{\mathrm{w}}(\boldsymbol{x})$ is the volume fraction of water.

We want to identify the volume fraction of water $f_{\mathrm{w}}(\boldsymbol{x})$ and a material modeled by an instantaneous response $\epsilon_{\mathrm{L}}(\boldsymbol{x})$ in a volume Ω, *i.e.*, a permittivity

$$\epsilon(x, s) = 1 + \epsilon_{\mathrm{L}}(x) + f_{\mathrm{w}}(x) \left(\epsilon_{\mathrm{w}}(\infty) - 1 + \frac{\epsilon_{\mathrm{w}}(0) - \epsilon_{\mathrm{w}}(\infty)}{1 + \tau s} \right),$$

from a set of given fields

$$E^{(\mathrm{m})}(x, t; m) \quad \text{and} \quad H^{(\mathrm{m})}(x, t; m) \quad \text{for} \quad m = 1, \ldots, M \tag{8.52}$$

at the boundary of Ω. Following the procedure described in Section 8, we minimize the misfit functional (8.3) with the algorithm outlined in Section 8.5. The forward problem is given by the Maxwell equations together with a Debye type equation

$$\begin{cases} \left(\epsilon_{\mathrm{L}}(\boldsymbol{x}) + f_{\mathrm{w}}(\boldsymbol{x})(\epsilon_{\mathrm{w}}(\infty) - \epsilon_{\mathrm{m}})\right) \partial_t \boldsymbol{E} - \nabla \times \boldsymbol{H} + \partial_t \boldsymbol{P} = \boldsymbol{0}, \\ \mu \partial_t \boldsymbol{H} + \nabla \times \boldsymbol{E} = \boldsymbol{0}, \\ \tau \partial_t \boldsymbol{P} + \boldsymbol{P} = f_{\mathrm{w}}(\boldsymbol{x}) \left(\epsilon_{\mathrm{w}}(0) - \epsilon_{\mathrm{w}}(\infty)\right) \boldsymbol{E}. \end{cases} \tag{8.53}$$

The fields are assumed to be quiescent before time $t = 0$, this gives the zero initial values (8.2) of the fields and the polarization

$$\boldsymbol{E}(\boldsymbol{x}, 0) = \boldsymbol{H}(\boldsymbol{x}, 0) = \boldsymbol{P}(\boldsymbol{x}, 0) = \boldsymbol{0}.$$

At the boundary, the split fields are used as input field, *i.e.*,

$$E_+(\boldsymbol{x}, t; m) = E_+^{(\mathrm{m})}(\boldsymbol{x}, t; m) \quad \text{where} \quad \boldsymbol{x} \in \partial\Omega.$$

To get the gradient, we also have to solve the adjoint problem. The adjoint (backward) problem consists of the Maxwell equations together with a Debye type equation

$$\begin{cases} \left(\epsilon_{\mathrm{L}}(\boldsymbol{x}) + f_{\mathrm{w}}(\boldsymbol{x}) \left(\epsilon_{\mathrm{w}}(\infty) - \epsilon_{\mathrm{m}}\right)\right) \partial_t \widetilde{\boldsymbol{E}} - \nabla \times \widetilde{\boldsymbol{H}} + f_{\mathrm{w}}(\boldsymbol{x}) \left(\epsilon_{\mathrm{w}}(0) - \epsilon_{\mathrm{w}}(\infty)\right) \partial_t \widetilde{\boldsymbol{P}} = \boldsymbol{0}, \\ \mu \partial_t \widetilde{\boldsymbol{H}} + \nabla \times \widetilde{\boldsymbol{E}} = \boldsymbol{0}, \\ -\tau \partial_t \widetilde{\boldsymbol{P}} + \widetilde{\boldsymbol{P}} = \widetilde{\boldsymbol{E}}. \end{cases}$$

The adjoint problem is solved backwards in time, from $t = T$ to $t = 0$, the 'initial values' at $t = T$ are

$$\widetilde{\boldsymbol{E}}(\boldsymbol{x}, T) = \widetilde{\boldsymbol{H}}(\boldsymbol{x}, T) = \widetilde{\boldsymbol{P}}(\boldsymbol{x}, T) = \boldsymbol{0}.$$

At the boundary, the difference between the calculated and the given output fields are used, *i.e.*,

$$\tilde{\boldsymbol{e}}_{-}(\boldsymbol{x}, t) = \Phi(t)\left(E_{-}(\boldsymbol{x}, t) - E_{-}^{(\mathrm{m})}(\boldsymbol{x}, t)\right) \quad \text{where} \quad \boldsymbol{x} \in \partial\Omega. \tag{8.54}$$

Following the derivation in Section 8.8, we get the gradient $\boldsymbol{G} = (G_{\epsilon_{\mathrm{L}}}, G_{f_{\mathrm{w}}/\langle f_{\mathrm{w}}\rangle})$, where

$$\begin{cases} G_{\epsilon_{\mathrm{L}}} & = -2\sum_{m=1}^{M}\int_0^T \widetilde{\boldsymbol{E}} \cdot \partial_t \boldsymbol{E}\,\mathrm{d}t, \\ G_{f_{\mathrm{w}}/\langle f_{\mathrm{w}}\rangle} & = 2\langle f_{\mathrm{w}}\rangle \sum_{m=1}^{M}\int_0^T \left(\epsilon_{\mathrm{w}}(0) - \epsilon_{\mathrm{w}}(\infty)\right)\,\partial_t \widetilde{\boldsymbol{P}} \cdot \boldsymbol{E} - \left(\epsilon_{\mathrm{w}}(\infty) - \epsilon_{\mathrm{m}}\right)\,\widetilde{\boldsymbol{E}} \cdot \partial_t \boldsymbol{E}\,\mathrm{d}t. \end{cases}$$

Assume a square region $\Omega = [0, 1] \times [0, 1]$ filled with a mixture of water and a lattice of circular inclusions (crystal). We use a Debye type model for the water (blue, solid line) and a Lorentz model for the crystal (red, dashed line), the frequency characteristics are shown in Figure 8.13a. The static value, the high frequency value, and the relaxation time of water are chosen to be

$$\epsilon_{\mathrm{w}}(0) = 80, \quad \epsilon_{\mathrm{w}}(\infty) = 5, \quad \text{and } \tau = 0.2 = 667\,\mathrm{ps}, \tag{8.55}$$

respectively, see Ref. [132] for more realistic values. The background medium is set to the free space value, *i.e.*, $\epsilon_{\mathrm{m}} = 1$. The Lorentz medium has resonance frequency and a collision frequency

$$\omega_0 = 77 = 3.7\,\mathrm{GHz} \quad \text{and} \quad \nu = 5, \tag{8.56}$$

respectively. We use a source with bandlimited frequency characteristics as shown by the shaded region in Figure 8.13a.

The given boundary fields $E^{(\mathrm{m})}(x, t; m)$ and $H^{(\mathrm{m})}(x, t; m)$ $m = 1, \ldots, 8$ are simulated on a 512×512 grid with a leapfrog scheme. The boundary fields are scaled down to a 128×128 grid and a small amount of noise is added to the fields.

From the given fields $E^{(\mathrm{m})}(x, t; m)$ and $H^{(\mathrm{m})}(x, t; m)$, we try to identify a high frequency permittivity $\epsilon_{\mathrm{L}}(x)$ and the volume fraction of water $f_{\mathrm{w}}(\boldsymbol{x})$. Notice that, we do not identify the parameters of the simulation, *i.e.*, we try to identify a high frequency permittivity $\epsilon_{\mathrm{L}}(x)$ instead of the Lorentz parameter $\alpha(x)$. In the identification of the water content, we assume a priori information about the relaxation time τ. Following the flowchart of the identification algorithm presented in Section 8.5, we first parameterize the constitutive map $\boldsymbol{\varepsilon}$. The permittivity is

$$\epsilon(x, s) = 1 + \epsilon_{\mathrm{L}}(x) + f_{\mathrm{w}}(x)\left(\epsilon_{\mathrm{w}}(\infty) - \epsilon_{\mathrm{m}} + \frac{\epsilon_{\mathrm{w}}(0) - \epsilon_{\mathrm{w}}(\infty)}{1 + \tau s}\right)$$

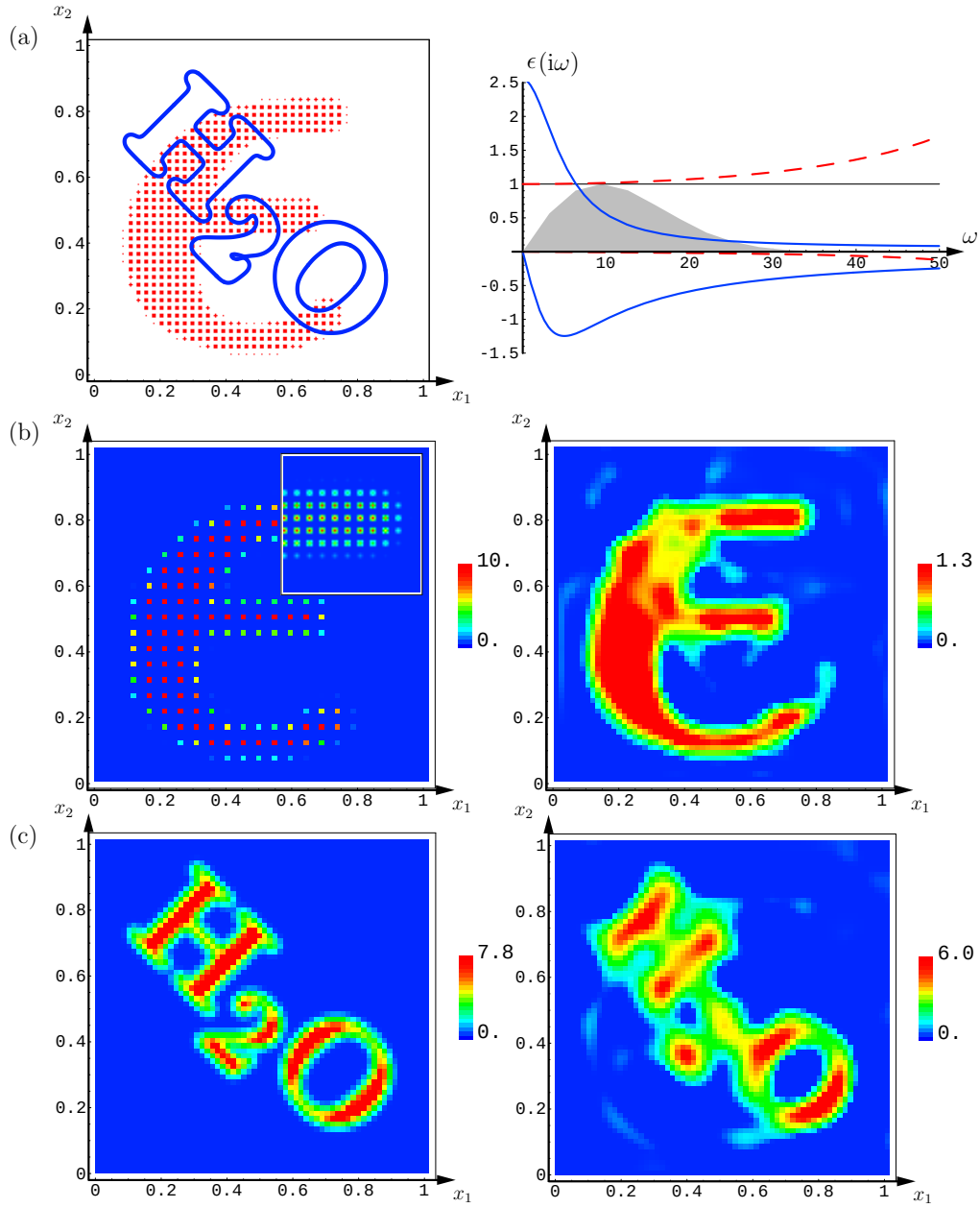

Figure 8.13: Identification of the volume fraction of water and a high frequency permittivity. From top to bottom: (a) the Lorentz medium in (red) dotted structure and the moisture in the (blue) H_2O-shaped region, (b) the true Lorentz constituent and the identified high frequency permittivity, (c) the true moisture constituent and the identified moisture constituent, respectively.

and the parameters are initiated to their free-space values

$$\epsilon_{\mathrm{L}}^{(0)}(x) = 0 \quad \text{and} \quad f_{\mathrm{w}}^{(0)}(x) = 0.$$

The scaling of the identification parameters are determined to

$$\langle \epsilon_{\mathrm{L}} \rangle = 1 \quad \text{and} \quad \langle f_{\mathrm{w}} \rangle = 2.5.$$

We use a Tikhonov parameter $\nu_{\mathrm{T}} = 0.0001$ and a boundary parameter $\nu_{\mathrm{B}} = 0.1$. The discretization is initiated to $\Delta x = 1/64$ and $\Delta t = \Delta x/2$. First 10 iterations are performed on a 64×64 grid, and the identified parameters are used to initiate 5 additional iterations on a 128×128 grid. The original and identified parameters are shown in Figure 8.13. Observe that the fine structure of the crystal is identified as an effective smooth structure. The algorithm succeeds to capture most of the moisture structure, the maximum water amount is identified to 6% compared to the original 7.8%.

As in Section 8.9, the same type of finite-difference scheme was used in both the simulation of the data and in the solution of the inverse problem, *i.e.*, we might have committed an inverse crime. However, the data was simulated on a 512×512-grid whereas the inverse problem was solved on 64×64 and 128×128-grids. Moreover, the data was simulated with a Lorentz material together with a Debye material whereas the inverse problem was solved with a instantaneous response together with a Debye model.

8.11 Effective medium models

In Figure 8.13, we observed that a smooth ϵ-profile was identified even though the true profile consists of several small particles. This is a typical case of the ill-posedness of the identification problem, *i.e.*, we do not have the resolution to separate a smooth obstacle from an object that is varying on a fine scale. In the identification algorithm this ill-posedness is a fundamental difficulty. However, there are several types of problems where the ill-posedness of the identification is used to simplify the solution of the problem.

For example if a FDTD scheme is used to determine the wave field in a region we discretize the material properties in the region. With an equidistant grid the discretization is typically determined by 10–15 samples per wavelength. Of course, this requires that it is possible to give a reasonable representation of the material properties on this grid. If the material properties varies much faster than the fields, it is possible to determine effective medium properties of the material. This property is utilized in homogenization [215, 130, 248, 27, 207] and mixing formulas [212]. Here we use the identification algorithm to determine effective medium properties.

In a first example, we consider a random distribution of particles in two spatial dimensions, see Figure 8.14a. The particles are dielectric with a permittivity $\epsilon_{\mathrm{i}} = 2$ and the background by a permittivity $\epsilon_{\mathrm{b}} = 1$. The size of the inclusions increases in the x_2-direction and the volume fraction of the particles increases in the x_1-direction.

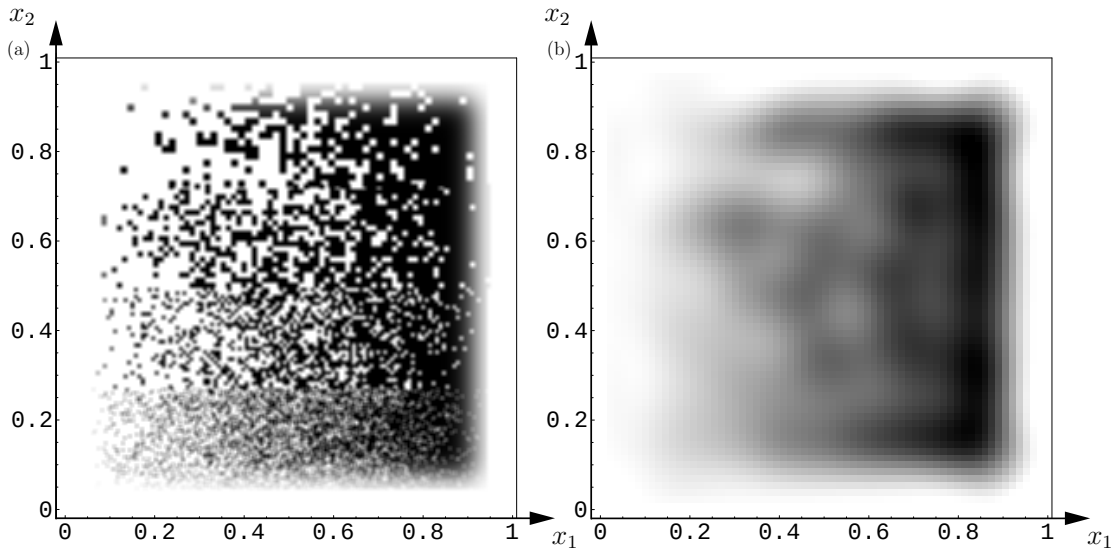

Figure 8.14: Resolution/homogenization of a random non-dispersive permittivity.

The region is discretized with $\Delta x = 1/512$. For small values of x_2, single cell (size Δx^2) inclusions are used, the size increases to $(4\Delta x)^2$ inclusions as x_2 approaches 1. The probability for an inclusion increases linearly from $x_1 = 0$ to $x_1 = 1$ to give an average permittivity of roughly $1 + x_1$, see Figure 8.14.

Eight sets of boundary fields

$$E^{(\mathrm{m})}(x, t; m) \quad \text{and} \quad H^{(\mathrm{m})}(x, t; m)$$

are simulated on the 512×512 grid with the leapfrog scheme (5.10). The temporal and spatial characters of the boundary fields are roughly as depicted in Figures 8.4 and 8.7. The boundary fields have a center wavelength of 0.5 and a bandwidth corresponding to wavelengths up to 0.25. Observe that the upper frequency is sampled with 128 samples per wavelength.

We use the identification algorithm presented in Section 8.5 to determine an effective permittivity for the region. The initial values of the permittivity are chosen to the free-space value $\epsilon^{(0)} = 1$. Notice that we could have used a better initial guess such that an average of the random samples. The boundary fields are interpolated to a 64×64 grid, This corresponds to 32 samples per wavelength. The identified permittivity is shown in Figure 8.14b. Here we notice that the fine structure of the permittivity has disappeared. However, part of the clustering structure is identified.

As a second example we consider a dielectric scatterer in the shape of a half cylinder, see Figure 8.15. The scatterer has a permittivity $\epsilon_{\mathrm{i}} = 2$ and the background is free space $\epsilon_{\mathrm{b}} = 1$. A set of boundary fields $E^{(\mathrm{m})}(x, t; m)$ and $H^{(\mathrm{m})}(x, t; m)$, $x \in \partial\Omega$, $t \in [0, T]$, and $m = 1, \ldots, 8$ are known at the boundary for eight different excitations. The given fields are determined with the leapfrog scheme on a 512×512 grid and interpolated to a 32×32 grid. The latter corresponds to the 'rule of thumb'

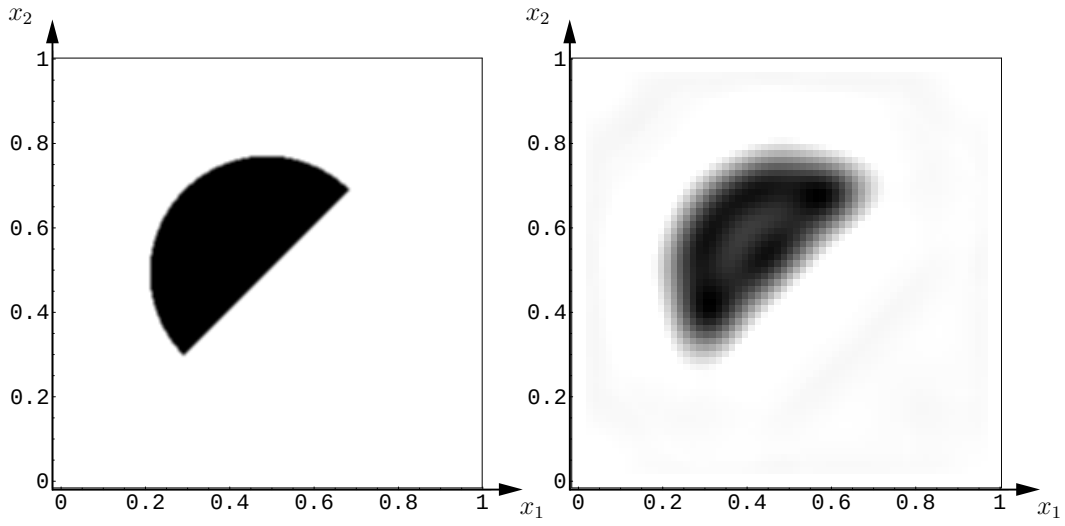

Figure 8.15: Resolution/homogenization of a half cylindrical permittivity.

10−15 samples per wavelength. We use the least-squares algorithm to get an effective representation of the scatterer on the 32×32 grid, see Figure 8.15.

8.12 Bi-anisotropic models

It is straightforward to generalize the gradient derivation from the isotropic models to the bi-anisotropic models. Here we consider the class of constitutive relations that can be modeled by a local operator, see Section 2.7. We use the six-vector notation (2.6) of the Maxwell equations. The dispersive effects are given by n (polarization) states, *i.e.*, $\boldsymbol{p} = \boldsymbol{p}(\boldsymbol{x}, t)$ is an $n \times 1$ matrix.

The electromagnetic field intensity and state vector satisfy the equation

$$\begin{cases} \partial_t \boldsymbol{\varepsilon}_\infty(\boldsymbol{x})\boldsymbol{e} - \nabla \times \mathrm{J}\boldsymbol{e} + \boldsymbol{\alpha}(\boldsymbol{x})\dot{\boldsymbol{p}} = \boldsymbol{0} & \text{in } \Omega \times [0,T] \\ \boldsymbol{\gamma}(\boldsymbol{x})\partial_t^2 \boldsymbol{p} + \boldsymbol{\nu}(\boldsymbol{x})\partial_t \boldsymbol{p} + \boldsymbol{\omega}(\boldsymbol{x})\boldsymbol{p} = \boldsymbol{\beta}(\boldsymbol{x})\boldsymbol{e} & \text{in } \Omega \times [0,T] \\ E_+(\boldsymbol{x},t) = E_+^{(\mathrm{m})}(\boldsymbol{x},t) & \text{at } \partial\Omega \times [0,T] \\ \boldsymbol{e}(\boldsymbol{x},0) = \boldsymbol{0}, \quad \boldsymbol{p}(\boldsymbol{x},0) = \boldsymbol{\gamma}\dot{\boldsymbol{p}}(\boldsymbol{x},0) = \boldsymbol{0} & \text{in } \Omega \end{cases} \tag{8.57}$$

where the instantaneous response $\boldsymbol{\varepsilon}_\infty = \boldsymbol{\varepsilon}_\infty(\boldsymbol{x})$ is a symmetric and positive definite 6×6 matrix, $\boldsymbol{\alpha} = \boldsymbol{\alpha}(\boldsymbol{x})$ is a $6 \times n$ matrix, $\boldsymbol{\beta} = \boldsymbol{\beta}(\boldsymbol{x})$ a $n \times 6$ matrix, and $\boldsymbol{\gamma} = \boldsymbol{\gamma}(\boldsymbol{x}), \boldsymbol{\nu} = \boldsymbol{\nu}(\boldsymbol{x})$, and $\boldsymbol{\omega} = \boldsymbol{\omega}(\boldsymbol{x})$ are $n \times n$ matrices. The matrix $\boldsymbol{\varepsilon}_\infty$ models the instantaneous response and $\boldsymbol{\alpha}$, $\boldsymbol{\gamma}$, $\boldsymbol{\nu}$ and $\boldsymbol{\omega}$ models the slower dispersive effects of the medium. At the boundary the split fields $E_\pm$ are used.

As in the isotropic case, we find the gradient of the objective functional (8.3) with respect to the parameters $\boldsymbol{\varepsilon}_\infty, \boldsymbol{\alpha}, \boldsymbol{\gamma}, \boldsymbol{\nu}$ and $\boldsymbol{\omega}$ by calculating the increment of the functional to the first order, *i.e.*,

$$\mathcal{J}'[\boldsymbol{\varepsilon}] = \lim_{\delta \to 0} \frac{\mathcal{J}[\boldsymbol{\varepsilon} + \delta\boldsymbol{\varepsilon}'] - \mathcal{J}[\boldsymbol{\varepsilon}]}{\delta} = 4 \sum_{m=1}^{M} \int_0^T \int_{\partial\Omega} \Phi E'_- \cdot (E_- - E_-^{(\mathrm{m})}) \, \mathrm{dS} \, \mathrm{d}t$$

where $\boldsymbol{\varepsilon} + \delta\boldsymbol{\varepsilon}'$ is a short-hand notation for the perturbations

$$\begin{aligned} &\boldsymbol{\varepsilon}_\infty \to \boldsymbol{\varepsilon}_\infty + \delta\boldsymbol{\varepsilon}'_\infty, \quad \boldsymbol{\alpha} \to \boldsymbol{\alpha} + \delta\boldsymbol{\alpha}', \quad \boldsymbol{\gamma} \to \boldsymbol{\gamma} + \delta\boldsymbol{\gamma}', \\ &\boldsymbol{\nu} \to \boldsymbol{\nu} + \delta\boldsymbol{\nu}', \quad \boldsymbol{\omega} \to \boldsymbol{\omega} + \delta\boldsymbol{\omega}', \quad \boldsymbol{\beta} \to \boldsymbol{\beta} + \delta\boldsymbol{\beta}' \end{aligned} \tag{8.58}$$

and

$$\boldsymbol{e} + \delta\boldsymbol{e}' + \mathrm{O}(\delta^2), \quad \boldsymbol{p} + \delta\boldsymbol{p}' + \mathrm{O}(\delta^2) \quad \text{as} \quad \delta \to 0$$

are the solutions to (8.57) with the perturbed parameters (8.58). The increments in the perturbed fields $\boldsymbol{e}'$ and $\boldsymbol{p}'$ satisfy the equation

$$\begin{cases} \partial_t \boldsymbol{\varepsilon}_\infty \boldsymbol{e}' - \nabla \times \mathrm{J}\boldsymbol{e}' + \boldsymbol{\alpha}\partial_t \boldsymbol{p}' = -\boldsymbol{\varepsilon}'_\infty \dot{\boldsymbol{e}} - \boldsymbol{\alpha}'\dot{\boldsymbol{p}} & \text{in } \Omega \times [0,T] \\ \boldsymbol{\gamma}\partial_t^2 \boldsymbol{p}' + \boldsymbol{\nu}\partial_t \boldsymbol{p}' + \boldsymbol{\omega}\boldsymbol{p}' - \boldsymbol{\beta}\boldsymbol{e}' = -\boldsymbol{\gamma}'\ddot{\boldsymbol{p}} - \boldsymbol{\nu}'\dot{\boldsymbol{p}} - \boldsymbol{\omega}'\boldsymbol{p} + \boldsymbol{\beta}'\boldsymbol{e} & \text{in } \Omega \times [0,T] \\ E'_+(x,t) = \boldsymbol{0} & \text{at } \partial\Omega \times [0,T] \\ \boldsymbol{e}'(\boldsymbol{x},0) = \boldsymbol{0}, \quad \boldsymbol{p}'(\boldsymbol{x},0) = \boldsymbol{\gamma}\dot{\boldsymbol{p}}'(\boldsymbol{x},0) = \boldsymbol{0} & \text{in } \Omega \end{cases}$$

where $\dot{\boldsymbol{e}} = \partial_t \boldsymbol{e}$, $\dot{\boldsymbol{p}} = \partial_t \boldsymbol{p}$, and $\ddot{\boldsymbol{p}} = \partial_t^2 \boldsymbol{p}$ are the partial derivatives with respect to time t of the solution to (8.57). To find the gradient of the objective functional, we introduce the adjoint problem

$$\begin{cases} \partial_t \boldsymbol{\varepsilon}_\infty \tilde{\boldsymbol{e}} - \nabla \times \mathrm{J}\tilde{\boldsymbol{e}} + \boldsymbol{\beta}^{\mathrm{T}}\dot{\tilde{\boldsymbol{p}}} = \boldsymbol{0} & \text{in } \Omega \times [0,T] \\ \boldsymbol{\gamma}^{\mathrm{T}}\partial_t^2 \tilde{\boldsymbol{p}} - \boldsymbol{\nu}^{\mathrm{T}}\partial_t \tilde{\boldsymbol{p}} + \boldsymbol{\omega}^{\mathrm{T}}\tilde{\boldsymbol{p}} - \boldsymbol{\alpha}^{\mathrm{T}}\tilde{\boldsymbol{e}} = \boldsymbol{0} & \text{in } \Omega \times [0,T] \\ \widetilde{E}_-(x,t) = \Phi(E_-(x,t) - E_-^{(\mathrm{m})}(x,t)) & \text{at } \partial\Omega \times [0,T] \\ \tilde{\boldsymbol{e}}(\boldsymbol{x},T) = \boldsymbol{0}, \quad \tilde{\boldsymbol{p}}(\boldsymbol{x},T) = \boldsymbol{\gamma}^{\mathrm{T}}\dot{\tilde{\boldsymbol{p}}}(\boldsymbol{x},T) = \boldsymbol{0} & \text{in } \Omega. \end{cases}$$

The adjoint equation is essentially the original equation (8.57) solved backwards in time with an input field depending on the difference between the calculated output and the measured output fields. Multiply the fields of the perturbed equation with the fields of the adjoint problem and and vice versa and add the contributions. We get the product

$$\begin{aligned} \partial_t \left[\tilde{\boldsymbol{e}}^{\mathrm{T}}\boldsymbol{\varepsilon}_\infty \boldsymbol{e}' + \dot{\tilde{\boldsymbol{p}}}^{\mathrm{T}}\boldsymbol{\gamma}\dot{\boldsymbol{p}}' + \tilde{\boldsymbol{p}}^{\mathrm{T}}\boldsymbol{\omega}\boldsymbol{p}'\right] + \nabla \cdot (\widetilde{\boldsymbol{E}} \times \boldsymbol{H}' + \boldsymbol{E}' \times \widetilde{\boldsymbol{H}}) \\ = -\tilde{\boldsymbol{e}}^{\mathrm{T}}\boldsymbol{\varepsilon}'_\infty \dot{\boldsymbol{e}} - \tilde{\boldsymbol{e}}^{\mathrm{T}}\boldsymbol{\alpha}'\dot{\boldsymbol{p}} - \dot{\tilde{\boldsymbol{p}}}^{\mathrm{T}}\boldsymbol{\gamma}'\ddot{\boldsymbol{p}} - \dot{\tilde{\boldsymbol{p}}}^{\mathrm{T}}\boldsymbol{\nu}'\dot{\boldsymbol{p}} - \dot{\tilde{\boldsymbol{p}}}^{\mathrm{T}}\boldsymbol{\omega}'\boldsymbol{p} + \dot{\tilde{\boldsymbol{p}}}^{\mathrm{T}}\boldsymbol{\beta}'\boldsymbol{e}. \end{aligned}$$

Integrate this equation over time $[0,T]$ and space Ω. The first term vanishes according to the initial values of the perturbed and adjoint problems, and the second term gives an integral over the boundary

$$\begin{aligned} &\int_0^T \int_{\partial\Omega} (\widetilde{\boldsymbol{E}} \times \boldsymbol{H}' + \boldsymbol{E}' \times \widetilde{\boldsymbol{H}}) \cdot \boldsymbol{n} \,\mathrm{dS}\,\mathrm{d}t \\ &\quad = \int_0^T \int_\Omega -\tilde{\boldsymbol{e}}^{\mathrm{T}}\boldsymbol{\varepsilon}'_\infty \dot{\boldsymbol{e}} - \tilde{\boldsymbol{e}}^{\mathrm{T}}\boldsymbol{\alpha}'\dot{\boldsymbol{p}} - \dot{\tilde{\boldsymbol{p}}}^{\mathrm{T}}\boldsymbol{\gamma}'\ddot{\boldsymbol{p}} - \dot{\tilde{\boldsymbol{p}}}^{\mathrm{T}}\boldsymbol{\nu}'\dot{\boldsymbol{p}} - \dot{\tilde{\boldsymbol{p}}}^{\mathrm{T}}\boldsymbol{\omega}'\boldsymbol{p} + \dot{\tilde{\boldsymbol{p}}}^{\mathrm{T}}\boldsymbol{\beta}'\boldsymbol{e} \,\mathrm{dV}\,\mathrm{d}t. \end{aligned} \tag{8.59}$$

The perturbation of the objective functional is

$$\begin{aligned}\mathcal{J}'[\boldsymbol{\varepsilon}] &= 4\sum_{m=1}^{M}\int_0^T\int_{\partial\Omega}\Phi E'_-\cdot(E_- - E_-^{(\mathrm{m})})\,\mathrm{dS}\,\mathrm{d}t\\ &= 2\int_0^T\int_\Omega -\tilde{\boldsymbol{e}}^{\mathrm{T}}\boldsymbol{\varepsilon}'_\infty\dot{\boldsymbol{e}} - \tilde{\boldsymbol{e}}^{\mathrm{T}}\boldsymbol{\alpha}'\dot{\boldsymbol{p}} - \dot{\tilde{\boldsymbol{p}}}^{\mathrm{T}}\boldsymbol{\gamma}'\ddot{\boldsymbol{p}} - \dot{\tilde{\boldsymbol{p}}}^{\mathrm{T}}\boldsymbol{\nu}'\dot{\boldsymbol{p}} - \dot{\tilde{\boldsymbol{p}}}^{\mathrm{T}}\boldsymbol{\omega}'\boldsymbol{p} + \dot{\tilde{\boldsymbol{p}}}^{\mathrm{T}}\boldsymbol{\beta}'\boldsymbol{e}\,\mathrm{dV}\,\mathrm{d}t\\ &= \langle\mathbf{G}_{\epsilon_\infty},\boldsymbol{\varepsilon}'_\infty\rangle + \langle\mathbf{G}_\alpha,\boldsymbol{\alpha}'\rangle + \langle\mathbf{G}_\gamma,\boldsymbol{\gamma}'\rangle + \langle\mathbf{G}_\nu,\boldsymbol{\nu}'\rangle + \langle\mathbf{G}_\omega,\boldsymbol{\omega}'\rangle + \langle\mathbf{G}_\beta,\boldsymbol{\beta}'\rangle\end{aligned}$$

where matrix-valued gradients are identified as

$$\begin{cases}\mathbf{G}_{\epsilon_\infty} = -\sum_{m=1}^{M}\int_0^T \tilde{\boldsymbol{e}}\dot{\boldsymbol{e}}^{\mathrm{T}} + \dot{\boldsymbol{e}}\tilde{\boldsymbol{e}}^{\mathrm{T}}\,\mathrm{d}t, \quad \mathbf{G}_\alpha = -2\sum_{m=1}^{M}\int_0^T \tilde{\boldsymbol{e}}\dot{\boldsymbol{p}}^{\mathrm{T}}\,\mathrm{d}t,\\ \mathbf{G}_\gamma = -2\sum_{m=1}^{M}\int_0^T \dot{\tilde{\boldsymbol{p}}}\ddot{\boldsymbol{p}}^{\mathrm{T}}\,\mathrm{d}t, \quad \mathbf{G}_\nu = -2\sum_{m=1}^{M}\int_0^T \dot{\tilde{\boldsymbol{p}}}\dot{\boldsymbol{p}}^{\mathrm{T}}\,\mathrm{d}t,\\ \mathbf{G}_\omega = -2\sum_{m=1}^{M}\int_0^T \dot{\tilde{\boldsymbol{p}}}\boldsymbol{p}^{\mathrm{T}}\,\mathrm{d}t, \quad \text{and} \quad \mathbf{G}_\beta = 2\sum_{m=1}^{M}\int_0^T \dot{\tilde{\boldsymbol{p}}}\boldsymbol{e}^{\mathrm{T}}\,\mathrm{d}t.\end{cases}$$

The elements of the matrix-valued gradients are, *e.g.*, given by

$$(\mathbf{G}_\alpha)_{i,j}(\boldsymbol{x}) = 2\sum_{m=1}^{M}\int_0^T \tilde{\boldsymbol{e}}_i(\boldsymbol{x},t;m)\dot{\boldsymbol{p}}_j(\boldsymbol{x},t;m)\,\mathrm{d}t$$

for $i = 1, 2, \ldots, 6$ and $j = 1, 2, \ldots, n$. The inner product is defined as

$$\langle\mathbf{G}_\alpha,\boldsymbol{\alpha}'\rangle = \sum_{i=1}^{6}\sum_{j=1}^{n}\int_\Omega (\mathbf{G}_{\boldsymbol{\alpha}})_{i,j}\,\boldsymbol{\alpha}'_{i,j}. \tag{8.60}$$

Observe that the symmetry requirement (2.13) is enforced on the instantaneous response.

Chapter 9

Time-reversal mirrors and time-reversal cavities

Time-reversal mirrors and time-reversal cavities are used to convert an acoustic wave field issued from a source into a wave field focusing at the source positions. The areas of application include medical imaging, lithotripsy and non-destructive testing. In Section 9.1, we discuss the time-reversal cavity and in Section 9.2, we consider the time-reversal mirror. Time-reversal mirrors and time-reversal cavities have been extensively studied by M. Fink *et al.*, see *e.g.*, Refs [**?**, **?**]. The results reported in this chapter is part of a joint project together with M. V. de Hoop and J. L. Rousseau.

9.1 Time-reversal cavities

The time-reversal cavity unfolds a wave field in a region from measurements of the field at the boundary of the region. We consider the time-reversal cavity for the acoustic wave equation, *i.e.*, a linear combination of the pressure and particle velocity is recorded, for a long period of time, at a surface surrounding the sources, see Figure 9.1. From these recorded fields, we try to recreate the original pressure field $p(\boldsymbol{x}, t)$ and velocity field $\boldsymbol{v}(\boldsymbol{x}, t)$ in Ω and hence refocus the wave field at the source positions. To accomplish this, the recorded field is time reversed and used to remit the acoustic wave field into the volume.

We assume that the region is source free for positive times and that the support of the fields is contained in Ω at $t = 0$. Furthermore, the original fields are assumed to be non-static. Let $b(\boldsymbol{x}, t)$ be the recorded linear combination of the acoustic pressure and the normal component of the particle velocity for time $0 \leq t \leq T$, *i.e.*,

$$b(\boldsymbol{x}, t) = \alpha p(\boldsymbol{x}, t) + (1 - \alpha) v_n(\boldsymbol{x}, t) \quad \text{for} \quad \boldsymbol{x} \in \partial\Omega, \tag{9.1}$$

where $v_n = \boldsymbol{v} \cdot \boldsymbol{n}$, see Figure 9.3. We restrict the analysis to convex combinations of p and v_n, *i.e.*, the parameter α is restricted to $0 \leq \alpha \leq 1$.

The remitted time-reversed fields are denoted by a check ($\check{}$). The remitted

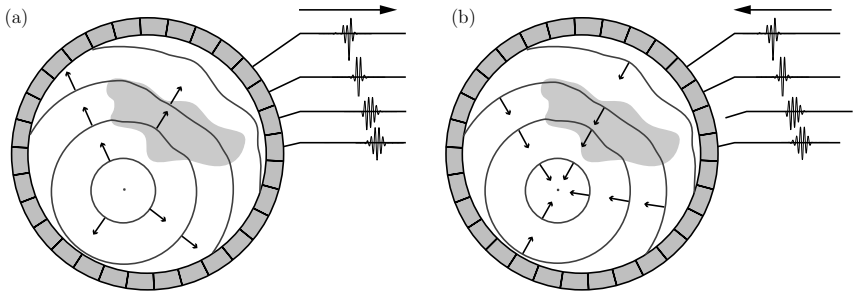

Figure 9.1: The time-reversal cavity: (a) the recording situation and (b) the remitted time-reversed fields.

pressure $\check{p}(\boldsymbol{x},t)$ and particle velocity $\check{\boldsymbol{v}}(\boldsymbol{x},t)$ satisfy the acoustic wave equation in Ω

$$\kappa\partial_t\check{p}+\nabla\cdot\check{\boldsymbol{v}}=0 \quad \text{and} \quad \rho\partial_t\check{\boldsymbol{v}}+\nabla\check{p}=\boldsymbol{0} \quad \text{in } \Omega\times[-T,\infty] \tag{9.2}$$

together with the boundary condition

$$\alpha\check{p}(\boldsymbol{x},t)-(1-\alpha)\check{v}_n(\boldsymbol{x},t)|_{\boldsymbol{x}\in\partial\Omega}=b(\boldsymbol{x},-t) \quad \text{for } t>-T. \tag{9.3}$$

Observe that the sign change of the velocity field in (9.3) redirect the energy flux to propagate into the region.

To determine the time-reversal cavity fields, we need to specify a set of initial values at $t=-T$. The value of the original field p and $\boldsymbol{v}$ are not a priori known in the region Ω. Instead we use that the fields decay for large times. This gives the initial values

$$\check{p}(\boldsymbol{x},-T)=0 \quad \text{and} \quad \check{\boldsymbol{v}}(\boldsymbol{x},-T)=\boldsymbol{0} \quad \text{in } \Omega \tag{9.4}$$

on the time-reversed fields, see Figure 9.2.

The goal with the time-reversal cavity can now be formulated: the remitted fields $\check{p}$ and $\check{\boldsymbol{v}}$ approach the original pressure and particle velocity as the time of recording increases, *i.e.*,

$$\check{p}(\boldsymbol{x},-t)\to p(\boldsymbol{x},t) \quad \text{and} \quad \check{\boldsymbol{v}}(\boldsymbol{x},-t)\to-\boldsymbol{v}(\boldsymbol{x},t) \quad \text{in} \quad \mathrm{L}^2(\Omega) \tag{9.5}$$

for $t\geq 0$ as $T\to\infty$.

Due to the zero initial conditions (9.4), we cannot expect the remitted wave fields of the time-reversal cavity (9.2) to resemble the original wave field for small times T. However, if the recording is conducted for an infinite time interval, the wave fields $p(\boldsymbol{x},t)|_{\boldsymbol{x}\in\Omega}$ and $\boldsymbol{v}(\boldsymbol{x},t)|_{\boldsymbol{x}\in\Omega}$ decay and the resemblance is perfect. To see this, we let p_Ω and $\boldsymbol{v}_\Omega$ be the time-reversed restriction of p and $\boldsymbol{v}$ to the region Ω, *i.e.*,

$$p_\Omega(\boldsymbol{x},t)=p(\boldsymbol{x},-t)|_{\boldsymbol{x}\in\Omega} \quad \text{and} \quad \boldsymbol{v}_\Omega(\boldsymbol{x},t)=-\boldsymbol{v}(\boldsymbol{x},-t)|_{\boldsymbol{x}\in\Omega} \quad \text{for} \quad t\geq -T.$$

Uniqueness of the solution to the acoustic wave equation show that p_Ω and $\boldsymbol{v}_\Omega$ satisfy the acoustic wave equation in Ω with boundary condition (9.3) and initial values

$$p_\Omega(\boldsymbol{x},-T)=p(\boldsymbol{x},T) \quad \text{and} \quad \boldsymbol{v}_\Omega(\boldsymbol{x},-T)=-\boldsymbol{v}(x,T).$$

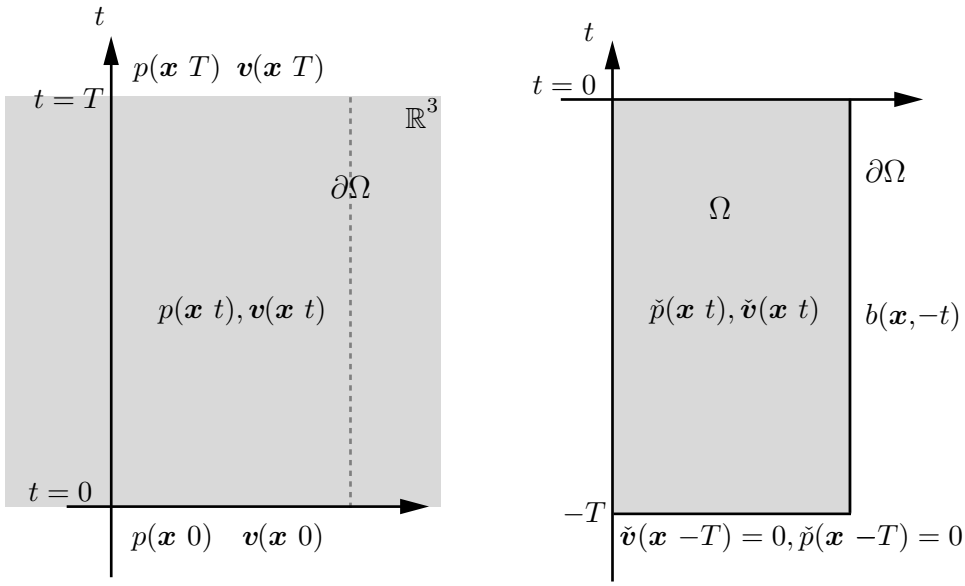

Figure 9.2: Initial-boundary value problems for the time-reversal cavity.

The remitted fields equal the original time-reversed fields minus an error term due to the vanishing initial values, *i.e.*,

$$\check{p}(\boldsymbol{x},t) = p_\Omega(\boldsymbol{x},t) - \tilde{p}(\boldsymbol{x},t) \quad \text{and} \quad \check{\boldsymbol{v}}(\boldsymbol{x},t) = \boldsymbol{v}_\Omega(\boldsymbol{x},t) - \tilde{\boldsymbol{v}}(\boldsymbol{x},t).$$

The error terms $\tilde{p}$ and $\tilde{\boldsymbol{v}}$ satisfy the acoustic equation (3.1) with the boundary condition

$$\alpha\tilde{p}(\boldsymbol{x},t) - (1-\alpha)\tilde{v}(\boldsymbol{x},t)|_{\boldsymbol{x}\in\partial\Omega} = 0 \quad \text{for } t > -T$$

and the original pressure and particle velocity field in Ω as initial conditions, *i.e.*,

$$\tilde{p}(\boldsymbol{x},-T) = p_\Omega(\boldsymbol{x},-T) \quad \text{and} \quad \tilde{\boldsymbol{v}}(\boldsymbol{x},-T) = -\boldsymbol{v}_\Omega(\boldsymbol{x},-T) \quad \text{for} \quad \boldsymbol{x}\in\Omega.$$

An energy estimate shows that the energy of the error field is bounded by the energy of the original field, *i.e.*,

$$\frac{1}{2}\int_\Omega \kappa|\tilde{p}(\boldsymbol{x},t)|^2 + \rho|\tilde{\boldsymbol{v}}(\boldsymbol{x},t)|^2\,\mathrm{dV} \le \frac{1}{2}\int_\Omega \kappa|p(\boldsymbol{x},T)|^2 + \rho|\boldsymbol{v}(\boldsymbol{x},T)|^2\,\mathrm{dV}\,.$$

Observe that the convex condition $0 \le \alpha \le 1$ is used in the energy estimate, see Chapter 5. For the cases $\alpha = 0$ or $\alpha = 1$ the energy in the volume is conserved. To get a perfect time-reversal cavity it is sufficient (and necessary for $\alpha = 0$ or $\alpha = 1$) that the restrictions of the fields p and $\boldsymbol{v}$ to the region Ω approach zero as time evolves. This follows from the decay of the local energy for the acoustic wave

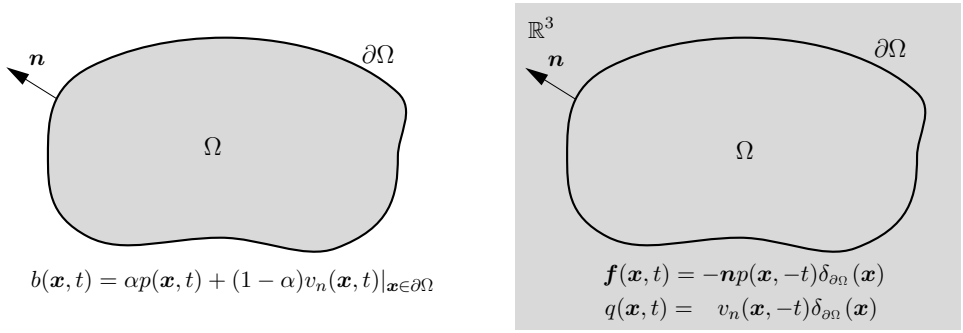

Figure 9.3: Boundary formulation and source formulation of the time-reversal cavity.

equation, see Refs [257, 11, 189, 190] and Section 5.4. Observe that the assumption of an irrotational particle velocity is necessary for the energy decay.

The Duhamel principle can be used to transform the boundary condition in the time-reversal cavity into sources, see Figure 9.3. The equivalent sources of the time-reversal cavity are

$$q(\boldsymbol{x},t) = v_n(\boldsymbol{x},-t)\delta_{\partial\Omega}(\boldsymbol{x}) \quad \text{and} \quad \boldsymbol{f}(\boldsymbol{x},t) = -\boldsymbol{n}(\boldsymbol{x})p(\boldsymbol{x},-t)\delta_{\partial\Omega}(\boldsymbol{x}) \tag{9.6}$$

in $\mathbb{R}^3 \times [-\infty, 0]$.

It is straight forward to generalize the time-reversal cavity to the Maxwell equations in a lossless medium.

9.2 Time-reversal mirrors and evanescent wave constituents

In this section, we consider the time-reversal mirror, *i.e.*, the recording of the fields is restricted to a single plane, see Figure 9.4. Due to the reduced amount of information, one only expects to retrieve the original wave field between the source and the plane of recording. Furthermore, it is difficult to handle reflections. To illustrate this, we consider the slab geometry depicted in Figure 9.5. A wave is generated by a source at $x_3 = X_3$. The up-going part of the wave field impinges on the slab. The reflection induces a down-going wave. We record the wave field at $x_3 = 0$ and $x_3 = X_3' > X_3$, time reverse the wave field, and remit the wave field into the volume with the equivalent sources (9.6). By the time-reversal cavity (9.5), the original wave field is retrieved as the time of recording increases. Use the linearity to analyze the time-reversal mirror with $x_3 = 0$ as the plane of recording. In this case, a single up-going wave is recorded and remitted into the half space $x_3 > 0$ as a down-going wave field. The down-going wave reflects at the layer interface. One observes that the time-reversal mirror does not account for the reflected field. Furthermore, the energy of the down-going wave field is reduced due to the reflection. In the time-reversal cavity, the remitted field from the recording at $x_3 = X_3$ compensates for the reflections, see Figure 9.5.

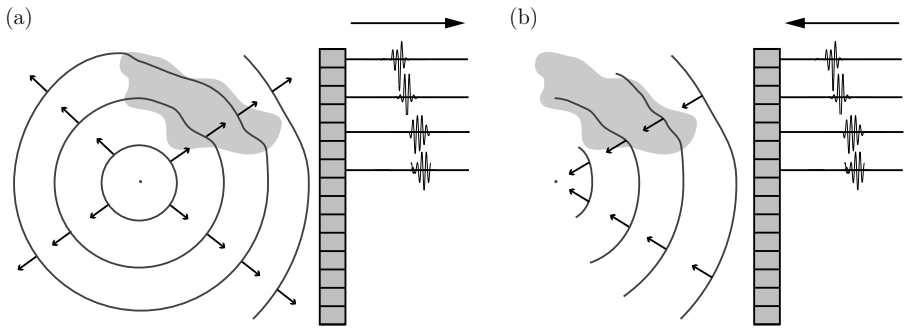

Figure 9.4: The time-reversal mirror: (a) the recording situation, (b) the remitted time-reversed fields.

To surmount the problems associated with reflections, we introduce a one-way time-reversal mirror. The acoustic wave equation is approximated by two separate equations propagating the wave field in the positive and negative directions, respectively. We start with a temporal Fourier transformation of the wave field. The wave field is decomposed with respect to the depth direction. The down- and up-going components $\hat{u}_+$ and $\hat{u}_-$ of the wave field are defined as

$$\begin{pmatrix} \hat{u}_+ \\ \hat{u}_- \end{pmatrix} = \frac{1}{2} \begin{pmatrix} 1 & \mathrm{i}\omega\rho\Gamma^{-1} \\ 1 & -\mathrm{i}\omega\rho\Gamma^{-1} \end{pmatrix} \begin{pmatrix} \hat{p} \\ \hat{v}_3 \end{pmatrix},$$

where the vertical-propagation operator Γ is defined as an approximation of the square-root operator, *i.e.*,

$$\Gamma \approx \lim_{\eta \searrow 0+} [-\mathrm{D}^2 + (\eta + \mathrm{i}\omega)^2 \rho_0 \kappa(\boldsymbol{x})]^{1/2}, \tag{9.7}$$

see Section 4.4. We formulate the time-reversal mirror in the language of one-way Green functions. The one-way Green functions are defined by the equations

$$(\partial_3 \pm \Gamma)\widehat{\mathcal{G}}^{(\pm)}(x, x_3, \mathrm{i}\omega; x', x_3') = 0 \quad \text{for} \quad x_3 \gtrless x_3' \tag{9.8}$$

together with the conditions

$$\widehat{\mathcal{G}}^{(\pm)}(x, x_3', \mathrm{i}\omega; x', x_3') = \delta(x - x') \quad \text{and} \quad \widehat{\mathcal{G}}^{(\pm)}(x, x_3, \mathrm{i}\omega; x', x_3') = 0 \quad \text{for} \quad x_3' \gtrless x_3. \tag{9.9}$$

For the time-reversal mirror, we assume an up-going wave field $\hat{u}_-(x, X_3, \mathrm{i}\omega)$ at the plane $x_3 = X_3$. Use the Green function (9.8) to propagate the field in the negative x_3-direction. At the surface $x_3 = 0$ the field

$$\hat{u}_-(x, 0, \mathrm{i}\omega) = \int_{\mathbb{R}^2} \widehat{\mathcal{G}}^{(-)}(x, 0, \mathrm{i}\omega; x', X_3) \hat{u}_-(x', X_3, \mathrm{i}\omega)\, \mathrm{d}x'$$

is recorded. We proceed by using the Duhamel principle to get an equivalent source distribution. Time reversal of a field corresponds to a complex conjugate, denoted

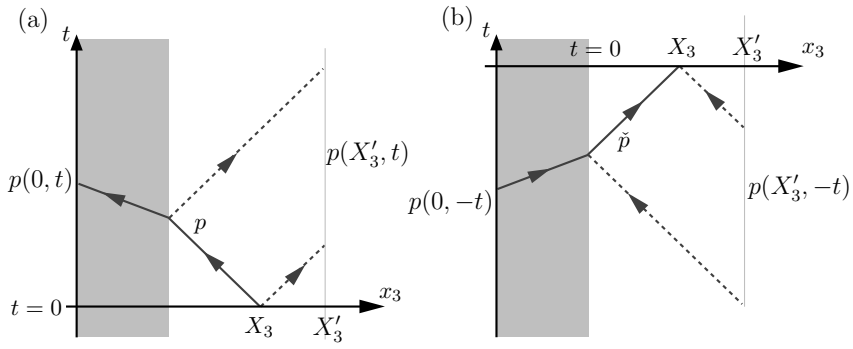

Figure 9.5: Time-reversal mirror for a layered media: (a) the recording situation and (b) the remitted time-reversed fields. The solid lines and the dashed lines correspond to the time-reversal mirror at $x_3 = 0$ and $x_3 = X_3'$, respectively. Observe that down (up) is in the positive (negative) x_3-direction.

by an asterix $(*)$, in the Fourier domain. The time reversed down-going wave field at $x_3 = 0$ is

$$\hat{u}_+(x, 0, \mathrm{i}\omega) = \frac{1}{2}(1 - \Gamma^{-1}\Gamma^*)\hat{u}_-(x, 0, \mathrm{i}\omega)^*.$$

Propagate the field back to x_3 and use the inverse Fourier transform to recover the time-domain field. This gives the one-way time-reversal mirror field

$$\check{u}_+(x'', x_3, t) = \frac{1}{4\pi}\int_{\mathbb{R}} \mathrm{e}^{\mathrm{i}\omega t}\int_{\mathbb{R}^2}\int_{\mathbb{R}^2} \widehat{\mathcal{G}}^{(+)}(x'', x_3, \mathrm{i}\omega; x, 0)(1 - \Gamma^{-1}\Gamma^*)$$
$$\widehat{\mathcal{G}}^{(-)}(x, 0, \mathrm{i}\omega; x', X_3)^*\hat{u}_-(x', X_3, \mathrm{i}\omega)^*\,\mathrm{d}x'\,\mathrm{d}x\,\mathrm{d}\omega. \quad (9.10)$$

As an example, we consider the one-way time-reversal mirror for the case of a homogeneous space, *i.e.*, $\rho = \rho_0$ and $\kappa(\boldsymbol{x}) = \kappa_0$. The one-way Green functions are

$$\mathcal{G}^{(\pm)}(x, x_3, t; x', x_3') = \frac{1}{8\pi^3}\int_{\mathbb{R}}\int_{\mathbb{R}^2} \mathrm{e}^{\mathrm{i}\xi\cdot(x-x')+\mathrm{i}\omega t\pm\gamma_0(\xi,\mathrm{i}\omega)(x_3-x_3')}\,\mathrm{d}\xi\,\mathrm{d}\omega \quad \text{for} \quad x_3 \gtrless x_3'$$

and zero elsewhere. The free-space vertical-propagation symbol γ_0 is defined by

$$\gamma_0(\xi, \mathrm{i}\omega) = \lim_{\eta \searrow 0} \sqrt{(\eta + \mathrm{i}\omega)^2\rho_0\kappa_0 + \xi^2}.$$

In the frequency representation, we observe the evanescent property of the one-way wave equation, *i.e.*, the low frequency wave constituents decay exponentially. Hence, it is not possible to simply propagate the field with $\mathcal{G}^{(-)}$, time reverse the signal and propagate it back with $\mathcal{G}^{(+)}$. In the time-reversal mirror, the evanescent wave constituents vanish in the reflection, *i.e.*,

$$\check{u}_+(x, x_3, t) = \frac{1}{8\pi^3}\int_{\mathbb{R}}\int_{|\xi|<|\omega|} \mathrm{e}^{\mathrm{i}\omega t+\mathrm{i}\xi\cdot(x-y)-\gamma_0(\xi,\mathrm{i}\omega)(X_3-x_3)}\hat{u}_+(y, X_3, \mathrm{i}\omega)^*\,\mathrm{d}y\,\mathrm{d}\xi\,\mathrm{d}\omega.$$

Due to the evanescent wave constituents, the wave field of the time-reversal mirror does not reduce to the original wave field, *i.e.*, in general

$$\check{u}_+(x, x_3, t) \neq u_+(x, x_3, -t).$$

However, half of the pressure or particle velocity is retrieved for symmetric fields, *e.g.*, in the case of an impulse pressure source $q(x, x_3, t) = \delta(t)\delta(x)\delta(x_3 - X_3)$, the time-reversal mirror gives half of the original pressure field at the plane of the source.

9.2.1 Time-reversal mirrors in the paraxial approximation

To get a numerically efficient implementation, we have to approximate the vertical-propagation operator (9.7). One common approximation is the paraxial (or parabolic) approximation, see Section 4.4.5. In this approximation, the one-way paraxial Green function $\widehat{\mathcal{G}}_{\mathrm{p}}^{(\pm)}$ satisfies (9.8) and (9.9) with the paraxial approximation of the vertical propagation operator, *i.e.*,

$$\Gamma_{\mathrm{p}} = \mathrm{i}\omega c^{-1}(\boldsymbol{x}) - \frac{\mathrm{D}^{\mathrm{T}}(c(\boldsymbol{x})\,\mathrm{D}\,)}{2\mathrm{i}\omega}. \tag{9.11}$$

We consider the paraxial approximation in a region $\Omega = \Omega' \times [0, X_3]$, where $\Omega' \in \mathbb{R}^2$. It is necessary to add boundary condition on $\partial\Omega'$. Here, we use the finite speed of propagation to impose zero fields at the boundary $\partial\Omega'$, *i.e.*,

$$\widehat{\mathcal{G}}_{\mathrm{p}}^{(\pm)}(x, x_3, \mathrm{i}\omega; x', x_3') = 0 \quad \text{for} \quad x \in \partial\Omega'.$$

With this set of boundary conditions, the paraxial operator Γ_{p} is skew symmetric, $\Gamma_{\mathrm{p}}^\dagger = -\Gamma_{\mathrm{p}}$, in the L^2 inner product over Ω', *i.e.*,

$$\int_{\Omega'} u^* \Gamma_{\mathrm{p}} v \,\mathrm{d}x = -\int_{\Omega'} (\Gamma_{\mathrm{p}} u)^* v \,\mathrm{d}x. \tag{9.12}$$

Moreover, Γ_{p} changes sign as $\mathrm{i} \to -\mathrm{i}$, *i.e.*, $\Gamma_{\mathrm{p}}^* = -\Gamma_{\mathrm{p}}$. This property eliminates the evanescent wave constituents, *i.e.*, $1 - \Gamma_{\mathrm{p}}^{-1}\Gamma_{\mathrm{p}}^* = 2$. We also have the reciprocity relation

$$\begin{aligned}
&\widehat{\mathcal{G}}_{\mathrm{p}}^{(-)}(x', x_3', \mathrm{i}\omega; x'', x_3'') \\
&= \int_{\mathbb{R}} \int_{\Omega'} \delta(x - x')\delta(x_3 - x_3') \widehat{\mathcal{G}}_{\mathrm{p}}^{(-)}(x, x_3, \mathrm{i}\omega; x'', x_3'') \,\mathrm{d}x \,\mathrm{d}x_3 \\
&= \int_{\mathbb{R}} \int_{\Omega'} \Big[(\partial_{x_3} + \Gamma_{\mathrm{p}}) \widehat{\mathcal{G}}_{\mathrm{p}}^{(+)}(x, x_3, \mathrm{i}\omega; x', x_3') \Big] \widehat{\mathcal{G}}_{\mathrm{p}}^{(-)}(x, x_3, \mathrm{i}\omega; x'', x_3'') \,\mathrm{d}x \,\mathrm{d}x_3 \\
&= \int_{\Omega'} \widehat{\mathcal{G}}_{\mathrm{p}}^{(+)}(x, x_3, \mathrm{i}\omega; x', x_3') \widehat{\mathcal{G}}_{\mathrm{p}}^{(-)}(x, x_3, \mathrm{i}\omega; x'', x_3'') \Big|_{x_3=-\infty}^{\infty} \mathrm{d}x \\
&\quad + \int_{\mathbb{R}} \int_{\Omega'} \widehat{\mathcal{G}}_{\mathrm{p}}^{(+)}(x, x_3, \mathrm{i}\omega; x', x_3') (-\partial_{x_3} + \Gamma_{\mathrm{p}}) \widehat{\mathcal{G}}_{\mathrm{p}}^{(-)}(x, x_3, \mathrm{i}\omega; x'', x_3'') \,\mathrm{d}x \,\mathrm{d}x_3 \\
&= \widehat{\mathcal{G}}_{\mathrm{p}}^{(+)}(x'', x_3'', \mathrm{i}\omega; x', x_3').
\end{aligned} \tag{9.13}$$

In the time-reversal mirror (9.10), we observe that there are no evanescent wave constituents in the paraxial approximation, *i.e.*, the skew symmetry (9.12) eliminates these waves. The time-reversed field is

$$\begin{aligned}
&\check{u}_+(x,x_3,\mathrm{i}\omega)\\
&=\int_{\Omega'}\int_{\Omega'}\widehat{\mathcal{G}}_{\mathrm{p}}^{(+)}(x,x_3,\mathrm{i}\omega;x'',0)\widehat{\mathcal{G}}_{\mathrm{p}}^{(-)}(x'',0,\mathrm{i}\omega;x',X_3)^*\hat{u}_-(x',X_3,\mathrm{i}\omega)^*\,\mathrm{d}x'\,\mathrm{d}x''\\
&=\int_{\Omega'}\int_{\Omega'}\widehat{\mathcal{G}}_{\mathrm{p}}^{(-)}(x'',0,\mathrm{i}\omega;x,x_3)\widehat{\mathcal{G}}_{\mathrm{p}}^{(-)}(x'',0,\mathrm{i}\omega;x',X_3)^*\hat{u}_-(x',X_3,\mathrm{i}\omega)^*\,\mathrm{d}x'\,\mathrm{d}x''\\
&=\int_{\Omega'}\widehat{\mathcal{G}}_{\mathrm{p}}^{(-)}(x,x_3,\mathrm{i}\omega;x',X_3)^*\hat{u}_-(x',X_3,\mathrm{i}\omega)^*\,\mathrm{d}x'=\hat{u}_-(x,x_3,\mathrm{i}\omega),
\end{aligned}$$

where we used the reciprocity (9.13) and the identity

$$\begin{aligned}
&\int_{x\in\Omega'}\widehat{\mathcal{G}}_{\mathrm{p}}^{(-)}(x,x_3,\mathrm{i}\omega;x',x_3')\widehat{\mathcal{G}}_{\mathrm{p}}^{(-)}(x,x_3,\mathrm{i}\omega;x'',x_3')^*\,\mathrm{d}x-\delta(x'-x'')\\
=&\int_{z=x_3'}^{x_3}\int_{x\in\Omega'}\widehat{\mathcal{G}}_{\mathrm{p}}^{(-)}(x,z,\mathrm{i}\omega;x',x_3')^*\Gamma_{\mathrm{p}}\widehat{\mathcal{G}}_{\mathrm{p}}^{(-)}(x,z,\mathrm{i}\omega;x'',x_3')\\
&\qquad+(\Gamma_{\mathrm{p}}\widehat{\mathcal{G}}_{\mathrm{p}}^{(-)}(x,z,\mathrm{i}\omega;x',x_3'))^*\widehat{\mathcal{G}}_{\mathrm{p}}^{(-)}(x,z,\mathrm{i}\omega;x'',x_3')\,\mathrm{d}x\,\mathrm{d}z\\
=&2\int_{z=x_3'}^{x_3}\int_{x\in\Omega'}\widehat{\mathcal{G}}_{\mathrm{p}}^{(-)}(x,z,\mathrm{i}\omega;x',x_3')^*\,\mathrm{Re}\{\Gamma_{\mathrm{p}}\}\widehat{\mathcal{G}}_{\mathrm{p}}^{(-)}(x,z,\mathrm{i}\omega;x'',x_3')\,\mathrm{d}x\,\mathrm{d}z=0.
\end{aligned}$$

Hence, the one-way time-reversal mirror is exact in the paraxial approximation.

Chapter A

Notation

Most of the used notation is described and explained in this section. The general (mathematical) notation is given in Section A.1, the electromagnetic notation in Section A.2, and the acoustic notation in Section A.3.

A.1 Mathematical notation

A region in $\mathbb{R}^3$ is denoted with Ω. The region is assumed to have a sufficiently smooth boundary $\partial\Omega$ with the outward normal $\boldsymbol{n}$ ($|\boldsymbol{n}| = 1$). The volume measure in $\mathbb{R}^3$ is given by dV and the surface measure by dS. Vectors in $\mathbb{R}^3$ are denoted with boldface letters, *e.g.*, $\boldsymbol{x} = (x_1, x_2, x_3)$ is the typical coordinate (or vector) in $\mathbb{R}^3$. The temporal coordinate is usually denoted with t or τ and a temporal interval by $[0, T]$.

The symbol ∂ is used to denote the differential operator. Partial differentiation with respect to a variable is denoted with a subscript, *e.g.*,

$$\partial_{x_3} = \partial_3 = \frac{\partial}{\partial x_3}. \tag{A.1}$$

For higher order differentiation, multi-index notation is used, *e.g.*,

$$\partial_x^\alpha = \partial_{x_1}^{\alpha_1} \partial_{x_2}^{\alpha_2} \quad \text{with} \quad |\alpha| = \alpha_1 + \alpha_2, \tag{A.2}$$

see Section 4.4.4. Spatial differentiation is also denoted with the 'nabla' symbol, *i.e.*,

$$\begin{aligned} &\operatorname{grad} \phi = \nabla \phi = \begin{pmatrix} \partial_1 \phi \\ \partial_2 \phi \\ \partial_3 \phi \end{pmatrix}, \quad \operatorname{curl} \boldsymbol{E} = \nabla \times \boldsymbol{E} = \begin{pmatrix} \partial_2 E_3 - \partial_3 E_2 \\ \partial_3 E_1 - \partial_1 E_3 \\ \partial_1 E_2 - \partial_2 E_1 \end{pmatrix} \\ &\operatorname{div} \boldsymbol{E} = \nabla \cdot \boldsymbol{E} = \partial_1 E_1 + \partial_2 E_2 + \partial_3 E_3. \end{aligned} \tag{A.3}$$

The transverse differential operator D is

$$\mathrm{D}\, \phi = \begin{pmatrix} \partial_1 \phi \\ \partial_2 \phi \end{pmatrix}, \quad \mathrm{D} \cdot E = \partial_1 E_1 + \partial_2 E_2. \tag{A.4}$$

symbol	equation	description
∂	A.1	Partial differential operator
∇	A.3	Nabla operator
D	A.4	Transverse differential operator
Ω		Spatial region in $\mathbb{R}^3$ or $\mathbb{R}^2$
$\partial\Omega$		Boundary of Ω
$\boldsymbol{n}$		Unit vector, typically the outward normal vector of Ω
$\boldsymbol{i}$	4.1	Unit vector, typically the preferred direction
dV		Volume measure
dS		Surface measure
$\boldsymbol{x}$		Spatial vector or coordinate (x_1, x_2, x_3)
x		Transverse part of a spatial vector or coordinate (x_1, x_2)
t		Temporal coordinate
s	A.9	Laplace transform parameter $s = \eta + \mathrm{i}\omega$
ω		Angular frequency
i		Imaginary unit $\mathrm{i}^2 = -1$
z^*		Complex conjugate: $z = a + \mathrm{i}b$, $a, b \in \mathbb{R} \Rightarrow z^* = a - \mathrm{i}b$
$\mathbf{A}^{\mathrm{T}}$	A.8	Transpose of the matrix $\mathbf{A}$
$\mathbf{A}^{\mathrm{H}}$	A.8	Hermitian conjugate of the matrix $\mathbf{A}$
e		exp 1
$\hat{u}(s)$	A.9	The Laplace transform of $u(t)$
L^2		The Lebesgue space of square integrable functions
$\langle u, v\rangle$	A.12	Inner product between u and v
$\|u\|$	A.11	The L^2 norm of u
$\mathrm{O}(\cdot)$	A.13	Big-Ordo
$\mathrm{o}(\cdot)$	A.14	Little-Ordo

Table A.1: General notation.

The transverse part of $\boldsymbol{x}$ with respect to the direction $\boldsymbol{n}$ is given by $x = \boldsymbol{n} \times (\boldsymbol{x} \times \boldsymbol{n})$. A field vector is decomposed into its transverse and normal components with respect to a direction $\boldsymbol{i}$, *e.g.*,

$$E_i = \boldsymbol{i} \cdot \boldsymbol{E} \quad \text{and} \quad E = \boldsymbol{i} \times (\boldsymbol{E} \times \boldsymbol{i}), \tag{A.5}$$

respectively. We have the power-flux identity

$$\boldsymbol{i} \cdot \boldsymbol{E} \times \boldsymbol{H} = E \cdot \mathrm{J}H. \tag{A.6}$$

In the wave decomposition (4.3), $\boldsymbol{i}$ denotes the vertical direction. This gives the transverse field

$$E = \begin{pmatrix} E_1 \\ E_2 \end{pmatrix}. \tag{A.7}$$

For the matrices, standard matrix algebra is used. Let $\mathbf{A}$ be a $M \times N$-matrix with elements $A_{m,n}$ for $m = 1, \ldots, M$ and $n = 1, \ldots, N$. The transpose $\mathbf{A}^{\mathrm{T}}$ and

Hermitian conjugate $\mathbf{A}^{\mathrm{H}}$ are defined as the matrices with elements

$$A_{n,m} \quad \text{and} \quad A^*_{n,m}, \tag{A.8}$$

respectively.

The temporal Laplace transform is defined by

$$\hat{u}(s) = \int_{0-}^{\infty} \mathrm{e}^{-st} u(t)\,\mathrm{d}t \tag{A.9}$$

with $\operatorname{Re} s \geq \eta_0$ for some $\eta_0 > -\infty$. The inverse Laplace transform is

$$u(t) = \frac{1}{2\pi} \int_{-\infty}^{\infty} \mathrm{e}^{(\eta+\mathrm{i}\omega)t} \hat{u}(\eta + \mathrm{i}\omega)\,\mathrm{d}\omega \quad \text{for} \quad \operatorname{Re} s = \eta \geq \eta_0. \tag{A.10}$$

The Laplace parameter s is decomposed into $s = \eta + \mathrm{i}\omega$, where ω is the angular frequency.

The Lebesgue space L^2 is given by functions such as

$$\|u\|_\Omega = \left(\int_\Omega |u(\boldsymbol{x})|^2\,\mathrm{dV} \right)^{1/2} \tag{A.11}$$

is bounded. The inner product in L^2 is

$$\langle u, v \rangle_\Omega = \int_\Omega u^*(\boldsymbol{x}) v(\boldsymbol{x})\,\mathrm{dV}\,. \tag{A.12}$$

For $\Omega = \mathbb{R}^n$, the notation $\langle u, v \rangle_n = \langle u, v \rangle_{\mathbb{R}^n}$ is used.

The big ordo $\mathrm{O}(\cdot)$ and little ordo $\mathrm{o}(\cdot)$ means, *e.g.*,

$$f(x) = \mathrm{O}(x^\alpha) \quad \text{as} \quad x \to 0 \iff f(x)/x^\alpha = B(x) \quad \text{as} \quad x \to 0, \tag{A.13}$$

where $B(x)$ is bounded in a neighborhood of $x = 0$ and

$$f(x) = \mathrm{o}(x^\alpha) \quad \text{as} \quad x \to 0 \iff f(x)/x^\alpha \to 0 \quad \text{as} \quad x \to 0. \tag{A.14}$$

A.2 Electromagnetic notation

The electromagnetic notation follows the standard by letting $\boldsymbol{E}$ and $\boldsymbol{H}$ denote the electric and magnetic field intensities, $\boldsymbol{D}$ and $\boldsymbol{B}$ the electric and magnetic flux densities, $\boldsymbol{J}$ the (electric) current, and ρ the (electric) source density. Occasionally, the magnetic current $\boldsymbol{J}^{(\mathrm{M})}$ and source density $\rho^{(\mathrm{M})}$ are used, see also Table 2.1.

The six-vectors are used instead of an index notation. The electromagnetic six-vectors are denoted with a lower case $\boldsymbol{e}$ and $\boldsymbol{d}$, respectively, *i.e.*,

$$\boldsymbol{e} = \begin{pmatrix} \boldsymbol{E} \\ \boldsymbol{H} \end{pmatrix}, \quad \text{and} \quad \boldsymbol{d} = \begin{pmatrix} \boldsymbol{D} \\ \boldsymbol{B} \end{pmatrix}. \tag{A.15}$$

symbol	equation	description
$\boldsymbol{E}$	2.1	Electric field intensity
$\boldsymbol{H}$	2.1	Magnetic field intensity
$\boldsymbol{D}$	2.1	Electric flux density
$\boldsymbol{B}$	2.1	Magnetic flux density
$\boldsymbol{J}$	2.1	Electric current density
ϱ	2.2	Electric charge density
$\nabla \times \mathrm{J}$	A.16	Maxwell's spatial differential operator
$\boldsymbol{e}$	A.15	Electromagnetic field intensity
$\boldsymbol{d}$	A.15	Electromagnetic flux densities
$E_{\pm}$		Electromagnetic split fields
$\boldsymbol{P}^{(\mathrm{D})}$	8.46	Debye polarization
$\boldsymbol{P}^{(\mathrm{L})}$	8.47	Lorentz polarization
$\boldsymbol{\varepsilon}$	2.4	The constitutive map $\boldsymbol{e} \to \boldsymbol{d}$

Table A.2: Electromagnetic notation.

The curl and divergence operators acts on the electric and magnetic fields, *i.e.*,

$$\nabla \times \mathrm{J}\boldsymbol{e} = \nabla \times \begin{pmatrix} 0 & 1 \\ -1 & 0 \end{pmatrix} \begin{pmatrix} \boldsymbol{E} \\ \boldsymbol{H} \end{pmatrix} = \nabla \times \begin{pmatrix} \boldsymbol{H} \\ -\boldsymbol{E} \end{pmatrix} = \begin{pmatrix} \nabla \times \boldsymbol{H} \\ -\nabla \times \boldsymbol{E} \end{pmatrix} \tag{A.16}$$

where

$$\mathrm{J} = \begin{pmatrix} 0 & 1 \\ -1 & 0 \end{pmatrix}. \tag{A.17}$$

The divergence is defined similarly

$$\nabla \cdot \boldsymbol{d} = \nabla \cdot \begin{pmatrix} \boldsymbol{D} \\ \boldsymbol{B} \end{pmatrix} = \begin{pmatrix} \nabla \cdot \boldsymbol{D} \\ \nabla \cdot \boldsymbol{B} \end{pmatrix}. \tag{A.18}$$

The constitutive map $\boldsymbol{\varepsilon}:\ \hat{\boldsymbol{e}} \to \hat{\boldsymbol{d}}$ is given by

$$\boldsymbol{\varepsilon} = \begin{pmatrix} \boldsymbol{\epsilon} & \boldsymbol{\xi} \\ \boldsymbol{\zeta} & \boldsymbol{\mu} \end{pmatrix} \quad \text{that is} \quad \begin{pmatrix} \widehat{\boldsymbol{D}} \\ \widehat{\boldsymbol{B}} \end{pmatrix} = \begin{pmatrix} \boldsymbol{\epsilon} & \boldsymbol{\xi} \\ \boldsymbol{\zeta} & \boldsymbol{\mu} \end{pmatrix} \begin{pmatrix} \widehat{\boldsymbol{E}} \\ \widehat{\boldsymbol{H}} \end{pmatrix}. \tag{A.19}$$

The quadratic form $\hat{\boldsymbol{e}}^{\mathrm{H}} \cdot \boldsymbol{\varepsilon}\hat{\boldsymbol{e}}$ is

$$\hat{\boldsymbol{e}}^{\mathrm{H}} \cdot \boldsymbol{\varepsilon}\hat{\boldsymbol{e}} = \left(\widehat{\boldsymbol{E}}^* \cdot \boldsymbol{\epsilon}\widehat{\boldsymbol{E}} + \widehat{\boldsymbol{E}}^* \cdot \boldsymbol{\xi}\widehat{\boldsymbol{H}} + \widehat{\boldsymbol{H}}^* \cdot \boldsymbol{\zeta}\widehat{\boldsymbol{E}} + \widehat{\boldsymbol{H}}^* \cdot \boldsymbol{\mu}\widehat{\boldsymbol{H}}\right). \tag{A.20}$$

As a final example, the first term in (2.38) is

$$\begin{aligned} &\left[\begin{pmatrix} 0 & 1 \\ -1 & 0 \end{pmatrix} \begin{pmatrix} \widehat{\boldsymbol{A}}^{(\mathrm{E})} \\ \widehat{\boldsymbol{A}} \end{pmatrix}\right]^{\mathrm{H}} \cdot \nabla \times \hat{\boldsymbol{a}} = \begin{pmatrix} \widehat{\boldsymbol{A}} \\ -\widehat{\boldsymbol{A}}^{(\mathrm{E})} \end{pmatrix}^{\mathrm{H}} \cdot \nabla \times \begin{pmatrix} \widehat{\boldsymbol{A}}^{(\mathrm{E})} \\ \widehat{\boldsymbol{A}} \end{pmatrix} \\ &= (\widetilde{\boldsymbol{A}}^* \ -(\widetilde{\boldsymbol{A}}^{(\mathrm{E})})^*) \cdot \nabla \times \begin{pmatrix} \widehat{\boldsymbol{A}}^{(\mathrm{E})} \\ \widehat{\boldsymbol{A}} \end{pmatrix} = \widetilde{\boldsymbol{A}}^* \cdot \nabla \times \widehat{\boldsymbol{A}}^{(\mathrm{E})} - (\widetilde{\boldsymbol{A}}^{(\mathrm{E})})^* \cdot \nabla \times \widehat{\boldsymbol{A}}. \end{aligned} \tag{A.21}$$

symbol	equation	description
p	3.1	Pressure field
$\boldsymbol{v}$	3.1	Particle velocity
ρ	3.1	Density
κ	3.1	Compressibility
c		Velocity $c = (\kappa\rho)^{-1/2}$

Table A.3: Acoustic notation.

In the analysis as well as in the state variable representation of the constitutive map, it is convenient to identify the fields $\hat{\boldsymbol{e}}$ and constitutive map $\boldsymbol{\varepsilon}$ with their matrix representation in a fixed coordinate system. The fields are identified with 6×1-matrices and the the constitutive map is identified with a 6×6-matrix, *i.e.*,

$$\hat{\boldsymbol{e}} = \begin{pmatrix} \widehat{E}_1 \\ \widehat{E}_2 \\ \widehat{E}_3 \\ \widehat{H}_1 \\ \widehat{H}_2 \\ \widehat{H}_3 \end{pmatrix} \quad \text{and} \quad \boldsymbol{\varepsilon} = \begin{pmatrix} \epsilon_{1,1} & \epsilon_{1,2} & \epsilon_{1,3} & \xi_{1,1} & \xi_{1,2} & \xi_{1,3} \\ \epsilon_{2,1} & \epsilon_{2,2} & \epsilon_{2,3} & \xi_{2,1} & \xi_{2,2} & \xi_{2,3} \\ \epsilon_{3,1} & \epsilon_{3,2} & \epsilon_{3,3} & \xi_{3,1} & \xi_{3,2} & \xi_{3,3} \\ \zeta_{1,1} & \zeta_{1,2} & \zeta_{1,3} & \mu_{1,1} & \mu_{1,2} & \mu_{1,3} \\ \zeta_{2,1} & \zeta_{2,2} & \zeta_{2,3} & \mu_{2,1} & \mu_{2,2} & \mu_{2,3} \\ \zeta_{3,1} & \zeta_{3,2} & \zeta_{3,3} & \mu_{3,1} & \mu_{3,2} & \mu_{3,3} \end{pmatrix} \tag{A.22}$$

respectively.

A.3 Acoustic notation

The acoustic wave-field quantities are reviewed in Table A.3, see also Table 3.1. The pressure $p(\boldsymbol{x}, t)$ and the velocity $\boldsymbol{v}(\boldsymbol{x}, t)$ are the fundamental acoustic fields. The interaction between the acoustic fields and matter is modeled by the compressibility κ and the density ρ.

Bibliography

[1] I. Åberg and A. Karlsson. The source problem—Transient waves propagating from internal sources in non-stationary media. *Wave Motion*, **26**, 43–68, 1997.

[2] I. Åberg, G. Kristensson, and D. J. N. Wall. Propagation of transient electromagnetic waves in time-varying media—direct and inverse scattering problems. *Inverse Problems*, **11**(1), 29–49, 1995.

[3] I. Åberg, G. Kristensson, and D. J. N. Wall. Transient waves in non-stationary media. *J. Math. Phys.*, **37**(5), 2229–2252, 1996.

[4] I. Åberg. *Transient Waves in Nonstationary Media.* PhD thesis, Lund Institute of Technology, Department of Electromagnetic Theory, P.O. Box 118, S-211 00 Lund, Sweden, 1996.

[5] M. S. Agranovich. *Elliptic Operators on Closed Manifolds*, volume VI of *Partial Differential Equations.* Springer-Verlag, Berlin, 1991.

[6] N. I. Akhiezer. *The classical moment problem.* Oliver and Boyd, 1965.

[7] R. A. Albanese, R. L. Medina, and J. W. Penn. Mathematics, medicine and microwaves. *Inverse Problems*, **10**, 995–1007, 1994.

[8] E. Ammicht, J. P. Corones, and R. J. Krueger. Direct and inverse scattering for viscoelastic media. *J. Acoust. Soc. Am.*, **81**, 827–834, 1987.

[9] W. A. Atherton. *From Compass to Computer.* Macmillan, New York, 1984.

[10] F. V. Atkinson. Wave propagation and the Bremmer series. *J. Math. Anal. Appl.*, **1**, 255–276, 1960.

[11] G. S. S. Ávila and D. G. Costa. Asymptotic properties of general symmetric hyperbolic systems. *Journal of Functional Physics*, **35**, 49–63, 1980.

[12] C. A. Balanis. *Advanced Engineering Electromagnetics.* John Wiley & Sons, New York, 1989.

[13] R. S. Beezley and R. J. Krueger. An electromagnetic inverse problem for dispersive media. *J. Math. Phys.*, **26**(2), 317–325, 1985.

[14] R. Bellman and G. N. Wing. *An Introduction to Invariant Imbedding*. John Wiley & Sons, New York, 1975.

[15] C. L. Bennett. Time domain inverse scattering. *IEEE Trans. Antennas Propagat.*, **29**(2), 213–219, March 1981.

[16] P. Bernekorn, A. Karlsson, and G. Kristensson. Propagation of transient electromagnetic waves in inhomogeneous and dispersive waveguides. *J. Electro. Waves Applic.*, **10**(9), 1263–1286, 1996.

[17] M. Bertero and P. Boccacci. *Introduction to Inverse Problems in Imaging*. Institute of Physics Publishing, Bristol, 1998.

[18] M. Bertero and E. R. Pike, editors. *Inverse Problems in Scattering and Imaging*, Bristol, 1991. Adam Hilger Ltd.

[19] A. K. Bhattacharyya. *High-Frequency Electromagnetic Techniques: Recent Advances and Applications*. John Wiley & Sons, New York, 1995.

[20] D. Billger. *Scattering on the Timoshenko beam–direct and inverse problems in the time domain*. PhD thesis, Chalmers University of Technology, 1998.

[21] D. Billger and P. Folkow. The imbedding equations for the Timoshenko beam. *Journal of Sound and Vibration*, **209**(4), 609–634, 1998.

[22] N. Bleistein, J. K. Cohen, and J. W. Stockwell. Mathematics of multidimensional seismic inversion. Lecture notes, May 1998.

[23] H. Blok and M. Oristaglio. Wavefield imaging and inversion in electromagnetics and acoustics. Technical report, Centre for Technical Geoscience, Delft University of Technology, 1995.

[24] C. O. Bloom. Energy decays locally even if total energy grows algebraically with time. *Journal of Differential Equations*, **16**, 352–372, 1974.

[25] B. Borden. *Radar Imaging of Airborne Targets. A Primer for Applied Mathematicians and Physicists*. Institute of Physics Publishing, Bristol, 1999.

[26] M. Born and E. Wolf. *Principles of Optics*. Pergamon, Oxford, 1980.

[27] A. Bossavit. On the homogenization of Maxwell equations. *COMPEL-The International Journal for Computation and Mathematics in Electrical and Electronic Engineering*, **14**(4), 23–26, 1995.

[28] H. Bremmer. The W.K.B. approximation as the first term of a geometric-optical series. *Comm. Pure Appl. Math.*, **4**, 105–115, 1951.

[29] K. Bube and R. J. Burrridge. The one-dimensional inverse problem of reflection seismology. *SIAM Review*, **25**(4), 497–559, 1983.

[30] F. X. Canning. A local description of the directional characteristics of the propagation of electromagnetic fields. *IEEE Trans. Antennas Propagat.*, **36**(8), 1088–1095, August 1988.

[31] M. Cheney. *Tesla: Man out of time*. Dell Publishing, New York, 1983.

[32] M. Cheney, D. Isaacson, and J. C. Newell. Electrical impedance tomography. *SIAM Review*, **41**(1), 85–101, 1999.

[33] M. Cheney and D. Isaacson. Issues in electrical impedance imaging. *IEEE Computational Science & Engineering*, pages 53–62, 1995.

[34] J. F. Claerbout. *Imaging the Earth's interior*. Blackwell Scientific Publications, Oxford, 1985.

[35] R. E. Collin. *Field Theory of Guided Waves*. IEEE Press, New York, second edition, 1991.

[36] M. D. Collins, R. J. Cederberg, D. B. King, and S. A. Chin-Bing. Comparison of algorithms for solving parabolic wave equations. *J. Acoust. Soc. Am.*, **100**(1), 178–182, July 1996.

[37] D. Colton, R. Ewing, and W. Rundell, editors. *Inverse Problems in Partial Differential Equations*. SIAM, Philadelphia, 1990.

[38] D. Colton and R. Kress. *Inverse Acoustic and Electromagnetic Scattering Theory*. Springer-Verlag, Berlin, 1992.

[39] J. P. Corones. Bremmer series that correct parabolic approximations. *J. Math. Anal. Appl.*, **50**, 361–372, 1975.

[40] J. P. Corones, M. E. Davison, and R. J. Krueger. Direct and inverse scattering in the time domain via invariant imbedding equations. *J. Acoust. Soc. Am.*, **74**(5), 1535–1541, 1983.

[41] J. P. Corones, M. E. Davison, and R. J. Krueger. The effects of dissipation in one-dimensional inverse problems. In A. J. Devaney, editor, *Inverse Optics, Proceedings of the SPIE*, pages 107–114, Bellingham, WA, 1983. Proc. SPIE 413, SPIE.

[42] J. P. Corones, M. E. Davison, and R. J. Krueger. Wave splittings, invariant imbedding and inverse scattering. In A. J. Devaney, editor, *Inverse Optics*, pages 102–106, Bellingham, WA, 1983. Proc. SPIE 413, SPIE.

[43] J. P. Corones, M. E. Davison, and R. J. Krueger. Dissipative inverse problems in the time domain. In W.-M. Boerner, editor, *Inverse Methods in Electromagnetic Imaging*, volume 143, pages 121–130, Reidel Dordrecht, 1985. NATO ASI series, Series C.

[44] J. P. Corones and A. Karlsson. Transient direct and inverse scattering for inhomogeneous viscoelastic media: obliquely incident SH mode. *Inverse Problems*, **4**, 643–660, 1988.

[45] J. P. Corones, G. Kristensson, P. Nelson, and D. L. Seth, editors. *Invariant Imbedding and Inverse Problems*. SIAM, Philadelphia, 1992.

[46] J. P. Corones and R. J. Krueger. Obtaining scattering kernels using invariant imbedding. *J. Math. Anal. Appl.*, **95**, 393–415, 1983.

[47] J. P. Corones, R. J. Krueger, and V. H. Weston. Some recent results in inverse scattering theory. In F. Santosa, Y. Pao, W. Symes, and C. Holland, editors, *Inverse Problems of Acoustic and Elastic Waves*, pages 65–81, SIAM Philadelphia, PA, 1985. Proc. SPIE 413.

[48] R. Courant and D. Hilbert. *Methods of Mathematical Physics*, volume 2. Interscience Publishers, New York, 1962.

[49] Y. Dai, E. J. Rothwell, K. M. Chen, and D. P. Nyquist. Time-domain imaging of radar targets using algorithms for reconstruction from projections. *IEEE Trans. Antennas Propagat.*, **45**(8), 1227–1235, August 1997.

[50] R. Dautray and J.-L. Lions. *Mathematical Analysis and Numerical Methods for Science and Technology, Volume 2: Functional and Variational Methods*. Springer-Verlag, Berlin Heidelberg, 1988.

[51] R. Dautray and J.-L. Lions. *Mathematical Analysis and Numerical Methods for Science and Technology, volume 6: Evolution Problems II*. Springer-Verlag, Berlin Heidelberg, 1993.

[52] M. V. de Hoop. Generalization of the Bremmer coupling series. *J. Math. Phys.*, **37**(7), 3246–3282, 1996.

[53] M. V. de Hoop and A. T. de Hoop. Scalar space-time waves in their spectral-domain first- and second-order Thiele approximations. *Wave Motion*, **15**, 229–265, 1992.

[54] M. V. de Hoop and A. K. Gautesen. Uniform asymptotic expansion of the generalized Bremmer series. *SIAM J. Appl. Math.*, 1999. To appear.

[55] S. R. deGroot. *The Maxwell equations*. North-Holland, Amsterdam, 1969.

[56] P. Delsarte, Y. Genin, and Y. Kamp. On the role of the Nevanlinna-Pick problem in circuit and system theory. *Circuit Theory and Applications*, **9**, 177–187, 1981.

[57] G. D. Dockery. Modeling electromagnetic wave propagation in the troposphere using the parabolic equation. *IEEE Trans. Antennas Propagat.*, **36**(10), 1464–1470, October 1988.

[58] R. P. Dougherty. *Direct and inverse scattering of classical waves at oblique incidence to stratified media via invariant imbedding equations*. PhD thesis, Iowa State University, Ames, Iowa, 1986.

[59] D. G. Dudley. Parametric identification of transient electromagnetic systems. *Wave Motion*, **5**, 369–384, 1983.

[60] I. Egorov. *Transient Electromagnetic Pulse Propagation in Temprally Dispersive Materials*. PhD thesis, Lund Institute of Technology, Department of Electromagnetic Theory, P.O. Box 118, S-211 00 Lund, Sweden, 1998.

[61] I. Egorov, A. Karlsson, and S. Rikte. Time-domain Green dyadics for temporally dispersive, simple media. *J. Phys. A: Math. Gen.*, **31**(14), 3219–3240, 1998. See [**?**] for corrections.

[62] I. Egorov and S. Rikte. Forerunners in bigyrotropic materials. *J. Opt. Soc. Am. A*, **15**(9), 2391–2403, 1998.

[63] B. Engquist and A. Majda. Absorbing boundary conditions for the numerical simulation of waves. *Mathematics of Computation*, **31**, 629–651, 1977.

[64] A. C. Eringen and G. A. Maugin. *Electrodynamics of Continua I*. Springer-Verlag, New York, 1990.

[65] A. C. Eringen and G. A. Maugin. *Electrodynamics of Continua II*. Springer-Verlag, New York, 1990.

[66] C. Eswarappa and W. J. R. Hoefer. One-way equation absorbing boundary conditions for 3-D TLM analysis of planar and quasi-planar structures. *IEEE Trans. Microwave Theory Tech.*, **42**(9), 1669–1677, September 1994.

[67] C. E. Evans. *Partial Differential Equations*, volume 3B. Center for Pure and Applied Mathematics at the Department of Mathematics, University of California, Berkeley, 1994.

[68] L. C. Evans. *Partial Differential Equations*. American Mathematical Society, Providence, Rhode Island, 1998.

[69] L. B. Felsen and N. Marcuvitz. *Radiation and scattering of waves*. IEEE Press, Piscataway, NJ, 1994. (Originally published by Prentice-Hall in 1973).

[70] E. M. Fernandez-Berdaguer. An iterative procedure for estimation of variable coefficients in a hyperbolic system. *Appl. Math. Comput.*, **76**, 213–250, 1996.

[71] E. M. Fernández-Berdaguer. Parameter estimation in acoustic media using the adjoint method. *SIAM J. Control Optim.*, **36**(4), 1315–1330, July 1998.

[72] R. P. Feynman. *Quantum Electrodynamics*. W. A. Benjamin, Inc., Reading, Massachusetts, 1961.

[73] R. P. Feynman. *QED — The Strange Theory of Light and Matter*. Princeton University Press, Princeton, New Jersey, 1985.

[74] R. P. Feynman, R. B. Leighton, and M. Sands. *The Feynman Lectures on Physics*. Addison-Wesley, Reading, MA, USA, 1965.

[75] L. Fishman. Phase space and functional integral methods in direct and inverse scattering. In P. Sabatier, editor, *Inverse Methods in Action*, page 182. Springer-Verlag, Berlin, 1990.

[76] L. Fishman. Exact and operator rational approximate solutions of the helmholtz, weyl composition equation in underwater acoustics—the quadratic profile. *J. Math. Phys.*, **33**(5), 1887–1914, 1992.

[77] L. Fishman, M. V. de Hoop, and M. J. N. van Stralen. Exact constructions of Helmholtz operator symbols. the focusing quadratic profile. 1999. Submitted to J. Math. Phys.

[78] L. Fishman, A. K. Gautesen, and Z. Sun. Uniform high-frequency approximations of the square root Helmholtz operator symbol. *Wave Motion*, **26**, 127–161, 1997.

[79] L. Fishman and J. J. McCoy. Derivation and application of extended parabolic wave theories. I. The factorized Helmholtz equation. *J. Math. Phys.*, **25**(2), 285–296, February 1984.

[80] L. Fishman and J. J. McCoy. Derivation and application of extended parabolic wave theories. II. Path integral representations. *J. Math. Phys.*, **25**(2), 297–308, February 1984.

[81] L. Fishman, J. J. McCoy, and S. C. Wales. Factorization and path integration of the Helmholtz equation: Numerical algorithms. *J. Acoust. Soc. Am.*, **81**(5), 1355–1376, May 1987.

[82] L. Fishman and S. C. Wales. Phase space methods and path integration: the analysis and computation of scalar wave equations. *J. Comp. Appl. Math.*, **20**, 219–238, 1987.

[83] P. D. Folkow, G. Kristensson, and P. Olsson. Time domain Green functions for the homogeneous Timoshenko beam. *Quart. J. Mech. Appl. Math.*, **51**(1), 125–141, 1998.

[84] G. B. Folland. *Introduction to Partial Differential Equations*. Princeton University Press, Princeton, New Jersey, 1995.

[85] A. Franchois and C. Pichot. Microwave imaging—complex permittivity reconstruction with a Levenburg-Marquardt method. *IEEE Trans. Antennas Propagat.*, **45**(2), 203–215, February 1997.

[86] J. Fridén. Inverse scattering for anisotropic mirror image symmetric media. *Inverse Problems*, **10**(5), 1133–1144, 1994.

[87] J. Fridén. Inverse scattering for the homogeneous dispersive anisotropic slab using transient electromagnetic fields. *Wave Motion*, **23**(4), 289–306, 1996.

[88] J. Fridén, G. Kristensson, and R. D. Stewart. Transient electromagnetic wave propagation in anisotropic dispersive media. *J. Opt. Soc. Am. A*, **10**(12), 2618–2627, 1993.

[89] J. Fridén. *Bartholinian Pleasures: Time Domain Direct and Inverse Electromagnetic Scattering for Dispersive Anisotropic Media*. PhD thesis, Göteborg University and Chalmers University of Technology, Institute of Theoretical Physics, 412 96 Göteborg, Sweden, 1995.

[90] J. Fridén, G. Kristensson, and A. Sihvola. Effect of dissipation on the constitutive relations of bi-anisotropic media–the optical response. *Electromagnetics*, **17**(3), 251–267, 1997.

[91] P. Fuks, A. Karlsson, and G. Larson. Direct and inverse scattering for dispersive media. *Inverse Problems*, **10**(3), 555–571, 1994.

[92] P. Fuks, G. Kristensson, and G. Larson. Permittivity profile reconstructions using transient electromagnetic reflection data. Technical Report LUTEDX/(TEAT-7009)/1–88/(1989), Lund Institute of Technology, Department of Electromagnetic Theory, P.O. Box 118, S-211 00 Lund, Sweden, 1990.

[93] P. Fuks, G. Kristensson, and G. Larson. Permittivity profile reconstructions using transient electromagnetic reflection data. *J. Electro. Waves Applic.*, **11**(2), 245–248, 1998.

[94] L. Garnero, A. Franchois, J.-P. Hugonin, C. Pichot, and N. Joachimovicz. Microwave imaging—complex permittivity reconstruction by simulated annealing. *IEEE Trans. Microwave Theory Tech.*, **39**(11), 1801–1807, November 1991.

[95] J. B. Garnett. *Bounded Analytic Functions*. Academic Press, New York, 1981.

[96] O. Gauthier, J. Virieux, and A. Tarantola. Two-dimensional nonlinear inversion of seismic waveforms: Numerical results. *Geophysics*, **51**(7), 1387–1403, July 1986.

[97] P. E. Gill, W. Murray, and M. H. Wright. *Practical Optimization*. Academic Press, London, 1981.

[98] O. A. Godin. Reciprocity and energy conservation within the parabolic approximation. *Wave Motion*, **29**, 175–194, 1999.

[99] S. H. Gray. On the convergence of the time-domain Bremmer series. *Wave Motion*, **5**, 249–255, 1983.

[100] R. E. Greene and S. G. Krantz. *Function theory of one complex variable*. John Wiley & Sons, New York, 1997.

[101] G. Grubb. *Functional Calculus of Pseudodifferential Boundary Problems*. Birkhäuser, Boston, 1996.

[102] B. Gustafsson, H.-O. Kreiss, and J. Oliger. *Time Dependent Problems and Difference Methods*. John Wiley & Sons, New York, 1995.

[103] M. Gustafsson. Time domain theory of the macroscopic Maxwell equations. Technical Report LUTEDX/(TEAT-7062)/1–24/(1997), Lund Institute of Technology, Department of Electromagnetic Theory, P.O. Box 118, S-211 00 Lund, Sweden, 1997.

[104] M. Gustafsson. *Inverse Electromagnetic Scattering Problems — A Time-Domain Optimization Approach*. Licentiate thesis, Lund Institute of Technology, Department of Electromagnetic Theory, P.O. Box 118, S-211 00 Lund, Sweden, 1998.

[105] M. Gustafsson. The Bremmer series for a multi-dimensional acoustic scattering problem. *J. Phys. A: Math. Gen.*, **33**(9–10), 1921–1932, 2000.

[106] M. Gustafsson and S. He. A wave-splitting based optimization approach to multi-dimensional time-domain electromagnetic inverse problems. *Mathematics and Computers in Simulation*, **50**, 541–551, 1999.

[107] M. Gustafsson and S. He. An optimization approach to multi-dimensional time domain acoustic inverse problems. *J. Acoust. Soc. Am.*, 2000. (In press).

[108] M. Gustafsson and S. He. An optimization approach to two-dimensional time domain electromagnetic inverse problems. *Radio Sci.*, **35**(2), 525–536, 2000.

[109] T. M. Habashy, M. Oristaglio, and A. T. de Hoop. Simultaneous nonlinear reconstruction of two-dimensional permittivity and conductivity. *Radio Sci.*, **29**(4), 1101–1118, 1994.

[110] J. Hadamard. *Lectures on the Cauchy Problem in Linear Partial Differential Equations*. Yale University Press, New Haven, 1923.

[111] H. Harada, D. J. N. Wall, T. Takenaka, and M. Tanaka. Conjugate gradient method applied to inverse scattering problem. *IEEE Trans. Antennas Propagat.*, **43**(8), 784–792, August 1995.

[112] R. F. Harrington. *Field Computation by Moment Methods*. Macmillan, New York, 1968.

[113] S. He. A 'compact Green function' approach to the time domain direct and inverse problems for a stratified dissipative slab. *J. Math. Phys.*, **34**(10), 4628–4645, 1993.

[114] S. He, R. Hellberg, and V. H. Weston. Simultaneous reconstruction for the telegraph equation in a stratified half space using 3D reflectivity. *IEICE Trans Commun.*, **E76-B**(12), 1538–1545, 1993.

[115] S. He and S. I. Kabanikhin. An optimization approach to a three-dimensional acoustic inverse problem in the time domain. *J. Math. Phys.*, **36**(8), 4028–4043, 1995.

[116] S. He, S. Ström, and V. H. Weston. *Time Domain Wave-splittings and Inverse Problems*. Oxford University Press, Oxford, 1998.

[117] S. He and V. H. Weston. Inverse problem for the dissipative wave equation in stratified half-space and linearization of the imbedding equations. *Inverse Problems*, **8**(3), 435–455, 1992.

[118] S. He and V. H. Weston. Determination of the permittivity and conductivity in $\mathbb{R}^3$ using wave-splitting of Maxwell's equations. *J. Math. Phys.*, **36**(4), 1776–1789, 1995.

[119] S. He, P. Fuks, and G. W. Larson. An optimization approach to time-domain electromagnetic inverse problem for a stratified dispersive and dissipative slab. *IEEE Trans. Antennas Propagat.*, **44**(9), 1277–1282, 1996.

[120] R. Hellberg and A. Karlsson. Design of reflectionless media for transient electromagnetic waves. *Inverse Problems*, **11**, 147–164, 1995.

[121] R. Hellberg, A. Karlsson, and P. Thärning. Non-reflecting dispersive media. *Smart Materials and Structures*, **1**, 341–346, 1992.

[122] G. T. Herman, H. K. Tuy, K. J. Langenberg, and P. C. Sabatier. *Basic Methods of Tomography and Inverse Problems*. Adam Hilger Ltd., 1988.

[123] H. P. Hiriyannaiah. X-ray computed tomography for medical imaging. *IEEE Signal Processing Magazine*, pages 42–59, March 1997.

[124] K. I. Hopcraft and P. R. Smith. *An Introduction to Electromagnetic Inverse Scattering*. Kluwer Academic Publishers Group, Dordrecht, 1992.

[125] L. Hörmander. *The Analysis of Linear Partial Differential Operators I*. Grundlehren der mathematischen Wissenschaften 256. Springer-Verlag, Berlin Heidelberg, 1983.

[126] R. G. Hunsperger. *Integrated Optics: Theory and Technology*. Springer-Verlag, Berlin, 1995.

[127] V. Isakov. *Inverse Problems for Partial Differential Equations*. Springer-Verlag, Berlin, 1998.

[128] J. D. Jackson. *Classical Electrodynamics*. John Wiley & Sons, New York, second edition, 1975.

[129] G. L. James. *Geometrical Theory of Diffraction for Electromagnetic Waves*. Peter Peregrinus Ltd., Stevenage, UK, 3rd edition, 1986.

[130] V. V. Jikov, S. M. Kozlov, and O. A. Oleinik. *Homogenization of Differential Operators and Integral Functionals*. Springer-Verlag, Berlin, 1994.

[131] L. Jonsson and M. V. de Hoop. Wave field decomposition in anisotropic fluids. Technical Report TRITA-TET 00-4, Department of Electromagnetic Theory, S100 44 Stockholm, Sweden, 2000. Submitted to SIAM J. Appl. Math.

[132] U. Kaatze. Microwave dielectric properties of water. In A. Kraszewski, editor, *Microwave Aquametry*, chapter 2, pages 37–53. IEEE Press, New York, 1996.

[133] A. Karlsson. Inverse scattering for viscoelastic media using transmission data. *Inverse Problems*, **3**, 691–709, 1987.

[134] A. Karlsson. Direct and inverse electromagnetic scattering from a dispersive medium. Technical Report TRITA-TET 89-2, Department of Electromagnetic Theory, S-100 44 Stockholm, Sweden, 1989.

[135] A. Karlsson. Wave propagators for transient waves in one-dimensional media. *Wave Motion*, **24**(1), 85–99, 1996.

[136] A. Karlsson. Determination of transition matrices for inhomogeneous dielectric bodies by a wave propagator method. Technical Report LUTEDX/(TEAT-7076)/1–17/(1998), Lund Institute of Technology, Department of Electromagnetic Theory, P.O. Box 118, S-211 00 Lund, Sweden, 1998.

[137] A. Karlsson and K. Kreider. Transient electromagnetic wave propagation in transverse periodic media. *Wave Motion*, **23**(2), 259–277, 1996.

[138] A. Karlsson, K. Kreider, and G. Kristensson. Wave splitting and imbedding equations for a spherically symmetric dispersive medium. In J. P. Corones, G. Kristensson, P. Nelson, and D. L. Seth, editors, *Invariant Imbedding and Inverse Problems*. SIAM, 1992.

[139] A. Karlsson and G. Kristensson. Constitutive relations, dissipation and reciprocity for the Maxwell equations in the time domain. *J. Electro. Waves Applic.*, **6**(5/6), 537–551, 1992.

[140] A. Karlsson, G. Kristensson, and H. Otterheim. Transient wave propagation in gyrotropic media. In J. P. Corones, G. Kristensson, P. Nelson, and D. L. Seth, editors, *Invariant Imbedding and Inverse Problems*. SIAM, 1992.

[141] A. Karlsson and S. Rikte. The time-domain theory of forerunners. *J. Opt. Soc. Am. A*, **15**(2), 487–502, 1998.

[142] I. Kay. Some remarks concerning the Bremmer series. *J. Math. Anal. Appl.*, **3**, 40–49, 1961.

[143] H. B. Keller and J. B. Keller. Exponential-like solutions of systems of linear ordinary differential equations. *J. Soc. Indust. Appl. Math.*, **10**(2), 246–259, 1962.

[144] J. B. Keller. Geometrical theory of diffraction. *J. Opt. Soc. Am.*, **52**, 116–130, 1962.

[145] J. B. Keller. Inverse problems. *Am. Math. Mon.*, **83**, 107–118, 1976.

[146] J. B. Keller and J. S. Papadakis, editors. *Wave Propagation and Underwater Acoustics*. Springer-Verlag, Berlin, 1977.

[147] A. Kirsch. *An Introduction to the Mathematical Theory of Inverse Problems*. Springer-Verlag, New York, 1996.

[148] A. Kirsch. Characterization of the shape of a scattering obstacle using the spectral data of the far field operator. *Inverse Problems*, **14**, 1489–1512, 1998.

[149] R. E. Kleinman and P. M. van den Berg. Non-linearized approach to profile inversion. *Int. J. Imaging Systems Tech.*, **2**, 119–126, 1990.

[150] M. V. Klibanov. Carleman estimates and inverse problems. *Inverse Problems*, **8**, 575–96, 1992.

[151] M. V. Klibanov, T. R. Lucas, and R. M. Frank. A fast and accurate imaging algorithm in optical/diffusion tomography. *Inverse Problems*, **13**, 1341–1361, 1997.

[152] M. Kline. An asymptotic solution of Maxwell's equations. *Comm. Pure Appl. Math.*, **4**, 225–262, 1951.

[153] J. A. Kong. *Electromagnetic Wave Theory*. John Wiley & Sons, New York, 1986.

[154] H.-O. Kreiss and J. Lorenz. *Initial-Boundary Value Problems and the Navier-Stokes Equations*. Academic Press, San Diego, 1989.

[155] G. Kristensson. Direct and inverse scattering problems in dispersive media—Green's functions and invariant imbedding techniques. In R. Kleinman, R. Kress, and E. Martensen, editors, *Direct and Inverse Boundary Value Problems*, Methoden und Verfahren der Mathematischen Physik, Band 37, pages 105–119, Frankfurt am Main, 1991. Peter Lang.

[156] G. Kristensson. Transient electromagnetic wave propagation in waveguides. *J. Electro. Waves Applic.*, **9**(5/6), 645–671, 1995.

[157] G. Kristensson, J. K. Krueger, and R. C. Winther. Existence and construction of solutions of dissipative inverse problems. *J. Math. Anal. Appl.*, **157**(2), 542–554, 1991.

[158] G. Kristensson and R. J. Krueger. Direct and inverse scattering in the time domain for a dissipative wave equation. Part 1: Scattering operators. *J. Math. Phys.*, **27**(6), 1667–1682, 1986.

[159] G. Kristensson and R. J. Krueger. Direct and inverse scattering in the time domain for a dissipative wave equation. Part 2: Simultaneous reconstruction of dissipation and phase velocity profiles. *J. Math. Phys.*, **27**(6), 1683–1693, 1986.

[160] G. Kristensson and R. J. Krueger. Direct and inverse scattering in the time domain for a dissipative wave equation. Part 3: Scattering operators in the presence of a phase velocity mismatch. *J. Math. Phys.*, **28**(2), 360–370, 1987.

[161] G. Kristensson and R. J. Krueger. Direct and inverse scattering in the time domain for a dissipative wave equation. Part 4: Use of phase velocity mismatches to simplify inversions. *Inverse Problems*, **5**(3), 375–388, 1989.

[162] G. Kristensson and S. Rikte. The inverse scattering problem for a homogeneous bi-isotropic slab using transient data. In L. Päivärinta and E. Somersalo, editors, *Inverse Problems in Mathematical Physics*, pages 112–125. Springer-Verlag, Berlin, 1993.

[163] G. Kristensson and C. R. Vogel. Inverse problems for acoustic waves using the penalised likelihood method. *Inverse Problems*, **2**(4), 461–479, 1986.

[164] G. Kristensson. Direct and inverse scattering problems in the time domain. Lecture notes, 1993.

[165] G. Kristensson and D. J. N. Wall. Direct and inverse scattering for transient electromagnetic waves in nonlinear media. *Inverse Problems*, **14**, 113–137, 1998.

[166] R. J. Krueger and R. L. Ochs, Jr. A Green's function approach to the determination of internal fields. *Wave Motion*, **11**, 525–543, 1989.

[167] L. D. Landau, E. M. Lifshitz, and L. P. Pitaevskiĭ. *Electrodynamics of Continuous Media*. Pergamon, Oxford, second edition, 1984.

[168] K. J. Langenberg. Applied inverse problems for acoustic, electromagetic, and elastic wave scattering. In Sabatier, editor, *Basic Methods of Tomography and Inverse Problems*. Adam Hilger Ltd., Bristol, 1987.

[169] K. J. Langenberg. Introduction to the special issue on inverse problems. *Wave Motion*, **11**(2), 99–112, 1989.

[170] D. Lee and A. D. Pierce. Parabolic equation development in recent decade. *Journal of Computational Acoustics*, **3**(2), 95–173, 1995.

[171] D. Lesselier. Optimization techniques and inverse problems: Reconstruction of conductivity profiles in the time domain. *IEEE Trans. Antennas Propagat.*, **30**(1), 59–65, January 1982.

[172] D. Lesselier and W. Tabbara. 1-D inverse scattering problems in acoustics and electromagnetics. bibliographic study. *Journal d'Acoustique*, **1**(4), 363–84, 1988.

[173] M. F. Levy. Parabolic wave equation techniques for radiowave propagation. *Radio Science Bulletin*, (282), 6–13, September 1997.

[174] M. Lilja. *Controller Design by Frequency Domain Approximation*. PhD thesis, Lund Institute of Technology, Department of Automatic Control, P.O. Box 118, S-221 00 Lund, Sweden, 1989.

[175] C.-Y. Lin and Y.-W. Kiang. Inverse scattering for conductors by the equivalent source method. *IEEE Trans. Antennas Propagat.*, **44**(3), 310–316, March 1996.

[176] I. V. Lindell. *Methods for Electromagnetic Field Analysis*. Clarendon Press, Oxford, 1992.

[177] I. V. Lindell, A. H. Sihvola, S. A. Tretyakov, and A. J. Viitanen. *Electromagnetic Waves in Chiral and Bi-isotropic Media*. Artech House, Boston, London, 1994.

[178] A. K. Louis. Medical imaging: state of the art and future development. *Inverse Problems*, **8**, 709–738, 1992.

[179] J. Lundstedt and S. Ström. Simultaneous reconstruction of two parameters from the transient response of a nonuniform LCRG transmission line. *J. Electro. Waves Applic.*, **10**(1), 19–50, 1996.

[180] R. M. Luneberg. *Mathematical Theory of Optics*. Brown Univ. Press, Providence, RI, 1944.

[181] J. C. Maxwell. *A Treatise on Electricity and Magnetism*, volume 1. Dover Publications, New York, 1954.

[182] J. C. Maxwell. *A Treatise on Electricity and Magnetism*, volume 2. Dover Publications, New York, 1954.

[183] H. McMaken. On the convergence of the Bremmer series for the Helmholtz equation in 2-D. *Wave Motion*, **8**, 277–283, 1986.

[184] T. Melamed, E. Heyman, and L. B. Felsen. Local spectral analysis of short-pulse excited scattering from weakly inhomogeneous media–part II: Inverse scattering. *IEEE Trans. Antennas Propagat.*, **47**(7), 1218–1227, July 1999.

[185] Z. Q. Meng, T. Takenaka, and T. Tanaka. Image reconstruction of two-dimensional impenetrable objects uding genetic algorithm. *J. Electro. Waves Applic.*, **13**, 95–118, 1999.

[186] E. L. Miller and A. S. Willsky. Wavelet-based methods for the nonlinear inverse scattering problem using: The extended Born approximation. *Radio Sci.*, **31**(1), 51–65, Jan-Feb 1996.

[187] R. Mittra, O. Ramahi, A. Khebir, R. Gordon, and A. Kouki. A review of absorbing boundary conditions for two and three-dimensional electromagnetic scattering problems. *IEEE Trans. Magnetics*, **25**(4), 3034–3039, July 1989.

[188] M. Moghaddam and W. C. Chew. Nonlinear two-dimensional velocity profile inversion using time-domain data. *IEEE Trans. Geoscience and Remote Sensing*, **30**(1), 147–156, January 1992.

[189] C. S. Morawetz. Exponential decay for solutions of the wave equation. *Comm. Pure Appl. Math.*, pages 439–444, 1966.

[190] C. S. Morawetz. *Notes on time decay and scattering for some hyperbolic problems*, volume 19. SIAM, Philadelphia, 1975.

[191] P. M. Morse and H. Feshbach. *Methods of Theoretical Physics*, volume 1. McGraw-Hill, New York, 1953.

[192] P. M. Morse and H. Feshbach. *Methods of Theoretical Physics*, volume 2. McGraw-Hill, New York, 1953.

[193] C. Müller. *Foundations of the Mathematical Theory of Electromagnetic Waves*. Springer-Verlag, Berlin, 1969.

[194] A. I. Nachman. Global uniqueness for a two-dimensional inverse boundary value problem. *Ann. of Math.*, **143**, 71–96, 1996.

[195] R. G. Newton. *Inverse Schrödinger Scattering in Three Dimensions*. Springer-Verlag, Berlin, 1989.

[196] H. Otterheim. *Time domain direct and inverse scattering for gyrotropic media*. PhD thesis, Royal institute of technology, Stockholm, Sweden, 1993.

[197] M. Pastorino. Modern microwave inverse-scattering techniques for image reconstruction. *IEEE Instrumentation & Measurement Magazine*, pages 20–25, December 1998.

[198] E. Polack. *Computational Methods in Optimization, a Unified Approach*. Academic Press, New York, 1971.

[199] E. J. Post. *Formal Structure of Electromagnetics*. North-Holland, Amsterdam, 1962.

[200] S. Pourjavid and O. Tretiak. Ultrasound imaging through time-domain diffraction tomography. *IEEE Transactions on Ultrasonics, Ferroelectrics, and Frequency Control*, **38**(1), 74–85, January 1991.

[201] S. W. R. Coifman, V. Rokhlin. The fast multipole method for the wave equation: A pedestrian prescription. *IEEE Antennas and Propagation Magazine*, **35**(3), 7–12, 1993.

[202] I. T. Rekanos, T. V. Yioultsis, and T. D. Tsiboukis. Inverse scattering using the finite-element method and a nonlinear optimization technique. *IEEE Trans. Microwave Theory Tech.*, **47**(3), 336–344, March 1999.

[203] S. Rikte. Transient Inverse Scattering in Dispersive Homogeneous Bi-isotropic Media. In R. Kleinman, T. Angell, D. Colton, F. Santosa, and I. Stakgold, editors, *Mathematical and Numerical Aspects of Wave Propagation*. SIAM, 1993.

[204] S. Rikte. *Propagation of transient electromagnetic waves in stratified bi-isotropic media and related inverse scattering problems*. PhD thesis, Lund Institute of Technology, Department of Electromagnetic Theory, P.O. Box 118, S-211 00 Lund, Sweden, 1994.

[205] S. Rikte. Reconstruction of bi-isotropic material parameters using transient electromagnetic fields. *Wave Motion*, **28**(1), 41–58, July 1998.

[206] S. Rikte. The theory of the propagation of TEM-pulses in dispersive bi-isotropic slabs. *Wave Motion*, **29**(1), 1–21, January 1999.

[207] S. Rikte, M. Andersson, and G. Kristensson. Homogenization of woven materials. *Archiv für Elektronik und Übertragungstechnik (AEÜ)*, **53**(5), 261–271, 1999.

[208] V. Rokhlin. Raplid solution of integral equations of scattering theory in two dimansions. *Journal of Computational Physics*, **10**(1), 14–19, 1995.

[209] V. G. Romanov and S. I. Kabanikhin. *Inverse Problems for Maxwell's Equations*. VSP, Utrecht, 1994.

[210] E. J. Rothwell, K. M. Chen, D. P. Nyquist, and J. E. Ross. Time-domain imaging of airborne targets using ultra-wideband or short-pulse radar. *IEEE Trans. Antennas Propagat.*, **43**(3), 327–329, March 1995.

[211] Y. Saad. *Iterative Methods for Sparse Linear Systems*. PWS Publishing Company, Boston, 1996.

[212] K. Sarabandi and P. R. Siqueira. Numerical scattering analysis for two-dimensional dense random media: Characterization of effective permittivity. *IEEE Trans. Antennas Propagat.*, **45**(5), 858–867, May 1997.

[213] J. A. Scales and M. L. Smith. *Introductory Geophysical Inverse Theory: Part I.* Samizdat Press, `http://samizdat.mines.edu`, March 1996. Release 1.2.

[214] M. A. Shubin. *Pseudodifferential Operators and Spectral Theory.* Springer-Verlag, Berlin, 1987.

[215] A. Sihvola. Homogenization of a dielectric mixture with anisotropic spheres in anisotropic background. *Electromagnetics*, **17**(3), 269–286, 1997.

[216] M. P. Simon, M. J. Schuh, and A. C. Woo. Bistatic ISAR images from a time-domain code. *IEEE Antennas and Propagation Magazine*, **37**(5), 25–32, October 1995.

[217] D. Sjöberg. Reconstruction of nonlinear material properties for homogeneous, isotropic slabs using electromagnetic waves. *Inverse Problems*, **15**(2), 431–444, April 1999.

[218] R. Snieder, M. Y. Xie, A. Pica, and A. Tarantola. Retrieving both the impedance contrast and background velocity: A global strategy for the seismic reflection problem. *Geophysics*, **54**(8), 991–1000, August 1989.

[219] I. Stakgold. *Boundary Value Problems of Mathematical Physics*, volume 2. Macmillan, New York, 1968.

[220] J. C. Strikwerda. *Finite Difference Schemes and Partial Differential Equations.* Chapman & Hall, New York, 1989.

[221] T. Sueta and M. Izutsu. Integrated optic devices for microwave applications. *IEEE Trans. Microwave Theory Tech.*, **38**(5), 477–482, May 1990.

[222] Z. Sun. Direct scattering and reconstruction of internal source. *Wave Motion*, **16**, 249–263, 1992.

[223] Z. Sun. Time domain direct scattering and inverse source problems. In J. P. Corones, G. Kristensson, P. Nelson, and D. L. Seth, editors, *Invariant Imbedding and Inverse Problems.* SIAM, 1992.

[224] Z. Sun. Reconstruction of source and medium parameters via wave-splitting and green function equations. *SIAM J. Appl. Math.*, **56**(4), 1146–1163, 1996.

[225] Z. Sun and J. Corones. Invariant imbedding method and inverse source problems. *Inverse Problems in Scattering and Imaging, SPIE Proc.*, **1767**, 13–20, 1992.

[226] J. Sylvester and G. Uhlmann. A global uniqueness theorem for an inverse boundary value problem. *Ann. of Math.*, **125**, 153–169, 1987.

[227] J. Sylvester and G. Uhlmann. The Dirichlet to Neumann map and applications. In D. Colton, R. Ewing, and W. Rundell, editors, *Inverse Problems in Partial Differential Equations*, pages 101–139. SIAM, Philadelphia, 1990.

[228] A. Taflove. *Computational electrodynamics: The Finite-Difference Time-Domain Method*. Artech House, Boston, London, 1995.

[229] T. Takenaka, D. J. N. Wall, H. Harada, and M. Tanaka. Reconstruction algorithm of the refractive index of a cylindrical object from the intensity measurements of the total field. *Microwave Opt. Techn. Lett.*, **14**(3), 182–188, February 1997.

[230] L. S. Tamil and A. K. Jordan. Spectral inverse scattering theory for inhomogeneous dielectric waveguides and devices. *Proc. IEEE*, **79**(10), 1519–1528, October 1991.

[231] A. Tarantola. Inversion of seismic reflection data in the acoustic approximation. *Geophysics*, **49**(8), 1259–1266, August 1984.

[232] A. Tarantola. *Inverse Problem Theory*. Elsevier Science Publishers, Amsterdam, 1987.

[233] M. E. Taylor. *Pseudodifferential Operators*. Princeton University Press, Princeton, New Jersey, 1981.

[234] A. G. Tijhuis. *Electromagnetic Inverse Profiling. Theory and Numerical Implementation*. VNU Science Press BV, Utrecht, 1987.

[235] F. Trevers. *Introduction to pseudodifferential and Fourier integral operators*, volume 1. Plenum Press, New York, 1980.

[236] P. Y. Ufimtsev. Elementary edge waves and the physical theory of diffraction. *Electromagnetics*, **11**, 125–160, 1991.

[237] P. M. van den Berg. Profile inversion though contrast sources. Department of Electromagnetic Theory, S100 44 Stockholm, Sweden, 1999.

[238] P. M. van den Berg, M. G. Cote', and R. E. Kleinman. "blind" shape reconstruction from experimental data. *IEEE Trans. Antennas Propagat.*, **43**, 1389–1396, 1995.

[239] P. M. van den Berg and R. E. Kleinman. A contrast source inversion method. *Inverse Problems*, **13**, 1607–1620, 1997.

[240] P. M. van den Berg, B. J. Kooij, and R. E. Kleinman. Image reconstruction from ipswich data–III. *IEEE Antennas and Propagation Magazine*, **41**(2), 27–32, April 1999.

[241] P. van den Berg and R. E. Kleinman. The conjugate gradient spectral iterative technique for planar structures. *IEEE Trans. Antennas Propagat.*, **36**(10), 1418–1423, October 1988.

[242] M. van Stralen. *Directional decomposition of electromagnetic and acoustic wave-fields*. PhD thesis, Delft University of Technology, 1997.

[243] G. Wahba. Practical approximate solutions to linear operator equations when the data are noisy. *SIAM Journal on Numerical Analysis*, **14**, 651–667, 1977.

[244] D. J. N. Wall and P. Olsson. Invariant imbedding and hyperbolic heat waves. *J. Math. Phys.*, **38**(3), 1723–1749, 1997.

[245] T. Wang and M. L. Oristaglio. An inverse algorithm for velocity reconstruction. *Inverse Problems*, **14**(5), 1345–1351, October 1998.

[246] T. L. Wang, M. Oristaglio, A. Tripp, and G. Hohmann. Inversion of diffusive transient electromagnetic data by a conjugate-gradient method. *Radio Sci.*, **29**(4), 1143–1156, Jul-Aug 1994.

[247] R. Weinstock. *Calculus of variation: with applications to physics and engineering*. Dover Publications, New York, 1974.

[248] N. Wellander. *Homogenization of Some Linear and Nonlinear Partial Differential Equations*. PhD thesis, Luleå University of Technology, Luleå, Sweden, 1998.

[249] V. H. Weston. Factorization of the dissipative wave equation and inverse scattering. *J. Math. Phys.*, **29**(10), 2205–2218, 1988.

[250] V. H. Weston. Invariant imbedding for the wave equation in three dimensions and the applications to the direct and inverse problems. *Inverse Problems*, **6**, 1075–1105, 1990.

[251] V. H. Weston. Invariant imbedding and wave splitting in $\mathbb{R}^3$: II. The Green function approach to inverse scattering. *Inverse Problems*, **8**, 919–947, 1992.

[252] V. H. Weston. Root of a second order hyperbolic differential operator and wave splitting. In J. P. Corones, G. Kristensson, P. Nelson, and D. L. Seth, editors, *Invariant Imbedding and Inverse Problems*. SIAM, 1992.

[253] W. H. Weston and S. He. Wave splitting of the telegraph equation in $\mathbb{R}^3$ and its application to inverse scattering. *Inverse Problems*, **9**(6), 789–812, 1993.

[254] A. E. Yagle and J. L. Frolik. On the feasibility of impulse reflection response data for the two-dimensional inverse scattering problem. *IEEE Trans. Antennas Propagat.*, **44**(12), 1551–1564, December 1996.

[255] D. Yevick and D. J. Thomson. Split-step/finite difference and split-step/Lanczos algorithms for solving alternative higher-order parabolic equations. *J. Acoust. Soc. Am.*, **96**(1), 396–405, July 1994.

[256] W. Yu, Z. Peng, and L. Jen. A fast convergent method in electromagnetic inverse scattering. *IEEE Trans. Antennas Propagat.*, **44**(11), 1529–1532, November 1996.

[257] E. C. Zachmanoglou. The decay of solutions of the initial-boundary value problem for hyperbolic equations. *J. Math. Anal. Appl.*, **13**, 504–515, 1966.

Index